



The University of
Nottingham

UNITED KINGDOM • CHINA • MALAYSIA

Ionic Liquids as Designer Molecules for XPS Peak Fitting

Coby Clarke, M.Sci.

Thesis submitted to the University of Nottingham
for the degree of Doctor of Philosophy

September 2015

This *Thesis* is dedicated to my sister, Paige, the strongest person I know.

Abstract

X-ray photoelectron spectroscopy (XPS) of ionic liquids (ILs) has become a valuable tool for the investigations of IL interfacial and physicochemical properties. The complex signals that result from elements which occupy a variety of chemical states, for example the C 1s photoemission, are often interpreted through chemical intuition and peak fitting parameters. This *Thesis* will present a new method to determine exact photoemission binding energies (B.E.s), through the comparison of multiple spectra.

The designer aspect of ILs has been exploited in order to produce salts with small structural modifications. By comparing the C 1s and N 1s photoemissions of the structurally related samples, difference spectra have been produced. These spectra show the relative shifting of electron density between the two signals, revealing the initial and final locations of the changing photoemission. Using this technique, the current C 1s peak fitting models of imidazolium and pyridinium ILs have been examined.

A variety of 4,4'-bipyridinium salts have also been used as a structural variation of pyridinium ILs to show how molecular symmetry and normalisation may be utilised in order to produce photoemissions equivalent to fragments of molecules. The subsequent C 1s difference spectra have provided carbon peak fitting models for mono- and di-alkylated 4,4'-bipyridinium salts. Without the use of XP difference spectra, these known fitting models would be almost impossible to determine.

Finally, multiple complex difference spectra have been used to identify the exact B.E.s of C 1s photoemissions from a series of nitrile functionalised ILs. The complex difference spectra have also been analysed by inverse Gaussian fittings to show how additional information may be extracted from the characteristic shapes. The 'construction' of photoemissions is also demonstrated, whereby known B.E. peaks are assembled to accurately reproduce experimentally determined XP spectra.

Declaration

This work has not previously been accepted in substance for any degree and is not being concurrently submitted in candidature for any degree.

Signed _____ (Candidate)

Date _____

Statement 1

This Thesis is the result of my own investigations, except where otherwise stated. Other sources are acknowledged by footnotes giving explicit references.

Bibliographies are appended.

Signed _____ (Candidate)

Date _____

Signed _____ (Supervisor)

Date _____

Statement 2

I hereby give consent for my Thesis, if accepted, to be available for photocopying and for inter-library loan, and for the title and summary to be made available to outside organisations.

Signed _____ (Candidate)

Date _____

Acknowledgements

Firstly, I would like to thank my supervisor, Prof. Peter Licence for his excellent guidance and support throughout this Ph.D. project. I would also like to thank Dr. Emily Smith for XPS training, help with data interpretation and stimulating conversation throughout the past 4 years. I must also thank Jason B. Harper and Rebecca R. Hawker of the University of New South Wales (UNSW) for donating the 4-chloroimidazolium ionic liquids presented in this work.

I am indebted to Matthew Buckley for help with Igor Pro. Without Matthew's help with peak fitting and Igor procedures, this work would have been impossible to achieve alone. I must also thank Alex Dear for the preparation of the 4,4'-bipyridinium bromides used in this work. It was a pleasure to mentor Alex throughout his Masters' project.

I would like to thank the recent members of the Licence group for making long hours in the lab enjoyable: Zoë, Becca, Ana, Ejike, Amelina, Steven, Rossella, Laís, Luiz, Graziela, Andinet, Astrid, Alex, Ed, Darrell, Matt, Sandra and Bogdan. I would also like to extend my gratitude to Zoë and Ana for proof reading this thesis, especially Zoë who has also provided love, support and encouragement throughout my research.

For teaching me at the beginning of my Ph.D. and for inspiring my interest in ionic liquid research, I am grateful to the past members of the Licence group: Dr. Simon Puttick, Dr. Al Taylor, Dr. Shuang Men, Dr. Bitu Hurriso, Dr. Ignacio Villar-Garcia, Dr. Emma Steeds, Dr. Dan Mitchell and Dr. Kevin Lovelock.

The reference XP spectra used in this thesis were previously acquired by Dr. Shuang Men (pyridiniums) and Dr. Ignacio Villar-Garcia (imidazoliums). I would like to thank them for the use of this data.

I must also thank the technical staff for all of their help, especially Mark Guyler, Neil Barnes, Clive Dixon and Conor Howell.

Finally, I would like to thank my family for all of their love and support throughout my Ph.D.

Abbreviations

[A] ⁻	Anion
Arb. Units	Arbitrary Units
B.E.	Binding energy
CHA	Concentric hemispheric analyser
C ^{ali}	Aliphatic carbon component
-CF ₃	Trifluoromethane group
C ⁿ	Carbon component(s) of n
CPS	Counts Per Second
DLD	Delay line detector
ESI-MS	Electrospray Ionisation Mass Spectrometry
eV	Electron volts
EWG	Electron Withdrawing Group
FWHM	Full Width at Half Maximum
h	Planck's constant ($6.626 \times 10^{-34} \text{ m}^2 \text{ kg s}^{-1}$)
IC	Ion Chromatography
ILs	Ionic Liquids
IR	Infrared
J	Coupling constant
K.E.	Kinetic energy
Km	Kilometer
kV	Kilovolts
mA	Milliampere
mbar	Millibar
n	Number of carbon atoms in an alkyl chain
nm	Nanometer
NMR	Nuclear Magnetic Resonance
NIP	Neutral ion pair
RSF	Relative Sensitivity Factor
RTILs	Room Temperature Ionic Liquids
TSILs	Task Specific Ionic Liquids
UHV	Ultra-High Vacuum ($1 \times 10^{-8} \text{ mbar}$)
V	Volts
XPS	X-ray Photoelectron Spectroscopy
δ	Chemical shift
Φ_s	Work function
λ	Mean free path
θ	Emission angle

Table of structural abbreviations

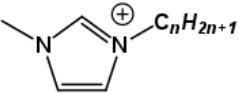
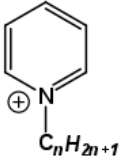
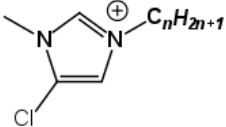
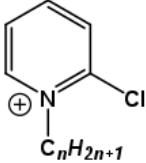
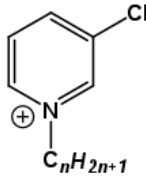
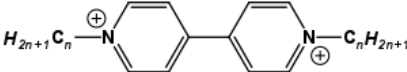
Structure	Name	Abbreviation
	1-alkyl-3-methylimidazolium	$[\text{C}_n\text{C}_1\text{Im}]^+$
	1-alkylpyridinium	$[\text{C}_n\text{Py}]^+$
	1-alkyl-1-methylpyrrolidinium	$[\text{C}_n\text{C}_1\text{Pyr}]^+$
	1-alkyl-3-methyl-4-chloroimidazolium	$[\text{C}_n\text{C}_1\text{-4-ClIm}]^+$
	1-alkyl-2-chloropyridinium	$[\text{C}_n\text{-2-ClPy}]^+$
	1-alkyl-3-chloropyridinium	$[\text{C}_n\text{-3-ClPy}]^+$
	1,1'-dialkyl-4,4'-bipyridinium	$[(\text{C}_n)_2\text{bipy}]^+$
	1-alkyl-4,4'-bipyridinium	$[\text{C}_n\text{bipy}]^+$

Table of structural abbreviations continued...

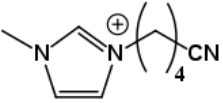
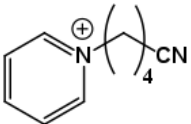
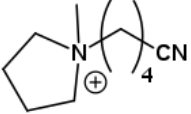
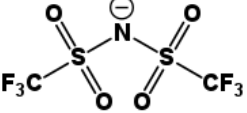
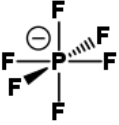
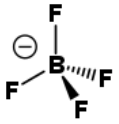
Structure	Name	Abbreviation
	1-valeronitrile-3-methylimidazolium	$[(C_4CN)C_1Im]^+$
	1-valeronitrile-pyridinium	$[(C_4CN)Py]^+$
	1-valeronitrile-1-methylpyrrolidinium	$[(C_4CN)Pyr]^+$
	Bis(trifluoromethanesulfonyl)imide	$[NTf_2]^-$
	Hexafluorophosphate	$[PF_6]^-$
	Tetrafluoroborate	$[BF_4]^-$

Table of Contents

1	INTRODUCTION	12
1.1	IONIC LIQUIDS	12
1.2	VOLATILITY OF ILS	13
1.3	SOLVATION PROPERTIES	13
1.4	XPS ANALYSIS OF ILS	14
1.5	AIMS AND OBJECTIVES	15
1.6	REFERENCES	18
2	THEORY AND EXPERIMENTAL	24
2.1	THEORY	25
2.1.1	<i>X-ray Photoelectron Spectroscopy</i>	25
2.1.1.1	The Photoelectric Effect	25
2.1.1.2	The Auger Effect	26
2.1.1.3	Shake Up and Shake Off Effects	27
2.1.1.4	The XPS Experiment	28
2.1.1.5	The Vacuum Environment	29
2.1.1.6	Charge Neutralisation	29
2.1.2	<i>Data Analysis</i>	30
2.1.2.1	XP Spectra	30
2.1.2.2	Wide Scans	30
2.1.2.3	High Resolution Scans	31
2.1.2.4	Chemical Shift	32
2.1.2.5	Peak Fittings	33
2.1.2.6	Charge Correcting IL XP Spectra	37
2.2	EXPERIMENTAL	38
2.2.1	<i>Data Analysis of XP Spectra</i>	38
2.2.2	<i>Instrumentation</i>	38
2.2.2.1	XPS	38
2.2.2.2	NMR Analysis	39
2.2.2.3	Mass Spectrometry	40
2.2.2.4	Ion Chromatograph	40
2.2.3	<i>Synthesis</i>	40
2.2.3.1	General Comments	40
2.2.3.2	Materials	41
2.2.3.3	Synthetic Procedures	42
2.3	REFERENCES	62
3	CHLORINATED IONIC LIQUIDS	ERROR! BOOKMARK NOT DEFINED.
3.1	INTRODUCTION	65
3.2	CHLORINATED IMIDAZOLIUM ILS	67
3.2.1	<i>The XPS of Chlorinated Imidazolium Salts</i>	68
3.2.2	<i>[C₁C_n-4-ClIm][NTf₂] C 1s Difference Spectra</i>	72
3.2.2.1	Peak Positions in [C ₁ C _n -4-ClIm][NTf ₂] Difference Spectra	75
3.2.2.2	Peak Shifting in [C ₁ C _n -4-ClIm][NTf ₂] Difference Spectra	75
3.3	CHLORINATED PYRIDINIUM ILS	81
3.3.1	<i>N-Alkyl-2-Chloropyridinium Salts</i>	82
3.3.1.1	XPS of [C _n -2-ClPy][NTf ₂] salts	83
3.3.1.2	Peak Shifting in the [C _n -2-ClPy][NTf ₂] C 1s Region	88
3.3.1.3	Peak Fitting the [C _n -2-ClPy][NTf ₂] C 1s region	91
3.3.2	<i>N-Alkyl-3-Chloropyridinium ILS</i>	94
3.3.2.1	XPS of [C _n -3-ClPy][A] Salts	94

3.3.2.2	[C _n -3-CIPy][NTf ₂] C 1s Difference Spectra	98
3.3.2.3	Peak Fitting the [C _n -3-CIPy][A] C 1s region.....	101
3.4	CONCLUSIONS	103
3.5	REFERENCES.....	106
4	4,4'-BIPYRIDINIUM C 1S PEAK FITTING	111
4.1	SYNTHESIS OF 4,4'-BIPYRIDINIUM IONIC LIQUIDS	112
4.2	XPS ANALYSIS OF 4,4-BIPYRIDINIUM SALTS	113
4.2.1	<i>1,1'-Dialkyl-4,4'-bipyridinium bis(trifluoromethane-sulfonyl)imide Ionic Liquids, [(C_n)₂Bipy][NTf₂]₂</i>	<i>113</i>
4.2.1.1	Wide and High Resolution Scans	114
4.2.1.2	[(C _n) ₂ Bipy][NTf ₂] ₂ and [C _n Py][NTf ₂] C 1s Difference Spectra.....	117
4.2.1.3	Confirmation of the [C _n Py][A] C 1s Peak Fitting Model.....	121
4.2.1.4	Peak Fitting the [(C _n) ₂ Bipy][NTf ₂] ₂ C 1s Region	122
4.2.2	<i>XPS of Alkyl-4,4'-bipyridinium Ionic Liquids</i>	<i>124</i>
4.2.2.1	Wide and High Resolution Scans	125
4.2.2.2	N 1s Peak Fitting	127
4.2.2.3	C 1s Peak Fitting.....	129
4.3	CONCLUSIONS	137
4.4	REFERENCES.....	139
5	NITRILE FUNCTIONALISED IONIC LIQUIDS	142
5.1	STRUCTURES AND SYNTHESIS.....	144
5.2	XPS OF NITRILE FUNCTIONALISED ILS.....	146
5.2.1	<i>Wide and High Resolution Scans for Nitrile Functionalised ILS</i>	<i>146</i>
5.2.1.1	Nitrile Functionalised ILS with [NTf ₂] ⁻ anions	146
5.2.1.2	Nitrile Functionalised ILS with [PF ₆] ⁻ , [BF ₄] ⁻ and Cl ⁻ anions.....	151
5.2.2	<i>Shake up/off Quantification of Nitrile Functionalised ILS</i>	<i>154</i>
5.2.3	<i>Nitrile Interactions with Anions and Cations</i>	<i>155</i>
5.2.4	<i>C 1s Difference Spectra Examples: [(C₄CN)Py][NTf₂].....</i>	<i>157</i>
5.2.5	<i>Cationic Variation: [(C₄CN)C₁Im][NTf₂] and [(C₄CN)C₁Pyrr][NTf₂] C 1s Difference Spectra</i>	<i>165</i>
5.2.5.1	[(C ₄ CN)C ₁ Im][NTf ₂] Difference Spectra	165
5.2.5.2	[(C ₄ CN)C ₁ Pyrr][NTf ₂] Difference Spectra.....	168
5.2.6	<i>Anionic Variation: [(C₄CN)C₁Im][A] C 1s Difference Spectra.....</i>	<i>171</i>
5.2.7	<i>Accurate C 1s Peak Fitting for Nitrile ILS.....</i>	<i>179</i>
5.3	CONCLUSIONS	182
5.4	REFERENCES.....	185
6	CONCLUSIONS AND FUTURE WORK.....	188
7	APPENDIX.....	193
7.1	GAUSSIAN PEAK FITTINGS:	194
7.2	GAUSSIAN PEAK FITTING RESULTS:	195
7.3	RESIDUAL STDs FOR NITRILE ILS:.....	201
7.4	REFERENCE SPECTRA:.....	202

Chapter 1: **Introduction**

1 Introduction

1.1 Ionic Liquids

Ionic liquids (ILs) are salts with low melting points (generally $< 100^{\circ}\text{C}$) that are composed of large, bulky organic cations with simple anions. The study of ILs has gained considerable interest over the past few decades, due to their outstanding physiochemical properties which provide exceptional performances in a wide range of applications.¹⁻⁵ From energy devices⁶ and biomass processing⁷ to rocket fuels⁸ and sweat activated perfumes,⁹ ILs are remarkable materials with unique features. There are a number of excellent publications for a thorough introduction to ILs and their unusual properties.¹⁰⁻¹²

The most important practical feature of ILs is the ability to select specific physical and chemical properties by choosing particular anion and cation combinations,^{13,14} **Figure 1.1.** Potentially there are millions of cation-anion pairs, each providing an IL with individual characteristics. It is important to thoroughly understand the processes that govern the nature of ILs, especially when designing new materials for a specialised application. The following sections will introduce a few relevant properties of ILs that are directly related to this thesis. Furthermore, previous IL XPS experiments will be discussed in order to provide a foundation for the work presented here.

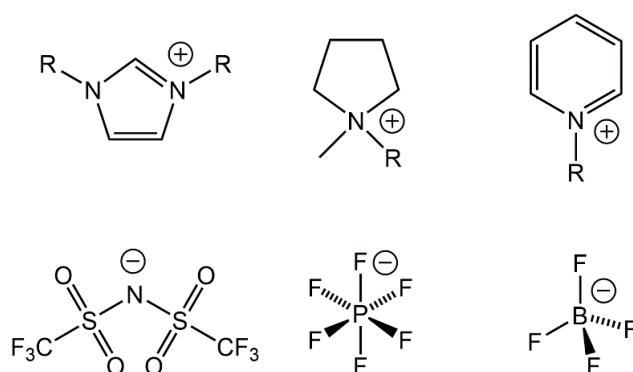


Figure 1.1 A selection of common IL cations (top row) and anions (bottom row).

1.2 Volatility of ILs

ILs were initially thought to be involatile, with decomposition of the salts occurring long before evaporation.¹⁵ However, recent experiments have shown that ILs may be vaporised under reduced pressures and high temperatures.^{16–20} Distillations of ILs are even possible,^{21,22} although for imidazolium ILs with $[\text{PF}_6]^-$ and $[\text{BF}_4]^-$ anions, a decomposition process whereby the anions and cations of the IL fuse to form an adduct of the two has been noted.^{23,24} The vapour phase of traditional ILs has been found to consist of neutral ion pairs (NIPs),^{25,26} while the vapour phase of dicationic ILs has been found to consist of neutral ion triplets (NITs).^{27,28} Despite this, the extremely high enthalpies of vaporisation render ILs non-volatile under ambient conditions.^{29–31} ILs may even be introduced into ultra-high vacuum (UHV) chambers without suffering significant evaporation.^{32–34} This has allowed the use of XPS for the investigation of a range of IL at room temperature.

1.3 Solvation Properties

ILs have long been suggested as alternative solvents to replace traditional volatile organic compounds (VOCs).^{35–38} The major incentive being that the low volatilities of ILs prevents evaporation into the environment. Although the use of bulk ILs as solvents has come under scrutiny,³⁹ ILs still possess certain properties that make them potentially useful as solvents. For example, the solvation properties of ILs can be altered by the selection of different anion and cation types. Dissolved species may experience a range of inter-molecular forces, including van der Waals, coulombic, hydrogen bonding, π - π stacking and dipole interactions,^{11,40–42} depending upon the IL that is chosen. The segregation of ILs into polar and non-polar domains^{43–45} may even lead to preferred solvation of the solutes into the various parts of the ILs.^{46,47}

ILs are able to dissolve a wide range of materials, including organic compounds,⁴⁸ gasses,⁴⁹ proteins,⁵⁰ enzymes⁵¹ and polymers.⁵² Unfortunately,

neutral organometallic complexes exhibit poor solubilities in traditional ILs. This problem may be overcome by functionalisation of the IL with one or more coordinating groups.⁵³⁻⁵⁵ Generally, these ILs are referred to as task-specific ionic liquids (TSILs), as they are designed and suited to a particular purpose.^{56,57} The ability to modify the solvation properties of ILs has resulted in rapid growth for homogeneous catalysis in ILs.^{41,58,59} Supported ionic liquids (SILs), whereby IL layers are either adsorbed or covalently bound to a solid support, may also be used in order to eliminate issues associated with bulk ILs, such as mass transport of solutes.^{60,61}

The performance of a homogeneous catalyst depends upon the electronic environment of the catalytically active metal centre. For IL solutions, the anion has been shown to express the highest influence over the majority of IL-catalyst interactions.⁶²⁻⁶⁴ An IL with a highly basic anion provides a liquid medium that is capable of coordinating, and hence stabilising, a metallic catalyst. For weakly coordinating anions such as [NTf₂]⁻, functionalities are required in order to coordinate the metal species. A common coordinating group that may be used for this particular purpose is the nitrile functional group.^{65,66} The XPS analysis of a range of nitrile functionalised ILs will be discussed later in this thesis. The data presented here may form the basis for future XPS experiments involving IL metallic solutions.

1.4 XPS Analysis of ILs

As previously stated, ILs may be introduced into ultra-high vacuum chambers without incurring significant evaporation.⁶⁷⁻⁷⁰ This lack of volatility has allowed X-ray photoelectron spectroscopy (XPS) to become a prominent analytical method for the investigation of the physicochemical properties of IL samples.⁷¹⁻⁷⁵ The Licence group has dedicated a considerable amount of time and resources into advancing this research. The group's efforts began in 2005 with the successful XPS analysis of [C₁C₂Im][EtOSO₃],⁷⁶ before this time the investigations of ILs under UHV conditions were unknown. The samples were found to be resistant to X-ray beam damage and also provided a strong

photoelectron flux, resulting in short collection times and excellent XPS data. A multi-component model was proposed for the C 1s region of the IL, which was based upon chemical knowledge and parameter constraints (areas, FWHMs). Subsequent investigations using other imidazolium ILs provided an updated fitting model that was shown to effectively fit the profiles of multiple IL C 1s spectra.⁷⁷

Reproducible and accurate binding energies are important for the comparison of various IL XPS experiments. In 2011 the Licence group observed peak shifting in prolonged XPS experiments of liquid samples, due to surface charging. In response they outlined a general charge correction method in order to obtain absolute binding energies of imidazolium ILs,⁷⁸ this process will be explained later in this *Thesis*. Since these initial investigations, the XPS of ILs has rapidly expanded to include the monitoring of *in situ* organic reactivity using ILs as solvents,^{79,80} the speciation of organometallics in ILs,^{62,64} the investigations of cation-anion interactions^{75,81,82} and the XPS analysis of a wide range of unique IL systems.^{73,83-85}

1.5 Aims and Objectives

The low vapour pressure of ILs makes them ideal for UHV spectroscopies, such as XPS. As a surface sensitive technique, XPS can offer vital information on the liquid-vacuum interface and thin film-substrate interface.^{86,87} XPS has also recently become an important tool for investigating bulk IL properties. Since XPS is element specific, all components of the constituent anions and cations may be monitored *in situ*. B.E.s of core orbitals vary depending upon the chemical state, chemical bond type and inter- or intra- molecular interactions of the element in question. This allows the determination and quantification of the different chemical environments present within each sample, potentially providing key additional information on the nature of IL interactions.

Unfortunately, when an element occupies many different chemical environments, photoemission peaks often become convoluted and

unresolvable. This problem is most pronounced in the C 1s region of XP spectra,⁸⁸ where signals appear as complex “fingerprints” that provide little information upon the electronic distribution of the carbon backbone. Crude peak fitting models are often employed in an attempt to deconvoluted and interpret this carbon photoemission,⁸⁶ however this process is based upon chemical knowledge and peak fitting parameters. Peak assignments are therefore not conclusive, and the acquired B.E.s may not accurately represent the individual carbon photoemissions. This *Thesis* aims to develop upon the existing C1s peak fitting procedures that are already in place and also produce new protocols for the extraction of usable, reliable data from XP spectra.

Multiple XP spectra will be analysed relative to each other to produce difference spectra. These spectra show the relative shifting of electron density between the two samples. Through this method, peak positions may be located and exact B.E.s for individual carbon environments may be obtained. This method will progress in the following way:

➤ *Chapter 3: Chlorinated ILs*

- Chlorine is used as an electron withdrawing (EWG) in order to shift electron density away from one carbon atom.
- The shifting electron density is measured through the C 1s XP spectra, and the initial and final locations of the photoemissions are revealed.
- This process is applied to imidazolium and pyridinium ILs, providing exact B.E.s for a range of carbon environments. The current peak fitting models are therefore scrutinised and updated accordingly.

➤ *Chapter 4: 4,4'-Bipyridinium ILs*

- The C 1s XP spectra for dialkyl-4,4'-bipyridinium ILs are used as symmetrical pyridinium analogues. Normalisation of the C 1s regions show how their photoemissions may be halved in

order to provide photoemissions equivalent to fragments of molecules.

- The acquired photoemissions are used to further analyse and peak fit the C 1s regions of pyridinium and mono-alkylated 4,4'-bipyridinium ILs.

➤ *Chapter 5: Nitrile Functionalised ILs*

- A series of nitrile functionalised IL XP spectra are compared to traditional alkyl-chain ILs and C 1s difference spectra are produced.
- Analysis of the difference spectra shows the simultaneous addition and shifting of individual C 1s peaks. Hence, the complexity of the difference spectra are increased and require a more detailed investigation.
- The C 1s regions of the nitrile ILs therefore provide ideal carbon photoemissions that may be used to test the 'building' of C 1s spectra from known B.E. peaks.

1.6 References

- 1 L. C. Branco, G. V. S. M. Carrera, J. Aires-de-sousa, I. L. Martin, R. Frade and C. A. M. Afonso, in *Ionic Liquids: Theory, Properties, New Approaches*, 2011, pp. 61–95.
- 2 H. Tokuda, K. Hayamizu, K. Ishii, A. Bin and H. Susan, *J. Phys. Chem. B.*, **108**, 2004, 16593–16600.
- 3 C. Chiappe and S. Rajamani, *Eur. J. Org. Chem.*, 2011, **2011**, 5517–5539.
- 4 H. Tokuda, S. Tsuzuki, M. A. B. H. Susan, K. Hayamizu and M. Watanabe, *J. Phys. Chem. B*, 2006, **110**, 19593–600.
- 5 H. Olivier-Bourbigou, L. Magna and D. Morvan, *Appl. Catal. A Gen.*, 2010, **373**, 1–56.
- 6 R. Kawano, H. Matsui, C. Matsuyama, A. Sato, M. A. B. H. Susan, N. Tanabe and M. Watanabe, *J. Photochem. Photobiol. A Chem.*, 2004, **164**, 87–92.
- 7 I. Kilpeläinen, H. Xie, A. King, M. Granstrom, S. Heikkinen and D. S. Argyropoulos, *J. Agric. Food Chem.*, 2007, **55**, 9142–9148.
- 8 Y. Zhang, H. Gao, Y. H. Joo and J. M. Shreeve, *Angew. Chem. Int. Ed.*, 2011, **50**, 9554–9562.
- 9 H. Q. N. Gunaratne, P. Nockemann and K. R. Seddon, *Chem. Commun.*, 2015, **51**, 4455–4457.
- 10 P. Wasserscheid and T. Welton, *Ionic Liquids in Synthesis*, Wiley, 2nd edn., 2008.
- 11 C. Chiappe and D. Pieraccini, *J. Phys. Org. Chem.*, 2005, **18**, 275–297.
- 12 J. Dupont and P. a Z. Suarez, *Phys. Chem. Chem. Phys.*, 2006, **8**, 2441–2452.
- 13 P. Bonhôte, A.-P. Dias, N. Papageorgiou, K. Kalyanasundaram and M. Grätzel, *Inorg. Chem.*, 1996, **35**, 1168–1178.
- 14 H. Weingärtner, *Angew. Chem. Int. Ed.*, 2008, **47**, 654–670.
- 15 H. L. Ngo, K. Lecompte, L. Hargens and A. B. Mcewen, 2000, **358**.
- 16 K. R. J. Lovelock, J. P. Armstrong, P. Licence and R. G. Jones, *Phys. Chem. Chem. Phys.*, 2014, **16**, 1339–53.

- 17 J. M. S. S. Esperança, J. N. C. Lopes, M. Tariq, L. M. N. B. F. Santos, J. W. Magee and L. P. N. Rebelo, *J. Chem. Eng. Data*, 2010, **55**, 3–12.
- 18 A. Deyko, K. R. J. Lovelock, J.-A. Corfield, A. W. Taylor, P. N. Gooden, I. J. Villar-Garcia, P. Licence, R. G. Jones, V. G. Krasovskiy, E. a Chernikova and L. M. Kustov, *Phys. Chem. Chem. Phys.*, 2009, **11**, 8544–8555.
- 19 D. H. Zaitsau, G. J. Kabo, A. A. Strechan and Y. U. Paulechka, *J. Phys. Chem. A*, 2006, **110**, 7303–7306.
- 20 A. Deyko, S. G. Hessey, P. Licence, E. A. Chernikova, V. G. Krasovskiy, L. M. Kustov and R. G. Jones, *Phys. Chem. Chem. Phys.*, 2012, **14**, 3181–3193.
- 21 A. W. Taylor, K. R. J. Lovelock, A. Deyko, P. Licence and R. G. Jones, *Phys. Chem. Chem. Phys.*, 2010, 12, 1772.
- 22 M. J. Earle, J. M. S. S. Esperança, M. A. Gilea, J. N. C. Lopes, L. P. N. Rebelo, J. W. Magee, K. R. Seddon and J. A. Widegren, *Nature*, 2006, **439**, 831–834.
- 23 A. W. Taylor, K. R. J. Lovelock, R. G. Jones and P. Licence, *Dalton Trans.*, 2011, **40**, 1463–70.
- 24 C. Tian, W. Nie, M. V. Borzov and P. Su, *Organometallics*, 2012, **31**, 1751–1760.
- 25 J. P. Leal, J. M. S. S. Esperança, M. E. M. da Piedade, J. N. C. Lopes, L. P. N. Rebelo and K. R. Seddon, *J. Phys. Chem. A*, 2007, **111**, 6176–82.
- 26 A. Deyko, K. R. J. Lovelock, P. Licence and R. G. Jones, *Phys. Chem. Chem. Phys.*, 2011, 13, 16841.
- 27 K. R. J. Lovelock, A. Deyko, J.-A. Corfield, P. N. Gooden, P. Licence and R. G. Jones, *ChemPhysChem*, 2009, **10**, 337–40.
- 28 J. Vitorino, J. P. Leal, P. Licence, K. R. J. Lovelock, P. N. Gooden, M. E. Minas Da Piedade, K. Shimizu, L. P. N. Rebelo and J. N. Canongia Lopes, *ChemPhysChem*, 2010, **11**, 3673–3677.
- 29 Y. U. Paulechka, G. J. Kabo, A. V. Blokhin, O. A. Vydrov, J. W. Magee and M. Frenkel, *J. Chem. Eng. Data*, 2003, **48**, 457–462.
- 30 Y. U. Paulechka, D. H. Zaitsau, G. J. Kabo and A. A. Strechan, *Thermochim. Acta*, 2005, **439**, 158–160.
- 31 M. Diedenhofen, A. Klamt, K. Marsh and A. Schäfer, *Phys. Chem. Chem. Phys.*, 2007, **9**, 4653–4656.

- 32 H.-P. Steinrück, J. Libuda, P. Wasserscheid, T. Cremer, C. Kolbeck, M. Laurin, F. Maier, M. Sobota, P. S. Schulz and M. Stark, *Adv. Mater.*, 2011, **23**, 2571–87.
- 33 H.-P. Steinrück, *Surf. Sci.*, 2010, **604**, 481–484.
- 34 E. F. Smith, F. J. M. Rutten, I. J. Villar-Garcia, D. Briggs and P. Licence, *Langmuir*, 2006, **22**, 9386–9392.
- 35 N. V Plechkova and K. R. Seddon, *Chem. Soc. Rev.*, 2008, **37**, 123–150.
- 36 J. P. Hallett and T. Welton, *Chem. Rev.*, 2011, **111**, 3508–3576.
- 37 R. D. Rogers and K. R. Seddon, *Science*, 2003, **302**, 792–793.
- 38 P. Wasserscheid and W. Keim, *Angew. Chem. Int. Ed.*, 2000, **39**, 3772–3789.
- 39 P. G. Jessop, *Green Chem.*, 2011, **13**, 1391.
- 40 J. Wang, H. Chu and Y. Li, *ACS Nano*, 2008, **2**, 2540–2546.
- 41 R. Sheldon, *Chem. Commun.*, 2001, 2399–2407.
- 42 L. Crowhurst, P. R. Mawdsley, J. M. Perez-Arlandis, P. a. Salter and T. Welton, *Phys. Chem. Chem. Phys.*, 2003, **5**, 2790.
- 43 C. Hardacre, J. D. Holbrey, M. Nieuwenhuyzen and T. G. a Youngs, *Acc. Chem. Res.*, 2007, **40**, 1146–1155.
- 44 L. a. Aslanov, *J. Mol. Liq.*, 2011, **162**, 101–104.
- 45 J. N. a Canongia Lopes and A. a H. Pádua, *J. Phys. Chem. B*, 2006, **110**, 3330–3335.
- 46 K. Shimizu, M. F. Costa Gomes, A. a H. Pádua, L. P. N. Rebelo and J. N. Canongia Lopes, *J. Mol. Struct. THEOCHEM*, 2010, **946**, 70–76.
- 47 J. N. Canongia Lopes, M. F. Costa Gomes and A. a H. Pádua, *J. Phys. Chem. B*, 2006, **110**, 16816–16818.
- 48 K. N. Marsh, A. Deev, A. C.-T. Wu, E. Tran and a. Klamt, *Korean J. Chem. Eng.*, 2002, **19**, 357–362.
- 49 J. L. Anthony, E. J. Maginn and J. F. Brennecke, *J. Phys. Chem. B*, 2002, **106**, 7315–7320.
- 50 K. Fujita, D. R. MacFarlane and M. Forsyth, *Chem. Commun.*, 2005, **70**, 4804–4806.

- 51 U. Kragl, M. Eckstein and N. Kaftzik, *Curr. Opin. Biotechnol.*, 2002, **13**, 565–571.
- 52 N. Winterton, *J. Mater. Chem.*, 2006, **16**, 4281.
- 53 Z. Fei, D. Zhao, D. Pieraccini, W. H. Ang, T. J. Geldbach, R. Scopelliti, C. Chiappe and P. J. Dyson, *Organometallics*, 2007, **26**, 1588–1598.
- 54 L. C. Branco, J. N. Rosa, J. J. Moura Ramos and C. a M. Afonso, *Chemistry*, 2002, **8**, 3671–3677.
- 55 P. Nockemann, B. Thijs, T. N. Parac-Vogt, K. Van Hecke, L. Van Meervelt, B. Tinant, I. Hartenbach, T. Schleid, T. N. Vu, T. N. Minh and K. Binnemans, *Inorg. Chem.*, 2008, **47**, 9987–9999.
- 56 R. Giernoth, *Angew. Chem. Int. Ed.*, 2010, 49, 2834–2839.
- 57 S. Lee, *Chem. Commun.*, 2006, 1049–1063.
- 58 V. I. Pârvulescu and C. Hardacre, *Chem. Rev.*, 2007, **107**.
- 59 P. Wasserscheid and W. Keim, *Angew. Chem. Int. Ed.*, 2000, **39**, 3772–3789.
- 60 A. Riisager, R. Fehrmann, M. Haumann and P. Wasserscheid, *Top. Catal.*, 2006, **40**, 91–102.
- 61 C. Van Doorslaer, J. Wahlen, P. Mertens, K. Binnemans and D. De Vos, *Dalton Trans.*, 2010, **39**, 8377–90.
- 62 A. W. Taylor, S. Men, C. J. Clarke and P. Licence, *RSC Adv.*, 2013, **3**, 9436.
- 63 J. Estager, P. Nockemann, K. R. Seddon, M. Swadźba-Kwaśny and S. Tyrrell, *Inorg. Chem.*, 2011, **50**, 5258–5271.
- 64 M. Currie, J. Estager, P. Licence, S. Men, P. Nockemann, K. R. Seddon, M. Swadźba-Kwaśny and C. Terrade, *Inorg. Chem.*, 2013, **52**, 1710–1721.
- 65 D. Zhao, Z. Fei, C. André Ohlin, G. Laurency and P. J. Dyson, *Chem. Commun.*, 2004, 2500–2501.
- 66 K. C. Lethesh, K. Van Hecke, L. Van Meervelt, P. Nockemann, B. Kirchner, S. Zahn, T. N. Parac-Vogt, W. Dehaen and K. Binnemans, *J. Phys. Chem. B*, 2011, **115**, 8424–38.
- 67 A. Deyko, K. R. J. Lovelock, J.-A. Corfield, A. W. Taylor, P. N. Gooden, I. J. Villar-Garcia, P. Licence, R. G. Jones, V. G. Krasovskiy,

- E. A. Chernikova and L. M. Kustov, *Phys. Chem. Chem. Phys.*, 2009, **11**, 8544–8555.
- 68 A. Deyko, S. G. Hesse, P. Licence, E. A. Chernikova, V. G. Krasovskiy, L. M. Kustov and R. G. Jones, *Phys. Chem. Chem. Phys.*, 2012, **14**, 3181.
- 69 J. P. Armstrong, C. Hurst, R. G. Jones, P. Licence, K. R. J. Lovelock, C. J. Satterley and I. J. Villar-Garcia, *Phys. Chem. Chem. Phys.*, 2007, **9**, 982–990.
- 70 K. R. J. Lovelock, A. Deyko, P. Licence and R. G. Jones, *Phys. Chem. Chem. Phys.*, 2010, **12**, 8893–8901.
- 71 C. Kolbeck, T. Cremer, K. R. J. Lovelock, N. Paape, P. S. Schulz, P. Wasserscheid, F. Maier and H. P. Steinrück, *J. Phys. Chem. B*, 2009, **113**, 8682–8688.
- 72 P. Licence, *Angew. Chem. Int. Ed.*, 2012, **51**, 4789–4791.
- 73 B. B. Hurisso, K. R. J. Lovelock and P. Licence, *Phys. Chem. Chem. Phys.*, 2011, **13**, 17737–48.
- 74 A. W. Taylor, F. Qiu, I. J. Villar-Garcia and P. Licence, *Chem. Commun.*, 2009, 5817–5819.
- 75 T. Cremer, C. Kolbeck, K. R. J. Lovelock, N. Paape, R. Wölfel, P. S. Schulz, P. Wasserscheid, H. Weber, J. Thar, B. Kirchner, F. Maier and H.-P. Steinrück, *Chem. Eur. J.*, 2010, **16**, 9018–33.
- 76 E. F. Smith, I. J. V. Garcia, D. Briggs and P. Licence, *Chem. Commun.*, 2005, 5633–5.
- 77 E. F. Smith, F. J. M. Rutten, I. J. Villar-Garcia, D. Briggs and P. Licence, *Langmuir*, 2006, **22**, 9386–9392.
- 78 I. J. Villar-Garcia, E. F. Smith, A. W. Taylor, F. Qiu, K. R. J. Lovelock, R. G. Jones and P. Licence, *Phys. Chem. Chem. Phys.*, 2011, **13**, 2797.
- 79 C. Kolbeck, I. Niedermaier, N. Taccardi, P. S. Schulz, F. Maier, P. Wasserscheid and H. P. Steinrück, *Angew. Chem. Int. Ed.*, 2012, **51**, 2610–2613.
- 80 I. Niedermaier, C. Kolbeck, N. Taccardi, P. S. Schulz, J. Li, T. Drewello, P. Wasserscheid, H.-P. Steinrück and F. Maier, *ChemPhysChem*, 2012, **13**, 1725–1735.
- 81 S. Men, K. R. J. Lovelock and P. Licence, *Phys. Chem. Chem. Phys.*, 2011, **13**, 15244–15255.

- 82 I. J. Villar-Garcia, E. F. Smith, A. W. Taylor, F. Qiu, K. R. J. Lovelock, R. G. Jones and P. Licence, *Phys. Chem. Chem. Phys.*, 2011, **13**, 2797–2808.
- 83 D. S. Mitchell, *Thesis*, University of Nottingham, 2014.
- 84 A. W. Taylor and P. Licence, *ChemPhysChem*, 2012, **13**, 1917–1926.
- 85 R. K. Blundell and P. Licence, *Phys. Chem. Chem. Phys.*, 2014, **16**, 15278–88.
- 86 K. R. J. Lovelock, I. J. Villar-Garcia, F. Maier, H. P. Steinrück and P. Licence, *Chem. Rev.*, 2010, **110**, 5158–5190.
- 87 V. Lockett, R. Sedev, C. Bassell and J. Ralston, *Phys. Chem. Chem. Phys.*, 2008, **10**, 1330–1335.
- 88 A. Walton, John; Wincott, Paul; Fairley, Neal; Carrick, *Peak Fitting with CasaXPS: a Casa Pocket Book*, Acolyte Science, 2010.

Chapter 2:
Theory and Experimental

2 Theory and Experimental

2.1 Theory

2.1.1 X-ray Photoelectron Spectroscopy

XPS is a semi-quantitative, surface sensitive spectroscopic technique that measures the binding energies of electrons that are ejected from samples when ionised by X-ray radiation *in vacuo*. Developed by Kai Siegbahn in the 1960s, for which he was later awarded the 1981 Nobel Prize in physics,¹ XPS is now a widespread analytical tool used in many research fields, including polymer chemistry, catalysis, nanoscience and microelectronics.²⁻⁵

2.1.1.1 The Photoelectric Effect

The photoelectric effect is the principle upon which XPS operates. Samples that are exposed to X-ray radiation become ionised as electrons are ejected from the surface as photoelectrons, **Figure 2.1**.⁶ When the emitted photoelectrons do not lose energy due to inelastic scattering, their resulting kinetic energies (K.E.) may be measured and the binding energy (B.E.) of the core orbital may be calculated according to the Einstein equation:

$$K.E. = h\nu - B.E. - \Phi_s$$

The K.E. of the photoelectron is therefore also dependent upon the energy of the incident photon ($h\nu$) and the work function of the spectrometer (Φ_s), which is the energy required to move an electron from the Fermi level to the Vacuum level. The XP spectrometer automatically corrects for the work function, a typical value being 4.5 eV.

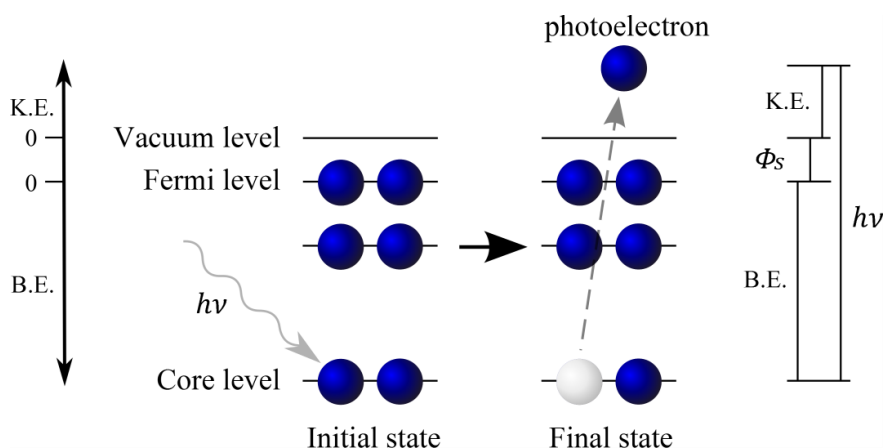


Figure 2.1 A diagram depicting the photoelectric effect. The ionisation of a core level electron (blue sphere) from the initial state. The ejected photoelectron leaves behind a positive hole (white sphere). The schematic on the right describes how the Einstein equation relates the K.E. of the photoelectron to the B.E. of the core level electron.

X-rays penetrate several micrometres into the sample, however the inelastic mean free path (λ) of photoelectrons in organic samples is typically 3nm. The information depth (I.D., 3λ), the depth at which 95% of all photoelectrons are scattered by the time they reach the surface, is therefore between 7-9 nm at the normal emission angle, $\theta = 0^\circ$.⁷ If the emission angle is increased to $\theta = 80^\circ$ from the surface normal, the I.D. is decreased to the top 1-1.5 nm of the sample. This is known as angle resolved X-ray photoelectron spectroscopy, ARXPS.⁸ It is important to note that at $\theta = 0^\circ$ the information obtained from XPS data is indicative of the bulk ionic liquid.⁹

2.1.1.2 The Auger Effect

During XPS measurements the photoionisation process leaves “positive holes” in the core-levels of atoms. When these vacancies are filled by higher energy electrons, the excess energy is either emitted as a photon (visible light, UV or X-rays) or transferred to another electron, ejecting it as an Auger electron, **Figure 2.2.** XPS survey scans always contain Auger peaks between 800 eV and 1400 eV. The energy of an Auger electron only depends upon the states of this secondary emission process, it is therefore independent of the incident photon energy.¹⁰

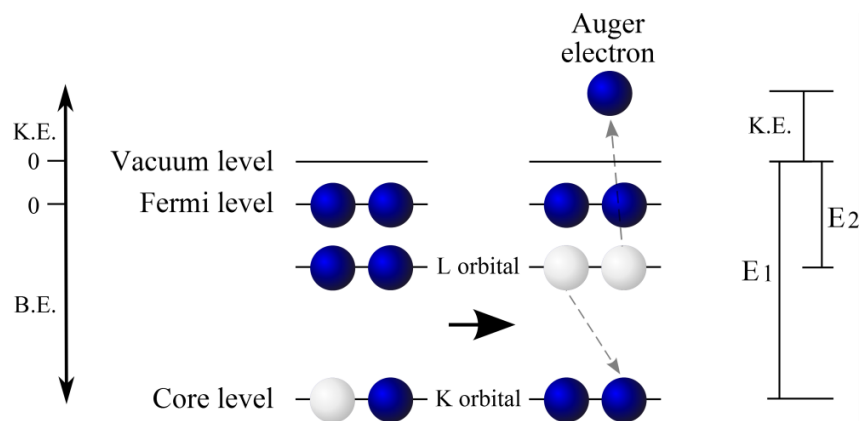


Figure 2.2 A diagram depicting the Auger effect. The positive hole allows a higher energy electron to relax, resulting in the emission of a photon or the ejection of an Auger electron. The schematic on the right describes how the K.E. of the Auger electron is derived.

Each element has a characteristic set of Auger peaks that may be used in elemental identification. Three consecutive letters denote the quantum energy levels involved in the emission process. For example, the Auger transition KLL involves a primary photoionisation from the K orbital (principal quantum number, $n = 1$), a relaxing electron originating from an L orbital ($n = 2$) and the resulting Auger electron is also ejected from the L orbital ($n = 2$).

2.1.1.3 Shake Up and Shake Off Effects

For samples containing π orbitals, e.g. the aromatic regions of imidazolium and pyridinium ionic liquids, outgoing photoelectrons may interact with the valence electrons that occupy these energy states. When the photoelectron causes a π - π^* excitation it loses some kinetic energy and hence appears at a higher binding energy. This is known as the ‘shake up’ phenomenon and it is often observed in C 1s and N 1s high resolution XP spectra (when the sample contains a relatively large proportion of π -bonded atoms). A parallel process known as ‘shake off’ also occurs whereby the outgoing photoelectron completely ionises the valence π -electron, leaving vacancies in both the core level and valence band. ‘Shake off’ signals contribute to the background of the XP spectrum and are not directly observed. Both processes reduce the intensity of the

photoelectron peaks for π -bonded atoms by 5-20%.^{11,12} By measuring the ‘shake up’ region in the C 1s spectra and calculating the degree of loss due to these processes (the ‘shake off’ process is assumed to be equal to the ‘shake up’ process), more accurate fitting model may be developed in order to accurately represent complex photoemission signal.

2.1.1.4 The XPS Experiment

A simplified schematic of a typical XP spectrometer is shown in **Figure 2.3**. X-ray radiation is produced by bombarding a metal source with high energy electrons. For this work an aluminium targeted anode was used to generate Al $K\alpha$ radiation of 1486.6 eV. The X-rays are monochromated by selective diffraction through an array of quartz crystals which remove satellite lines and Bremsstrahlung radiation. The beam is consequently narrowed to 0.3 eV, at 1486.6 eV, to produce an intense photoelectron flux that can be focused onto an area of only a 10 μm diameter. The monochromator also acts to separate the anode and sample, preventing back-scattered electrons causing unwanted damage or overheating during experiments.

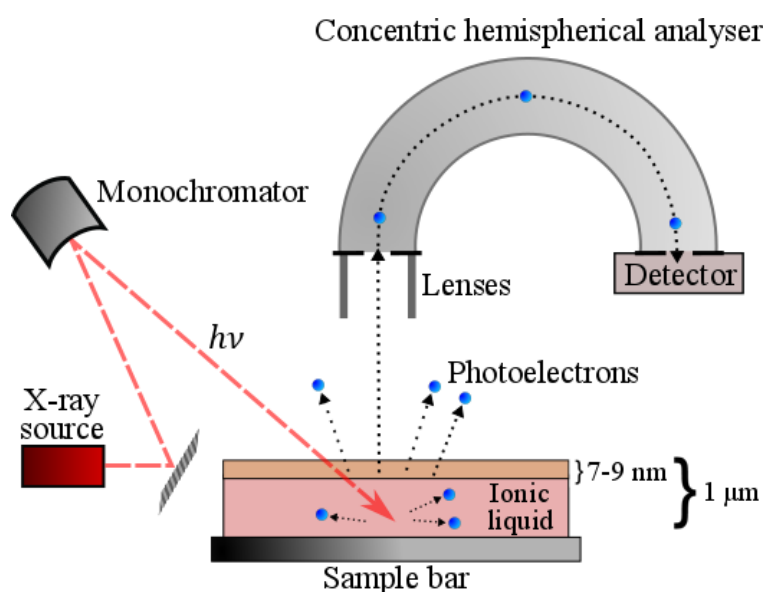


Figure 2.3 A simplified depiction of the XPS setup used for this work.

Photoelectrons emitted from the sample surface are collected, slowed down and focused by transfer lenses before entering the concentric hemispherical analyser (CHA). By varying the voltage between two concentric plates, the CHA is able to scan the energy range of the emitted photoelectrons one at a time. Only photoelectrons of the correct pass energy, as selected at the analyser, may travel through the path of the CHA before reaching the detector. In this setup a multi-channel plate then multiplies the photoelectron signal and a delay line detector (DLD) counts the electron pulses.

2.1.1.5 The Vacuum Environment

To retain the kinetic energy of the emitted photoelectrons an ultra-high vacuum environment is used in order to minimise gas phase collisions. The sample analytical chamber used for this work maintains a steady UHV pressure between 10^{-8} and 10^{-9} mbar. The mean free path of an electron under UHV is $1-10^5$ Km, whereas at ambient pressure λ is below 70 nm. Samples are initially degassed in a sample transfer chamber ($\approx 10^{-7}$ mbar) for a minimum of 3 hours. Volatile impurities and adsorbed gasses are removed from the bulk sample and its surface under these conditions.¹³ Typically, turbomolecular and sputter ion sublimation pumps are used to maintain the UHV environment.

2.1.1.6 Charge Neutralisation

For electrically conducting samples, such as ionic liquids and metals, the positive vacancies that form as a result of photoionisation recombine with electrons flowing from the spectrometer. Non-conducting samples cannot be earthed in this way and as a result positive charge builds up at the surface during XPS measurements. Consequently, the Fermi levels of the sample and the spectrometer are unaligned and as a result the magnitude of the work function is unknown and no longer correctly compensated for. Sample charging will also lead to line broadening which can significantly diminish spectral resolution.¹⁴ Low kinetic energy electrons are flooded into non-

conducting samples to compensate for this build-up of positive charge. However this technique often results in overcompensation and photoemission peaks appear at higher binding energies as a result. Accurate binding energies may be achieved by charge correcting to known B.E. peaks, these are discussed further later in this section.

2.1.2 Data Analysis

2.1.2.1 XP Spectra

XPS can provide two types of spectra for data analysis, wide scans (or survey scans) and high resolution scans. Wide scans show elemental composition as the whole accessible energy range is scanned (≈ 1400 eV) for photoelectron emissions. High resolution scans focus on an energy region that contains a particular photoemission peak.

2.1.2.2 Wide Scans

XP wide scans are presented as counts per second (CPS) plotted against B.E. in reverse. The spectra show sharp peaks protruding from a rising background (from low to high B.E.). Core photoelectron peaks appear between 35 eV and 800 eV and are the dominant feature in an XP survey scan. **Figure 2.4** shows a wide scan taken for the ionic liquid $[\text{C}_8\text{C}_1\text{Im}][\text{NTf}_2]$, each photoemission is labelled with the corresponding element and originating orbital. Since the whole accessible energy range is scanned (≈ 1400 eV), the spectrum allows elemental identification and semi-quantitative analysis by comparing the relative areas of each signal. Hydrogen and helium do not appear on XP wide scans as they have low cross-sectional areas that do not allow for photoionisation.¹⁵ Relative sensitivity factors (RSF) must be employed for semi-quantitative analysis of atomic concentrations. The Kratos library was used for the determination of atomic percentages in this work (10-20% error).¹⁶

As more orbitals become accessible at progressively higher energies, steps often appear as the higher number of emitted photoelectrons undergo more gas phase collisions and hence contribute to the background in larger quantities. Wide scans are often recorded with a step of 0.5 eV and a pass energy of 80 eV at the analyser. This allows for greater signal intensity but at the cost of spectral resolution. In addition to core photoemissions, wide scans always contain Auger peaks at higher B.E. (800-1400 eV)¹⁷ and valence band signals at lower B.E. (0-35 eV).¹⁸

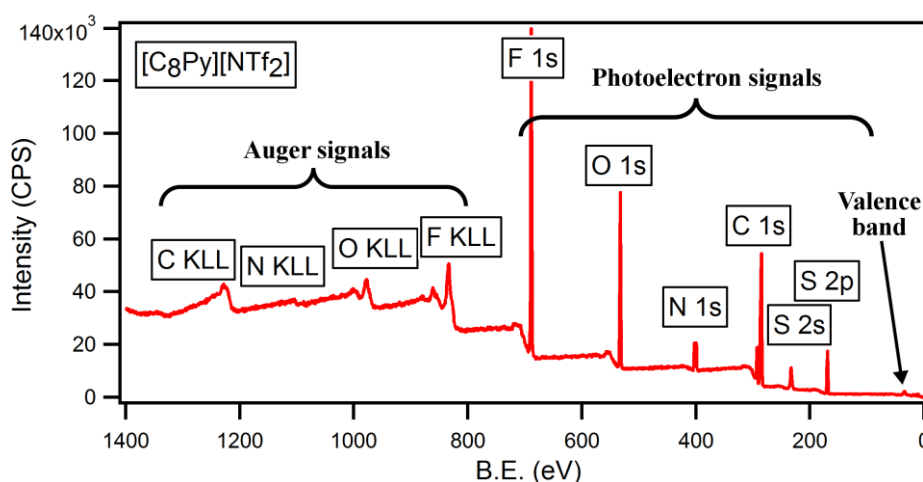


Figure 2.4 An example wide scan, showing the Auger signals, photoelectron signals and the valence band. The spectrum shown here is for the pyridinium [C₈Py][NTf₂] IL.

2.1.2.3 High Resolution Scans

By analysing a shorter range (10-40 eV) for a longer dwell time, coupled with a smaller energy step (0.1 eV) and lower pass energy (20 eV), the resolution of the spectrum can be significantly increased (albeit at a cost to the signal-to-noise ratio). Usually the most intense photoemission for each element is studied and therefore more valuable information, such as chemical states and electronic environments, can be discerned. The detection limit under these conditions is close to 0.01 atomic %, ^{19,20} any element present in lower concentrations will go undetected by XPS. **Figure 2.5** shows an N 1s high resolution scan for [C₈Py][NTf₂]. The individual chemical environments for the cationic and anionic nitrogen species are easily discerned.

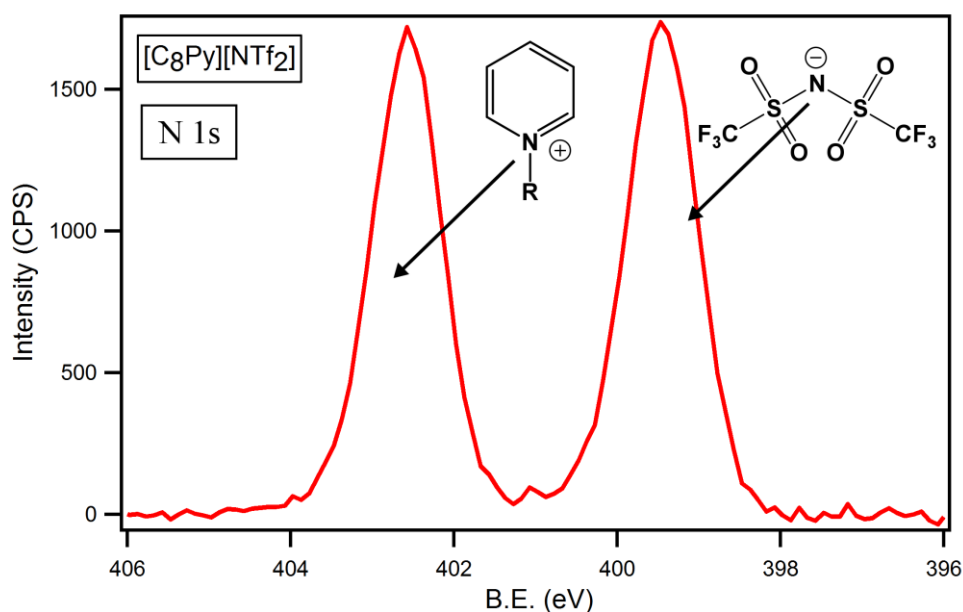


Figure 2.5 The N 1s high resolution scan of $[\text{C}_8\text{Py}][\text{NTf}_2]$, showing two peaks. The peak at higher B.E. originates from the nitrogen of the $[\text{C}_8\text{Py}]^+$ cation and the peak at lower B.E. originates from the nitrogen of the $[\text{NTf}_2]^-$ anion.

2.1.2.4 Chemical Shift

When a particular element is present in multiple chemical states, photoemission corresponding to each environment are observed, as seen in **Figure 2.4**. The local electronic environment of an element alters the B.E. of the core level electrons, due to increased or decreased electrostatic attraction to the nucleus.²¹ Therefore factors such as oxidation state (O.S.), chemical bond type and intra- or inter-molecular interactions will cause changes in the observed B.E.s, due to the varying amounts of electron density.²² This is referred to as chemical shift in XP spectroscopy. When a larger amount of electron density is present about the element in question, the electrostatic shielding from the nuclear charge is greater and hence the core level electron experiences a lower effective electrostatic interaction to the nucleus. The result is a shift towards a lower B.E., for example the N 1s signal from the $[\text{NTf}_2]^-$ anion in **Figure 2.5** has a significantly lower B.E. photoemission when compared to the positive nitrogen of the cation. The reverse process situation occurs for decreased amounts of electron density, see **Figure 2.6**.

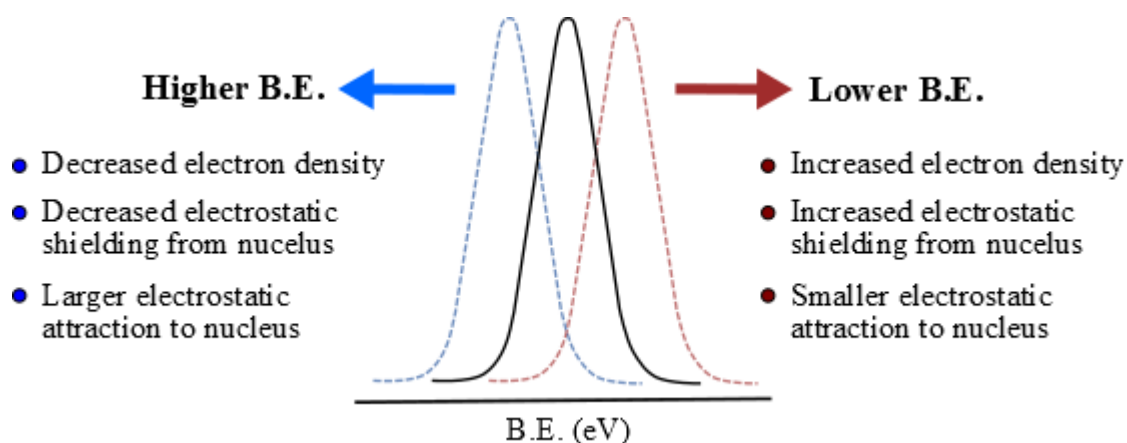


Figure 2.6 The peak shifting that occurs for varying degrees of electron density. The change in B.E. due to the local electronic environment is referred to as chemical shift.

XPS is therefore capable of identifying and quantifying the various chemical states of elements in a particular sample. By comparing the observed B.E.s to XPS data bases, it is possible to determine chemical bond types and O.S.s for samples.

2.1.2.5 Peak Fittings

When an element is present in multiple similar chemical states, photoemission peaks may appear complex and unresolved. For this reason, peak fitting models are often employed in attempts to interpret the ‘fingerprint’ structures of convoluted photoemission signals. The peak fitting of XP spectra has become a popular post-acquisition analysis procedure used by chemists from a wide range of disciplinary backgrounds. The Foreword of Peak Fitting with CasaXPS²¹ by John Walton *et al.* contains perhaps the best piece of advice for the beginner analyst:

“It must be emphasised that there is no ‘absolute’ or ‘scientifically correct’ method, methodology, or algorithm for peak fitting which will inevitably produce the ‘right’ answer, and that the possibilities for mistakes, misunderstanding and interpretation are legion.”

By constraining peak full width at half maximums (FWHMs) and areas, crude models can often be produced that are able to reproduce the observed photoemission spectra. Robust models are able to peak fit multiple photoemissions from similar samples, however the obtained B.E.s still represent components of a model and not real photoemission peaks.

2.1.2.5.1 IL C 1s Peak Fitting

The C 1s photoemissions of IL XP spectra are ideal examples of complex photoemissions that are regularly deconvoluted by peak fitting procedures. Since this thesis will deal with imidazolium and pyridinium ILs, the two current C 1s peak fitting models for these two salts are presented.

Pyridinium C 1s Peak Fitting:

The C 1s high resolution scan for the [C₈Py][NTf₂] IL is presented in **Figure 2.7**. The main photoemission signal is clearly composed of a complex arrangement of unresolved peaks, each representing the various chemical environment of the carbon atoms present within the IL. The shake up signal is visible on the high resolution scan, although it is coincident with the -CF₃ photoemission from the [NTf₂]⁻ anion. The current pyridinium peak fitting model^{12,23} has been applied to the C 1s scan and the individual signals are colour coded to the structure shown on the plot.

The C^{2,6,7} (blue) component represents the carbon atoms bound to the nitrogen heteroatom. The C^{3,4,5} (orange) component represents the carbon atoms from the back of the pyridinium ring and the C^{ali} (black) component represents the carbons of the long aliphatic tail. The C^{2,6,7} component (287.1 eV) appears at a higher B.E. due to the charge withdrawal from the electropositive cationic nitrogen atom. The C^{3,4,5} component (286.0 eV) appears at a slightly lower B.E. as there is no neighbouring electropositive heteroatom. The C^{ali} component (285.0 eV) appears at the lowest B.E. due to the electron rich environment of the long aliphatic tail. The C^{ali} component has been used to charge correct the spectrum, this will be explained in the following section.

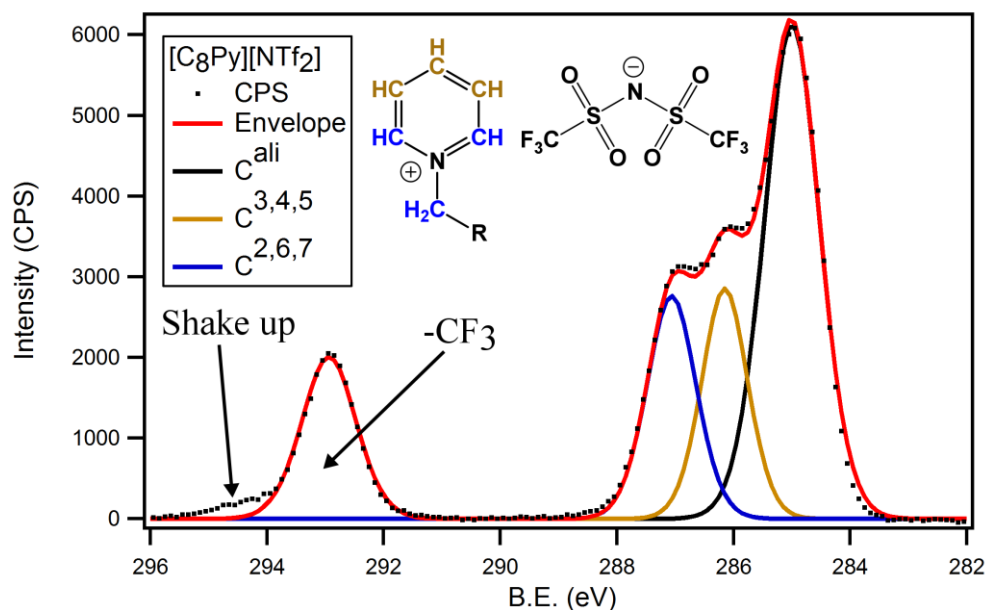


Figure 2.7 The current C 1s peak fitting model for pyridinium ILs. The spectrum shows the $[C_8Py][NTf_2]$ C 1s photoemissions (black dots) with the individual carbon components and their resulting sum, the envelope (red). The shake up and $-CF_3$ signals are also labelled.

The FWHMs of the components have been constrained to 0.8-1.2 eV for $C^{2,6,7}$ and $C^{3,4,5}$ and 0.8-1.5 eV for C^{ali} . The larger FWHM window for C^{ali} is due to the overlapping of multiple C 1s photoemissions. Peak areas are also constrained to the relative proportions of the carbon environments. For example, $[C_8Py][NTf_2]$ has the following components $C^{2,6,7}:C^{3,4,5}:C^{ali}$ in the following ratio 3:3:7. Measurements of the shake up signals from the C 1s regions of pyridinium ILs have found that sp^2 pyridinium carbon atoms appear to lose an average of 10% of their signal.²³ Therefore, after accounting for shake up/off losses, the ratio of the areas now becomes 2.8:2.7:7. This model has been found to accurately represent a range of pyridinium IL XP spectra.

Imidazolium C 1s Peak Fitting:

Figure 2.8 shows the current C 1s peak fitting model^{9,14,18,24,25} as applied to the [C₈C₁Im][NTf₂] C1s high resolution scan. Each component is colour coded to the attached structure, C² (green), C^{4,5} (blue), C^{6,7} (orange) and C^{ali} (black). The CF₃ peak and the shake up signal are also labelled on the plot. The C² carbon is flanked by two neighbouring electronegative nitrogen atoms, meaning that the photoemission signal should appear at higher B.E. (287.7 eV). The C^{4,5} and C^{6,7} carbon components appear at lower B.E.s as they are only bonded to one nitrogen atom. In this model, the C^{4,5} component (287.1 eV) appears at a higher B.E. than the C^{6,7} component (286.6 eV), this assignment has been made through chemical intuition. The C^{ali} component (285.0 eV) represents the electron rich aliphatic tail and has been used to charge correct the spectrum, as with the [C₈Py][NTf₂] salt.

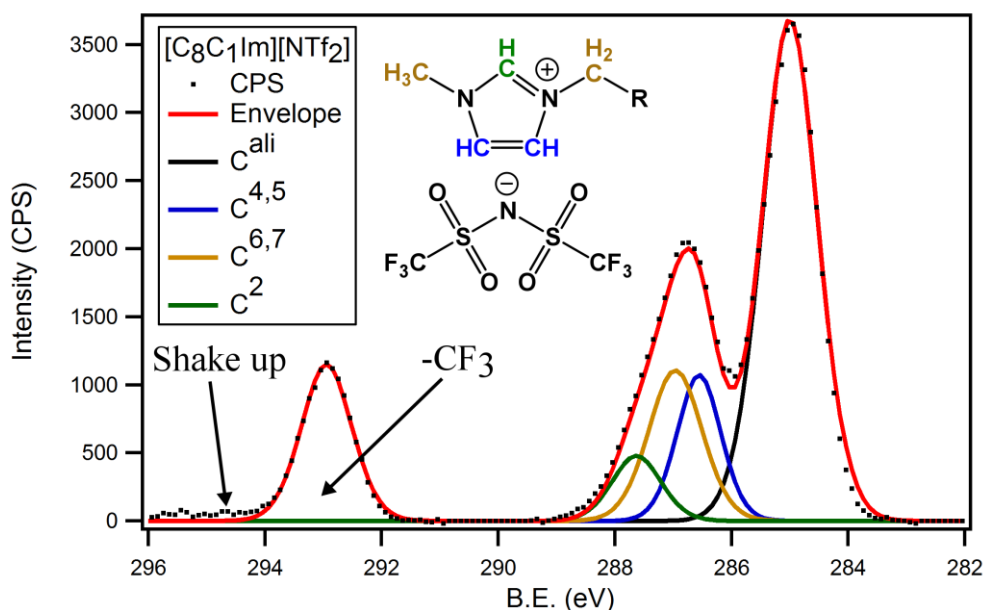


Figure 2.8 The current C 1s peak fitting model for imidazolium ILs. The spectrum shows the [C₈C₁Im][NTf₂] C 1s photoemissions (black dots) with the individual carbon components and their resulting sum, the envelope (red). The shake up and –CF₃ signals are also labelled.

Previous shake up measurements have calculated 20% signals loss for each sp^2 carbon atom of imidazolium ILs.¹¹ Therefore the $C^2:C^{4,5}:C^{6,7}:C^{ali}$ components have the ratio 0.8:1.6:1.8:7, after accounting for shake up/off losses.

The majority of the XP spectra that have been acquired and analysed in this *Thesis* are for $[NTf_2]^-$ salts. The low basicity of the $[NTf_2]^-$ anion results in C 1s spectra that are spread across a wide B.E. range. This makes the interpretation of the C 1s photoemissions easier than with high basicity anion (e.g. Halides or acetates). The presence of the $-CF_3$ C 1s signal also aids the charge correction and normalisation of the main C 1s photoemissions.

2.1.2.6 Charge Correcting IL XP Spectra

As previously mentioned, when photoelectrons are emitted from a sample surface, positive holes that are left behind cause differential charging in non-conductors. For conductors such as metal and liquid IL samples, electrons flow from the spectrometer and combine with the positive holes. Despite this, XP spectra still require calibration to a known B.E. signal in order to produce reliable data that may be used to compare signals across multiple data sets. Internal charge referencing has been established as the most convenient and reliable method for calibration of IL spectra. The aliphatic carbon signal (C^{ali}) for ILs with alkyl chains of C_8 or higher has been used extensively for charge correction in this way.^{9,23,26-29} The signal may be referenced to 285.0 eV (the value for aliphatic carbon) and the associated spectra may be corrected accordingly. Spectra that are referenced in this way appear to provide consistent B.E.s the fluorine environments if different anions. Therefore charge correction to the F 1s signals of $[BF_4]^-$, $[PF_6]^-$ and $[NTf_2]^-$ anions is also a viable method of spectral calibration.

2.2 Experimental

2.2.1 Data Analysis of XP Spectra

For this work, all heteroatom XP spectra (N 1s, O 1s, F 1s, B 1s, P 2p, S 2p, Cl 2p...) were fitted with a two point linear background. The C 1s spectra were fitted with a spline linear background to allow incorporation of the $-\text{CF}_3$ photoemissions from the $[\text{NTf}_2]^-$ anions and measurement of the shake up signal. Peak fittings were done using either GL(30) curves (70% Gaussian characteristics with 30% Lorentzian characteristics) or Gaussian curves. All GL(30) fittings were performed using CasaXPS software and Gaussian fittings were custom made in Igor Pro (See *Appendix* for details). Relative sensitivity factors (RSF) used in the determination of atomic percentages were taken from the Kratos library.¹⁶ The RSF values and the measurement error of 0.1 eV (spectrometer specific) are determined by Kratos Analytical Ltd. All peak C 1s peaks are constrained to 0.8-1.2 eV, with the exception of large C^{ali} components ($> \text{C}_8$) which are constrained to 0.8-1.5 eV. When position constraints are used, the B.E.s are constrained to the error or the known B.E. value, i.e. ± 0.1 eV.

2.2.2 Instrumentation

2.2.2.1 XPS

All XP spectra were recorded using a Krato Axis Ultra Spectrometer equip with a monochromated Al $\text{K}\alpha$ source (1486.6 eV), hybrid (magnetic/electrostatic) optics, concentric hemispherical analyser (CHA) and a multi-channel plate and delay line detector (DLD). The incident angle of the X-rays is 30° and the collection angle is 0° , relative to the surface normal. An entrance aperture of $300 \times 700 \mu\text{m}^2$ with pass energies of either 80 eV (wide scans) or 20 eV (high resolution scans) were used. For a clean Ag surface, the Ag $3d_{5/2}$ photoemission had an intensity of 7.5×10^5 CPS and an FWHM of 0.55 eV, with a pass energy of 20 eV at the analyser and a 450 W emission power. B.E.s were calibrated to the Au $4f_{7/2}$ (83.96 eV), Ag $3d_{5/2}$ (368.21 eV)

and Cu $2p_{3/2}$ (932.62 eV) photoemissions. The experimental error is determined by the manufacturer and quoted as ± 0.1 eV.

For ILs that are solid at room temperature, charge neutralisation was applied. A standard Bayonet Neill Concelman (BNC) connector was used to earth sample bars through the instrument stage. A filament that is coaxial with the electrostatic and magnetic transfer lenses was used for charge neutralisation, as well as a balance plate to create a potential gradient between the neutraliser and the sample. A filament current of 1.9 A and a balance voltage of 3.3 V were used for neutralisation of solid samples. This neutralisation method was not used for liquid samples as they are electrically conducting and therefore do not experience differential charging.

For XPS analysis, IL samples were placed onto a stainless steel sample bar of Kratos design. Liquid samples were placed as a single drop (≈ 20 mg) that was spread thinly to avoid variable sample heights. Solid samples were held down with double sided sticky tape to avoid contamination of the XPS chamber. Samples were introduced to a sample transfer chamber which was initially degassed to high vacuum ($\approx 10^{-7}$ mbar) over night. Samples were then transferred to the sample analytical chamber which maintained pressures $\leq 1 \times 10^{-8}$ mbar at all times.

2.2.2.2 NMR Analysis

The majority of NMR experiments were recorded using a Bruker DPX-300 spectrometer with operating frequencies of 300 (^1H), 75 (^{13}C), 282 (^{19}F) and 121 (^{31}P) MHz. The 4,4'-bipyridinium bromide salts were analysed using a JEOL EX270 NMR spectrometer with operating frequencies of 270 (^1H) and 68 (^{13}C) MHz. Chemical shifts (δ) are reported in parts per million (ppm) and spectra are referenced to the residual solvent peaks of commercial deuterated solvents. For this work DMSO- d_6 (δ_{H} 2.50 and δ_{C} 39.51 ppm), MeOD- d_4 (δ_{H} 3.31/4.87 and δ_{C} 49.1 ppm), CDCl $_3$ (δ_{H} 7.27 and δ_{C} 77.0 ppm) and D $_2$ O (δ_{H} 4.75 ppm) were used at room temperature. Coupling constants (J) are presented in Hz.

2.2.2.3 Mass Spectrometry

Electrospray ionisation mass spectrometry (ESI-MS) was recorded on a Bruker microTOF mass spectrometer with both positive and negative ionisation sources. Solutions were made using analytical grade solvents, acetonitrile or methanol were used for this work.

2.2.2.4 Ion Chromatograph

Anion chromatography was recorded using a DIONEX ICS-3000 chromatograph fitted with a Dionex AS20 (2 x 250 mm) analytical column and a Dionex CG20 (2 x 50 mm) guard column. An isocratic eluent consisting of water (60%), acetonitrile (25%) and an aqueous 100 mM NaOH solution (15%) was used. The columns were kept at 40 °C during analysis and the flow rate was set to 0.25 mL/min. Samples were prepared by dissolving \approx 5 mg of ionic liquid in 10 mL of ultrapure water or an acetonitrile:water mixture (< 25% HPLC grade acetonitrile).

2.2.3 Synthesis

2.2.3.1 General Comments

ILs are usually synthesised *via* alkylation of an amine or phosphine nucleophile with an alkylhalide to form a quaternised cationic species.³⁰ The halide counterions may then be exchanged for other polyatomic anions by salt metathesis in water or an organic solvent, **Figure 2.9**. This process usually exploits the precipitation of the IL (or an inorganic salt from an organic solvent) as the thermodynamic driving force, in order to obtain the pure IL products.

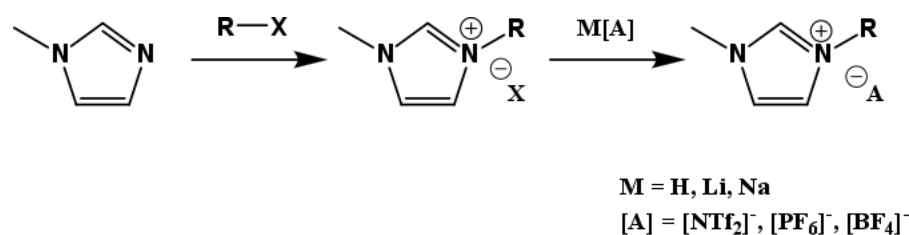


Figure 2.9 An example preparation of a typical IL. Alkylation with a haloalkane, followed by salt metathesis is shown for methyl imidazole to form imidazolium ILs. The same procedure is often used for most other IL salts.

The major source of IL impurities in this work are residual halides that remain from incomplete anion metathesis. For this reason, ion chromatography (IC) is employed in order to monitor the residual halide content. The ILs presented in this work have all been found to contain <10 ppm residual halide content (the detection limit for IC). Where IC is not a viable option, the silver nitrate test has been used to detect trace quantities of residual halides. A concentrated aqueous solution of AgNO₃ is mixed with a solution of the IL (or IL washings) in either water or water/acetone (2:1, V:V). Any precipitated AgX indicates the presence of halides in solution, hence the ILs require further washing. XPS analysis is also informative in terms of elemental composition. The absence of residual halide photoemissions indicates that the impurities do not exceed 0.1 at.%, which is the detection limit for XPS scans.

The 1-alkyl-3-methyl-4-chloroimidazolium salts ([C₄C₁-4-ClIm]Cl, [C₈C₁-4-ClIm]Cl, [C₄C₁-4-ClIm][NTf₂]⁻ and [C₄C₁-4-ClIm][NTf₂]⁻) presented in this *Thesis* were synthesised by Rebecca R. Hawker and Jason B. Harper of the University of New South Wales. The 4,4'-bipyridinium mono- and dicationic bromide salts ([C₂Bipy]Br, [C₄Bipy]Br, [C₆Bipy]Br, [C₈Bipy]Br, [(C₂)₂Bipy]Br, [(C₄)₂Bipy]Br, [(C₆)₂Bipy]Br and [(C₈)₂Bipy]Br) were synthesised by Alex Dear at the University of Nottingham.

2.2.3.2 Materials

All reagents were purchased from a range of commercial suppliers and used as received. Lithium bis(trifluoromethanesulfonyl)imide was purchased from 3M

and also used as received. All solvents were analytical reagent grade. All water used in this work was Millipore Milli-Q 18 M Ω ultrapure deionised water.

2.2.3.3 Synthetic Procedures

2.2.3.3.1 Chlorinated ILs:

1-Butyl-3-methyl-4-chloroimidazolium chloride, [C₄C₁-4-ClIm]Cl

5-Chloro-1-methylimidazole (15.2 g, 130.0 mmol) and 1-chlorobutane (35.2 g, 380.0 mmol, 2.9 eq.) were combined and heated to 80 °C for 9 days. After cooling, the solidified product was suspended in ethyl acetate (200 mL) and left to stir for 2 hr. The product was isolated by filtration and the process was repeated two more times. The isolated white solid (17.46 g, 64.0%) was dried under reduced pressure. m.p. 114-116°C. ¹H NMR (400 MHz, d₃-acetonitrile) δ 0.94 (t, J = 7.4 Hz, 3H, CH₂CH₃), 1.32 (m, 2H, CH₃CH₂), 1.83 (m, 2H, NCH₂CH₂), 3.83 (s, 3H, NCH₃), 4.22 (t, J = 7.2 Hz, 2H, NCH₂CH₂), 7.70 (d, J = 1.9 Hz, 1H, NCCICHN), 10.08 (d, J = 1.5 Hz, 1H, NCHN). ¹³C NMR (100 MHz, d₃-acetonitrile) δ 13.64 (CH₂CH₃), 19.83 (CH₂CH₃), 32.34 (NCH₂CH₂), 34.49 (NCH₃), 50.93 (NCH₂CH₂), 120.24 (NCCICHN), 123.17 (NCCICHN), 138.39 (NCHN). IR (solid): ν_{max} 2930, 1557, 1346, 1154, 894, 836 cm⁻¹. Found HR-MS (ESI) m/z: 173.0837 (100), 175.0807 (32), ([C₄C₁-4-ClIm]⁺, C₈H₁₄^{35/37}ClN₂ requires m/z: 173.0840 (100), 175.0811 (32)). Anal. Calcd for C₈H₁₄Cl₂N₂: C, 43.45; H, 6.99; N 12.67. Found: C, 43.27; H, 7.18; N, 12.60.

1-Octyl-3-methyl-4-chloroimidazolium iodide, [C₈C₁-4-ClIm]I

5-Chloro-1-methylimidazole (1.00 mL, 10.9 mmol) and 1-iodooctane (2.4 mL, 13.0 mmol) were stirred at room temperature for 3 days. Due to a slow reaction rate, the temperature was increased to 40°C and the reaction mixture was stirred under reflux for a further 2 days. The reaction mixture was cooled to room temperature, during which time it solidified. This isolated solid was

suspended in diethyl ether (40 mL). After stirring this mixture for 2 hours, the diethyl ether was decanted and the process repeated five times on the residual solid. The remaining yellow solid was dried under reduced pressure to give 1-octyl-4-chloro-3-methylimidazolium iodide (2.50 g, 7.00 mmol, 65%). m.p. 82.3-84.2°C. ^1H NMR (300 MHz, *d*-chloroform) δ 0.87 (m, 3H, CH_2CH_3), 1.29 (m, 10H, $\text{CH}_3(\text{CH}_2)_5$), 1.95 (m, 2H, NCH_2CH_2), 4.03 (s, 3H, NCH_3), 4.37 (t, $J = 7.5$ Hz, 2H, $\text{NCH}_2\text{CH}_2(\text{CH}_2)_5\text{CH}_3$), 7.48 (s, 1H, NCCICHN), 10.45 (s, 1H, NCHN). ^{13}C NMR (75 MHz, *d*-chloroform) δ 14.05 (CH_2CH_3), 22.57 ($\text{N}(\text{CH}_2)_6\text{CH}_2\text{CH}_3$), 26.21 ($\text{N}(\text{CH}_2)_5\text{CH}_2\text{CH}_2\text{CH}_3$), 28.92 ($\text{N}(\text{CH}_2)_4\text{CH}_2(\text{CH}_2)_2\text{CH}_3$), 29.00 ($\text{N}(\text{CH}_2)_3\text{CH}_2(\text{CH}_2)_3\text{CH}_3$), 29.98 ($\text{N}(\text{CH}_2)_2\text{CH}_2(\text{CH}_2)_4\text{CH}_3$), 31.66 ($\text{NCH}_2\text{CH}_2(\text{CH}_2)_5\text{CH}_3$), 34.62 (NCH_3), 51.25 ($\text{NCH}_2(\text{CH}_2)_6\text{CH}_3$), 118.68 (NCCICHN), 122.81 (NCCICHN), 137.37 (NCHN). ν_{max} 2997, 2916, 2850, 1564, 1460, 1356, 1248, 1160, 860, 810, 723, 667 cm^{-1} . Found HR-MS (ESI) m/z : 229.1465 (100), 231.1431 (32), ($[\text{C}_8\text{C}_1\text{-4-ClIm}]^+$, $\text{C}_{12}\text{H}_{22}^{35/37}\text{ClN}_2$ requires m/z : 229.1466 (100), 231.1437 (32)); 585.1981 (100), 587.1950 (62), 589.1919 (6), ($[\text{C}_8\text{C}_1\text{-4-ClIm}]_2\text{I}$, $\text{C}_{24}\text{H}_{44}^{35/37}\text{Cl}_2\text{N}_4\text{I}$ requires m/z : 585.1982 (100), 587.1953 (62), 589.1923 (6)).

1-Butyl-3-methyl-4-chloroimidazolium

bis(trifluoromethanesulfonyl)imide, $[\text{C}_4\text{C}_1\text{-4-ClIm}][\text{NTf}_2]$

$[\text{C}_4\text{C}_1\text{-4-ClIm}]\text{Cl}$ (16.4 g, 78.4 mmol) was dissolved in water (20 mL) and a solution of $\text{Li}[\text{NTf}_2]$ (24.8 g, 109.0 mmol) in water (35 mL) was added to form an instantaneous precipitate. The mixture was left to stir at room temperature overnight, after which point the water was removed and the lower ionic liquid layer was washed with water (5 x 30 mL) until the washings tested negative to the silver nitrate test. The resulting viscous liquid solidified to a white solid (25.8 g, 60.0%). m.p. 41-44 °C. ^1H NMR (DMSO- d_6 , 300MHz): $\delta = 9.24$ (d, $J=1.7$ Hz, 1 H), 8.09 (d, $J=1.7$ Hz, 1 H), 4.15 (t, $J=7.1$ Hz, 2 H), 3.77 (s, 3 H), 1.65 - 1.84 (m, 2 H), 1.12 - 1.41 (m, 2 H), 0.90 ppm (t, $J=7.4$ Hz, 3 H). ^{13}C NMR (DMSO- d_6 , 75MHz): $\delta = 136.9$, 121.4, 119.5 (q, $J_{\text{CF}} = 322$ Hz, 2C, CF_3), 119.4, 49.4, 33.7, 31.0, 18.6, 13.2 ppm. ^{19}F NMR (DMSO- d_6 , 282 MHz) $\delta = -78.72$ (s, 6 F, CF_3) ppm. ESI-MS: m/z 173.08 [M^+]. Anal. Calcd for

C₁₀H₁₄ClN₃F₆O₄S₂: C, 26.47; H, 3.11; N 9.32. Found: C, 26.72; H, 2.93; N, 9.32.

1-Octyl-3-methyl-4-chloroimidazolium

bis(trifluoromethanesulfonyl)imide, [C₈C₁-3-ClIm][NTf₂]

[C₈C₁-4-ClIm]I (2.11 g, 59.1 mmol) was dissolved in water (20 mL) and a solution of Li[NTf₂] (2.50 g, 87.0 mmol) in water (20 mL) was added to form an instantaneous precipitate. The mixture was left to stir at room temperature for 24 hr, after which point the water was removed and DCM (50 mL) was added. The solution was washed with water (10 x 50 mL) until the washings tested negative to the silver nitrate test. The organic solvent was removed and the viscous yellow liquid (2.00 g, 66.0%) was dried under reduced pressure. ¹H NMR (DMSO-d₆, 300MHz): δ = 9.24 (d, *J*=1.8 Hz, 1 H), 8.08 (d, *J*=1.8 Hz, 1 H), 4.14 (t, *J*=7.2 Hz, 2 H), 3.78 (s, 3 H), 1.59 - 1.95 (m, 2 H), 1.08 - 1.44 (m, 10 H), 0.86 ppm (t, *J*=6.7 Hz, 3 H). ¹³C NMR (DMSO-d₆, 75MHz): δ = 136.8, 121.4, 119.5 (q, *J*_{CF} = 322 Hz, 2C, CF₃), 119.4, 49.7, 33.7, 31.2, 29.0, 28.4, 28.3, 25.4, 22.0, 13.9 ppm. ¹⁹F NMR (DMSO-d₆, 282 MHz) δ = -78.78 (s, 6 F, CF₃) ppm. ESI-MS: m/z 229.14 [M⁺].

1-Butyl-2-pyridone, C₄-2-OPy

2-Hydroxypyridine (2.00 g, 21.0 mmol), potassium carbonate (5.81 g, 42.1 mmol, 2.0 eq.), tetrabutylammonium bromide (0.68 g, 2.10 mmol, 0.1 eq.) and 1-bromobutane (4.32 g, 3.40 mL, 31.6 mmol, 1.5 eq.) were combined with toluene (200 mL) and 1-2 mL of water was added. The mixture was heated to 50 °C and left to stir for 1 hr. The temperature was raised to 130 °C and mixture was left to reflux for 2 hr. After cooling, the insoluble material was removed by filtration and the solvent was evaporated to give a crude oil. The crude product was then purified by column chromatography (hexane:Ethyl acetate, 30:70) to give a yellow oil (2.06 g, 64.8%). ¹H NMR (CHLOROFORM-d, 400MHz): δ = 7.15 - 7.35 (m, 2 H), 6.52 (d, *J*=9.0 Hz, 1 H), 6.05 - 6.17 (m, 1 H), 3.89 (t, *J*=7.1 Hz, 2 H), 1.58 - 1.77 (m, 2 H), 1.26 -

1.45 (m, 2 H), 0.92 ppm (t, $J=7.3$ Hz, 3 H). ^{13}C NMR (CHLOROFORM-d, 101MHz): $\delta = 162.5, 139.0, 137.4, 120.9, 105.7, 49.5, 31.2, 19.7, 13.6$ ppm.

This data is consistent with other literature reports.³¹

1-Octyl-2-pyridone, C₈-2-OPy

The same procedure used to prepare C₄-2-OPy was used to prepare C₈-2-OPy from 2-hydroxypyridine (4.85 g, 50.0 mmol), potassium carbonate (13.8 g, 100.0 mmol, 2.0 eq.), tetrabutylammonium bromide (1.63 g, 5.00 mmol, 0.1 eq.) and 1-bromooctane (14.5 g, 13.0 mL, 75.0 mmol, 1.5 eq.) to give a crude product was purified by column chromatography (hexane:ethyl acetate, 30:70) to give a yellow oil (7.69 g, 74.2%). ^1H NMR (CHLOROFORM-d, 300MHz): $\delta = 7.19 - 7.33$ (m, 2 H), 6.53 (d, $J=9.1$ Hz, 1 H), 6.12 (td, $J=6.7, 1.4$ Hz, 1 H), 3.89 (t, $J=7.5$ Hz, 2 H), 1.63 - 1.81 (m, 2 H), 1.13 - 1.41 (m, 10 H), 0.85 ppm (t, $J=6.7$ Hz, 3 H). ^{13}C NMR (CHLOROFORM-d, 75MHz): $\delta = 162.5, 139.1, 137.4, 121.0, 105.7, 49.8, 31.6, 29.2, 29.1, 29.0, 26.5, 22.5, 14.0$ ppm.

1-Butyl-2-chloropyridinium bis(trifluoromethanesulfonyl)imide, [C₄-2-ClPy][NTf₂]

C₄-2-OPy (2.00 g, 13.2 mmol) was introduced to a dried schlenk flask under an inert atmosphere and phosphorus oxychloride (17.2 g, 10.5 mL, 112.4 mmol, 8.5 eq.) was slowly added. The mixture was heated to 110 °C and left to stir for 2 hrs. After cooling, the phosphorus oxychloride was evaporated and the resulting viscous brown liquid was dried at 70 °C and $\approx 8 \times 10^{-2}$ mbar for 2 hr. Water (50 mL) was slowly added, ensuring the temperature remained below 40 °C. A solution of Li[NTf₂] (4.55 g, 15.8 mmol, 1.2 eq.) in water (10 mL) was added dropwise and the mixture was left to stir for 2 hr. A small portion of DCM was added and the mixture was stirred vigorously. The aqueous layer was removed and the organic layer was further washed with water (3 x 30 mL). The solvent was evaporated to give a brown liquid (4.14 g, 69.5%) that was dried at 70 °C and $\approx 8 \times 10^{-2}$ mbar for 24 hr. ^1H NMR (DMSO-d₆, 300MHz): $\delta = 9.20$ (dd, $J=6.2, 1.6$ Hz, 1 H), 8.60 (td, $J=8.1, 1.6$ Hz, 1 H), 8.38 (dd, $J=8.1, 1.3$

Hz, 1 H), 8.13 (ddd, $J=7.6, 6.2, 1.3$ Hz, 1 H), 4.70 (t, $J=7.7$ Hz, 2 H), 1.78 - 1.99 (m, 2 H), 1.29 - 1.54 (m, 2 H), 0.94 ppm (t, $J=7.3$ Hz, 3 H). ^{13}C NMR (DMSO- d_6 , 75MHz): $\delta = 147.6, 147.2, 146.1, 130.3, 126.6, 119.5$ (q, $J_{CF} = 322$ Hz, 2C, CF_3), 59.6, 30.8, 18.8, 13.3 ppm. ^{19}F NMR (DMSO- d_6 , 282 MHz) $\delta = -78.73$ (s, 6 F, CF_3) ppm.

**1-Octyl-2-chloropyridinium bis(trifluoromethanesulfonyl)imide,
[C₈-2-ClPy][NTf₂]**

The same procedure used to prepare [C₄-3-ClPy][NTf₂] was used to prepare [C₈-2-ClPy][NTf₂] from C₈-2-OPy (2.00 g, 9.65 mmol), phosphorus oxychloride (12.6 g, 82.1 mmol, 8.5 eq.) and Li[NTf₂] (3.33 g, 11.6 mmol, 1.2 eq.) to give a brown liquid (3.47 g, 71.0%) that was dried at 70 °C and $\approx 8 \times 10^{-2}$ mbar for 24 hr. ^1H NMR (CHLOROFORM- d , 300MHz): $\delta = 8.95$ (dd, $J=6.2, 1.7$ Hz, 1 H), 8.49 (td, $J=8.1, 1.7$ Hz, 1 H), 8.09 (dd, $J=8.1, 1.3$ Hz, 1 H), 8.00 (ddd, $J=7.7, 6.2, 1.3$ Hz, 1 H), 4.74 (t, $J=7.8$ Hz, 2 H), 1.90 - 2.08 (m, 2 H), 1.19 - 1.51 (m, 10 H), 0.79 - 0.94 ppm (m, 3 H). ^{13}C NMR (CHLOROFORM- d , 75MHz): $\delta = 147.6, 147.3, 146.4, 130.5, 127.1, 119.7$ (q, $J_{CF} = 322$ Hz, 2C, CF_3), 61.1, 31.5, 29.8, 28.8, 28.7, 26.0, 22.5, 13.9 ppm. ^{19}F NMR (DMSO- d_6 , 282 MHz) $\delta = -78.91$ (s, 6 F, CF_3) ppm. Anal. Calcd for C₁₅H₂₁ClF₆N₂O₄S₂: C, 35.54; H, 4.18; N 5.53. Found: C, 35.63; H, 3.88; N, 5.44.

1-Butyl-3-chloropyridinium bromide, [C₄-3-ClPy]Br

3-Chloropyridine (10.0 g, 88.1 mmol) and 1-bromobutane (14.5 g, 11.35 mL, 105.7 mmol, 1.2 eq.) were combined under an inert atmosphere at room temperature. The mixture was heated to 90 °C and left to stir for 48 hr. After cooling, diethyl ether (100 mL) was added and the mixture was agitated until it solidified. The solid was isolated by filtration and recrystallised from methanol/diethyl ether to give a hygroscopic brown solid (16.9 g, 76.8%) that was dried at 70 °C and $\approx 8 \times 10^{-2}$ mbar for 24 hr. ^1H NMR (DMSO- d_6 , 300MHz): $\delta = 9.59 - 9.67$ (m, 1 H), 9.25 (d, $J=6.1$ Hz, 1 H), 8.77 - 8.84 (m, 1 H), 8.22 (dd, $J=8.4, 6.1$ Hz, 1 H), 4.68 (t, $J=7.5$ Hz, 2 H), 1.83 - 2.00 (m, 2 H),

1.20 - 1.39 (m, 2 H), 0.89 ppm (t, $J=7.4$ Hz, 3 H). ^{13}C NMR (DMSO- d_6 , 75MHz): $\delta = 145.1, 144.1, 143.7, 133.9, 128.7, 60.7, 32.5, 18.7, 13.3$ ppm. ESI-MS: m/z 170.07 [M^+].

1-Octyl-3-chloropyridinium bromide, [$\text{C}_8\text{-3-ClPy}$]Br

3-Chloropyridine (10.0 g, 88.1 mmol) and 1-bromooctane (20.4 g, 18.3 mL, 1.2 eq.) were combined under an inert atmosphere at room temperature. The mixture was heated to 80 °C and left to stir for 48 hr. After cooling, ethyl acetate (100 mL) was added and the viscous liquid was agitated until it solidified. The solid was collected and recrystallised from methanol/diethyl ether to give a hygroscopic brown solid (22.9 g, 84.8%) that was dried at 70 °C and $\approx 8 \times 10^{-2}$ mbar for 24 hr. ^1H NMR (DMSO- d_6 , 300MHz): $\delta = 9.61$ (s, 1 H), 9.23 (d, $J=6.1$ Hz, 1 H), 8.74 - 8.86 (m, 1 H), 8.22 (dd, $J=8.5, 6.1$ Hz, 1 H), 4.66 (t, $J=7.5$ Hz, 2 H), 1.80 - 2.02 (m, 2 H), 1.15 - 1.43 (m, 10 H), 0.84 ppm (t, $J=7.1$ Hz, 3 H). ^{13}C NMR (DMSO- d_6 , 75MHz): $\delta = 145.6, 144.7, 144.2, 134.4, 129.2, 61.5, 31.6, 31.1, 28.9, 28.8, 25.8, 22.5, 14.4$ ppm. ESI-MS: m/z 226.13 [M^+].

1-Octyl-3-chloropyridinium tetrafluoroborate, [$\text{C}_8\text{-3-ClPy}$][BF_4]

[$\text{C}_8\text{-3-ClPy}$]Br (5.00 g, 16.3 mmol) was dissolved in water (100 mL) and the solution was heated to 40 °C. A solution of sodium tetrafluoroborate (2.15g, 19.6 mmol, 1.2 eq.) in water (10 mL) was added dropwise and the mixture was left to stir for 2 hr. After cooling, a small portion of DCM was added and the mixture was left to stir overnight. The aqueous layer was separated and the organic layer was washed with water (5 x 30 mL). The organic solvent was removed to give a viscous brown liquid (4.21 g, 82.4%) that was dried at 70 °C and $\approx 8 \times 10^{-2}$ mbar for 24 hr. ^1H NMR (CHLOROFORM- d , 300MHz): $\delta = 8.76 - 8.89$ (m, 2 H), 8.39 - 8.51 (m, 1 H), 8.08 (dd, $J=8.4, 6.5$ Hz, 1 H), 4.66 (t, $J=7.5$ Hz, 2 H), 1.91 - 2.10 (m, 2 H), 1.16 - 1.42 (m, 10 H), 0.86 ppm (t, $J=6.7$ Hz, 3 H). ^{13}C NMR (CHLOROFORM- d , 75MHz): $\delta = 145.3, 143.4, 143.3, 136.1, 129.4, 63.0, 31.6, 31.5, 28.9, 28.9, 26.0, 22.5, 14.0$ ppm. ^{19}F

NMR (282 MHz, DMSO- d_6) δ ppm -151.2 (br. s, 4 F, BF₄), -151.3 ppm (q, J_{BF} = 1.51 Hz, 4 F, BF₄). ESI-MS: m/z 226.13 [M⁺].

1-Octyl-3-chloropyridinium hexafluorophosphate, [C₈-3-CIPy][PF₆]

The same procedure used to prepare [C₈-3-CIPy][BF₄] was used to prepare [C₈-3-CIPy][PF₆] from [C₈-3-CIPy]Br (5.00 g, 16.3 mmol) and H[PF₆] (60% w/w, 2.86 g, 2.75 mL, 19.6 mmol, 1.2 eq.) to give a viscous brown liquid (5.27 g, 87.0%) that solidified upon agitation. The solid was dried at 70 °C and $\approx 8 \times 10^{-2}$ mbar for 24 hr. ¹H NMR (CHLOROFORM- d , 300MHz): δ = 8.63 - 8.70 (m, 2 H), 8.39 - 8.45 (m, 1 H), 8.00 (dd, $J=8.3, 6.4$ Hz, 1 H), 4.56 (t, $J=7.5$ Hz, 2 H), 1.86 - 2.10 (m, 2 H), 1.13 - 1.49 (m, 10 H), 0.85 ppm (t, $J=6.9$ Hz, 3 H). ¹³C NMR (CHLOROFORM- d , 75MHz): δ = 145.4, 143.0, 136.2, 129.3, 63.1, 31.6, 31.3, 28.9, 28.8, 25.9, 22.5, 14.0 ppm. ¹⁹F NMR (282 MHz, DMSO- d_6) δ ppm -72.13 (d, $J_{PF} = 712.00$ Hz, 6 F, PF₆). ³¹P NMR (121 MHz, DMSO- d_6) δ ppm -144.56 (spt, $J_{FP} = 712.00$ Hz, 1 P, PF₆). ESI-MS: m/z 226.13 [M⁺].

1-Butyl-3-chloropyridinium bis(trifluoromethanesulfonyl)imide, [C₄-3-CIPy][NTf₂]

The same procedure used to prepare [C₈-3-CIPy][BF₄] was used to prepare [C₄-3-CIPy][NTf₂] from [C₄-3-CIPy]Br (5.00 g, 19.95 mmol) and Li[NTf₂] (6.90 g, 23.9 mmol, 1.2 eq.) to give a brown liquid (5.98 g 66.5%) that was dried at 70 °C and $\approx 8 \times 10^{-2}$ mbar for 24 hr. ¹H NMR (CHLOROFORM- d , 300MHz): δ = 8.71 - 8.80 (m, 2 H), 8.43 - 8.49 (m, 1 H), 8.00 (dd, $J=8.4, 6.1$ Hz, 1 H), 4.59 (t, $J=7.7$ Hz, 3 H), 1.89 - 2.08 (m, 2 H), 1.29 - 1.50 (m, 2 H), 0.94 ppm (t, $J=7.3$ Hz, 3 H). ¹³C NMR (CHLOROFORM- d , 75MHz): δ = 145.3, 143.0, 136.5, 129.2, 119.7 (q, $J_{CF} = 322$ Hz, 2C, CF₃), 63.0, 33.3, 30.9, 19.1, 13.2 ppm. ¹⁹F NMR (DMSO- d_6 , 282 MHz) δ = -78.92 (s, 6 F, CF₃) ppm. ESI-MS: m/z 170.07 [M⁺].

**1-Octyl-3-chloropyridinium bis(trifluoromethanesulfonyl)imide,
[C₈-3-ClPy][NTf₂]**

The same procedure used to prepare [C₈-3-ClPy][BF₄] was used to prepare [C₈-3-ClPy][NTf₂] from [C₈-3-ClPy]Br (5.00 g, 16.3 mmol) and Li[NTf₂] (5.62 g, 19.6 mmol, 1.2 eq.) to give a brown liquid (7.04 g 85.2%) that was dried at 70 °C and $\approx 8 \times 10^{-2}$ mbar for 24 hr. ¹H NMR (CHLOROFORM-d, 300MHz): δ = 8.78 - 8.86 (m, 2 H), 8.44 (ddd, $J=8.4, 1.9, 1.2$ Hz, 1 H), 8.06 (dd, $J=8.4, 6.0$ Hz, 1 H), 4.63 (t, $J=7.8$ Hz, 2 H), 1.91 - 2.10 (m, 2 H), 1.15 - 1.47 (m, 10 H), 0.87 ppm (t, $J=6.8$ Hz, 3 H). ¹³C NMR (CHLOROFORM-d, 75MHz): δ = 145.3, 143.2, 143.1, 136.5, 129.2, 119.7 (q, $J_{CF} = 322$ Hz, 2C, CF₃), 63.1, 31.5, 31.4, 28.8, 28.7, 25.8, 22.5, 13.9 ppm. ¹⁹F NMR (DMSO-d₆, 282 MHz) δ = -78.95 (s, 6 F, CF₃) ppm. ESI-MS: m/z 226.13 [M⁺].

2.2.3.3.2 4,4'-Bipyridinium ILs:

1-Ethyl-4,4'-bipyridinium bromide, [C₂Bipy]Br

4,4'-Bipyridine (6.00 g, 38.0 mmol) was dissolved in toluene (60 mL) and 1-bromoethane (43.8 g, 30.0 mL, 400 mmol, 10.5 eq.) was added dropwise, under an inert atmosphere. The mixture was heated to 90 °C and left to stir for 18 hr. The resulting solid precipitate was removed by filtration and recrystallised from hot acetonitrile to give a yellow solid (4.87 g, 48.0%) that was dried at 50 °C and $\approx 8 \times 10^{-2}$ mbar for 24 hr. ¹H NMR (METHANOL-D₃, 270MHz): δ = 9.18 (d, $J=6.9$ Hz, 2 H), 8.82 (dd, $J=4.5, 1.8$ Hz, 2 H), 8.55 (d, $J=6.5$ Hz, 2 H), 8.02 (dd, $J=4.6, 1.8$ Hz, 2 H), 4.77 (q, $J=7.3$ Hz, 2 H), 1.71 ppm (t, $J=7.3$ Hz, 3 H). ¹³C NMR (METHANOL-D₃, 68MHz): δ = 153.6, 150.5, 145.1, 142.4, 125.9, 122.3, 56.9, 15.5 ppm. ESI-MS: m/z 185.11 [M⁺].

This data is consistent with other literature reports.³²

1-Butyl-4,4'-bipyridinium bromide, [C₄Bipy]Br

4,4'-Bipyridine (8.00 g, 51.0 mmol) was dissolved in acetonitrile (90 mL) and 1-bromobutane (8.87 g, 7.00 mL, 61.0 mmol, 1.2 eq.) was added dropwise,

under an inert atmosphere. The mixture was heated to 80 °C and left to stir for 48 hr. After cooling, the solution was concentrated and the resulting precipitate was isolated by filtration. The solid product was suspended in hot chloroform and left to stir overnight. The insoluble material was separated and the solution was evaporated to give an off white solid (10.27 g, 69.0 %) that was dried at 50 °C and $\approx 8 \times 10^{-2}$ mbar for 24 hr. ^1H NMR (METHANOL- D_3 , 270MHz): $\delta = 9.17$ (d, $J=6.9$ Hz, 2 H), 8.82 (dd, $J=4.6, 1.7$ Hz, 2 H), 8.54 (d, $J=6.6$ Hz, 2 H), 8.02 (dd, $J=4.6, 1.7$ Hz, 2 H), 4.72 (t, $J=7.5$ Hz, 2 H), 2.06 (app. quin, $J=7.6$ Hz, 2 H), 1.47 (app. sxt, $J=7.7$ Hz, 2 H), 1.03 ppm (t, $J=7.3$ Hz, 3 H). ^{13}C NMR (METHANOL- D_3 , 68MHz): $\delta = 153.7, 150.5, 145.3, 142.4, 125.9, 122.3, 61.2, 33.1, 19.2, 12.5$ ppm. ESI-MS: m/z 213.13 [M^+].

This data is consistent with other literature reports.³³

1-Hexyl-4,4'-bipyridinium bromide, [C_6Bipy] Br

4,4'-Bipyridine (6.00 g, 38.4 mmol) was dissolved in acetonitrile (70 mL) and 1-bromohexane (7.06 g, 6.00 mL, 42.7 mmol, 1.10 eq.) was added dropwise, under an inert atmosphere. The mixture was heated to 70 °C and left to stir for 18 hr. The solid precipitate was suspended in hot chloroform and left to stir overnight. The insoluble material was separated and the solvent was removed to give a white solid (4.08 g, 33.1%) that was dried at 50 °C and $\approx 8 \times 10^{-2}$ mbar for 24 hr. ^1H NMR (METHANOL- D_3 , 270MHz): $\delta = 9.17$ (d, $J=6.9$ Hz, 2 H), 8.82 (dd, $J=4.6, 1.7$ Hz, 2 H), 8.54 (d, $J=6.6$ Hz, 2 H), 8.02 (dd, $J=4.6, 1.8$ Hz, 2 H), 4.71 (t, $J=7.6$ Hz, 2 H), 2.08 (quin, $J=7.4$ Hz, 2 H), 1.26 - 1.60 (m, 6 H), 0.92 ppm (t, $J=6.9$ Hz, 3 H). ^{13}C NMR (METHANOL- D_3 , 68MHz): $\delta = 153.7, 150.5, 145.3, 142.4, 125.9, 122.3, 61.5, 31.2, 31.0, 25.6, 22.2, 13.0$ ppm. ESI-MS: m/z 241.17 [M^+].

This data is consistent with other literature reports.³⁴

1-Octyl-4,4'-bipyridinium bromide, [C_8Bipy] Br

4,4'-Bipyridine (18.8 g, 120.0 mmol) was dissolved in DMF (160 mL) and 1-bromooctane (12.3 g, 11.0 mL, 63.7 mmol, 0.53 eq.) was added dropwise,

under an inert atmosphere. The mixture was heated to 85 °C and left to stir for 18 hr. After cooling, the solution was concentrated and diethyl ether was added until a precipitate formed. The isolated solid material was suspended in hot acetonitrile and left to stir overnight. The insoluble material was separated and the solution was removed to give an off white solid (7.02 g, 30.4%) that was dried at 50 °C and $\approx 8 \times 10^{-2}$ mbar for 24 hr. ^1H NMR (DMSO- d_6 , 300MHz): δ = 9.33 (d, $J=7.0$ Hz, 2 H), 8.86 (dd, $J=4.5, 1.7$ Hz, 2 H), 8.68 (d, $J=7.0$ Hz, 2 H), 8.07 (dd, $J=4.5, 1.7$ Hz, 2 H), 4.69 (t, $J=7.4$ Hz, 2 H), 1.96 (t, $J=6.9$ Hz, 2 H), 1.17 - 1.39 (m, 10 H), 0.84 ppm (t, $J=6.7$ Hz, 3 H). ^{13}C NMR (DMSO- d_6 , 75MHz): δ = 151.4, 145.8, 141.3, 128.7, 125.9, 122.4, 60.8, 31.6, 31.2, 28.9, 28.9, 25.9, 22.5, 14.4 ppm. ESI-MS: m/z 269.20 [M^+].

This data is consistent with other literature reports.³⁵

1,1'-Diethyl-4,4'-bipyridinium dibromide, [(C₂)₂Bipy][Br]₂

4,4'-Bipyridine (2.00 g, 12.8 mmol) was dissolved in acetonitrile (20 mL) and 1-bromoethane (13.9 g, 9.50 mL, 128.0 mmol, 10.0 eq.) was added dropwise, under an inert atmosphere. The mixture was heated to 80 °C and left to stir for 18 hr. The solid precipitate was isolated by filtration and washed with excess hot chloroform to give a yellow solid (4.04 g, 84.3%) that was dried at 50 °C and $\approx 8 \times 10^{-2}$ mbar for 24 hr. ^1H NMR (DEUTERIUM OXIDE- d_2 , 400 MHz): δ = 8.98 (d, $J=5.6$ Hz, 4 H), 8.39 (d, $J=5.6$, 4 H), 4.59-4.63 (m, 4 H), 1.55 ppm (t, $J=7.2$, 6 H). ^{13}C NMR (DEUTERIUM OXIDE, 68MHz): δ = 150.1, 145.4, 127.2, 57.8, 15.8 ppm. ESI-MS: m/z 214.14 [M^+].

This data is consistent with other literature reports.³⁶

1,1'-Dibutyl-4,4'-bipyridinium dibromide, [(C₄)₂Bipy][Br]₂

Separated from [C₄Bipy]Br by MeCN/EtOAc recrystallization to yield a bright yellow solid (3.01 g, 13.7%) that was dried at 50 °C and $\approx 8 \times 10^{-2}$ mbar for 24 hr. ^1H NMR (METHANOL- D_3 , 270 MHz): δ = 9.31 (d, $J=6.9$ Hz, 4 H), 8.71 (d, $J=6.5$ Hz, 4 H), 4.77 (t, $J=7.6$ Hz, 4 H), 2.01 - 2.19 (m, 4 H), 1.26 - 1.54 (m, 12 H), 0.86 - 1.00 ppm (m, 6 H). ^{13}C NMR (METHANOL- D_3 , 68

MHz): $\delta = 150.0, 145.8, 127.0, 62.0, 31.2, 31.0, 25.6, 22.2, 13.0$ ppm. ESI-MS: m/z 270.20 [M^+].

This data is consistent with other literature reports.³⁷

1,1'-Dihexyl-4,4'-bipyridinium dibromide, [(C₆)₂Bipy][Br]₂

Separated from [C₆Bipy]Br by MeCN/EtOAc recrystallization to yield a bright yellow solid (1.28 g, 6.99%) that was dried at 50 °C and $\approx 8 \times 10^{-2}$ mbar for 24 hr. ¹H NMR (METHANOL-D₃, 270 MHz): $\delta = 9.31$ (d, $J=6.9$ Hz, 4 H), 8.71 (d, $J=6.5$ Hz, 4 H), 4.77 (t, $J=7.6$ Hz, 4 H), 2.01 - 2.19 (m, 4 H), 1.26 - 1.54 (m, 12 H), 0.86 - 1.00 ppm (m, 6 H). ¹³C NMR (METHANOL-D₃, 68 MHz): $\delta = 150.0, 145.8, 127.0, 62.0, 31.2, 31.0, 25.6, 22.2, 13.0$ ppm. ESI-MS: m/z 326.27 [M^+].

This data is consistent with other literature reports.³⁸

1,1'-Dioctyl-4,4'-bipyridinium dibromide, [(C₈)₂Bipy][Br]₂

Separated from [C₈Bipy]Br by MeCN/EtOAc recrystallization to yield a bright yellow solid (1.71 g, 2.63%) that was dried at 50 °C and $\approx 8 \times 10^{-2}$ mbar for 24 hr. ¹H NMR (METHANOL-D₃, 270 MHz): $\delta = 9.30$ (d, $J=6.9$ Hz, 4 H), 8.70 (d, $J=6.5$ Hz, 4 H), 4.76 (t, $J=7.6$ Hz, 4 H), 2.01 - 2.23 (m, 4 H), 1.22 - 1.56 (m, 20 H), 0.82 - 1.02 ppm (m, 6 H). ¹³C NMR (METHANOL-D₃, 68 MHz): $\delta = 150.0, 145.8, 127.0, 62.0, 31.6, 31.3, 28.9, 28.8, 25.9, 22.4, 13.1$ ppm. ESI-MS: m/z 382.33 [M^+].

This data is consistent with other literature reports.³⁹

1,1'-Diethyl-4,4'-bipyridinium Di[bis(trifluoromethanesulfonyl)imide], [(C₂)₂Bipy][NTf₂]₂

[(C₂)₂Bipy]Br (1.00 g, 2.67 mmol) was dissolved in water and an aqueous solution of lithium bistriflimide (1.79 g, 3.21 mmol, 2.4 eq.) was slowly added, causing an instantaneous precipitate. The mixture was left to stir for 16 hr at

R.T., then the solid was filtered off and washed with excess water to give a bright white powder (1.27 g, 61.4%) that was dried at 70 °C and $\approx 8 \times 10^{-2}$ mbar for 24 hr. ^1H NMR (DMSO- d_6 , 300MHz): $\delta = 9.39$ (d, $J=6.8$ Hz, 2 H), 8.77 (d, $J=6.8$ Hz, 2 H), 4.72 (q, $J=7.3$ Hz, 2 H), 1.61 ppm (t, $J=7.3$ Hz, 3 H). ^{13}C NMR (DMSO- d_6 , 75MHz): $\delta = 149.0, 146.1, 127.0, 119.9$ (q, $J_{CF} = 322$ Hz, 2C, CF_3), 57.1, 16.7 ppm. ^{19}F NMR (DMSO- d_6 , 282 MHz) $\delta = -78.73$ (s, 6 F, CF_3) ppm. ESI-MS: m/z 214.14 [M^+].

**1,1'-Dibutyl-4,4'-bipyridinium Di[bis(trifluoromethanesulfonyl)imide],
[(C₄)₂Bipy][NTf₂]₂**

The same procedure used to prepare [(C₂)₂Bipy][NTf₂]₂ was used to prepare [(C₄)₂Bipy][NTf₂]₂ from [(C₄)₂Bipy][Br]₂ (1.00 g, 2.32 mmol) and Li[NTf₂] (1.56 g, 2.79 mmol, 2.4 eq.) to give a bright white solid (1.31 g, 67.9%) that was dried at 70 °C and $\approx 8 \times 10^{-2}$ mbar for 24 hr. ^1H NMR (DMSO- d_6 , 300MHz): $\delta = 9.38$ (d, $J=6.6$ Hz, 2 H), 8.77 (d, $J=6.6$ Hz, 2 H), 4.69 (t, $J=7.3$ Hz, 2 H), 1.97 (app. quin, $J=7.4$ Hz, 2 H), 1.35 (app. sxt, $J=7.3$ Hz, 2 H), 0.95 ppm (t, $J=7.3$ Hz, 3 H). ^{13}C NMR (DMSO- d_6 , 75MHz): $\delta = 148.7, 145.7, 126.6, 119.5$ (q, $J_{CF} = 322$ Hz, 2C, CF_3), 60.7, 32.7, 18.8, 13.2 ppm. ^{19}F NMR (DMSO- d_6 , 282 MHz) $\delta = -78.79$ (s, 6 F, CF_3) ppm. ESI-MS: m/z 270.20 [M^+].

This data is consistent with other literature reports.⁴⁰

**1,1'-Dihexyl-4,4'-bipyridinium Di[bis(trifluoromethanesulfonyl)imide],
[(C₆)₂Bipy][NTf₂]₂**

The same procedure used to prepare [(C₂)₂Bipy][NTf₂]₂ was used to prepare [(C₆)₂Bipy][NTf₂]₂ from [(C₆)₂Bipy][Br]₂ (1.00 g, 2.06 mmol) and Li[NTf₂] (1.38 g, 2.45 mmol, 2.4 eq.) to give a bright white solid (1.34 g, 73.3%) that was dried at 70 °C and $\approx 8 \times 10^{-2}$ mbar for 24 hr. ^1H NMR (DMSO- d_6 , 300MHz): $\delta = 9.38$ (d, $J=6.5$ Hz, 2 H), 8.77 (d, $J=6.5$ Hz, 2 H), 4.68 (t, $J=7.3$ Hz, 2 H), 1.98 (br. s., 2 H), 1.32 (br. s., 6 H), 0.88 ppm (t, $J=6.9$ Hz, 3 H). ^{13}C NMR (DMSO- d_6 , 75MHz): $\delta = 148.7, 145.7, 126.6, 119.5$ (q, $J_{CF} = 322$ Hz,

2C, CF₃), 60.9, 30.7, 30.5, 25.1, 21.8, 13.8 ppm. ¹⁹F NMR (DMSO-*d*₆, 282 MHz) δ = -78.74 (s, 6 F, CF₃) ppm. ESI-MS: m/z 163.13 [M²⁺].

This data is consistent with other literature reports.⁴¹

**1,1'-Dioctyl-4,4'-bipyridinium Di[bis(trifluoromethanesulfonyl)imide],
[(C₈)₂Bipy][NTf₂]₂**

The same procedure used to prepare [(C₂)₂Bipy][NTf₂]₂ was used to prepare [(C₈)₂Bipy][NTf₂]₂ from [(C₈)₂Bipy][Br]₂ (1.00 g, 1.85 mmol) and Li[NTf₂] (1.23 g, 2.21 mmol, 2.4 eq.) to give a bright white solid (1.41 g, 80.8%) that was dried at 70 °C and ≈ 8x10⁻² mbar for 24 hr. ¹H NMR (DMSO-*d*₆, 300MHz): δ = 9.38 (d, *J*=7.0 Hz, 2 H), 8.77 (d, *J*=7.0 Hz, 2 H), 4.68 (t, *J*=7.4 Hz, 2 H), 1.84 - 2.10 (m, 2 H), 1.17 - 1.39 (m, 10 H), 0.86 ppm (t, *J*=6.9 Hz, 3 H). ¹³C NMR (DMSO-*d*₆, 75MHz): δ = 148.9, 146.0, 126.9, 119.7 (q, *J*_{CF} = 322 Hz, 2C, CF₃), 61.2, 31.4, 31.0, 28.7, 28.6, 25.7, 22.3, 14.1 ppm. ¹⁹F NMR (DMSO-*d*₆, 282 MHz) δ = -78.75 (s, 6 F, CF₃) ppm. ESI-MS: m/z 191.16 [M²⁺].

This data is consistent with other literature reports.³⁹

**1-Ethyl-4,4'-bipyridinium bis(trifluoromethanesulfonyl)imide,
[C₂Bipy][NTf₂]**

The same procedure used to prepare [(C₂)₂Bipy][NTf₂]₂ was used to prepare [C₂Bipy][NTf₂] from [C₂Bipy]Br (1.00 g, 3.77 mmol) and Li[NTf₂] (1.26 g, 4.53 mmol, 1.2 eq.) to give a bright white solid (1.25 g, 71.5%) that was dried at 70 °C and ≈ 8x10⁻² mbar for 24 hr. ¹H NMR (DMSO-*d*₆, 300MHz): δ = 9.24 (d, *J*=6.8 Hz, 2 H), 8.87 (dd, *J*=4.5, 1.7 Hz, 2 H), 8.63 (d, *J*=6.8 Hz, 2 H), 8.03 (dd, *J*=4.5, 1.7 Hz, 2 H), 4.67 (q, *J*=7.3 Hz, 2 H), 1.59 ppm (t, *J*=7.3 Hz, 3 H). ¹³C NMR (DMSO-*d*₆, 75MHz): δ = 152.3, 151.0, 145.1, 140.9, 125.4, 121.9, 119.5 (q, *J*_{CF} = 322 Hz, 2C, CF₃), 56.0, 16.2 ppm. ¹⁹F NMR (DMSO-*d*₆, 282 MHz) δ = -78.27 (s, 6 F, CF₃) ppm. ESI-MS: m/z 185.10 [M⁺].

**1-Butyl-4,4'-bipyridinium bis(trifluoromethanesulfonyl)imide,
[C₄Bipy][NTf₂]**

The same procedure used to prepare [(C₂)₂Bipy][NTf₂]₂ was used to prepare [C₄Bipy][NTf₂] from [C₄Bipy]Br (1.00 g, 3.41 mmol) and Li[NTf₂] (1.14 g, 4.10 mmol, 1.2 eq.) to give a viscous brown liquid (1.15 g, 68.6%) that was dried at 70 °C and $\approx 8 \times 10^{-2}$ mbar for 24 hr. ¹H NMR (DMSO-d₆, 300MHz): δ = 9.24 (d, $J=7.1$ Hz, 2 H), 8.87 (dd, $J=4.6, 1.7$ Hz, 2 H), 8.63 (d, $J=7.1$ Hz, 2 H), 8.04 (dd, $J=4.6, 1.7$ Hz, 2 H), 4.64 (t, $J=7.4$ Hz, 2 H), 1.87 - 2.02 (m, 2 H), 1.21 - 1.45 (m, 2 H), 0.94 ppm (t, $J=7.3$ Hz, 2 H). ¹³C NMR (DMSO-d₆, 75MHz): δ = 152.8, 151.4, 145.7, 141.3, 125.9, 122.4, 119.9 (q, $J_{CF} = 322$ Hz, 2C, CF₃), 60.7, 33.1, 19.2, 13.7 ppm. ¹⁹F NMR (DMSO-d₆, 282 MHz) δ = -78.73 (s, 6 F, CF₃) ppm. ESI-MS: m/z 213.13 [M⁺].

This data is consistent with other literature reports.⁴⁰

**1-Hexyl-4,4'-bipyridinium bis(trifluoromethanesulfonyl)imide,
[C₆Bipy][NTf₂]**

The same procedure used to prepare [(C₂)₂Bipy][NTf₂]₂ was used to prepare [C₆Bipy][NTf₂] from [C₆Bipy]Br (1.00 g, 3.11 mmol) and Li[NTf₂] (1.04 g, 3.74 mmol, 1.2 eq.) to give a viscous brown liquid (1.37 g, 84.7%) that was dried at 70 °C and $\approx 8 \times 10^{-2}$ mbar for 24 hr. ¹H NMR (DMSO-d₆, 300MHz): δ = 9.24 (d, $J=7.1$ Hz, 2 H), 8.87 (dd, $J=4.6, 1.7$ Hz, 2 H), 8.63 (d, $J=7.1$ Hz, 2 H), 8.04 (dd, $J=4.6, 1.7$ Hz, 2 H), 4.63 (t, $J=7.4$ Hz, 2 H), 1.86 - 2.05 (m, 2 H), 1.22 - 1.38 (m, 6 H), 0.87 ppm (t, $J=6.9$ Hz, 3 H). ¹³C NMR (DMSO-d₆, 75MHz): δ = 152.8, 151.4, 145.7, 141.3, 125.9, 122.4, 119.9 (q, $J_{CF} = 322$ Hz, 2C, CF₃), 60.9, 31.1, 31.0, 25.5, 22.3, 14.3 ppm. ¹⁹F NMR (DMSO-d₆, 282 MHz) δ = -78.74 (s, 6 F, CF₃) ppm. ESI-MS: m/z 241.16 [M⁺].

This data is consistent with other literature reports.⁴¹

**1-Octyl-4,4'-bipyridinium bis(trifluoromethanesulfonyl)imide,
[C₈Bipy][NTf₂]**

The same procedure used to prepare [(C₂)₂Bipy][NTf₂]₂ was used to prepare [C₈Bipy][NTf₂] from [C₈Bipy]Br (1.00 g, 2.54 mmol) and Li[NTf₂] (0.85 g, 3.04 mmol, 1.2 eq.) to give a viscous brown liquid (1.23 g, 88.3%) that solidified upon agitation. The solid was dried at 70 °C and $\approx 8 \times 10^{-2}$ mbar for 24 hr. ¹H NMR (DMSO-d₆, 300MHz): $\delta = 9.23$ (d, $J=7.1$ Hz, 2 H), 8.87 (dd, $J=4.5, 1.8$ Hz, 2 H), 8.63 (d, $J=7.1$ Hz, 2 H), 8.04 (dd, $J=4.5, 1.8$ Hz, 2 H), 4.63 (t, $J=7.4$ Hz, 2 H), 1.86 - 2.05 (m, 2 H), 1.18 - 1.42 (m, 10 H), 0.86 ppm (t, $J=6.9$ Hz, 3 H). ¹³C NMR (DMSO-d₆, 75MHz): $\delta = 152.8, 151.4, 145.7, 141.3, 125.9, 122.4, 119.9$ (q, $J_{CF} = 322$ Hz, 2C, CF₃), 60.9, 31.6, 31.1, 28.9, 28.8, 25.9, 22.5, 14.4 ppm. ¹⁹F NMR (DMSO-d₆, 282 MHz) $\delta = -78.73$ (s, 6 F, CF₃) ppm. ESI-MS: m/z 269.20 [M⁺].

2.2.3.3.3 Nitrile Functionalised ILs:

1-Valeronitrile-3-methylimidazolium chloride, [(C₄CN)C₁Im]Cl

N-Methylimidazole (27.9 g, 27.0 mL, 339.3 mmol) and 5-chlorovaleronitrile (50 g, 424.1 mmol, 1.2 eq.) were mixed under an inert atmosphere and heated to 80 °C for 4hr, then to 110 °C for 2 hr. After cooling the viscous brown liquid was washed with Et₂O (3 x 50 mL) and dried at $\approx 8 \times 10^{-2}$ mbar for 24 hr, during which time the liquid solidified to a brown solid (61.7 g, 91.1%). ¹H NMR (DMSO-d₆, 300MHz): $\delta = 9.61$ (s, 1 H), 7.93 (t, $J=1.7$ Hz, 1 H), 7.84 (t, $J=1.7$ Hz, 1 H), 4.28 (t, $J=6.9$ Hz, 2 H), 3.87 (s, 3 H), 2.60 (t, $J=7.2$ Hz, 2 H), 1.80 - 1.95 (m, 2 H), 1.45 - 1.59 ppm (m, 2 H). ¹³C NMR (DMSO-d₆, 75MHz): $\delta = 136.9, 123.6, 122.2, 120.4, 47.6, 35.7, 28.5, 21.5, 15.7$ ppm. ESI-MS: m/z 164.11 [M⁺].

This data is consistent with other literature reports.⁴²

**1-Valeronitrile-3-methylimidazolium tetrafluoroborate,
[(C₄CN)C₁Im][BF₄]**

1-Valeronitrile-3-methylimidazolium chloride (5.00 g, 25.0 mmol) was dissolved in acetone (100 mL) and sodium tetrafluoroborate (3.02 g, 27.5 mmol, 1.1 eq.) was added to the solution. The mixture was stirred at 40 °C for 48 hr, then the solid was removed by filtration and the solvent removed to yield a brown liquid (4.24g , 63.6%) which was dried at 50 °C and $\approx 8 \times 10^{-2}$ mbar for 24 hr. ¹H NMR (DMSO-*d*₆ ,300MHz): δ = 9.06 (s, 1 H), 7.74 (t, *J*=1.8 Hz, 1 H), 7.69 (t, *J*=1.8 Hz, 1 H), 4.20 (t, *J*=7.0 Hz, 2 H), 3.84 (s, 3 H), 2.54 (t, *J*=7.2 Hz, 2 H), 1.81 - 1.94 (m, 2 H), 1.48 - 1.61 ppm (m, 2 H). ¹³C NMR (DMSO-*d*₆ ,75MHz): δ = 136.6, 123.7, 122.2, 120.4, 47.9, 35.8, 28.5, 21.5, 15.7 ppm. ¹⁹F NMR (DMSO-*d*₆, 282 MHz) δ = -148.3 (s, 4 F, BF₄) ppm ESI-MS: *m/z* 164.11 [M⁺].

This data is consistent with other literature reports.⁴³

**1-Valeronitrile-3-methylimidazolium hexafluorophosphate,
[(C₄CN)MIm][PF₆]**

1-Valeronitrile-3-methylimidazolium chloride (5.00 g, 25.0 mmol) was dissolved in water (50 mL) and hexafluorophosphoric acid (60% w/w, 3.83 mL, 27.5 mmol, 1.1 eq.) was added dropwise to the vigorously stirred solution at room temperature. The mixture was left for 2 hr at room temperature and the resulting viscous brown liquid was separated from the aqueous phase and washed with water (4 x 20 mL), then dried at 50 °C and $\approx 8 \times 10^{-2}$ mbar for 24 hr to yield the pure product (5.98 g, 77.2%). ¹H NMR (DMSO-*d*₆ ,300MHz): δ = 9.08 (s, 1 H), 7.74 (t, *J*=1.7 Hz, 1 H), 7.69 (t, *J*=1.7 Hz, 1 H), 4.20 (t, *J*=7.0 Hz, 2 H), 3.84 (s, 3 H), 2.55 (t, *J*=7.0 Hz, 2 H), 1.79 - 1.95 (m, 2 H), 1.48 - 1.62 ppm (m, 2 H). ¹³C NMR (DMSO-*d*₆ ,75MHz): δ = 136.6, 123.7, 122.2, 120.4, 47.9, 35.8, 28.5, 21.5, 15.7 ppm. ¹⁹F NMR (282 MHz, DMSO-*d*₆) δ ppm -70.18 (d, *J*_{PF}=712.00 Hz, 6 F, PF₆). ³¹P NMR (121 MHz, DMSO-*d*₆) δ ppm -144.21 (spt, *J*_{FP}=712.00 Hz, 1 P, PF₆). ESI-MS: *m/z* 164.11 [M⁺].

This data is consistent with other literature reports.⁴³

1-Valeronitrile-3-methylimidazolium bistriflimide, [(C₄CN)MIm][NTf₂]

The same procedure used to prepare [(C₄CN)Im][PF₆] was used to prepare [(C₄CN)Im][NTf₂] from 1-valeronitrile-3-methylimidazolium chloride (5.00 g, 25.0 mmol) and an aqueous solution of lithium bistriflimide (7.91 g, 27.5 mmol, 1.1 eq.) to yield a brown liquid (9.37 g, 84.3%) which was dried at 50 °C and $\approx 8 \times 10^{-2}$ mbar for 24 hr. ¹H NMR (DMSO-d₆, 300MHz): δ = 9.09 (s, 1 H), 7.76 (t, J =1.8 Hz, 1 H), 7.70 (t, J =1.7 Hz, 1 H), 4.20 (t, J =7.0 Hz, 2 H), 3.84 (s, 3 H), 2.55 (t, J =7.1 Hz, 2 H), 1.81 - 1.95 (m, 2 H), 1.48 - 1.62 ppm (m, 2 H). ¹³C NMR (DMSO-d₆, 75MHz): δ = 137.1, 124.2, 122.7, 120.8, 119.9 (q, J_{CF} = 322 Hz, 2C, CF₃), 48.4, 36.2, 29.0, 22.0, 16.1 ppm ESI-MS: m/z 164.11 [M⁺].

1-Valeronitrilepyridinium chloride, [(C₄CN)Py]Cl

Pyridine (13.0 g, 13.3 mL, 164.3 mmol) and 5-chlorovaleronitrile (23.3 g, 22.3 mL, 197.2 mmol, 1.2 eq.) were mixed under an inert atmosphere and heated to 70 °C for 72 hr, then 100 °C for 2 hr. After cooling, the viscous brown liquid was washed with Et₂O (3 x 50 mL) and recrystallized from MeOH/Et₂O. The liquid crystallised overnight to give a glassy brown solid (WARNING: extremely hygroscopic) that showed the presence of the 5-chlorovaleronitrile starting material by ¹H NMR. The solid was broken up and refluxed in EtOAc (100 mL) for 2 hr and finally dried at 50 °C and $\approx 8 \times 10^{-2}$ mbar for 24 hr to give the pure product (21.55 g, 85.2%). ¹H NMR (DMSO-d₆, 300MHz): δ = 9.36 (dd, J =6.7, 1.3 Hz, 2 H, CH), 8.64 (tt, J =7.7, 1.3 Hz, 1 H, CH), 8.20 (dd, J =7.7, 6.7 Hz, 2 H, CH), 4.79 (t, J =7.2 Hz, 2 H, CH₂), 2.62 (t, J =7.2 Hz, 2 H, CH₂), 1.93 - 2.09 (m, 2 H, CH₂), 1.51 - 1.65 ppm (m, 2 H, CH₂) ¹³C NMR (DMSO-d₆, 75MHz): δ = 145.6, 144.9, 128.1, 120.4, 59.4, 29.8, 21.4, 15.7 ppm. ESI-MS: m/z 161.10 [M⁺].

This data is consistent with other literature reports.⁴⁴

**1-Valeronitrilepyridinium bis(trifluoromethanesulfonyl)imide,
[(C₄CN)Py][[NTf₂]]**

[(C₄CN)Py]Cl (6.00 g, 30.5 mmol) was dissolved in water (50 mL) and an aqueous solution of Li[NTf₂] (10.51 g, 36.6 mmol, 1.2 eq.) was added dropwise with vigorous stirring, causing an instant phase separation. A small amount of DCM was added to reduce the viscosity of the lower layer and the mixture was left to stir for 2 hr. The lower layer was separated and washed with water (4 x 20 mL) and the solvent removed to give a viscous yellow liquid (11.5 g, 85.4%) that was dried at 50 °C and $\approx 8 \times 10^{-2}$ mbar for 24 hr. ¹H NMR (DMSO-d₆, 300MHz): δ = 9.08 (dd, $J=6.6, 1.3$ Hz, 2 H), 8.61 (tt, $J=7.8, 1.3$ Hz, 1 H), 8.17 (dd, $J=7.8, 6.6$ Hz, 2 H), 4.63 (t, $J=7.3$ Hz, 2 H), 2.56 (t, $J=7.1$ Hz, 2 H), 1.91 - 2.09 (m, 2 H), 1.49 - 1.66 ppm (m, 2 H). ¹³C NMR (DMSO-d₆, 75MHz): δ = 145.6, 144.8, 128.2, 120.3, 119.5 (q, $J_{CF} = 322$ Hz, 2C, CF₃), 59.9, 29.7, 21.5, 15.7 ppm. ¹⁹F NMR (DMSO-d₆, 282 MHz) δ = -78.27 (s, 6 F, CF₃) ppm. ESI-MS: m/z 161.10 [M⁺]

**1-Valeronitrilepyridinium bis(trifluoromethanesulfonyl)imide,
[(C₄CN)Py][PF₆]]**

The same procedure used to prepare [(C₄CN)Py][[NTf₂]] was used to prepare [(C₄CN)Py][[PF₆]] from [(C₄CN)Py]Cl (6.00 g, 30.5 mmol) and H[PF₆] (60 wt.%, 4.25 mL, 36.6 mmol, 1.2 eq.) to give a white solid (6.05 g, 64.8%) that was dried at 50 °C and $\approx 8 \times 10^{-2}$ mbar for 24 hr. ¹H NMR (DMSO-d₆, 300MHz): δ = 9.07 (dd, $J=6.6, 1.1$ Hz, 2 H), 8.61 (tt, $J=7.7, 1.3$ Hz, 1 H), 8.17 (dd, $J=7.7, 6.7$ Hz, 2 H), 4.63 (t, $J=7.3$ Hz, 2 H), 2.56 (t, $J=7.1$ Hz, 2 H), 1.93 - 2.10 (m, 2 H), 1.50 - 1.67 ppm (m, 2 H). ¹³C NMR (DMSO-d₆, 75MHz): δ = 146.0, 145.2, 128.6, 120.8, 60.4, 30.2, 21.9, 16.2 ppm. ³¹P NMR (DMSO-d₆, 121MHz): δ = -144.2 (spt, $J_{PF}=712$ Hz, PF₆) ppm. ¹⁹F NMR (DMSO-d₆, 282MHz): δ = -70.1 (d, $J_{FP}=712$ Hz, PF₆). ESI-MS: m/z 161.10 [M⁺].

1-Valeronitrile-1-methylpyrrolidinium chloride, [(C₄CN)C₁Pyrr]Cl

N-Methylpyrrolidine (13.0 g, 15.9 mL, 152.7 mmol) and 5-chlorovaleronitrile (21.6 g, 20.7 mL, 183.2 mmol, 1.2 eq.) were mixed under an inert atmosphere and heated to 70 °C for 72 hr, then 100 °C for 2 hr. The resulting dark red viscous oil was cooled and washed with Et₂O (3x 50 mL) and recrystallized from MeOH/Et₂O. ¹H NMR (DMSO-d₆, 300MHz): δ = 3.38 - 3.61 (m, 6 H), 3.03 (s, 3 H), 2.62 (t, *J*=7.1 Hz, 2 H), 2.07 (br. s., 4 H), 1.71 - 1.88 (m, 2 H), 1.52 - 1.67 ppm (m, 2 H). ¹³C NMR (DMSO-d₆, 75MHz): δ = 120.4, 63.3, 61.7, 47.3, 22.2, 22.0, 21.0, 15.8 ppm. NMR showed the presence of 5-chlorovaleronitrile and N-methylpyrrolidine so the sample was recrystallized from DCM/Et₂O and washed with EtOAc (50 mL) in a separating funnel. The liquid was dried at 50 °C and $\approx 8 \times 10^{-2}$ mbar for 24 hr, at which point it crystallised to give a red/brown solid (17.03 g, 69.4%). ¹H NMR (DMSO-d₆, 300MHz): δ = 3.38 - 3.61 (m, 6 H), 3.03 (s, 3 H), 2.62 (t, *J*=7.1 Hz, 2 H), 2.07 (br. s., 4 H), 1.71 - 1.88 (m, 2 H), 1.52 - 1.67 ppm (m, 2 H). ¹³C NMR (DMSO-d₆, 75MHz): δ = 120.4, 63.3, 61.7, 47.3, 22.2, 22.0, 21.0, 15.8 ppm. ESI-MS: *m/z* 167.15 [M⁺].

1-Valeronitrile-1-methylpyrrolidinium bistriflimide, [(C₄CN)C₁Pyrr][[NTf₂]]

The same procedure used to prepare [(C₄CN)Py][[NTf₂]] was used to prepare [(C₄CN)MPyrr][[NTf₂]] from [(C₄CN)MPyrr]Cl (6.00 g, 29.6 mmol) and Li[NTf₂] (10.2 g, 35.5 mmol, 1.2 eq.) to give a viscous orange liquid (12.0 g, 90.9%) that was dried at 50 °C and $\approx 8 \times 10^{-2}$ mbar for 24 hr. ¹H NMR (DMSO-d₆, 300MHz): δ = 3.25 - 3.58 (m, 6 H), 2.98 (s, 3 H), 2.57 (t, *J*=7.1 Hz, 2 H), 2.08 (br. s., 4 H), 1.73 - 1.89 (m, 2 H), 1.53 - 1.68 ppm (m, 2 H). ¹³C NMR (DMSO-d₆, 75MHz): δ = 120.2, 119.5 (q, *J*_{CF}=322 Hz, 2C, CF₃), 63.5, 62.1, 47.5, 22.2, 22.0, 21.1, 15.8 ppm. ¹⁹F NMR (DMSO-d₆, 282 MHz) δ = -78.72 (s, 6 F, CF₃) ppm. ESI-MS: *m/z* 167.15 [M⁺].

**1-Valeronitrile-1-methylpyrrolidinium hexafluorophosphate,
[(C₄CN)C₁Pyrr][PF₆]**

The same procedure used to prepare [(C₄CN)Py][NTf₂] was used to prepare [(C₄CN)MPyrr][PF₆] from [(C₄CN)MPyrr]Cl (6.00 g, 29.6 mmol) and H[PF₆] (60 wt.%, 5.00 mL, 35.5 mmol, 1.2 eq.) to give a viscous orange liquid (6.57 g, 71.1%) that was dried at 50 °C and $\approx 8 \times 10^{-2}$ mbar for 24 hr. ¹H NMR (DMSO-d₆, 300MHz): δ = 3.22 - 3.58 (m, 6 H), 2.98 (s, 3 H), 2.57 (t, $J=7.1$ Hz, 2 H), 2.08 (br. s., 4 H), 1.72 - 1.87 (m, 2 H), 1.53 - 1.69 ppm (m, 2 H). ¹³C NMR (DMSO-d₆, 75MHz): δ = 120.3, 63.5, 62.1, 47.5, 22.2, 22.0, 21.1, 15.8 ppm. ¹⁹F NMR (DMSO-d₆, 282MHz): δ = -70.2 (d, $J_{FP}=711$ Hz, 6F, PF₆) ppm. ³¹P NMR (DMSO-d₆, 121MHz): δ = -144.2 (spt, $J_{PF}=711$ Hz, 1P, PF₆) ppm. ESI-MS: m/z 167.15 [M⁺].

2.3 References

- 1 K. Siegbahn, University of Uppsala, 1981.
- 2 A. Knop-Gericke, E. Kleimenov, M. Haevecker, R. Blume, D. Teschner, S. Zafeiratos, R. Schloegl, V. I. Bukhtiyarov, V. V Kaichev, I. P. Prosvirin, A. I. Nizovskii, H. Bluhm, A. Barinov, P. Dudin and M. Kiskinova, in *Advances in Catalysis, Vol 52*, 2009, vol. 52, pp. 213–272.
- 3 R. L. Opila and J. Eng, *Prog. Surf. Sci.*, 2001, **69**, 125–163.
- 4 a. Paul Pijpers and R. J. Meier, *Chem. Soc. Rev.*, 1999, **28**, 233–238.
- 5 K. a. Wepasnick, B. a. Smith, J. L. Bitter and D. Howard Fairbrother, *Anal. Bioanal. Chem.*, 2010, **396**, 1003–1014.
- 6 P. K. Ghosh, *Introduction to Photoelectron Spectroscopy*, Wiley Interscience, 1983.
- 7 C. J. Powell and A. Jablonski, *Nucl. Instruments Methods Phys. Res. Sect. A Accel. Spectrometers, Detect. Assoc. Equip.*, 2009, **601**, 54–65.
- 8 C. S. Fadley, *Prog. Surf. Sci.*, 1984, **16**, 275–388.
- 9 K. R. J. Lovelock, I. J. Villar-Garcia, F. Maier, H. P. Steinrück and P. Licence, *Chem. Rev.*, 2010, **110**, 5158–5190.
- 10 C. C. Chang, *Surf. Sci.*, 1971, **25**, 53–79.
- 11 I. J. Villar García, The University of Nottingham, 2009.
- 12 S. Men, The University of Nottingham, 2011.
- 13 A. W. Taylor, K. R. J. Lovelock, A. Deyko, P. Licence and R. G. Jones, *Phys. Chem. Chem. Phys.*, 2010, **12**, 1772–1783.
- 14 I. J. Villar-Garcia, E. F. Smith, A. W. Taylor, F. Qiu, K. R. J. Lovelock, R. G. Jones and P. Licence, *Phys. Chem. Chem. Phys.*, 2011, **13**, 2797.
- 15 N. Stojilovic, *J. Chem. Educ.*, 2012, **89**, 1331–1332.
- 16 C. D. Wagner, L. E. Davis, M. V Zeller, J. a Taylor, R. H. Raymond and L. H. Gale, *Surf. Interface Anal.*, 1981, **3**, 211–225.
- 17 D. Briggs and J. T. Grant, in *Surface Analysis by Auger and X-Ray Photoelectron Spectroscopy*, 2003, pp. 31–56.
- 18 D. S. Mitchell, 2014.
- 19 D. R. Penn, *J. Electron Spectros. Relat. Phenomena*, 1976, **9**, 29–40.
- 20 I. Tilinin, *Prog. Surf. Sci.*, 1996, **52**, 193–335.
- 21 A. Walton, John; Wincott, Paul; Fairley, Neal; Carrick, *Peak Fitting with CasaXPS: a Casa Pocket Book*, Acolyte Science, 2010.
- 22 A. D. Baker and D. Betteridge, *Photoelectron Spectroscopy*, Pergamon Press, 1972.

- 23 S. Men, D. S. Mitchell, K. R. J. Lovelock and P. Licence, *ChemPhysChem*, 2015, **16**, 2211.
- 24 E. F. Smith, I. J. V. Garcia, D. Briggs and P. Licence, *Chem. Commun.*, 2005, 5633–5635.
- 25 A. W. Taylor and P. Licence, *ChemPhysChem*, 2012, **13**, 1917–1926.
- 26 I. J. Villar-Garcia, E. F. Smith, A. W. Taylor, F. Qiu, K. R. J. Lovelock, R. G. Jones and P. Licence, *Phys. Chem. Chem. Phys.*, 2011, **13**, 2797–2808.
- 27 B. B. Hurisso, K. R. J. Lovelock and P. Licence, *Phys. Chem. Chem. Phys.*, 2011, **13**, 17737–48.
- 28 I. J. Villar-Garcia, K. R. J. Lovelock, S. Men and P. Licence, *Chem. Sci.*, 2014, **5**, 2573–9.
- 29 A. W. Taylor, S. Men, C. J. Clarke and P. Licence, *RSC Adv.*, 2013, **3**, 9436.
- 30 P. Wasserscheid and T. Welton, *Ionic Liquids in Synthesis*, Wiley, 2nd edn., 2008.
- 31 S. M. Sieburth, C. Lin and D. Rucando, *J. Org. Chem.*, 1999, **64**, 950–953.
- 32 J. H. Mondal, S. Ahmed and D. Das, *Langmuir*, 2014, **30**, 8290–8299.
- 33 J. Joseph, N. V. Eldho and D. Ramaiah, *Chemistry*, 2003, **9**, 5926–35.
- 34 M. F. Pepitone, G. G. Jernigan, J. S. Melinger and O.K. Kim, *Org. Lett.*, 2007, **9**, 801–4.
- 35 X.-B. Shao, X.-K. Jiang, X.-Z. Wang, Z.-T. Li and S.-Z. Zhu, *Tetrahedron*, 2003, **59**, 4881–4889.
- 36 Y. Xiao, L. Chu, Y. Sanakis and P. Liu, *J. Am. Chem. Soc.*, 2009, **131**, 9931–9933.
- 37 H. Song, J. Chen, C. Xia and Z. Li, *Synth. Commun.*, 2012, **42**, 266–273.
- 38 V. Selvaraj, P. Sakthivel and V. Rajendran, *Ultrason. Sonochem.*, 2015, **22**, 265–271.
- 39 M. Kuroboshi, T. Shiba and H. Tanaka, *Tetrahedron Lett.*, 2013, **54**, 3666–3668.
- 40 A. Abebe, S. Admassie, I. J. Villar-Garcia and Y. Chebude, *Inorg. Chem. Commun.*, 2013, **29**, 210–212.
- 41 N. Jordão, L. Cabrita, F. Pina and L. C. Branco, *Chem. Eur. J.*, 2014, **20**, 3982–3988.
- 42 D. M. Drab, M. Smiglak, J. L. Shamshina, S. P. Kelley, S. Schneider, T. W. Hawkins and R. D. Rogers, *New J. Chem.*, 2011, **35**, 1701.
- 43 P. Dyson, D. Zhao and Z. Fei, US Pat., US20090143597 A1, 2009.
- 44 S. Zeng, H. He, H. Gao, X. Zhang, J. Wang, Y. Huang and S. Zhang, *RSC Adv.*, 2015, **5**, 2470–2478.

Chapter 3:
Chlorinated Ionic Liquids

3 Chlorinated Ionic Liquids

3.1 Introduction

As previously stated, the extremely low volatilities of ILs mean that they may be introduced into UHV environments without undergoing significant evaporation.¹⁻³ A wide range of vacuum dependant surface science methods have therefore been exploited in order to investigate the interfacial properties of ILs.⁴⁻⁷ Traditionally a surface characterisation technique, XPS has been shown to provide information indicative of the bulk liquid at the normal emission angle, $\theta = 0^\circ$. Since the element specific nature of XPS provides information on all atomic environments present within a sample, XPS has become a prominent technique in the investigations of anion-cation interactions, solvent-solute interactions and the solution phase chemistry of IL systems.⁸⁻¹²

Core level B.E.s are sensitive to the local chemical environment. This means that XPS may be used to identify and quantify the various chemical states of each element.¹³⁻¹⁵ This process becomes more problematic for elements that occupy a high number of diverse chemical states, for example the C 1s regions of most IL XP spectra. As complex unresolved photoemissions, these regions require peak fitting models in order to determine the individual signals that contribute to the observed spectrum.¹⁶⁻¹⁸ Although certain peak positions may be apparent, the majority of signals are fitted *via* parameter controlled peaks (e.g. FWHM and area constraints) and chemical intuition. For the XPS analysis of ILs to advance, exact photoemission B.E.s are required in order to extract the maximum amount of available data.

ILs may be customised with a range of functional groups to produce task specific ionic liquids (TSILs).¹⁹⁻²² The properties of ILs may therefore be altered to suit a particular application, depending upon the incorporated functional group.²³ Likewise, molecules may also be functionalised with ionic moieties, imparting IL-like properties to enhance the chemical and physical features of a particular molecular species.²⁴⁻²⁷ The ‘designer’ aspect of ILs

and the ease of their integration into existing systems has therefore resulted in their widespread adoption to a wide range of research fields. Examples include catalysis,²⁸ separations,²⁹ and gas capture.³⁰

TSILs have also been exploited in order to measure liquid phase organic reactions *via* XPS.^{8,31} Conventional reagents or solvents would evaporate under the UHV environment that is required for XPS analysis. ILs can be used to anchor functional groups to the involatile liquid medium, allowing organic reactions to proceed inside the XP spectrometer, without sacrificing the vacuum environment. In this particular example, imidazolium and phosphonium salts were functionalised with tertiary amines which were then combined with an analogous IL containing a chlorinated sulfonate anion. The resulting liquid mixtures allow the monitoring of the S_N2 reaction between the amine nucleophile and the chlorinated electrophile.

This chapter will present a range of ILs that have been functionalised with chlorine. The purpose of this functionalisation is not physical or chemical, but electronic. By introducing an electron withdrawing group (EWG) to the cationic heads of imidazolium and pyridinium ILs, B.E. shifts in the C 1s XP spectra should provide information on the initial and final locations of the chlorine bound carbon. This has significant implications for the C 1s peak fitting procedures that are used to model the XP spectra of ILs. Analysis of the C 1s region should be relatively simple, however in order to accurately determine peak positions difference spectra will be employed.

The procedures used to generate difference spectra were also described in the theory section. ILs with EWGs should produce a C 1s difference spectrum that show a loss of signal at low B.E. and a corresponding gain in signal at higher B.E. (when analysed relative to an analogous traditional IL). The loss of valence electron density on a carbon atom produces a slightly higher positive charge, this results in an increase in B.E. due to the decreased electrostatic shielding by electrons from the nucleus.

3.2 Chlorinated Imidazolium ILs

For this investigation imidazolium salts with chlorine bound to the C⁴ position of the aromatic ring were donated by Jason Harper of the University of New South Wales (UNSW). The salts contain the [NTf₂]⁻ anions and have butyl (C₄) or octyl (C₈) chain lengths, see **Figure 3.1**. The imidazolium salts are named according to the abbreviation [C₁C_n-4-ClIm][NTf₂], in order to denote that the chlorine is bound to the C⁴ carbon.

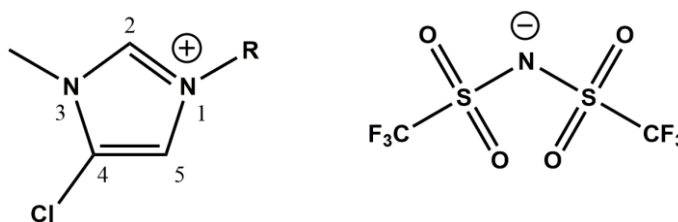


Figure 3.1 The structure of the [C₁C_n-4-ClIm][NTf₂] ILs used in this investigation. R is either the butyl (C₄) or octyl (C₈) aliphatic carbon chains.

The following sections will detail the C 1s peak fitting procedures of the [C₁C_n-4-ClIm][NTf₂] salts relative to the non-chlorinated [C₁C_nIm][NTf₂] salts. Since this analysis depends upon the existing C 1s peak fitting of the traditional imidazolium ILs, the [C₁C₈Im][NTf₂] C 1s model is presented in **Figure 3.2**. This fitting model¹⁶ was explained in detail in the previous chapter. The components are fixed to the relative areas of the carbon environments and the peak assignments are colour coded to the structure shown on the plot. The C^{4,5} (blue) component is located at a higher B.E., than the C^{6,7} (orange) component.

Through the shifting of electron density, chlorination of the C⁴ carbon of the imidazolium ring should allow the exact location of the C^{4,5} component to be identified. The subsequent fitting of the C 1s region should then provide a more accurate placement of the C^{6,7} component. Future experiments involving chlorination of the C⁶ component may be utilised in order to further expand this analysis. For the purpose of this investigation, the following experiments should provide sufficient data to either confirm or disprove the current C 1s fitting procedures.

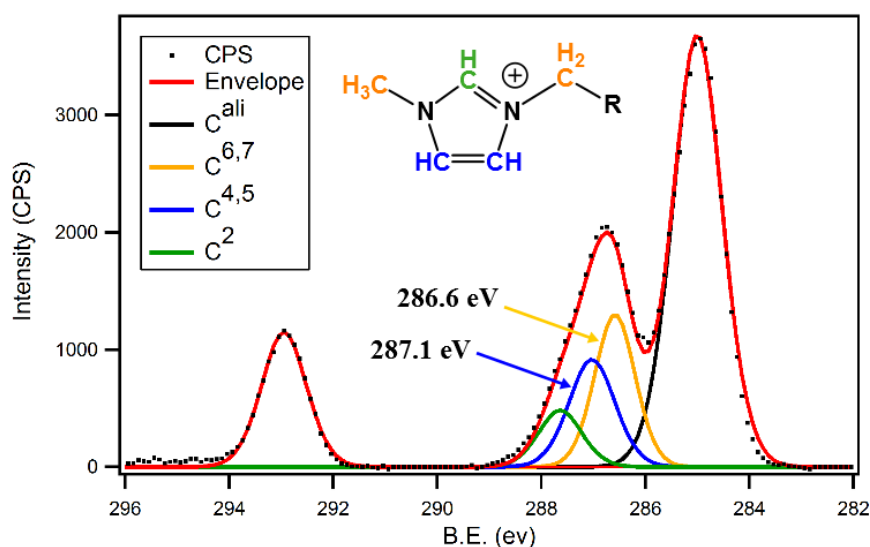


Figure 3.2 The current C 1s peak fitting model for the $[C_1C_8Im][NTf_2]$ salt. The spectrum is charge corrected to the C^{ali} signal which is set to 285.0 eV.

3.2.1 The XPS of Chlorinated Imidazolium Salts

The acquired wide scans for the $[C_1C_n-4-ClIm][NTf_2]$ salts are displayed in **Figure 3.3**, where only the expected elements are observed. This confirms the absence of residual halide impurities (< 0.1 at.%) and surface contamination from silicon containing compounds. The calculated and experimentally determined elemental compositions that were acquired from the wide scans are also presented in **Table 3.1**.

The $[C_1C_8-4-ClIm][NTf_2]$ sample was charge corrected to the aliphatic component (285.0 eV) and the $[C_1C_4-4-ClIm][NTf_2]$ sample was referenced to the cationic N 1s value of the imidazolium nitrogens, as measured from the corrected $[C_1C_8-4-ClIm][NTf_2]$ sample.³² All spectra were normalised to the F 1s signal of the anions. It should be noted that atomic compositions do not include hydrogen as it is not XPS observable.³³ The measured values are within 10.0% of the predicted compositions, however larger deviations are noted for chlorine. The low intensity of the Cl 2p photoemissions means that the error of measurement is relatively high compared to the measured atomic percentages.

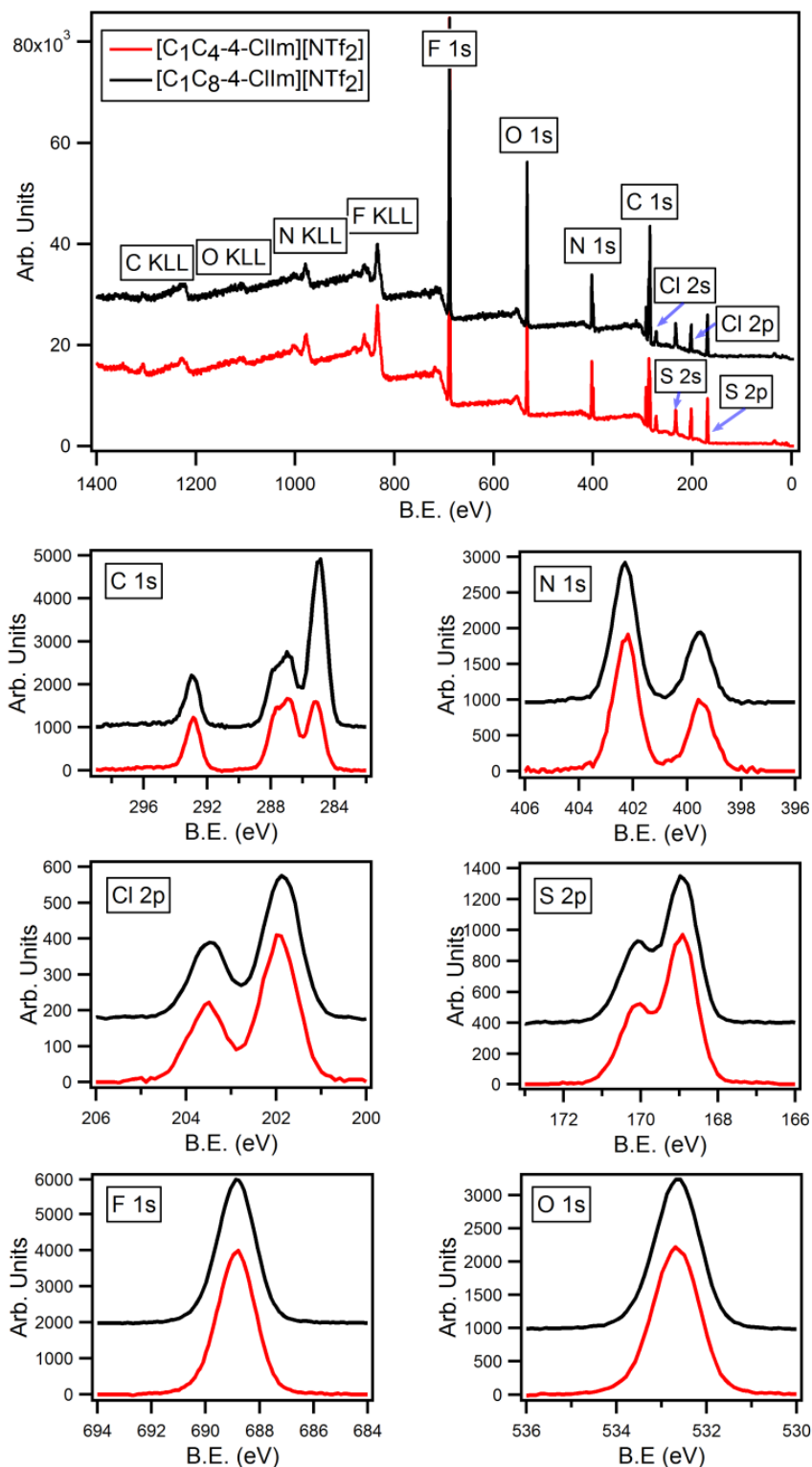


Figure 3.3 The XPS wide (top) and high resolution scans for the chlorinated imidazolium ILs $[C_1C_n-4-ClIm][NTf_2]$, where $n = 4$ (red) or 8 (black). The high resolution scans are colour coded to the wide scan spectra. Note: 2p photoemissions are doubly degenerate due to spin-orbit splitting. The signals have an intensity of 1 ($2p\ 1/2$) to 2 ($2p\ 3/2$).

Table 3.1 The measured and calculated atomic compositions measured from the XPS wide scans of the chlorinated imidazolium compounds.

		Composition (%)					
		C	N	O	F	S	Cl
[C ₁ C ₄ -4-ClIm][NTf ₂]	found	40.92	10.65	14.16	23.48	7.38	3.41
	calculated	38.46	11.54	15.38	23.08	7.69	3.85
	deviation (%)	-6.40	7.71	7.93	-1.73	4.03	11.42
[C ₁ C ₈ -4-ClIm][NTf ₂]	found	50.84	9.37	11.58	17.93	7.31	2.93
	calculated	46.67	10.00	13.33	20.00	6.67	3.33
	deviation (%)	-8.94	6.30	13.13	10.35	-9.60	12.01

The high resolution scans for each sample are also displayed in **Figure 3.3** and are colour coded to the wide scans. All scans show consistent photoemissions, with the exception of the C 1s region which shows the expected growth of the aliphatic signal. The B.E.s of the heteroatoms for the chlorinated imidazolium salts are displayed in **Table 3.2**. The analogous [C₁C_nIm][NTf₂] heteroatom B.E.s are also shown as a comparison. All B.E.s are consistent with the exception of the [C₁C_n-4-ClIm][NTf₂] cationic N 1s peaks which are shifted by 0.2 eV, relative to the traditional ILs. The measured shake up/off loss in the C 1s region for the [C₁C₄-4-ClIm][NTf₂] salt is 16.8%, while the loss measured for [C₁C₈-4-ClIm][NTf₂] is 22.2%. The average value of 19.8% is close to the previously measured 20.0% signal loss for the imidazolium C 1s region.¹⁶ Therefore sp² hybridised carbon atoms will incur a 20% signal deduction when peak fitting the chlorinated imidazolium regions.

Table 3.2 The heteroatom B.E.s for the chlorinated imidazolium ILs [C₁C_n-4-ClIm][NTf₂] (n = 4 and 8) and the traditional alkyl chain analogues, [C₁C_nIm][NTf₂].

		B.E. (eV)					
		N 1s		S 2p _{3/2}	F 1s	O 1s	Cl 2p _{3/2}
Cation	Anion	Cation	Anion				
[C ₁ C ₈ -4-ClIm] ⁺	[NTf ₂] ⁻	402.3	399.5	168.9	688.9	532.7	201.9
[C ₁ C ₈ Im] ⁺	[NTf ₂] ⁻	402.1	399.5	169.0	688.8	532.7	
[C ₁ C ₄ -4-ClIm] ⁺	[NTf ₂] ⁻	402.3	399.5	169.0	688.9	532.7	201.9
[C ₁ C ₄ Im] ⁺	[NTf ₂] ⁻	402.1	399.5	169.0	688.9	532.7	

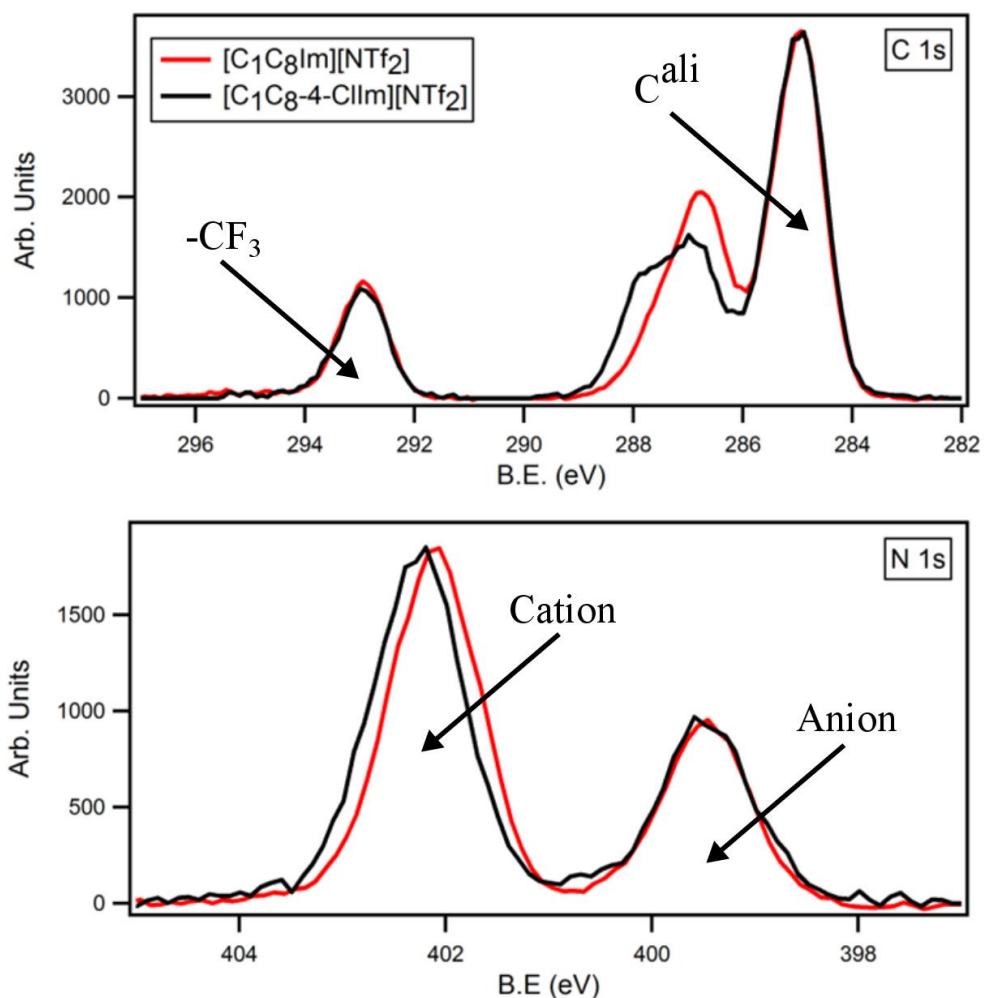


Figure 3.4 The overlaid C 1s (top) and N 1s (bottom) high resolution scans of the chlorinated $[C_1C_8-4-ClIm][NTf_2]$ salt (black) and the non-chlorinated analogue $[C_1C_8Im][NTf_2]$ (red).

The C 1s photoemissions will be presented later in the chapter. For a visual comparison of the effects of chlorination, the C 1s and N 1s regions of the $[C_1C_8Im][NTf_2]$ and $[C_1C_8-4-ClIm][NTf_2]$ ILs have been overlaid and are displayed in **Figure 3.4**. For the C 1s spectra, the only differences are within the region associated with nitrogen bound carbon. The CF₃ and aliphatic peaks remain identical between the two regions. Since a large portion of the $[C_1C_8-4-ClIm][NTf_2]$ signal now resides at a higher B.E. relative to the $[C_1C_8Im][NTf_2]$ C 1s photoemission, electron density has been removed from the imidazolium ring. Further analysis is required in order to deduce the initial and final locations of the shifting signals.

The N 1s spectra for the chlorinated and non-chlorinated ILs show two peaks, with the higher B.E. peaks integrating to twice the area of the lower B.E. peaks. The photoemission at 402.3 eV has been identified as the two imidazolium nitrogens, while the signal at 399.5 eV originates from the single nitrogen of the [NTf₂]⁻ anion. The 0.2 eV shift described above is visible in the overlaid spectra, with the [NTf₂]⁻ N 1s signals remaining at an identical B.E. for each salt. This suggests that chlorination of the C⁴ carbon results in a decrease in electron density for the whole imidazolium ring, as opposed to just the chlorine bound carbon. In order to further draw conclusions from this data, the B.E. shift observed for the C⁴ carbon will need to be examined further.

3.2.2 [C₁C_n-4-ClIm][NTf₂] C 1s Difference Spectra

If the C 1s photoemissions of the [C₁C_nIm][NTf₂] salts are subtracted from the photoemissions of the analogous [C₁C_n-4-ClIm][NTf₂] salts, difference spectra may be produced, **Figure 3.5**. Upon examination there appears to be a relatively simple shift for a small portion of the carbon signal. Quantification of this shift is possible by integration of the shifted peak area relative to the original photoemissions. The signal obtained from the [C₁C₈-4-ClIm][NTf₂] C 1s region corresponds to 0.9 carbon atoms, while the signal obtained from the [C₁C₄-4-ClIm][NTf₂] signal corresponds to 0.8 carbon atoms. Since the sp² hybridised carbon is subject to shake up/off losses, the expected values should be equal to 0.8 carbon atoms. These values support the data subtraction process, confirming that the observed signal originates from one sp² hybridised carbon atom of the imidazolium head.

The peaks from the difference spectra show a shift of +1.4 eV for the [C₁C₄-4-ClIm][NTf₂] salt and +1.3 eV for the [C₁C₈-4-ClIm][NTf₂] salt. This is a significant increase in B.E., highlighting that the C⁴ carbon is left electron deficient as a result of the EWG. Both difference spectra have FWHMs for the start and end peaks of 0.9 and 1.0 eV respectively, this value is typical for a single carbon photoemission.^{16-18,34}

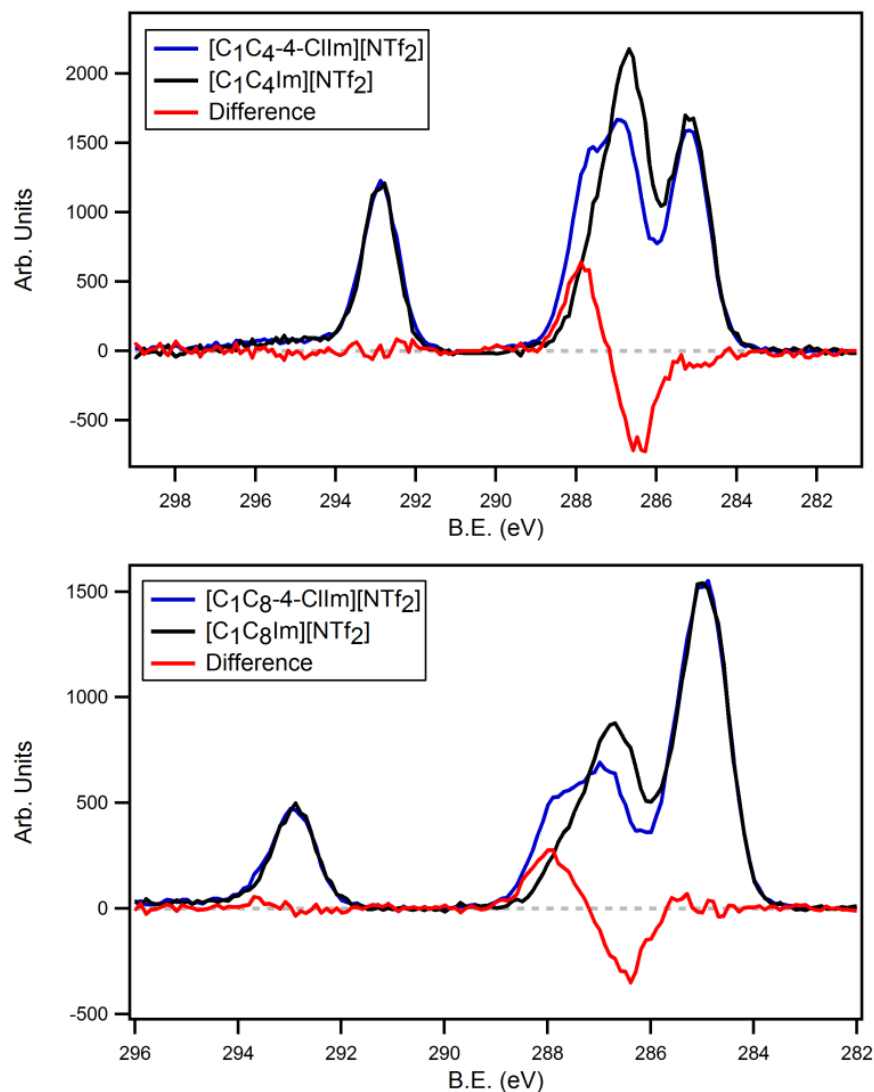


Figure 3.5 The C1s regions for [C₁C_n-4-ClIm][NTf₂] (blue), where $n = 4$ (top) and 8 (bottom). The analogous traditional [C₁C_nIm][NTf₂] C 1s regions (black) are overlaid and the resulting difference spectra are shown (red).

The two difference spectra have been overlaid and normalised to the area of the positive peak in order to examine any changes between the two shifts, **Figure 3.6**. The spectra appear to show remarkable similarities in their structures. The data subtraction process essentially cancels any photoemissions not involved in the shifting of electron density. The deviation about the 285.0 eV position may be a result of aliphatic carbon contamination or poor spectra alignment (during the generation of the difference spectrum). However, the inconsistency is small and situated away from the main shifts, therefore it may be considered negligible.

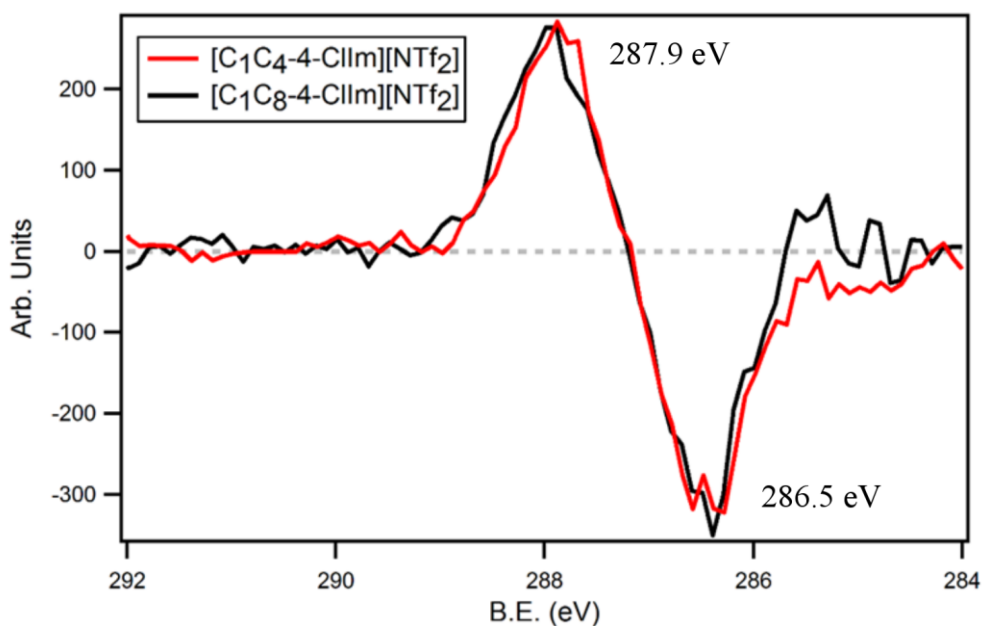


Figure 3.6 The overlaid difference spectra as obtained from the subtraction of the $[C_1C_n\text{Im}][\text{NTf}_2]$ C 1s photoemissions from the $[C_1C_n\text{-}4\text{-ClIm}][\text{NTf}_2]$ C 1s photoemissions. The spectra are normalised to the area of the positive signals.

A structural representation of the shifting signal between the chlorinated and non-chlorinated salts is presented in **Figure 3.7**. For the chlorinated salt, the $C^{4,5}$ component should now be split into two different peaks with significantly different B.E.s. The resulting 5 component model now contains the C^2 (green), C^4 (dark red), C^5 (blue), $C^{6,7}$ (orange) and C^{ali} (black) components with the respective ratios 1:1:1:2.5:3.75 for $[C_1C_4\text{-}4\text{-ClIm}][\text{NTf}_2]$ and 1:1:1:2.5:8.75 for $[C_1C_8\text{-}4\text{-ClIm}][\text{NTf}_2]$, after accounting for shake up off losses.

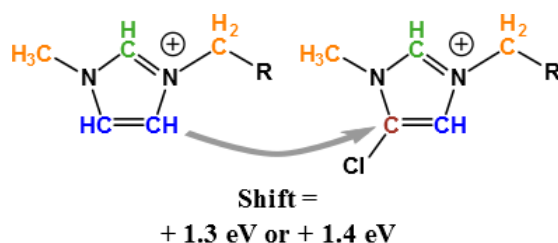


Figure 3.7 The structural representation of the shifts observed upon chlorination of the C^4 carbon atom of the imidazolium ring. The B.E. values have been obtained from the difference spectra presented above.

3.2.2.1 Peak Positions in [C₁C_n-4-ClIm][NTf₂] Difference Spectra

The negative signal of the difference spectrum appears at 286.5 eV and indicates the initial position of the C⁴ carbon photoemission, before the electronegative chlorine is bound to it. The positive signal of the difference spectrum appears at 287.9 eV, this indicates the C⁴ carbon with chlorine bound to it. The current peak fitting model places the C^{4,5} carbon atoms at a B.E. of 287.1 eV (the [C₁C₈Im][NTf₂] peak fitted C 1s region was shown at the beginning of this chapter, **Figure 3.2**). This suggests that the position of the C^{4,5} component in the imidazolium peak fitting model is incorrect. The true C^{4,5} photoemission actually occupies a B.E. position that has been previously assigned to the C^{6,7} carbon atoms. This means that the positions of the C^{4,5} and C^{6,7} peaks should be reversed, in order to more accurately represent the photoemissions of imidazolium salts. The B.E. shift between the initial and final locations of the C⁴ photoemission can also be utilised in order to confirm this result. Although the both chlorinated and non-chlorinated salts are charge corrected to the C^{ali} component, confirmation of the C^{4,5} component position without the need for accurate B.E.s provides an excellent method to check the observed result. Such methods may be implemented for future difference spectra, where robust charge correction procedures are not as developed for the originating photoemissions spectra (e.g. ILs without rich aliphatic tails or fluorinated anions).

3.2.2.2 Peak Shifting in [C₁C_n-4-ClIm][NTf₂] Difference Spectra

Figure 3.8 shows the structure of the [C₁C₈-4-ClIm][NTf₂] salt with the chlorinated imidazolium fitting model assignments. The addition of chlorine to the aromatic ring should not significantly affect the photoelectron signal of the C^{6,7} carbon environments. Therefore we can assume that the C^{6,7} component will remain stationary and at the same B.E. in both chlorinated and non-chlorinated imidazolium salts. A rigorous C 1s fitting model must utilise FWHM constraints. Peak width have been limited to 0.8-1.5 eV for the large

C^{ali} (C_8) photoemission and 0.8-1.2 eV for all other photoemissions.^{35,36} In this model, the C^2 , C^4 and C^5 peaks FWHMs have also been set to be equal.

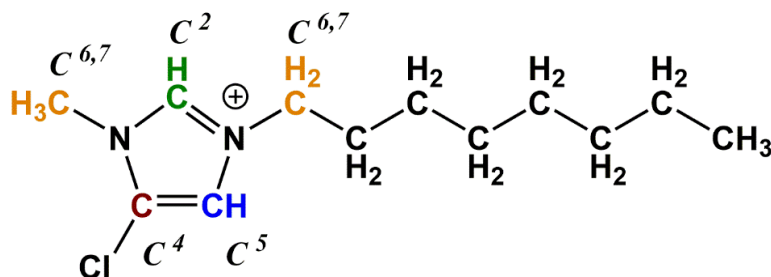


Figure 3.8 The structure of the $[C_1C_8-4-ClIm][NTf_2]$ salt with carbon components labels: C^2 (green), C^4 (dark red), C^5 (blue) and $C^{6,7}$ (orange).

As with the current C 1s model, the C^2 carbon of the imidazolium ring should have the highest B.E., while the electron rich aliphatic carbon chains should have the lowest B.E.s. The B.E. of the chlorinated C^4 carbon is now known from the generated difference spectra, i.e. the position of the positive peak at 287.9 eV. The C^5 and $C^{6,7}$ components are more difficult to accurately place. Although the negative peak of the difference does reveal the position of the C^5 component, peak variations should still be examined in order to provide a more comprehensive examination of the photoemission spectra.

The order of the $C^{4,5}$ and $C^{6,7}$ components may be reversed in the fitting model of the traditional $[C_1C_8Im][A]$ salts, without affecting the ability of the predicted photoemission to match the acquired data. **Figure 3.9** shows the current C 1s fitting for $[C_1C_8Im][NTf_2]$, labelled as model 1, and the alternative fitting whereby the $C^{4,5}$ and $C^{6,7}$ peaks are reversed, labelled as model 2. Both models accurately reproduce the measured CPS for the non-chlorinated imidazolium salt. The corresponding model may also be applied to the chlorinated $[C_1C_8-4-ClIm][NTf_2]$ C 1s photoemission, with the $C^{4,5}$ at a higher B.E. (model A) and lower B.E. (model B) than the $C^{6,7}$ component. Model A and model B also appear to accurately replicate the measured CPS for the chlorinated $[C_1C_8-4-ClIm][NTf_2]$ C 1s region. The B.E. shifts between the C^4 and C^5 components are also shown on the spectra.

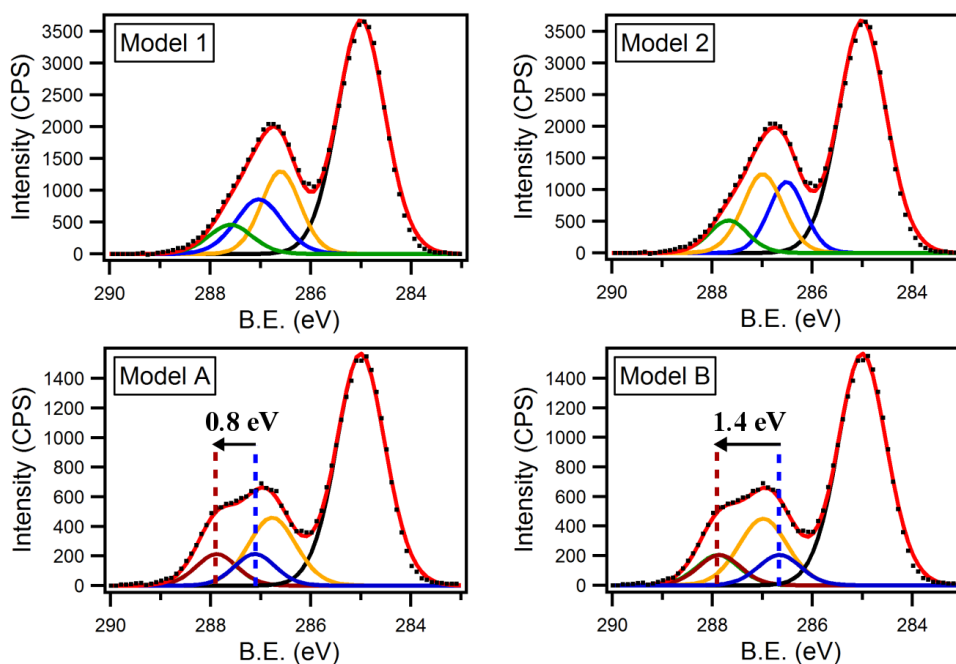


Figure 3.9 The two types of model that may be used to fit the C 1s regions of imidazolium salts. Model 1 is the current C 1s fitting used for imidazolium salts and model A is the corresponding adaption for the $[C_1C_8-4-ClIm][NTf_2]$ C 1s photoemission. Model 2 and model b have the $C^{4,5}$ and $C^{6,7}$ component orders reversed. Note: FWHMs may alter for each fitting, however only within the constraints.

The B.E.s obtained for the fittings of each model are presented in **Table 3.3**, where the analogous data obtained from the $[C_1C_4Im][NTf_2]$ and $[C_1C_4-4-ClIm][NTf_2]$ C 1s fittings is also summarised. Examination of the acquired B.E. values may provide a more detailed investigation of the two potential fitting models. The ability to provide reasonable B.E. values across multiple spectra of structurally related samples is an important and necessary feature of a photoemission model. For example, model 1 and model A both have the $C^{6,7}$ component at a lower B.E., relative to the C^4 and C^5 carbon photoemissions. These two models may therefore be compared in terms of the B.E. changes for each individual component. Any shifts in B.E. that are larger than the 0.1 eV error reflect an instability in the ‘robustness’ of the model. Also, the correct peak arrangement should show a component B.E. shift (between each model type: 1 to A or 2 to B) equal to the observed B.E. shift (as obtained from the difference spectrum). In this way the correct positions of the $C^{4,5}$ and $C^{6,7}$ components can be identified without the need for precise B.E. values.

Table 3.3 The B.E.s for the two potential fitting models that are obtained when swapping the order of the C 1s C^{4,5} and C^{6,7} components for [C₁C₈Im][NTf₂] or the C⁵ and C^{6,7} components for [C₁C₈-4-ClIm][NTf₂].

IL	model	Binding Energy (eV)						
		C ²	C ⁴	C ⁵	C ^{6,7}	C ^{ali}	CF ₃	
[C ₁ C ₈ Im][NTf ₂]	1	287.6		287.1		286.6	285.0	292.9
	2	287.7		286.5		287.0	285.0	293.0
[C ₁ C ₈ -4-ClIm][NTf ₂]	A	287.9	287.9		287.1	286.8	285.0	293.0
	B	287.9	287.9		286.7	287.0	285.0	293.0
[C ₁ C ₄ Im][NTf ₂]	1	287.7		287.1		286.6	285.2	293.0
	2	287.7		286.6		287.0	285.2	293.0
[C ₁ C ₄ -4-ClIm][NTf ₂]	A	287.7	287.9		287.2	286.7	285.2	292.9
	B	287.7	287.9		286.7	286.9	285.2	292.9

A visual representation of the B.E. shifts between each model has been constructed and is displayed in **Figure 3.10**, where each alkyl chain analogue (C₄ and C₈) is presented in a separate plot. For the [C₁C₄Im][NTf₂] and [C₁C₄-4-ClIm][NTf₂] shifts, both models appear to provide reasonable B.E.s, with no shifting larger than 0.1 eV between the two photoemissions (except for the C⁴ component). The [C₁C₈Im][NTf₂] and [C₁C₈-4-ClIm][NTf₂] B.E. shifts do not reflect this stability. Both fitting models appear to deviate by more than 0.1 eV for the majority of the photoemissions. At first this may be highlighting a weakness in the versatility of the models, however the 0.2 eV shift observed for the imidazolium N 1s signal does suggest that the imidazolium ring is left electron deficient after chlorination.

Inspection of the C⁴ B.E. shifts clearly shows that the model B and model 2 peak arrangement provides a reasonable value that coincides with the peak shifting observed in the difference spectrum. The shifts observed for the C⁴ component in the model A and model 1 peak arrangement are insufficient to explain the observed shift. This data also suggests that the current C 1s peak fitting model of the imidazolium salts is incorrect. In fact, the C^{6,7} component should occupy a higher B.E. than the imidazolium C^{4,5} component. Model B and model 2 are therefore a more accurate representation of the true photoemissions of imidazolium C 1s spectra.

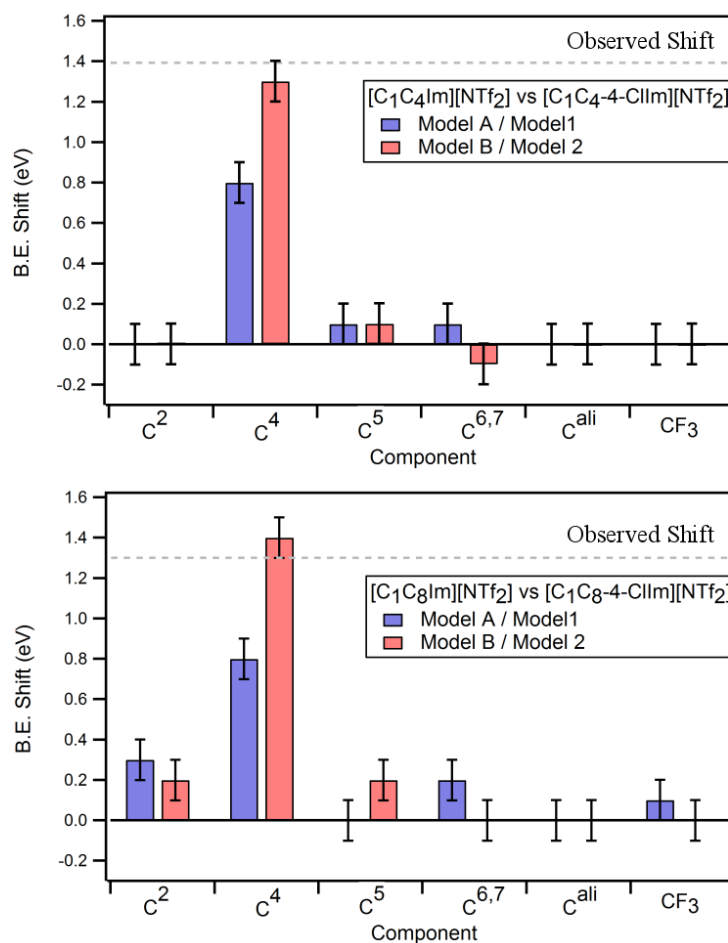


Figure 3.10 The B.E. shifts that occur upon chlorination of the imidazolium ring. The two alternative peak arrangements, Model A/Model 1 ($C_{4,5}$ or C_5 to the L.H.S of $C_{6,7}$) and Model B/Model 2 ($C_{4,5}$ or C_5 to the R.H.S of $C_{6,7}$) provide the shifts shown in the bar charts. The observed B.E. shift is labelled and shown as a dashed line.

The B.E.s obtained from each chlorinated and non-chlorinated C 1s region with the updated fitting model have been summarised in **Table 3.4**. The updated peak fitting of the [C₁C₈Im][NTf₂] C 1s region is also displayed in **Figure 3.11**. Overall, two methods of analysis have been used to determine the order of the C^{4,5} and C^{6,7} components from the data obtained from the difference spectra. The C⁴ carbon B.E.s obtained from the positive and negative peaks of the difference were used to confirm the initial and final locations of the C⁴ component. This suggested that the photoemission originates from the location previously assigned to the C^{6,7} component. This has been confirmed by implementation of two potential fitting models, and the subsequent correlation of the B.E. shifts to the shifts observed in the difference spectra.

Table 3.4 The updated C 1s B.E.s for the chlorinated imidazolium ILs $[C_1C_n-4-ClIm][NTf_2]$ and the traditional alkyl chain analogues, $[C_1C_nIm][NTf_2]$.

		B.E. (eV)					
		C 1s					
Cation	Anion	C ²	C ⁴	C ⁵	C ^{6,7}	C ^{ali}	CF ₃
$[C_1C_8-4-ClIm]^+$	$[NTf_2]^-$	287.7	287.9	286.7	286.9	285.0	292.9
$[C_1C_8Im]^+$	$[NTf_2]^-$	287.7	286.6	287.0	285.0	293.0	
$[C_1C_4-4-ClIm]^+$	$[NTf_2]^-$	287.9	287.9	286.7	287.0	285.2	293.0
$[C_1C_4Im]^+$	$[NTf_2]^-$	287.7	286.6	287.0	285.2	293.0	

The analysis of the C⁴ chlorinated imidazolium salts relative to the non-chlorinated analogues has provided sufficient proof of a previously incorrect imidazolium C 1s fitting model. The C⁵ carbon photoemission is most likely coincident with the C⁴ signal due to the similarity of the local environment. The C^{6,7} carbon has been located *via* the subsequent peak fitting of the imidazolium C 1s region. Although the known position of the C^{4,5} component will produce a more accurate B.E. for the C^{6,7} component, further analysis is required. Future experiments involving chlorination of the C⁶ or C⁷ carbon atoms may be utilised in the same way to identify the true B.E. of the C^{6,7} component.

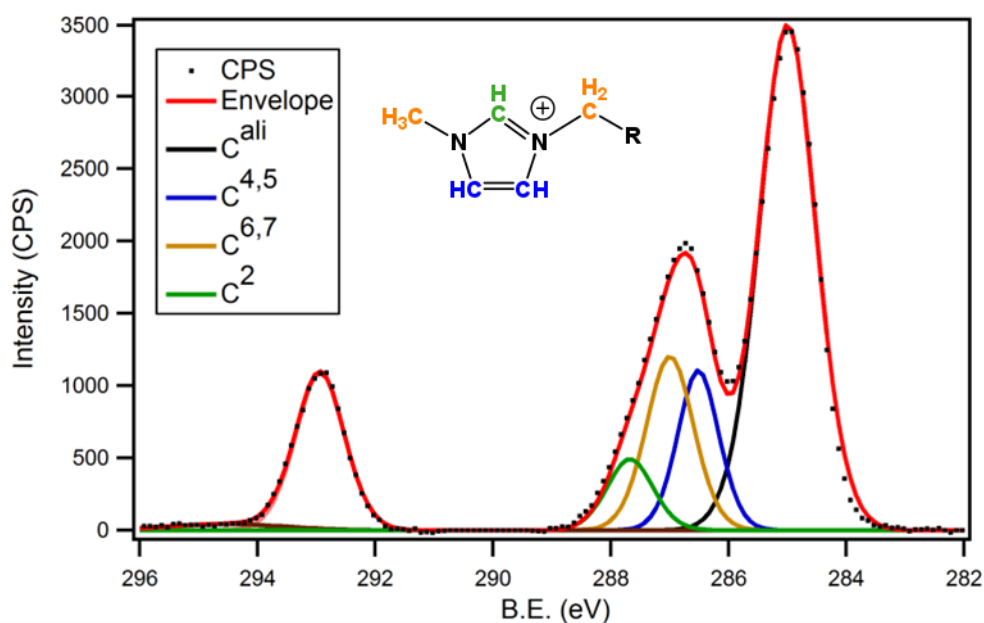


Figure 3.11 The updated fitting model for the $[C_1C_8Im][NTf_2]$ C 1s region, showing the C^{6,7} component at a higher B.E. than the C^{4,5} component.

3.3 Chlorinated Pyridinium ILs

A similar analysis may also be applied to chlorinated pyridinium ionic liquids. The pyridinium cation can be chlorinated at the 2, 3- or 4-positions of the pyridinium ring. By acquiring the XP spectra of these compounds and analysing their C 1s photoemissions relative to their non-chlorinated analogues, the current C 1s peak fitting of pyridinium ILs may also be scrutinised. Although the pyridinium C 1s region³⁷ does not appear as complex as the imidazolium, investigation of the true photoemission B.E.s is a necessary requirement for the development of robust and accurate peak fitting models.

The current pyridinium C 1s model is shown for [C₈Py][NTf₂] in **Figure 3.12**, where the carbon components are colour coded to the cationic structure shown on the plot. The simple peak fitting breaks the [C₈Py]⁺ cation into three components.¹⁶ The electron rich aliphatic tail (C^{ali}), the carbons at the back of the pyridinium ring (C^{3,4,5}) and the nitrogen bound carbon atoms (C^{2,6,7}). As with all ILs of C_n ≥ 8, the spectrum has been charge corrected to the C^{ali} component which is set at 285.0 eV. The resulting peak fitting of the [C₈Py][NTf₂] C 1s region places the C^{3,4,5} component at 286.1 eV and the C^{2,6,7} component at 287.1 eV.

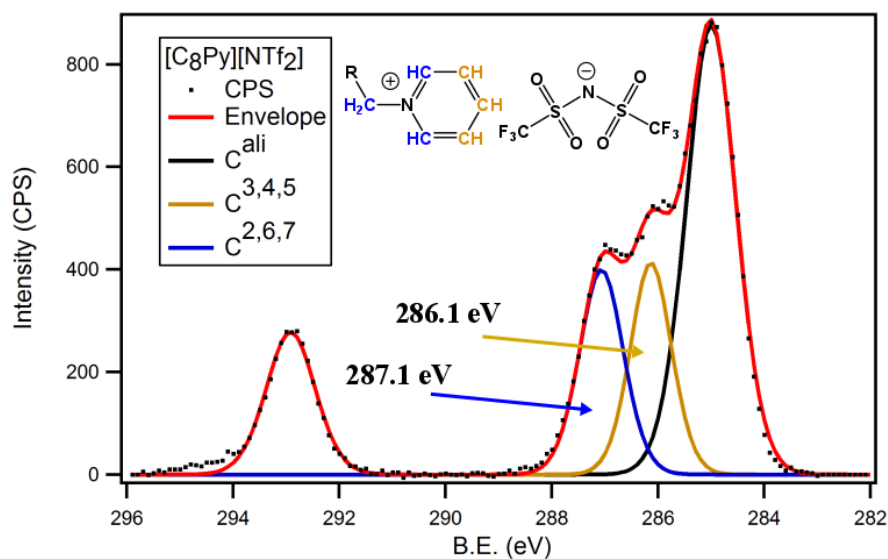


Figure 3.12 The peak fitted high resolution C 1s region for [C₈Py][NTf₂] with the colour coded structural representation. The XP spectrum is charge corrected to the C^{ali} component which is set at 285.0 eV.

The following section will present the XP spectra of 2-chloropyridinium and 3-chloropyridinium ILs, **Figure 3.13**. By subtracting the analogous non-chlorinated C 1s photoemissions from the acquired C 1s regions, a series of difference spectra may be produced. The initial and final locations of the chlorinated carbon will then be revealed through the observed shifting of electron density. The C 1s models for the chlorinated and non-chlorinated ILs may then be refined according to the acquired data, as with the imidazolium IL at the beginning of this chapter.

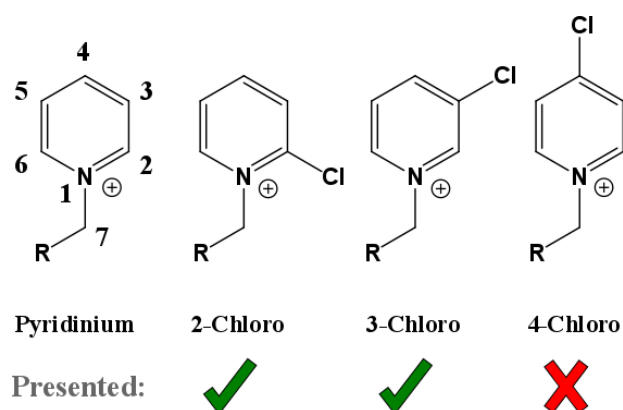


Figure 3.13 The numbering scheme for pyridinium ILs and the various chlorinated pyridinium analogues. The 2-chloropyridinium and 3-chloropyridinium salts are presented in this section.

3.3.1 N-Alkyl-2-Chloropyridinium Salts

The 2-chloropyridinium ILs are abbreviated as $[C_n\text{-2-ClPy}][A]$ in order to denote that the chlorine is bound to the 2-position of the pyridinium ring. The chlorinated salts were synthesised according to a known literature procedure.³⁸ Alkylation of 2-hydroxypyridine gave alkylpyridone oils that were chlorinated using phosphorus oxychloride at 100 °C for 2 hr, **Figure 3.14**. The subsequent anion metathesis with $\text{Li}[\text{NTf}_2]$ has not been reported, however under standard conditions (water, room temperature, air) the 2-chloropyridinium salts gave the corresponding $[\text{NTf}_2]^-$ ILs. Hydrolysis of the 2-chloropyridinium salts back to the starting 2-pyridone or 2-hydroxyl-pyridine was not observed.

Two $[C_n\text{-2-ClPy}][\text{NTf}_2]$ salts with alkyl chains of lengths $n = 4$ and $n = 8$ were prepared. Ion chromatography was not used in the determination of anionic

impurities as the basic sodium hydroxide (200 mM) eluent would most likely displace the chlorine of the pyridinium ring,^{39–41} potentially damaging the system. Instead, samples were tested with a concentrated aqueous solution of AgNO₃ to ensure no residual halide impurities remained. Chlorination of the pyridone could potentially result in a range of polyatomic phosphorus containing anions, due to the hydrolysis of POCl₃. XPS analysis is therefore the best potential method in the determination of anionic impurities for these particular samples.

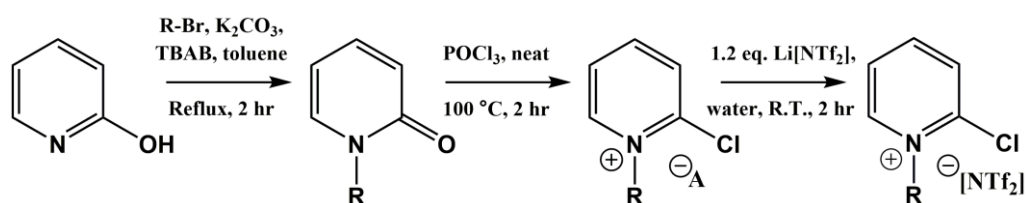


Figure 3.14 The synthetic scheme for the preparation of the chlorinated pyridinium salts used in this work. $R = C_4$ or C_8 .

3.3.1.1 XPS of [C_n-2-ClPy][NTf₂] salts

The wide scans for the two [C_n-2-ClPy][NTf₂] ILs are shown in **Figure 3.15**, where the photoelectron signals are labelled on the spectra. Only the expected elements are observed, confirming the absence of polyatomic phosphorus containing anions. The elemental compositions of the samples have been measured and compared to the calculated values, **Table 3.5**. The experimentally measured values are largely within 10% of the expected atomic compositions. The [C₈-2-ClPy][NTf₂] XP spectra are charge corrected to the aliphatic signal (C^{ali} component) which is set at 285.0 eV. The [C₄-2-ClPy][NTf₂] spectra have been charge referenced to the cationic N 1s signal that was obtained from the charge corrected [C₈-2-ClPy][NTf₂] spectra. The high resolution scans are also presented in **Figure 3.15**, where the spectra are colour coded to the signals of the wide scans.

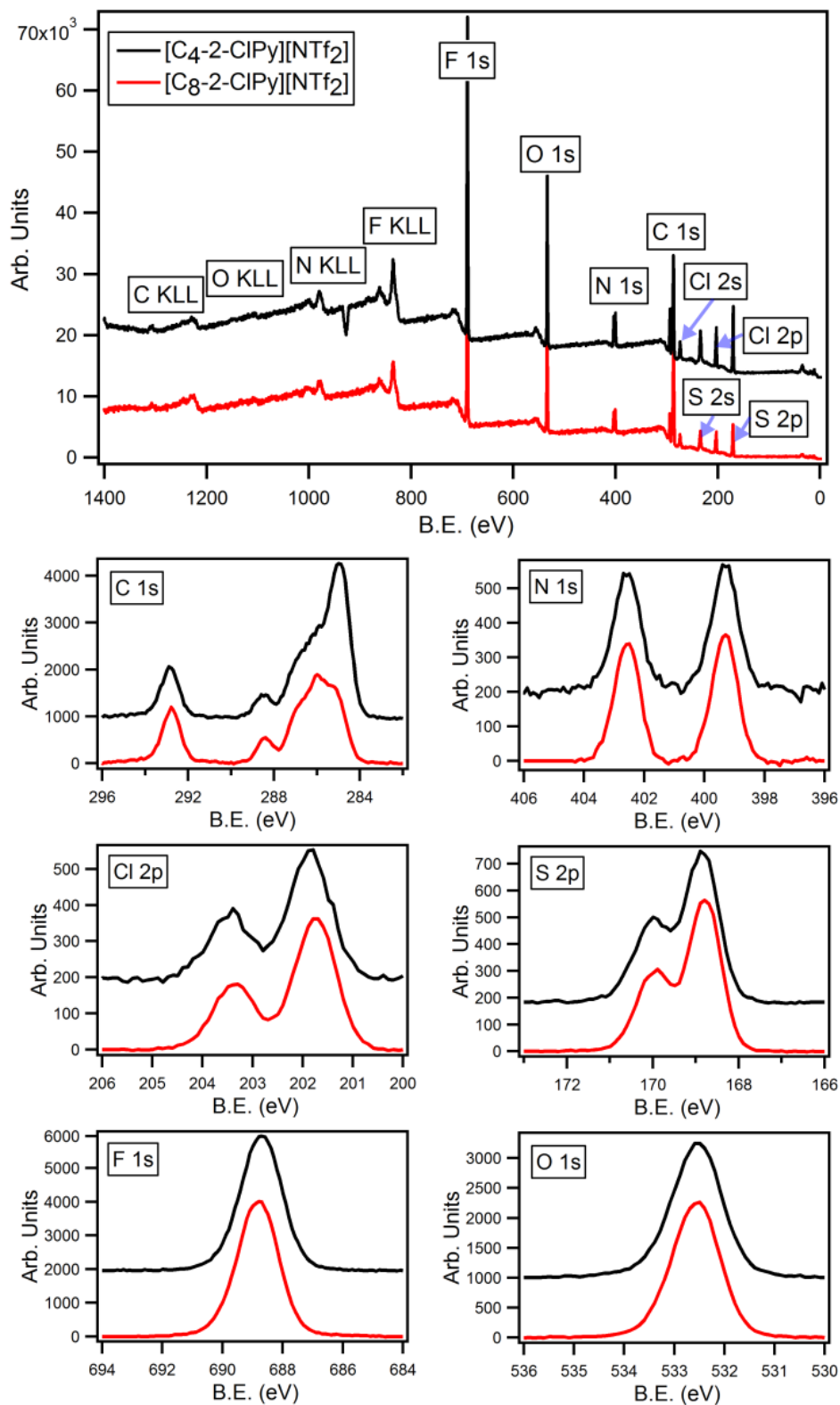


Figure 3.15 The XPS wide and high resolution scans for the chlorinated pyridinium ILs [C_n-2-ClPy][NTf₂], where $n = 4$ (black) and $n = 8$ (red). All scans are colour coded to the legend displayed on the top plot.

Table 3.5 The measured and calculated elemental compositions as measured from the XPS wide scans of the $[C_n-2-ClPy][NTf_2]$ salts, where $n = 4$ or $n = 8$. The deviation between the two values is also shown.

		Composition (%)					
		C	N	O	F	S	Cl
$[C_4-2-ClPy][NTf_2]$	found	46.61	7.14	13.37	21.31	7.47	3.74
	calculated	42.31	7.69	15.38	23.08	7.69	3.85
	deviation (%)	-10.16	7.15	10.73	7.67	2.86	2.86
$[C_8-2-ClPy][NTf_2]$	found	54.54	6.03	11.68	18.60	6.18	2.97
	calculated	50.00	6.67	13.33	20.00	6.67	3.33
	deviation (%)	-9.08	9.60	12.38	7.00	7.35	10.81

All high resolution regions show consistent photoemissions between the two salts, with the exception of the C 1s region which shows the expected growth of the aliphatic chain. The Cl 2p region shows a single chlorine environment (the 2p orbital appears as a doublet due to spin-orbit coupling), confirming the absence of residual chloride impurities. The N 1s scans show two nitrogen environments with a 1:1 area ratio upon integration. These signals originate from the cation (higher B.E.) and the anion (lower B.E.) nitrogen environments. The measured shake up/off signals from the C 1s regions correspond to 12.9% signal loss per sp^2 carbon for $[C_4-2-ClPy][NTf_2]$ and 9.9% for $[C_8-2-ClPy][NTf_2]$. The average value of 11.4% is relatively close to the previously measured 10.0% loss for pyridinium ILs, therefore sp^2 hybridised carbons will be deducted 10% of their area when developing pyridinium C 1s fitting models.

The heteroatom B.E.s obtained from the $[C_n-2-ClPy][NTf_2]$ salts are summarised in **Table 3.6**. The nitrogen N 1s signals of the cation are identical to those of the non-chlorinated ILs, however the N 1s signals originating from the $[NTf_2]^-$ anion appear to be 0.2 eV lower than expected. All other B.E.s appear consistent for both chlorinated and non-chlorinated ILs, with no deviation larger than the 0.1 eV error.

Table 3.6 The heteroatom B.E.s from the $[C_n\text{-}2\text{-ClPy}][\text{NTf}_2]$ salts, where $n = 4$ or 8 . The B.E.s of the non-chlorinated analogues are also presented as a comparison.

		B.E. (eV)					
		N 1s		F 1s	O 1s	S 2p _{3/2}	Cl 2p _{3/2}
Cation	Anion	Cationic	Anionic				
$[\text{C}_4\text{Py}]^+$	$[\text{NTf}_2]^-$	402.6	399.5	688.8	532.6	169.0	
$[\text{C}_4\text{-}2\text{-ClPy}]^+$	$[\text{NTf}_2]^-$	402.6	399.3	688.8	532.6	168.9	201.8
$[\text{C}_8\text{Py}]^+$	$[\text{NTf}_2]^-$	402.6	399.5	688.8	532.6	169.0	
$[\text{C}_8\text{-}2\text{-ClPy}]^+$	$[\text{NTf}_2]^-$	402.6	399.3	688.8	532.6	168.9	201.9

The shifted N 1s regions of the chlorinated and non-chlorinated pyridinium salts have been overlaid and normalised to the areas of the corresponding F 1s signals as a visual comparison, **Figure 3.16**. The N 1s signal of the pyridinium cation should theoretically be expected to increase in B.E. due to the proximity of the electron withdrawing chlorine atom. However, the cationic N 1s signals remain at a constant B.E. and the N 1s signal of the anion has shifted to a lower B.E.

The chlorine substituent could act to reduce charge transfer from the $[\text{NTf}_2]^-$ anion to the pyridinium nitrogen *via* steric hindrance. This may increase the charge upon the $[\text{NTf}_2]^-$ nitrogen, causing a decrease in the observed B.E. of the anion. A 0.2 eV shift may not be considered significant as both 399.5 eV and 399.3 eV are within the 0.1 eV error of 399.4 eV. Overall, the small 0.2 eV shift is not large enough to provide conclusive evidence of the anion-cation interactions of 2-chloropyridinium ILs. Further experimentation whereby progressively larger groups are appended to the 2- and 6-positions of the pyridinium cation may provide stronger evidence. For the purpose of this research these shifts may be considered negligible.

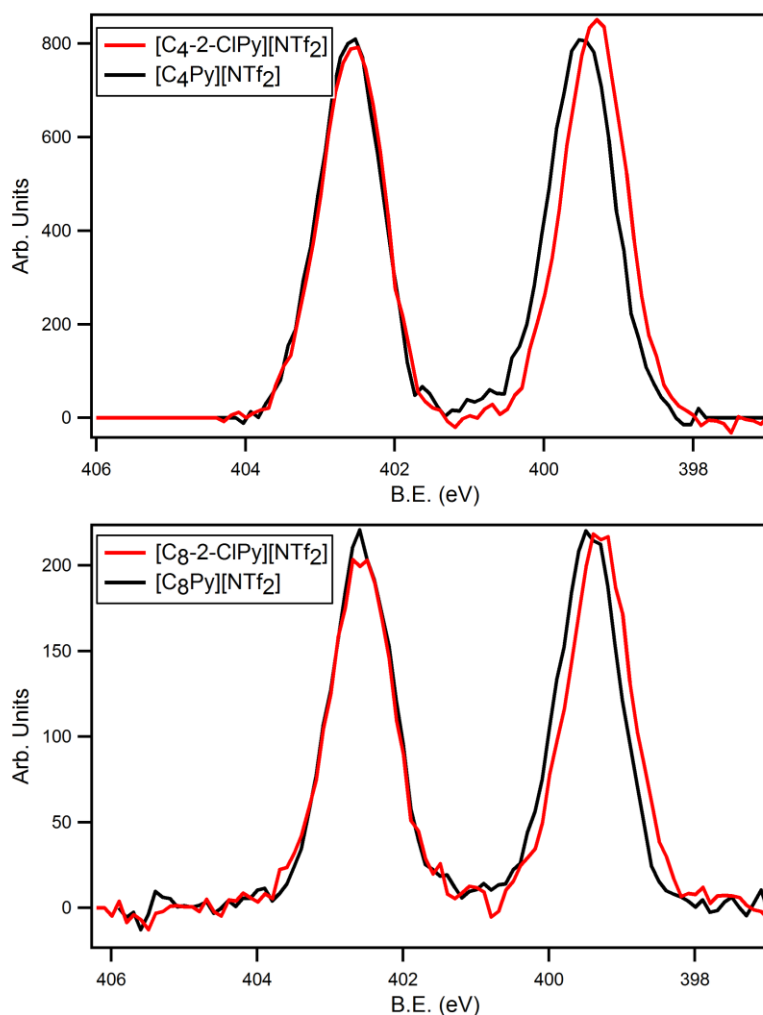


Figure 3.16 The N 1s high resolution regions for $[C_n-2-ClPy][NTf_2]$, $n = 4$ and 8 (red), with the analogous $[C_nPy][NTf_2]$ spectra overlaid (black). The spectra are charge corrected to the C^{ali} component for $n = 8$, and the $n = 4$ spectra are referenced to B.E. obtained for the N 1s imidazolium peak (402.6 eV). Charge correction to each individual F 1s peak (688.8 eV) also produces identical data.

However, similar B.E.s for the N 1s signal of $[NTf_2]^-$ have previously been observed for bulky ammonium and phosphonium ILs that possess long aliphatic chains, **Table 3.7**. The mobile electron rich alkyl groups are thought to wrap around the nitrogen core of the cation, shielding any potential charge transfer that may occur between the ion pairs.¹¹ Again, further experimentation is required in order to confirm that the observed shift is a result reduced charge transfer.

Table 3.7 The B.E. values of cationic and anionic N 1s peaks for a range of [NTf₂]⁻ ILs.

	B.E. (eV)			Reference
	Cation	Anion	Difference	
[C ₁ C ₈ Im] ⁺	402.1	399.5	0.6	
[C₁C₈-4-ClIm]⁺	402.3	399.5	0.8	
[C ₈ Py] ⁺	402.6	399.5	1.1	
[C₈-2-ClPy]⁺	402.6	399.3	1.3	
[C ₁ C ₈ Pyrr] ⁺	402.7 ^a	399.5 ^a	1.2	11
[N _{4,4,4,1}] ⁺	402.5 ^b	399.3 ^b	1.2	11
[P _{4,4,4,1}] ⁺		399.3 ^b		18

3.3.1.2 Peak Shifting in the [C_n-2-ClPy][NTf₂] C 1s Region

As before, by overlaying the C 1s photoemissions obtained from the chlorinated and non-chlorinated ILs, one spectrum may be subtracted from another to produce difference spectra. The original photoemissions and the resulting difference spectra are displayed in **Figure 3.17**. The positive signals of the difference spectra are equal to 0.8 carbons for both the C₄ and C₈, when measured relative to the [C_n-2-ClPy][NTf₂] photoemissions. When accounting for shake up/off losses each peak should integrate to an area that is equal to 0.9 carbon atoms. Although there is a small discrepancy, the shifting electron density is almost equal to one sp² hybridised carbon atom. The 1.3 eV (C₄) and 1.4 eV (C₈) shifts are similar to those found for the chlorinated imidazolium salts. This suggests that chlorine functionalisation produces a consistent level of electron withdrawal for the carbon atom that it is bound to.

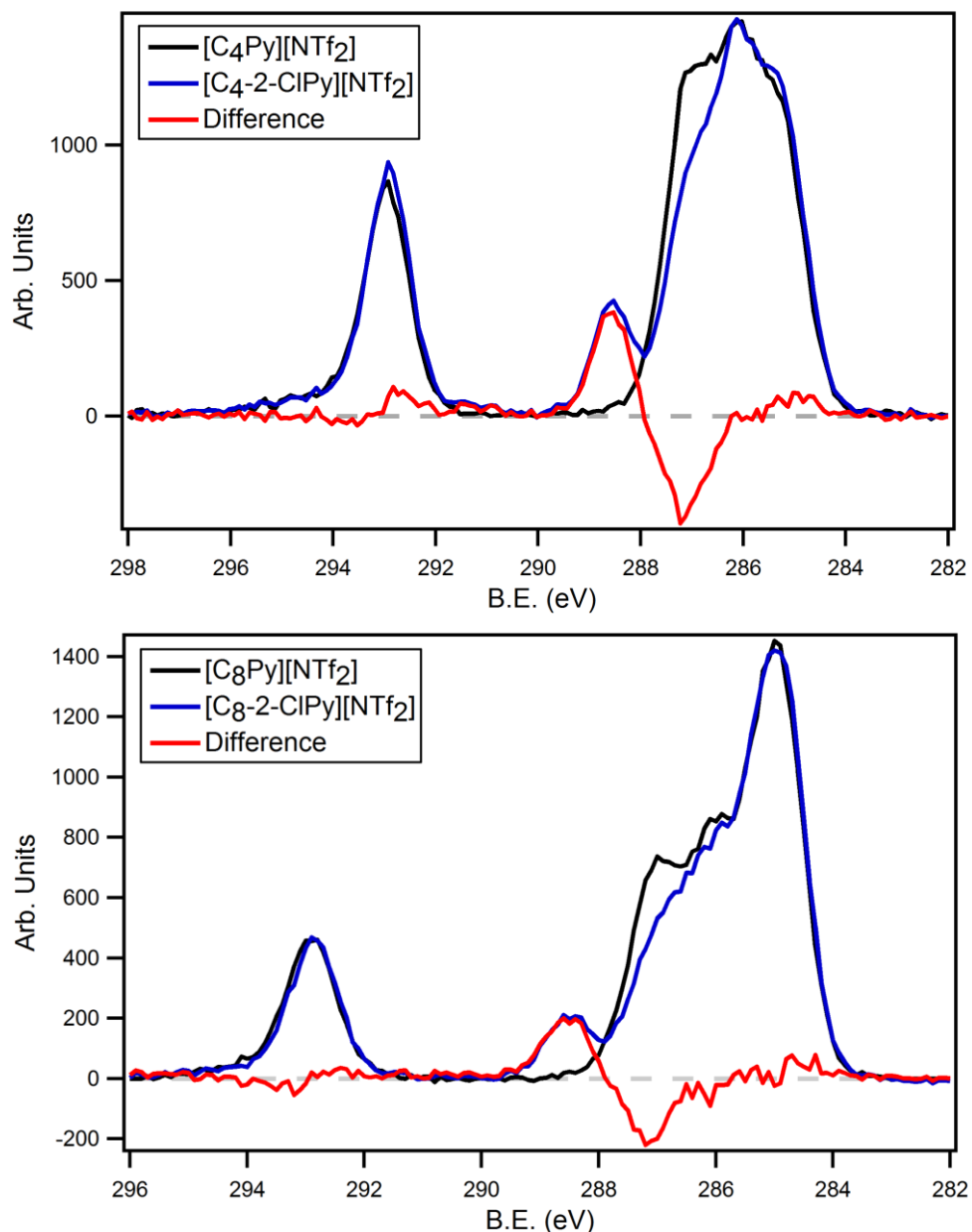


Figure 3.17 The difference spectra obtained by subtraction of the $[C_n\text{Py}][\text{NTf}_2]$ C 1s photoemissions from the $[C_n\text{-2-ClPy}][\text{NTf}_2]$ C 1s photoemissions. The signals are plotted against the $[C_n\text{-2-ClPy}][\text{NTf}_2]$ B.E.s.

The negative peaks for both $[C_n\text{-2-ClPy}][\text{NTf}_2]$ difference spectra appears at 287.1 eV, while the positive peaks appears at 288.4 eV. The similarities in the difference spectra become more apparent when they are overlaid and normalised to the area of the positive signal, **Figure 3.18**. As with the imidazolium difference spectra, both generated signals appear identical which supports the data subtraction process. The relative change in electron density is clearly visible by inspecting the original photoemissions relative to each

other. The only changes appear to occur at the locations of the positive and negative signals of the difference, i.e. the C^{ali} , $C^{3,4,5}$ and $-CF_3$ carbon photoemissions are consistent.

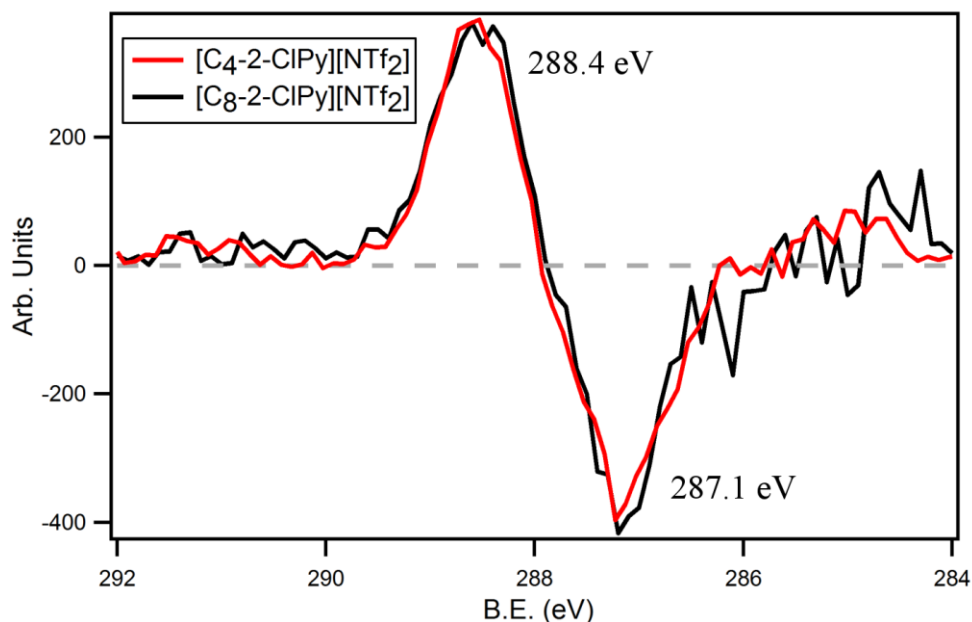


Figure 3.18 The overlaid difference spectra for $[C_n-2-ClPy][NTf_2]$ ($n = 4$ and 8), the spectra have been normalised to the area of the positive signal.

Figure 3.19 shows a structural representation of the shifting C^2 carbon photoemission upon chlorination of the pyridinium ring. The initial peak positions of the difference spectra (287.1 eV) reveals that the C^2 carbon has previously been correctly assigned, **Figure 3.2**. The C^6 carbon environment is identical to the C^2 , therefore both signals have been confirmed *via* the generation of difference spectra. Chlorination of the pyridinium ring has therefore provided XP spectra that support the current pyridinium C 1s peak fitting model. With knowledge of the C^2 position after chlorination, the $[C_n-2-ClPy][NTf_2]$ C 1s regions may be peak fitted to a higher level of certainty.

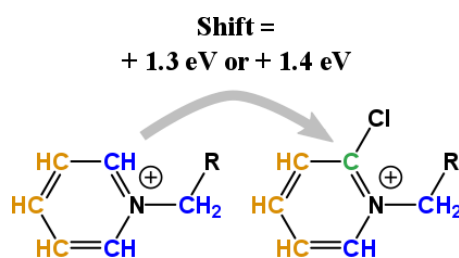


Figure 3.19 The B.E. shift observed for the C^2 carbon upon chlorination of the 2-position of the pyridinium ring.

3.3.1.3 Peak Fitting the $[C_n-2-ClPy][NTf_2]$ C 1s region

The location of the C^2 component is known as chlorination has shifted the peak from the bulk of the $[C_n-2-ClPy][NTf_2]$ C 1s photoemission. The location of the $C^{6,7}$ has been confirmed from the generated difference spectra, the signal should remain at the same position for the $[C_n-2-ClPy][NTf_2]$ salts. The $C^{3,4,5}$ component also appears to remain constant for the chlorinated pyridinium, as there are no other visual changes between the chlorinated and non-chlorinated photoemissions. Therefore, all peaks are expected to remain identical to the non-chlorinated analogues, with the exception of the shifting C^2 carbon. Following **Figure 3.20**, the new fitting model contains C^2 (green), $C^{3,4,5}$ (orange), $C^{6,7}$ (blue) and C^{ali} (black) components of the respective ratios 0.9:2.8:1.8:3 for $[C_4-2-ClPy][NTf_2]$ and 0.9:2.8:1.8:7 for $[C_8-2-ClPy][NTf_2]$. FWHMs were constrained to 0.8-1.5 eV for C^{ali} and 0.8-1.2 eV for all other components.

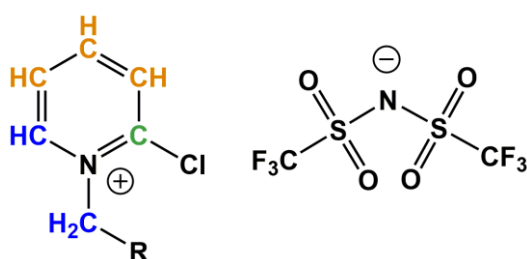


Figure 3.20 The new fitting model proposed for the chlorinated pyridinium salts, $[C_n-2-ClPy][NTf_2]$, where $n = 4$ or $n = 8$. The components shown have been assigned C^2 (green), $C^{3,4,5}$ (orange), $C^{6,7}$ (blue) and C^{ali} (black).

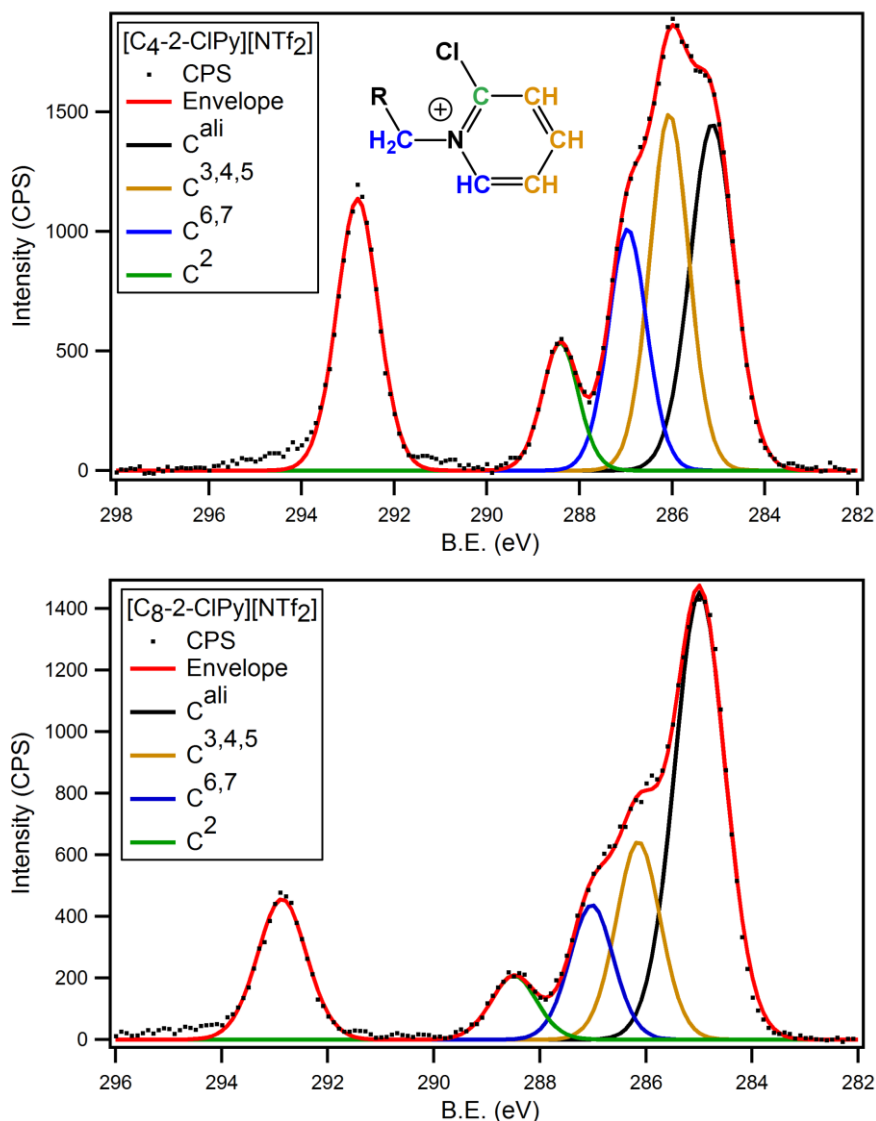


Figure 3.21 The peak fitted C 1s photoemissions of [C₄-2-ClPy][NTf₂] (top) and [C₈-2-ClPy][NTf₂] (bottom).

Figure 3.21 shows the C 1s regions of the [C_n-2-ClPy][NTf₂] salts with the applied fitting model. The envelope appears to accurately represent the observed photoemissions for both chlorinated pyridinium ILs. The obtained B.E.s for each component are displayed in **Table 3.8**, the analogous [C_nPy][NTf₂] C 1s components are included as a comparison. The shifts between each component for the chlorinated and non-chlorinated C 1s regions are also shown. The [C_n-2-ClPy][NTf₂] peak fittings provide B.E.s that are within 0.1 eV of each other. The [C_n-2-ClPy][NTf₂] C 1s components are also within 0.1 eV of the corresponding [C_nPy][NTf₂] components, with the exception of the C² component which shows the previously observed B.E. shift.

Table 3.8 The B.E. values obtained from the high resolution spectra for the samples $[C_n\text{-}2\text{-ClPy}][\text{NTf}_2]$, where $n = 4$ or $n = 8$. For $[C_8\text{-}2\text{-ClPy}][\text{NTf}_2]$ the spectra were charge corrected to the C^{ali} component (285.0 eV), the resulting N 1s pyridinium signal was then used

		B.E. (eV)				
		C 1s				
Cation	Anion	C ²	C ^{6,7}	C ^{3,4,5}	C ^{ali}	CF ₃
[C ₄ Py] ⁺	[NTf ₂] ⁻	287.1	287.1	286.2	285.2	292.9
[C ₄ -2-ClPy] ⁺	[NTf ₂] ⁻	288.4	287.0	286.1	285.1	292.8
Shift		1.3	0.1	0.1	0.1	0.1
[C ₈ Py] ⁺	[NTf ₂] ⁻	287.1	287.1	286.1	285.0	292.9
[C ₈ -2-ClPy] ⁺	[NTf ₂] ⁻	288.5	287.0	286.1	285.0	292.9
Shift		1.4	0.1	0.0	0.0	0.0

Overall the $[C_n\text{-}2\text{-ClPy}][\text{NTf}_2]$ salts appear to provide XPS spectra that are relatively easy to analyse. Chlorination of the 2-position of the pyridinium ring appears to cause a B.E. shift equal to that observed for the chlorinated imidazolium carbon atom. The C 1s XP spectra for $[C_n\text{-}2\text{-ClPy}][\text{NTf}_2]$ salts show that the C² carbon is removed from the main photoemission, making identification of the peak straight forward. The generated difference spectra show that the current C 1s peak fitting model for pyridinium ILs places the C² carbon at the correct B.E. value. The C⁶ carbon should also have the same B.E. value as its local environment is identical to that of the C² carbon. The following section will present the XP spectra for the 3-chloropyridinium ILs. Using the same analytical procedures, the true B.E. of the C³ carbon may be identified.

3.3.2 N-Alkyl-3-Chloropyridinium ILS

The 3-chloropyridinium ILS were synthesised by alkylation of 3-chloropyridine with bromoalkanes. Subsequent anion metathesis in water at room temperature over ≈ 16 hrs provided a range of ILS with various counterions. The ILS are named according to the formula $[C_n\text{-3-ClPy}][A]$, to denote that the 3-position of the pyridinium ring is chlorinated. Salts with $n = 4$ (with $A = \text{NTf}_2^-$ or Br^-) and 8 (with $A = \text{NTf}_2^-$, PF_6^- , BF_4^- or Br^-) were synthesised. The $[C_n\text{-3-ClPy}]\text{Br}$ salts were used as intermediates and therefore the XPS analysis of the 3-chloropyridinium halides is not presented. NMR analysis was used to determine the purity of the cation and aqueous AgNO_3 was used to test for residual halide impurities, after anion metathesis. Ion chromatography was not used in the determination of residual halides as the 3-chloropyridinium salts may hydrolyse in the presence of the NaOH eluent, as explained previously for the 2-chloropyridinium salts.³⁹⁻⁴¹

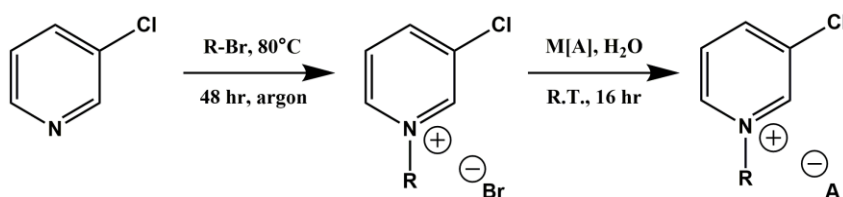


Figure 3.22 The synthetic scheme for the preparation of the 3-chloropyridinium ionic liquids. $M[A]$ was either $\text{Li}[\text{NTf}_2]$, $\text{K}[\text{PF}_6]$ or $\text{Na}[\text{BF}_4]$.

3.3.2.1 XPS of $[C_n\text{-3-ClPy}][A]$ Salts

The XP wide and high resolution scans acquired from the 3-chloropyridinium salts are displayed in **Figure 3.23**. All $[C_8\text{-3-ClPy}][A]$ XP spectra are charge corrected to the C^{ali} component which is set to 285.0 eV. The $[C_4\text{-3-ClPy}][\text{NTf}_2]$ spectra are referenced to the N 1s signal obtained from the charge corrected $[C_8\text{-3-ClPy}][\text{NTf}_2]$ salt. All scans are colour coded to the legend shown on the wide scan and all auger and photoemissions are labelled. Only the expected photoelectron signals are observed which confirms a successful anion metathesis for each salt, i.e. no residual bromide is observed.

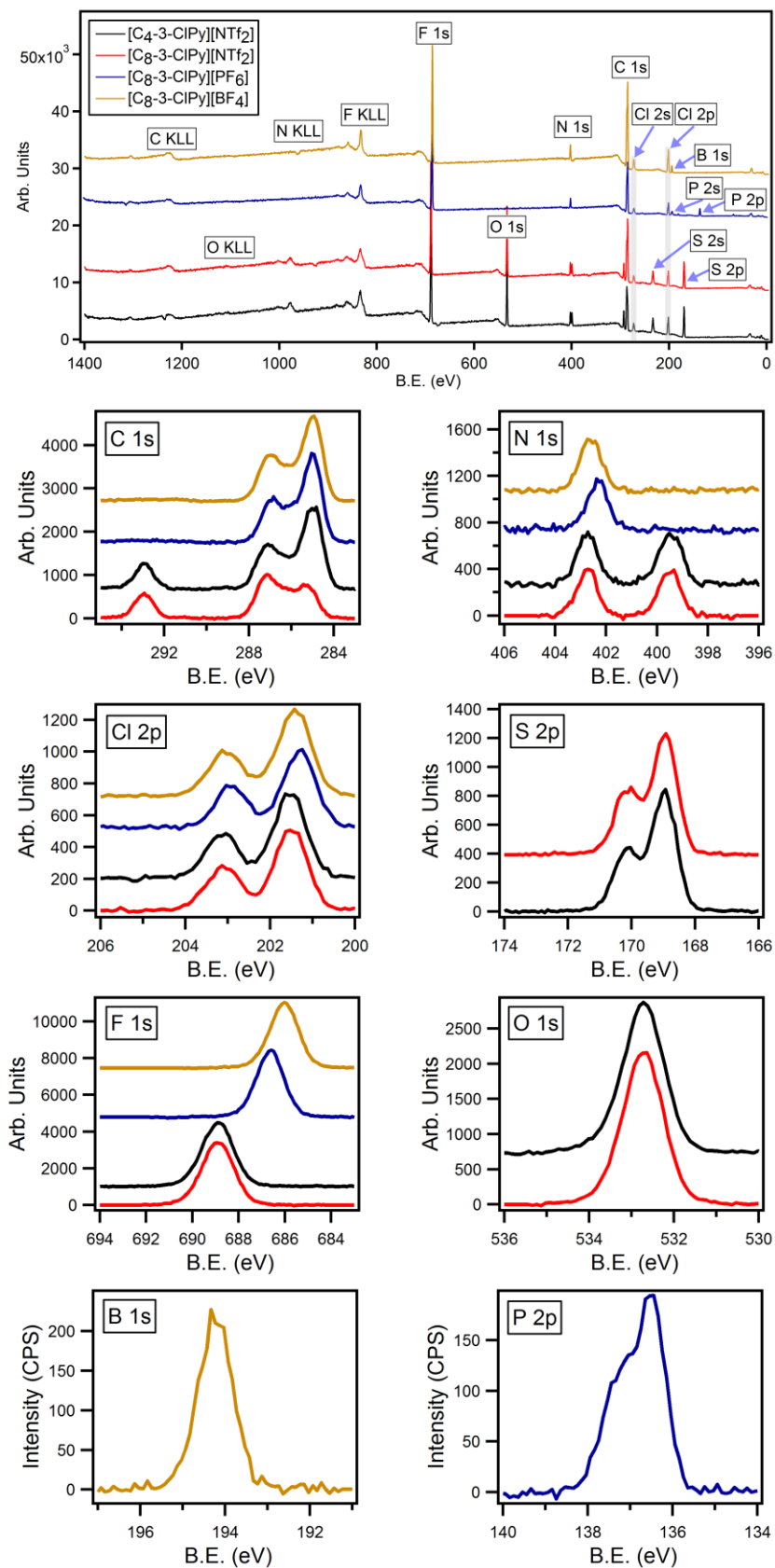


Figure 3.23 The acquired XPS wide (top) and high resolution scans for the 3-chloropyridinium ILs. All scans are colour coded to the legend displayed on the top plot.

The C 1s high resolution scans of the $[C_n\text{-3-ClPy}][\text{NTf}_2]$ salts show the growth of the aliphatic chain and the $-\text{CF}_3$ photoemissions from the $[\text{NTf}_2]^-$ anions. The $[C_n\text{-3-ClPy}][\text{PF}_6]$ and $[C_n\text{-3-ClPy}][\text{BF}_4]$ C 1s regions show a single photoemission that is similar in structure to the main photoelectron signal of the $[C_8\text{-3-ClPy}][\text{NTf}_2]$ C 1s region. Of course, the $[\text{PF}_6]^-$ and $[\text{BF}_4]^-$ anions do not contain the $-\text{CF}_3$ group and so no photoemission at 293.0 eV is observed. The N 1s regions for $[C_n\text{-3-ClPy}][\text{NTf}_2]$ show two peaks that integrate to give equal areas. The peak at higher B.E. is attributed to the pyridinium nitrogen, while the peak at lower B.E. is attributed to the nitrogen of the $[\text{NTf}_2]^-$ anion. A single peak originating from the pyridinium nitrogen is observed in the N 1s region of the 3-chloropyridinium $[\text{PF}_6]^-$ and $[\text{BF}_4]^-$ salts. The Cl 2p regions of each salt show consistent photoemissions with only one chemical state present. The F 1s high resolution scans show large B.E. differences for each type of anion and all other scans appear as expected. The atomic percentages acquired from the wide scans are presented in **Table 3.9** and the heteroatom B.E.s acquired from the high resolution scans are shown in **Table 3.10**.

Table 3.9 The measured and calculated elemental compositions as obtained from the XPS wide scans of the $[C_n\text{-3-ClPy}][A]$ salts. The deviations from the expected values are also shown.

Cation	Anion		Composition (%)							
			C	N	O	F	S	Cl	P	B
$[C_4\text{-3-ClPy}]^+$	$[\text{NTf}_2]^-$	found	45.53	7.02	13.81	21.7	8.05	3.89		
		calculated	42.31	7.69	15.38	23.08	7.69	3.85		
		deviation (%)	7.61	8.71	10.21	5.98	4.68	1.04		
$[C_8\text{-3-ClPy}]^+$	$[\text{NTf}_2]^-$	found	54.47	6.14	11.49	18.10	6.63	3.17		
		calculated	50.00	6.67	13.33	20.00	6.67	3.33		
		deviation (%)	8.94	7.95	13.8	9.50	0.60	4.80		
$[C_8\text{-3-ClPy}]^+$	$[\text{PF}_6]^-$	found	63.86	4.22		23.65		3.99	4.28	
		calculated	59.09	4.55		27.26		4.55	4.55	
		deviation (%)	8.07	7.25		3.61		12.31	5.93	
$[C_8\text{-3-ClPy}]^+$	$[\text{BF}_4]^-$	found	67.39	4.55		18.12		4.59		5.35
		calculated	65.00	5.00		20.00		5.00		5.00
		deviation (%)	3.68	9.00		9.40		8.20		7.00

The measured atomic percentages for each salt are relatively close to their expected values, with deviations well below the potential 20% error associated with quantification in this way. The heteroatom B.E.s for the [C₈Py][NTf₂] IL are included in **Table 3.10** as a comparison. The [C_n-3-ClPy][NTf₂] B.E.s are all within 0.1 eV of the analogous [C₈Py][NTf₂] salt, supporting the charge correction process. The B.E.s of the other [PF₆]⁻ and [BF₄]⁻ salts do not deviate by more than 0.2 eV from the [C_n-3-ClPy][NTf₂] B.E.s, with the exception of the F 1s photoemissions which originate from significantly different chemical environments ([PF₆]⁻ and [BF₄]⁻).

Table 3.10 The B.E.s of the heteroatoms from the high resolution scans of the [C_n-3-ClPy][A] salts.

		B.E. (eV)							
		N 1s		F 1s	O 1s	S 2p _{3/2}	Cl 2p _{3/2}	B 1s	P 2p _{3/2}
Cation	Anion	Cationic	Anionic						
[C ₈ Py] ⁺	[NTf ₂] ⁻	402.6	399.5	688.8	532.6	169.0			
[C ₄ -3-ClPy] ⁺	[NTf ₂] ⁻	402.7	399.5	688.9	532.7	169.0	201.5		
[C ₈ -3-ClPy] ⁺	[NTf ₂] ⁻	402.7	399.5	688.9	532.7	169.0	201.5		
[C ₈ -3-ClPy] ⁺	[PF ₆] ⁻	402.5		686.7			201.3		136.5
[C ₈ -3-ClPy] ⁺	[BF ₄] ⁻	402.6		686.0			201.4	194.2	

The shake up/off signals present in the C 1s regions of the 3-chloropyridinium salts have been measured relative to the main photoemissions and the values are presented in **Table 3.11**. The average value for the four samples is 11.08%, which is close to the previous 10% signal loss for sp² hybridised carbon observed for pyridinium ILs.¹⁸ For this reason, the standard 10% deductions will be taken for sp² hybridised carbon atom areas, when C 1s peak fitting models are developed. The following section will present the difference spectra of the 3-chloropyridinium ILs, when measured relative to their non-chlorinated analogues.

Table 3.11 The measured shake up/off losses per sp^2 carbon atom. The values are measured relative to the main photoemission of the C 1s region.

Cation	Anion	Shake up/off per Sp^2 carbon atom (%)
[C ₄ -3-ClPy] ⁺	[NTf ₂] ⁻	9.78
[C ₈ -3-ClPy] ⁺	[NTf ₂] ⁻	11.31
[C ₈ -3-ClPy] ⁺	[PF ₆] ⁻	11.07
[C ₈ -3-ClPy] ⁺	[BF ₄] ⁻	12.16
Average		11.08

3.3.2.2 [C_n-3-ClPy][NTf₂] C 1s Difference Spectra

As before, by overlaying the C 1s photoemissions of the chlorinated ILs and their non-chlorinated analogues, one spectrum may be subtracted from another to give a difference spectrum. **Figure 3.24** shows the resulting spectra with their original photoemissions. The negative peak appears at 286.1 eV for both C₄ and C₈ analogues, and the positive peaks appear at 287.5 eV for [C₄-3-ClPy][NTf₂] and 287.6 eV for [C₈-3-ClPy][NTf₂]. The positive peak positions are within the 0.1 eV measurement error. Although the chlorinated and non-chlorinated photoemissions show a B.E. shift between the two signals, the difference spectra simplify this shift to show two inverse Gaussian-like peaks.

The positive and negative peaks equate to 0.91 carbon atoms and 0.82 carbon atoms, respectively. As the shifting carbon environment is sp^2 hybridised and subject to shake up/off losses, the expected area should be equivalent to 0.9 carbon atoms. The values are therefore close enough to consider the shifting signal equal to one sp^2 hybridised carbon environment. The initial peak position of 286.1 eV coincides with the current pyridinium peak fitting model assignment for the C^{3,4,5} component. Since the C⁵ carbon is identical to the C³, the true photoemission B.E.s for both signals have been determined through the generated difference spectra. The C⁴ carbon will most likely emit photoelectrons of the same B.E., however using the data presented so far this may not be proven. The C⁴ peak position is addressed in the following chapter.

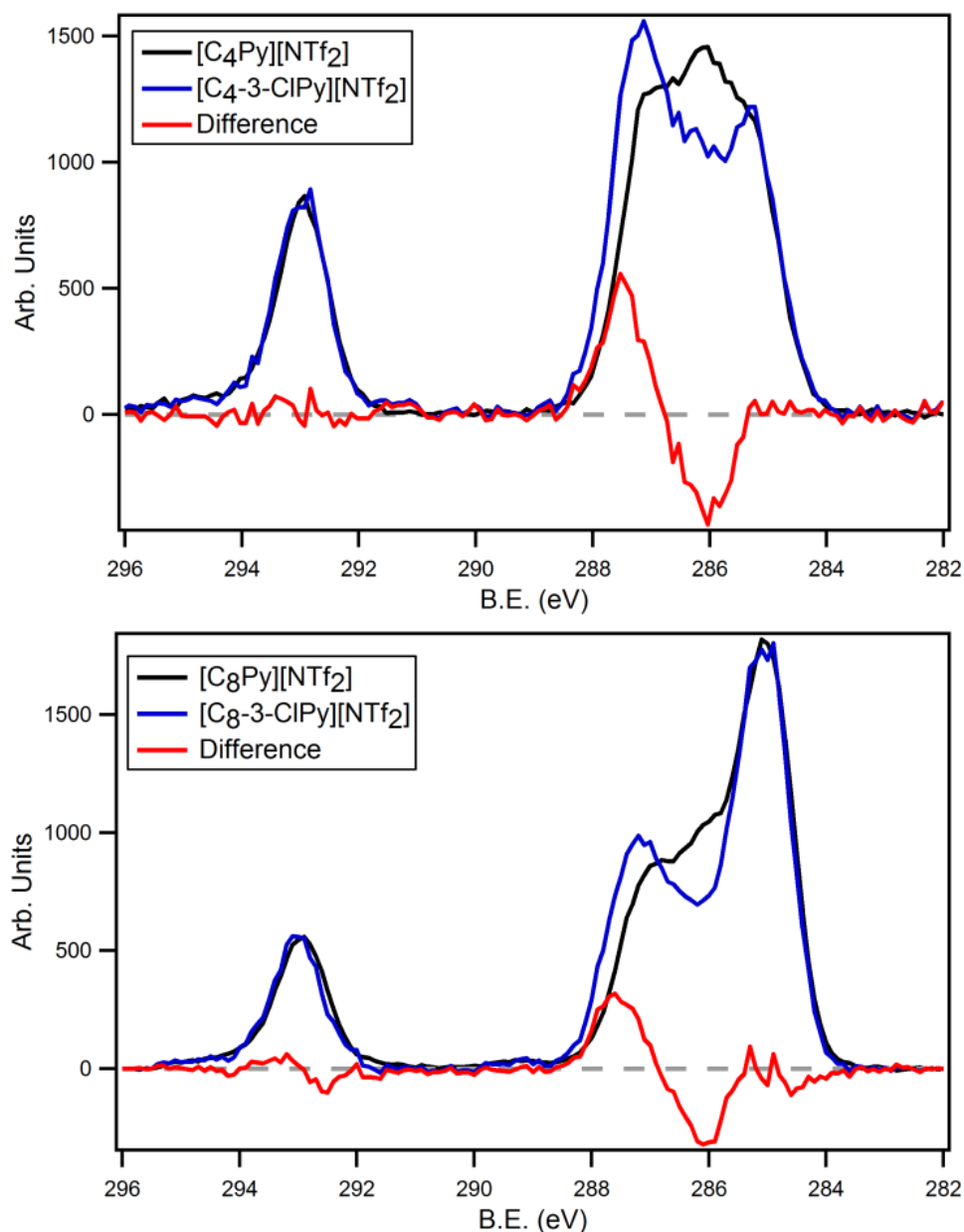


Figure 3.24 The difference spectra (red) generated from the subtraction of the $[C_n\text{Py}][\text{NTf}_2]$ photoemissions (black) from the $[C_n\text{-3-ClPy}][\text{NTf}_2]$ photoemissions (blue).

The measured B.E. shifts in the difference spectra are +1.4 eV for $[C_4\text{-3-ClPy}][\text{NTf}_2]$ and +1.5 eV for $[C_8\text{-3-ClPy}][\text{NTf}_2]$. These values are equal to the previously observed shifts for chlorination of the imidazolium C⁴ carbon and the pyridinium C² carbon environments. Again, this suggests that chlorination incurs a constant degree of electron withdrawal to aromatic carbon species.

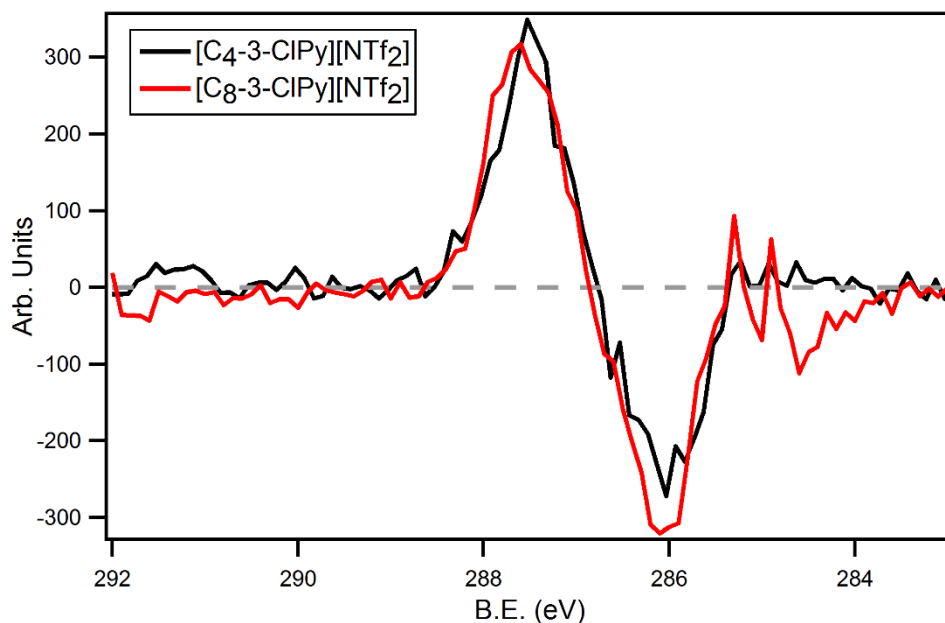


Figure 3.25 The overlaid difference spectra generated from the $[C_n\text{Py}][\text{NTf}_2]$ and the $[C_n\text{-3-ClPy}][\text{NTf}_2]$ C 1s photoemissions. The spectra are normalised to the area of the positive signal.

Both difference spectra have been overlaid and normalised to the area of the positive peak for a visual comparison, **Figure 3.25**. Although the signals are not as consistent as 2-chloropyridinium IL differences, the peak positions and shapes are still almost identical. A structural representation of the peak shifting observed upon chlorination of the 3-position of the pyridinium ring is shown in **Figure 3.26**. The positive signal of the difference spectrum shows the B.E. of the C^4 component with chlorine bound to it. Using this information, along with the known peak positions of the $C^{2,6,7}$ and $C^{4,5}$, the $[C_n\text{-3-ClPy}][A]$ C 1s regions may be accurately represented with known B.E. components.

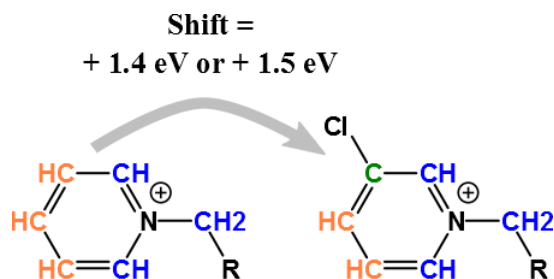


Figure 3.26 The structural representation for the peak shifting observed upon chlorination of the 3-position of the pyridinium ring.

3.3.2.3 Peak Fitting the $[C_n\text{-3-ClPy}][A]$ C 1s region

The C 1s fitting model for the $[C_n\text{-3-ClPy}][A]$ salts include the following components: C^3 (green), $C^{2,6,7}$ (blue), $C^{4,5}$ (orange) and C^{ali} (black), **Figure 3.27**. The areas of the components are set to equal the number of carbon environments, after accounting for shake up/off losses. For example, the $[C_8\text{-3-ClPy}][A]$ components have areas set to the respective ratio of 0.9:2.8:1.8:7 and the $[C_4\text{-3-ClPy}][\text{NTf}_2]$ components to 0.9:2.8:1.8:3. Again, the FWHMs have been constrained to 0.8-1.5 eV for C^{ali} and 0.8-1.2 eV for everything else.

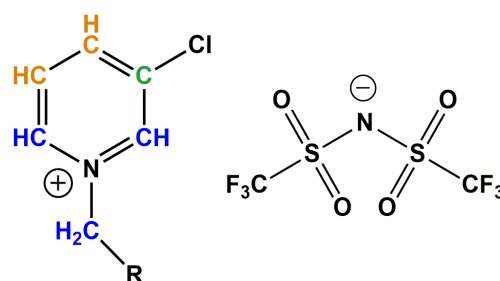


Figure 3.27 The 3-chloropyridinium structure with the colour coded carbon environments C^3 (green), $C^{2,6,7}$ (blue), $C^{4,5}$ (orange) and C^{ali} (black).

The resulting fits to the C 1s photoemissions are displayed in **Figure 3.28**. The model appears to accurately replicate the measured photoemissions for each C 1s region, with little to no discrepancies. The component B.E.s acquired from the peak fittings are summarised in **Table 3.12**, along with the B.E.s from the current $[C_8\text{Py}][\text{NTf}_2]$ peak fitting model. The only major differences between the two models are the shifting of the C^3 component, as expected. The peak fitting model for the 3-chloropyridinium salts therefore appears robust, with accurate B.E.s provided for each carbon component. The C^3 carbon component of the peak fitting coincides with the positive signal of the difference spectrum (287.6 eV), and the $C^{4,5}$ component coincides with the negative signal (286.1 eV). As with the 2-chloropyridinium photoemissions, the peak fitting of the C 1s region is relatively simple, and position restraints are not required in order to replicate the known B.E. positions of the chlorinated carbons. Additionally, the C 1s fittings suggest that only the chlorinated carbon environment experiences a B.E. shift, as observed in **Figure 3.24**.

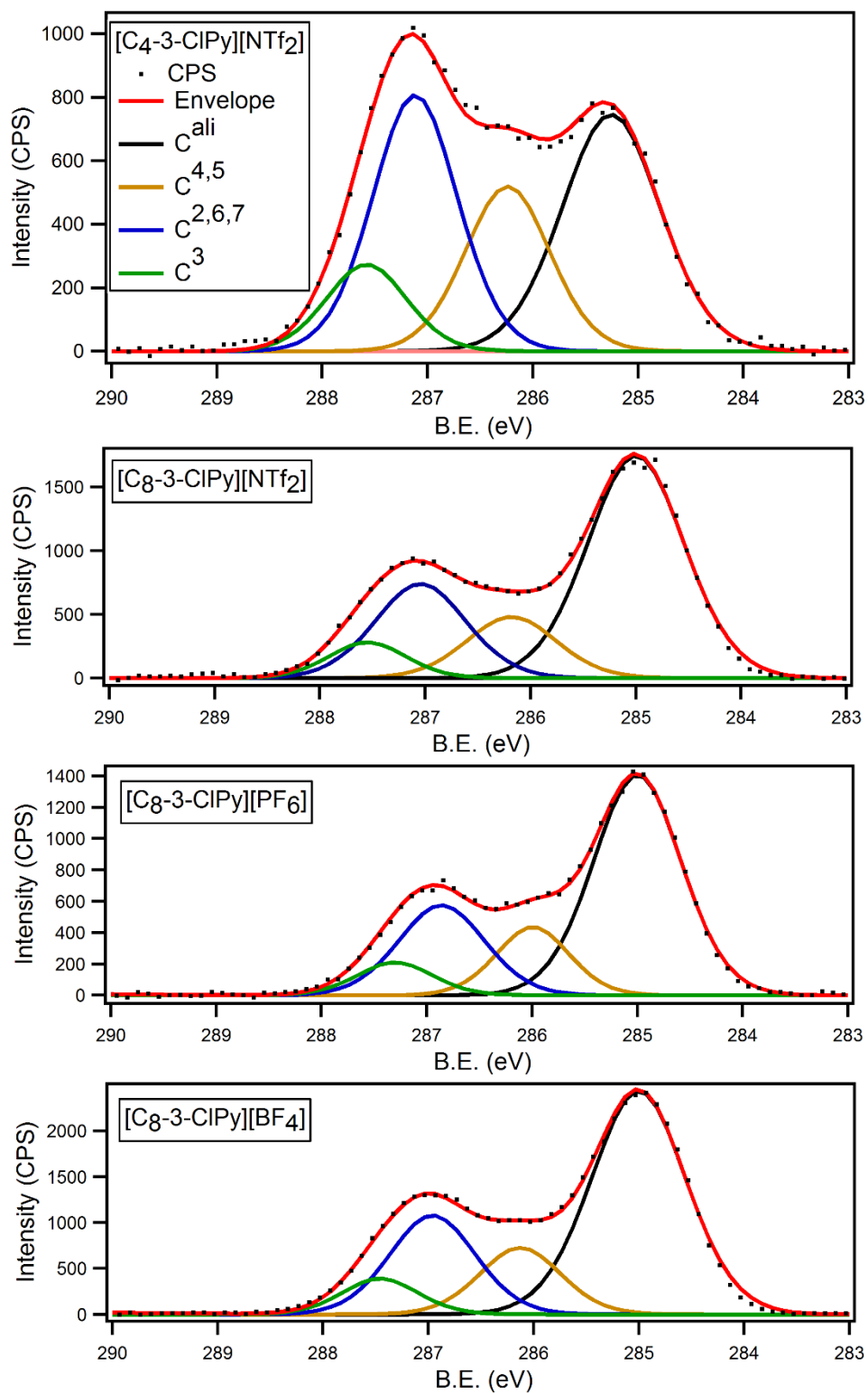


Figure 3.28 The peak fitted C 1s regions of the [C_n-3-ClPy][A] salts. The peaks are colour coded to the legend displayed on the top plot.

Table 3.12 The summarised B.E.s obtained from the peak fitting of the $[C_n-3-ClPy][A]$ C 1s regions. The $[C_8Py][NTf_2]$ B.E.s for the current peak fitting model are also presented as a comparison.

		B.E. (eV)				
		C 1s				
Cation	Anion	C ³	C ^{2,6,7}	C ^{4,5}	C ^{ali}	CF ₃
$[C_8Py]^+$	$[NTf_2]^-$	286.1	287.1	286.1	285.0	292.9
$[C_4-3-ClPy]^+$	$[NTf_2]^-$	287.6	287.1	286.2	285.3	293.0
$[C_8-3-ClPy]^+$	$[NTf_2]^-$	287.6	287.1	286.1	285.0	292.9
$[C_8-3-ClPy]^+$	$[PF_6]^-$	287.3	286.9	286.0	285.0	
$[C_8-3-ClPy]^+$	$[BF_4]^-$	287.5	287.0	286.0	285.0	

Through the shifting of electron density and the generation of difference spectra, the position of the C³ carbon has been confirmed. The C⁵ carbon will also emit photoelectrons of the same B.E. due to the similarities of its local environment to the C³ carbon. The current C 1s peak fitting model for pyridinium ILs is therefore correct with regards to the C^{3,5} (and most probably the C⁴) carbon photoemission B.E.s. The +1.4 eV shift is equal to the previous shifts observed when the C⁴ position of imidazolium and the C² position of pyridinium ILs are chlorinated. This implies that chlorination carries a constant and measurable degree of electron withdrawal from the carbon that it is bound to. This may aid in future studies that investigate the XP spectra of more complex chlorinated ILs.

3.4 Conclusions

This chapter has presented a new method for the determination of exact B.E.s from IL C 1s XP spectra. By utilising the designer aspect of ILs and appending structural modifications to certain carbon environments, the shifting of electron density relative to an unmodified analogue has provided true B.E. values for a range of carbon components. Specifically, chlorine has been used as an EWG to remove electron density from particular carbon atoms of ILs. The C 1s photoemissions of the chlorinated ILs have been examined relative to their non-chlorinated analogues, and a series of difference spectra have been produced. These spectra involve the subtraction

of one photoemission from another, which provides relatively simple positive and negative peaks that reveal the initial and final positions of the shifting carbon environments.

Chlorination of the 4-position of imidazolium ILs has shown that the current model used to interpret imidazolium C 1s XP spectra is incorrect. The C⁴ carbon (and therefore the C⁵ carbon) has been found to emit photoelectrons with B.E.s of 286.5 eV. This B.E. was previously attributed to the C^{6,7} carbons of the imidazolium IL through ‘best guess’ peak fittings. The + 1.4 eV shift of the C⁴ carbon upon chlorination was also used to show that the previous peak arrangement was incorrect. By altering the C^{4,5} and C^{6,7} peak positions in both chlorinated and non-chlorinated C 1s photoemissions, the B.E. shifts of two alternative models were found. The shifting observed in the difference spectrum was only reproduced by a peak arrangement that placed the C^{6,7} component at a higher B.E. than the C^{4,5} component. This analysis is independent of exact B.E.s and therefore the result strengthens the conclusion that the current C 1s peak fitting model is incorrect. A new imidazolium C 1s model was presented, where the C^{4,5} component occupies a B.E. of 286.6 eV and the C^{6,7} component occupies a B.E. of 287.0 eV.

Chlorination of the 2-position of pyridinium ILs has confirmed that the C² component in the current pyridinium C 1s fitting model is correct. The known B.E. of the C² (and therefore C⁶) carbon is 287.1 eV, this was found *via* the same methods described above. Chlorination of the 3-position of the pyridinium ring has also confirmed that the previous peak assignment for the C³ component was correct. The known B.E. of this component (and therefore the C⁵ component) is 286.1 eV, again found through the generation of difference spectra. The B.E. shifts observed for the chlorinated pyridinium ILs appear relatively simple. The only observed shift is upon the carbon bound directly to the chlorine atom, all other neighbouring carbon and nitrogen groups appear unaffected. The same B.E. shift of + 1.4 eV has been observed for both carbons in the chloropyridinium salts. This suggests that chlorination of a carbon atom results in a constant amount of electron withdrawal.

Although the chlorine substituents do act as EWGs, there may be other possible implications associated with the replacement of hydrogen atoms around the pyridinium rings. For example, for highly coordinating anions such as halides or acetates, hydrogen bonding may be disrupted. Potentially, the electron withdrawing effects of chlorine may then appear slightly larger as charge donation to the carbon atom may be hindered. The net result would be a larger shift to a higher B.E. value in any generated difference spectrum. However, for weakly coordinating anions such as $[\text{NTf}_2]^-$, charge transfer to the carbons of the pyridinium ring is already at a minimum. Therefore, the B.E. shifts observed for all chlorinated pyridinium salts with $[\text{NTf}_2]^-$ anion are assumed to be the result of electron withdrawal only.

Overall, this chapter has demonstrated the power of structural variation for XPS peak fitting. Although this technique is not limited to ILs, the ease of structural modification, the high photoelectron flux from liquid surfaces and the involatility of ILs are unique features that are ideally suited to this purpose. ILs therefore present a unique opportunity in the determination of accurate B.E.s for XP spectroscopy.

3.5 References

- 1 J. P. Armstrong, C. Hurst, R. G. Jones, P. Licence, K. R. J. Lovelock, C. J. Satterley and I. J. Villar-Garcia, *Phys. Chem. Chem. Phys.*, 2007, **9**, 982–990.
- 2 K. R. J. Lovelock, A. Deyko, P. Licence and R. G. Jones, *Phys. Chem. Chem. Phys.*, 2010, **12**, 8893–8901.
- 3 Y. U. Paulechka, D. H. Zaitsau, G. J. Kabo and A. A. Strechan, *Thermochim. Acta*, 2005, **439**, 158–160.
- 4 K. R. J. Lovelock, I. J. Villar-Garcia, F. Maier, H. P. Steinrück and P. Licence, *Chem. Rev.*, 2010, **110**, 5158–5190.
- 5 H.-P. Steinrück, *Surf. Sci.*, 2010, **604**, 481–484.
- 6 H.-P. Steinrück, J. Libuda, P. Wasserscheid, T. Cremer, C. Kolbeck, M. Laurin, F. Maier, M. Sobota, P. S. Schulz and M. Stark, *Adv. Mater.*, 2011, **23**, 2571–87.
- 7 I. J. Villar-Garcia, S. Fearn, G. F. De Gregorio, N. L. Ismail, F. J. V. Gschwend, A. J. S. McIntosh and K. R. J. Lovelock, *Chem. Sci.*, 2014, **5**, 4404–4418.
- 8 I. Niedermaier, C. Kolbeck, N. Taccardi, P. S. Schulz, J. Li, T. Drewello, P. Wasserscheid, H.-P. Steinrück and F. Maier, *ChemPhysChem*, 2012, **13**, 1725–1735.
- 9 E. F. Smith, I. J. V. Garcia, D. Briggs and P. Licence, *Chem. Commun.*, 2005, 5633–5635.
- 10 T. Cremer, C. Kolbeck, K. R. J. Lovelock, N. Paape, R. Wölfel, P. S. Schulz, P. Wasserscheid, H. Weber, J. Thar, B. Kirchner, F. Maier and H.-P. Steinrück, *Chem. Eur. J.*, 2010, **16**, 9018–9033.
- 11 R. K. Blundell and P. Licence, *Phys. Chem. Chem. Phys.*, 2014, **16**, 15278–88.
- 12 B. B. Hurisso, K. R. J. Lovelock and P. Licence, *Phys. Chem. Chem.*

- Phys.*, 2011, **13**, 17737–48.
- 13 D. C. Apperley, C. Hardacre, P. Licence, R. W. Murphy, N. V Plechkova, K. R. Seddon, G. Srinivasan, M. Swadźba-Kwaśny and I. J. Villar-Garcia, *Dalton Trans.*, 2010, **39**, 8679–8687.
- 14 A. W. Taylor, S. Men, C. J. Clarke and P. Licence, *RSC Adv.*, 2013, **3**, 9436.
- 15 M. Currie, J. Estager, P. Licence, S. Men, P. Nockemann, K. R. Seddon, M. Swadźba-Kwaśny and C. Terrade, *Inorg. Chem.*, 2013, **52**, 1710–1721.
- 16 I. J. Villar García, *Thesis*, The University of Nottingham, 2009.
- 17 A. W. Taylor, *Thesis*, The University of Nottingham, 2010.
- 18 S. Men, *Thesis*, The University of Nottingham, 2011.
- 19 P. Nockemann, B. Thijs, T. N. Parac-Vogt, K. Van Hecke, L. Van Meervelt, B. Tinant, I. Hartenbach, T. Schleid, T. N. Vu, T. N. Minh and K. Binnemans, *Inorg. Chem.*, 2008, **47**, 9987–9999.
- 20 S. Lee, *Chem. Commun.*, 2006, 1049–1063.
- 21 R. Giernoth, *Angew. Chem. Int. Ed.*, 2010, **49**, 2834–2839.
- 22 D. Zhao, Z. Fei, T. J. Geldbach, R. Scopelliti and P. J. Dyson, *J. Am. Chem. Soc.*, 2004, **126**, 15876–15882.
- 23 L. C. Branco, G. V. S. M. Carrera, J. Aires-de-sousa, I. L. Martin, R. Frade and C. A. M. Afonso, in *Ionic Liquids: Theory, Properties, New Approaches*, 2011, pp. 61–95.
- 24 J. Dupont, *Acc. Chem. Res.*, 2011, **44**, 1223–1231.
- 25 T. Fukushima and T. Aida, *Chem. Eur. J.*, 2007, **13**, 5048–5058.
- 26 J. Le Bideau, L. Viau and A. Vioux, *Chem. Soc. Rev.*, 2011, **40**, 907–25.

- 27 T. Morishita, H. Okamoto, Y. Katagiri, M. Matsushita and K. Fukumori, *Chem. Commun.*, 2015, **51**, 12068–12071.
- 28 V. I. Pârvulescu and C. Hardacre, *Chem. Rev.*, 2007, **107**.
- 29 H. Zhao, S. Xia and P. Ma, *J. Chem. Technol. Biotechnol.*, 2005, **80**, 1089–1096.
- 30 E. D. Bates, R. D. Mayton, I. Ntai and J. H. Davis, *J. Am. Chem. Soc.*, 2002, **124**, 926–927.
- 31 C. Kolbeck, I. Niedermaier, N. Taccardi, P. S. Schulz, F. Maier, P. Wasserscheid and H. P. Steinrück, *Angew. Chem. Int. Ed.*, 2012, **51**, 2610–2613.
- 32 I. J. Villar-Garcia, E. F. Smith, A. W. Taylor, F. Qiu, K. R. J. Lovelock, R. G. Jones and P. Licence, *Phys. Chem. Chem. Phys.*, 2011, **13**, 2797–2808.
- 33 N. Stojilovic, *J. Chem. Educ.*, 2012, **89**, 1331–1332.
- 34 C. Kolbeck, T. Cremer, K. R. J. Lovelock, N. Paape, P. S. Schulz, P. Wasserscheid, F. Maier and H. P. Steinrück, *J. Phys. Chem. B*, 2009, **113**, 8682–8688.
- 35 K. R. J. Lovelock, C. Kolbeck, T. Cremer, N. Paape, P. S. Schulz, P. Wasserscheid, F. Maier and H. P. Steinrück, *J. Phys. Chem. B*, 2009, **113**, 2854–2864.
- 36 I. J. Villar-Garcia, E. F. Smith, A. W. Taylor, F. Qiu, K. R. J. Lovelock, R. G. Jones and P. Licence, *Phys. Chem. Chem. Phys.*, 2011, **13**, 2797.
- 37 S. Men, D. S. Mitchell, K. R. J. Lovelock and P. Licence, *ChemPhysChem*, 2015, 2211–2218.
- 38 I. Rico, C. Dubrule and A. Lattes, *J. Org. Chem.*, 1994, **59**, 415–420.
- 39 H. A. Al-Iohedan, C. A. Bunton and L. S. Romsted, *J. Org. Chem.*, 1982, **47**, 3528–3532.

- 40 C. Fernandez, V. Toscano, H. Chaimovich, M. Politi and N. Hioka, *J. Phys. Org. Chem.*, 1998, **11**, 25–30.
- 41 H. A. Al-lohedan, *J. Phys. Chem.*, 1987, **91**, 4524–4527.

Chapter 4:
4,4'-Bipyridinium Ionic Liquids

4 4,4'-Bipyridinium C 1s Peak Fitting

Mono-alkylation of 4,4'-bipyridine to yield N-alkyl-4,4'-bipyridinium halide salts, $[C_n\text{Bipy}]X$, is a relatively facile process that uses inexpensive materials and simple reaction conditions.^{1,2} Anion metathesis using $\text{Li}[\text{NTf}_2]$ produces a range of RTILs that possess a free nitrogen atom that is capable of coordinating to metal centres,³ greatly enhancing the solubility of metal salts in the ionic liquid medium. For example, $[C_4\text{Bipy}][\text{NTf}_2]$ has been found to dissolve >20 mol% of NiCl_2 and $\text{Cu}(\text{NO}_3)_2$, whereas $[C_4\text{C}_1\text{Im}][\text{NTf}_2]$ is only capable of dissolving the same salts in quantities of <0.05 mol%.⁴ The ability to dissolve high concentrations of metal salts in ionic liquids presents exciting opportunities for a wide variety of research areas such as electrodeposition,^{5,6} metal recycling^{7,8} and catalysis⁹⁻¹¹.

4,4'-Bipyridine may be alkylated once to provide a mono-cationic species or twice to provide a dicationic species.¹²⁻¹⁵ Interestingly, the dicationic species is a symmetrical molecule which is akin to two pyridinium groups joined at the 4-position of the pyridine ring. This creates a unique situation for the XPS analysis of 4,4'-bipyridinium ILs, particularly when considering their C 1s photoemissions. An in depth XPS analysis of 4,4'-bipyridinium salts will provide a strong, reliable foundation for any future XP experiments involving the 4,4-bipyridinium cations, especially those focused on metal-IL interactions.^{16,17}

The following chapter will present the XP spectra of both mono- and dicationic 4,4'-bipyridinium salts with $[\text{NTf}_2]^-$ counter ions. As shown previously, additional data may be extracted from XP spectra when comparing multiple photoemissions of structurally related compounds. For this reason, the C 1s and N 1s spectra of both cationic cores will be compared and a series of difference spectra will be produced. Further comparisons to traditional mono-cationic pyridinium ILs will be made in order to extract the maximum amount of available data. This method of analysis should provide information on individual C 1s and N 1s components that would otherwise be unknown.

4.1 Synthesis of 4,4'-Bipyridinium Ionic Liquids

When using polar solvents to synthesis the mono-alkylated 4,4'-bipyridinium salts from bromoalkanes, mixtures of mono- and di-cationic species are always produced. Although the synthesis of pure mono-alkylated 4,4'-bipyridinium salts has been reported in dioxane,⁴ it was noted that even with variations in the reaction temperature, time and the ratio of starting materials, this was not possible for reactions conducted in acetonitrile or DMF. **Figure 4.1** shows a generalised synthetic scheme for the variety of conditions used in this work. The mono-alkylated compounds are denoted $[C_n\text{Bipy}]^+$ and the di-alkylated compounds are denoted $[(C_n)_2\text{Bipy}]^{2+}$. Salts with ethyl, butyl, hexyl and octyl alkyl chains were synthesised.

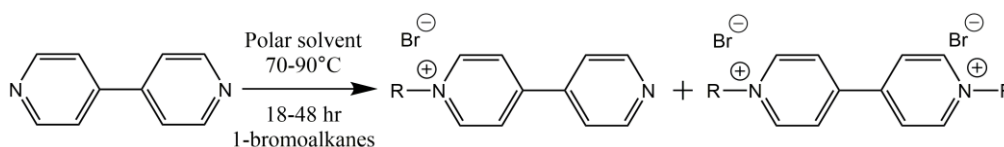


Figure 4.1 The synthetic scheme for the alkylation of 4,4'-bipyridinium bromide salts. $R = \text{ethyl } (C_2)$, $\text{butyl } (C_4)$, $\text{hexyl } (C_6)$ or $\text{octyl } (C_8)$ alkyl chains.

Table 4.1 shows the isolated yields for the pure mono- and di-cationic salts. The reaction conditions were adapted from existing literature procedures¹ and were designed to provide the mono-cationic 4,4'-bipyridinium salts as the major product. Unfortunately, the di-quaternised product is still produced in relatively high amounts, however the resulting mixture is easily separated due to the poor solubility of the dicationic species in both polar and non-polar solvents. See the *Chapter 2* for more details.

Sample purity is easily confirmed by NMR spectroscopy as mono-alkylation results in desymmetrisation of the 4,4'-bipyridine ring. Di-alkylation re-establishes this symmetry, therefore the starting materials and the alkylation products present characteristic peaks in an NMR spectra. Anion metatheses with aqueous solutions of $\text{Li}[\text{NTf}_2]$ at room temperature afford the pure mono- and di-cationic salts in relatively high yields. Ion chromatography and XPS analysis provide information on the purity of the anion with regards to residual bromide contamination.

Table 4.1 The reaction conditions used to synthesise each alkylated 4,4'-bipyridinium salt. The percentage of mono- and di-alkylated products are also shown.

Cation	Anion	Solvent	Temperature (°C)	Time (hr)	Ratio of reagents ^a	Product (%)	
						Mono	Di
[(C ₂)Bipy] ²⁺	Br ⁻	Toluene	90	18	1:10.5	48	-
[(C ₄)Bipy] ²⁺	Br ⁻	Acetonitrile	80	48	0.84	69	23
[(C ₆)Bipy] ²⁺	Br ⁻	Acetonitrile	70	18	0.9	33	13
[(C ₈)Bipy] ²⁺	Br ⁻	DMF	85	18	2	34	11

^a 4,4'-bipyridine : bromoalkane

4.2 XPS analysis of 4,4'-bipyridinium salts

It is important to note that the dicationic compounds that result from attempted mono-alkylation of 4,4'-bipyridine have been isolated and used for XPS analysis. These molecules were not initially targeted, however as purified samples they do provide an excellent opportunity to further examine the C 1s fitting procedures used for pyridinium ILs.¹⁸ The XP spectra for the dicationic salts may also be compared to the mono-alkylated [C_nBipy][NTf₂] products, potentially providing additional information on the B.E.s of the non-alkylated portion of the bipyridinium structure. The following sections will detail the XPS analysis of both mono- and di-alkylated 4,4'-bipyridinium salts, elaborating on the analytical procedures used so far for C 1s peak fitting.

4.2.1 1,1'-Dialkyl-4,4'-bipyridinium bis(trifluoromethanesulfonyl)imide Ionic Liquids, [(C_n)₂Bipy][NTf₂]₂

Di-alkylation of 4,4'-bipyridine results in a symmetrical molecule with a mirror plane that intersects the 4,4'-carbon to carbon bond, see **Figure 4.2**. The carbon groups about this plane are chemically equivalent, therefore each group should present a single binding energy in the C 1s XP spectra. This symmetry provides a unique opportunity to examine the shift in electron density about the C⁴ carbon of the pyridinium ring. By comparing the [(C_n)₂Bipy][NTf₂]₂ C1s spectra to the traditional [C_nPy][NTf₂] C 1s spectra,

the difference should indicate the initial and final location of the C⁴ carbon component. This data will not only help to refine and confirm the existing C 1s fitting procedures used for pyridinium ILs, but should also provide a degree of charge withdrawal that may be useful in developing future C 1s models for functionalised pyridinium ILs.

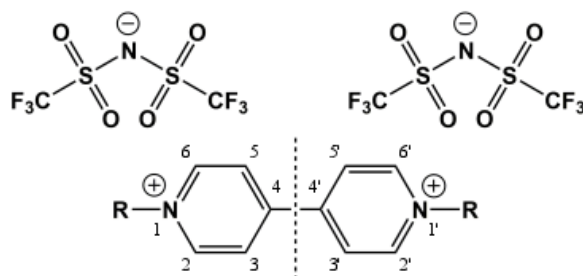


Figure 4.2 The structure of the $[(C_n)_2\text{Bipy}][\text{NTf}_2]_2$ salts, showing the mirror plane intersecting the 4,4'-carbon to carbon bond. R = ethyl (C_2), butyl (C_4), hexyl (C_6) or octyl (C_8) alkyl chains. The aromatic carbon positions are labelled with their respective numbers.

4.2.1.1 Wide and High Resolution Scans

The wide and high resolution scans for each alkyl chain analogue of $[(C_n)_2\text{Bipy}][\text{NTf}_2]_2$ are shown in **Figure 4.3**. The scans are summed and offset for ease of presentation. Only the expected photoemissions are observed in the wide scans, this confirms a successful anion metathesis and ensures samples are free from surface contamination.¹⁹ The calculated atomic percentages for each element are presented in **Table 4.2**. Most signals do not deviate by more than 10% of the expected values; the error is roughly 20% when quantifying regions in this way. The XP spectra are charge corrected to the C 1s C^{ali} component for $n = 8$, which is set to 285.0 eV.²⁰ The obtained value for the cationic N 1s signal (402.5 eV) has then been used to reference $[(C_n)_2\text{Bipy}][\text{NTf}_2]_2$, where $n = 2, 4$ and 6.

Table 4.2 The atomic percentages for the $[(C_n)_2\text{Bipy}][\text{NTf}_2]_2$ salts. The % deviations of the found and calculated values are also presented.

Cation	Anion		Composition (%)				
			C	N	O	F	S
$[(C_2)_2\text{Bipy}]^{2+}$	$2[\text{NTf}_2]^-$	Found	40.69	7.86	17.81	25.59	8.05
		Calculated	39.13	8.70	17.39	26.08	8.70
		Deviation (%)	-3.83	10.69	-2.36	1.91	8.07
$[(C_4)_2\text{Bipy}]^{2+}$	$2[\text{NTf}_2]^-$	Found	44.05	8.12	14.72	25.81	7.30
		Calculated	44.00	8.00	16.00	24.00	8.00
		Deviation (%)	-0.11	-1.48	8.70	-7.01	9.59
$[(C_6)_2\text{Bipy}]^{2+}$	$2[\text{NTf}_2]^-$	Found	47.28	7.48	14.18	23.73	7.33
		Calculated	48.15	7.41	14.81	22.22	7.41
		Deviation (%)	1.84	-0.94	4.44	-6.36	1.09
$[(C_8)_2\text{Bipy}]^{2+}$	$2[\text{NTf}_2]^-$	Found	55.52	6.38	13.29	18.47	6.34
		Calculated	51.72	6.90	13.79	20.69	6.90
		Deviation (%)	-6.84	8.15	3.76	12.02	8.83

The C 1s region shows the growing alkyl chain for $n = 2, 4, 6$ and 8 about the 285.0 eV position. The C 1s signals at higher binding energies remain constant, while the aliphatic region increases in width and height.²¹ This process was explained in the previous chapter. The N 1s signal shows two resolved peaks that represent the nitrogen from the anion (at lower B.E.) and the nitrogen from the cation (at higher B.E.), **Figure 4.3**. These two signals integrate to give equal areas, as expected. All scans show consistency in their positions which supports the charge correction and referencing that has been applied to the spectra.

The average value for the shake up/off per aromatic carbon is 11.11%, see **Table 4.3**. These losses are calculated from the high resolution C 1s spectra and are measured relative to the main C 1s photoemission. Since this value is close to the previously measured 10% loss for pyridinium ILs,²² all aromatic carbons will incur a 10% deduction when calculating component areas for $[(C_n)_2\text{Bipy}][\text{NTf}_2]_2$ salts.

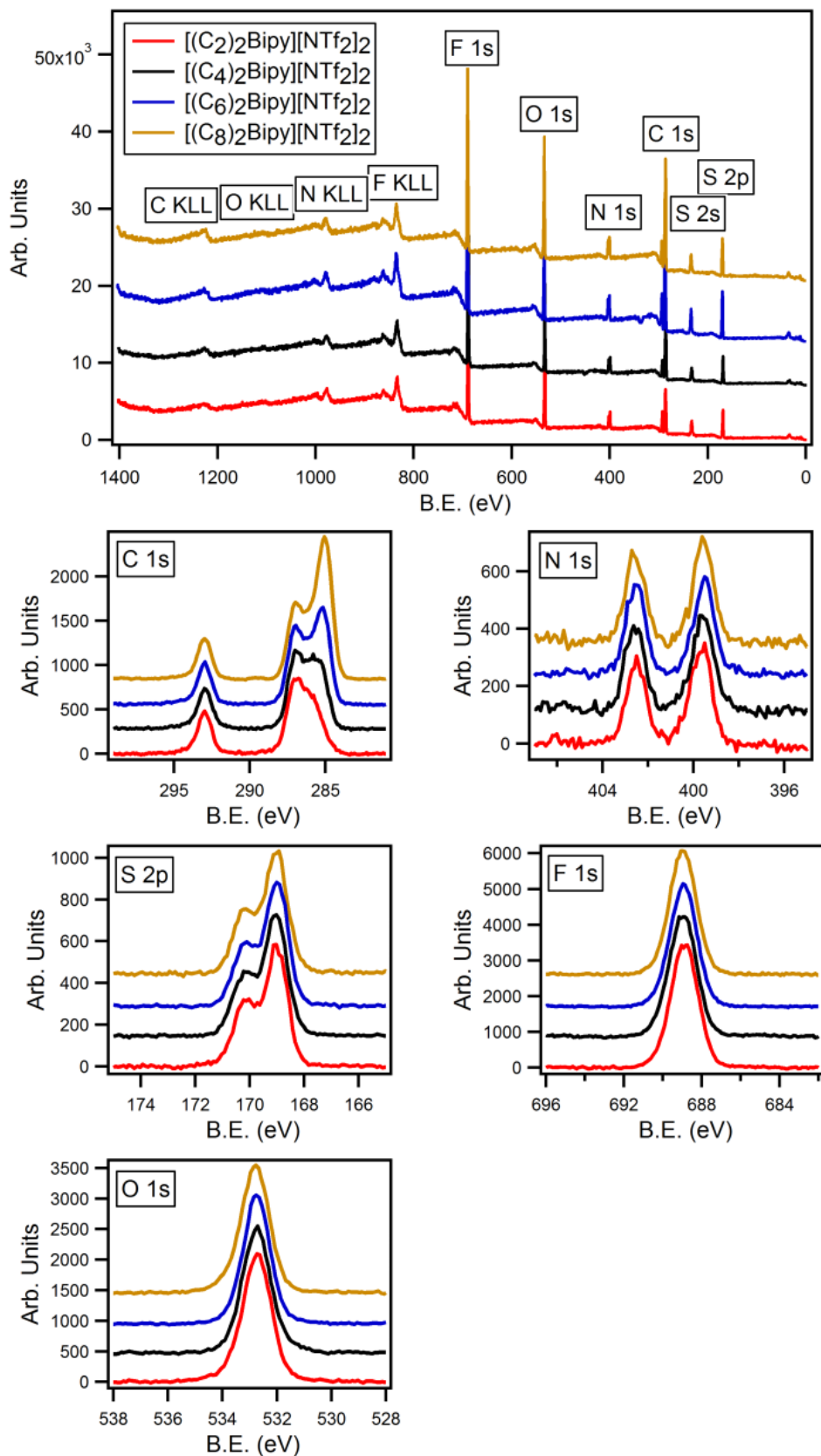


Figure 4.3 The wide and high resolution scans for $[(C_n)_2Bipy][NTf_2]_2$, where $n = 2$ (red), 4 (black), 6 (blue) and 8 (orange). The spectra are charge corrected to the C 1s C^{ali} component for $n = 8$, set to 285.0 eV. The corresponding value for the N 1s signal is then used to reference $n = 2, 4$ and 6.

Table 4.3 The percentage of shake up/off per aromatic carbon atom for the $[(C_n)_2\text{Bipy}][\text{NTf}_2]_2$ salts. The values are calculated relative to the main C 1s photoemission.

Cation	Anion	Shake up/off per aromatic carbon atom (%)
$[(C_2)_2\text{Bipy}]^{2+}$	$2[\text{NTf}_2]^-$	10.03
$[(C_4)_2\text{Bipy}]^{2+}$	$2[\text{NTf}_2]^-$	11.86
$[(C_6)_2\text{Bipy}]^{2+}$	$2[\text{NTf}_2]^-$	11.89
$[(C_8)_2\text{Bipy}]^{2+}$	$2[\text{NTf}_2]^-$	10.65
Average		11.11

The B.E.s for all heteroatoms are displayed in **Table 4.4**. As the C 1s photoemission contains unresolved signals, additional analysis is needed in order to present accurate B.E.s for the individual carbon components. As previously mentioned for the high resolution plots, the consistency between the B.E.s of the heteroatoms for each analogue of the $[(C_n)_2\text{Bipy}][\text{NTf}_2]_2$ salts supports the charge correction procedures employed for all dicationic salts.

Table 4.4 The binding energies for the heteroatoms of the $[(C_n)_2\text{Bipy}][\text{NTf}_2]_2$ salts (where $n = 2, 4, 6$ or 8). The error of measurement is 0.1 eV.

		Binding Energy (eV)				
		N 1s		F 1s	O 1s	S 2p _{3/2}
Cation	Anion	Cationic	Anionic			
$[(C_2)_2\text{Bipy}]^{2+}$	$2[\text{NTf}_2]^-$	402.5	399.5	688.8	532.7	196.0
$[(C_4)_2\text{Bipy}]^{2+}$	$2[\text{NTf}_2]^-$	402.5	399.5	688.9	532.7	196.0
$[(C_6)_2\text{Bipy}]^{2+}$	$2[\text{NTf}_2]^-$	402.5	399.5	688.9	532.7	196.0
$[(C_8)_2\text{Bipy}]^{2+}$	$2[\text{NTf}_2]^-$	402.5	399.5	688.9	532.8	196.0

4.2.1.2 $[(C_n)_2\text{Bipy}][\text{NTf}_2]_2$ and $[\text{C}_n\text{Py}][\text{NTf}_2]$ C 1s Difference Spectra

The structure of $[(C_n)_2\text{Bipy}][\text{NTf}_2]_2$ is equivalent to two pyridinium cations bound together at the 4-positions of the pyridine rings. Since the $[(C_n)_2\text{Bipy}][\text{NTf}_2]_2$ salt contains two $[\text{NTf}_2]^-$ counter ions, all photoemissions originating from the anion should have double the area of each monocationic $[\text{NTf}_2]^-$ photoemission. If the dicationic salts are normalised (by the F 1s

signal areas) to pyridinium XP spectra, then the resulting signal is equivalent to one side of the di-alkylated structure, e.g. the molecule is halved. Theoretically, the only resulting difference in the C 1s photoemissions should then be from the 4-position of the pyridinium ring. **Figure 4.4** shows how the carbon environments are grouped in both $[(C_n)_2Bipy]^{2+}$ and $[C_nPy]^+$ cations for XPS C 1s analysis.

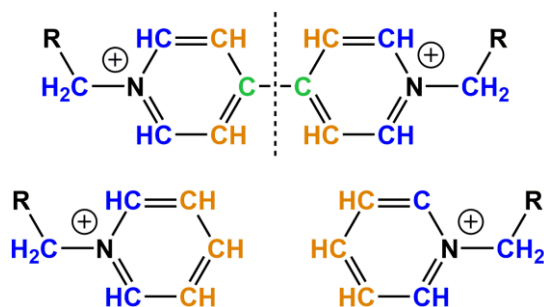


Figure 4.4 The structure of the $[(C_n)_2Bipy]^{2+}$ dication (top) with colour coded carbon environments. The $[C_nPy]^+$ cation is also shown with the corresponding carbon environments colour coded to those on the diquaternised structure.

The carbon regions for pyridinium C 1s spectral analysis were discussed in the previous chapter. The $[C_nPy]^+$ carbons are labelled as blue = $C^{2,6,7}$ and orange = $C^{3,4,5}$. For the $[(C_n)_2Bipy][NTf_2]_2$ salts the regions are labelled as: blue = $C^{2,6,7} + C^{2',6',7'}$, orange = $C^{3,5} + C^{3',5'}$ and green = $C^4 + C^{4'}$. However, upon normalisation to the pyridinium IL XP spectra, $[(C_n)_2Bipy][NTf_2]_2$ C 1s signals only represent half of the molecule, e.g. blue = $C^{2,6}$, orange = $C^{3,5}$ and green = C^4 .

Figure 4.5 shows the $[(C_6)_2Bipy][NTf_2]_2$ C 1s region overlaid with the $[C_6Py][NTf_2]$ C1s region as an example. The F 1s signal area from the dicationic salt has been normalised to the F 1s signal area of the pyridinium salt. As normalising in this way may leave slight deviations from element to element, any discrepancies are moderated by again normalising to the area of the C 1s signal from the $-CF_3$ anion. The difference between the two spectra, i.e. the pyridinium C 1s signal subtracted from the dicationic 4,4'-bipyridinium C1s signal, has been taken and is shown on the plot in red.

Relative to each other, both C 1s regions clearly show a shift in electron density. The $[(C_6)_2Bipy][NTf_2]_2$ C1s emission possesses an increased amount of electron density at 287.0 eV, and a corresponding lack of electron density at 286.2 eV. Since the 4-position of the halved bipyridinium unit is bound to another cationic pyridinium ring, electron density is therefore lost from the C⁴ carbon environment. A loss in electron density (relative to the pyridinium C 1s region) in this way should cause a signal shift from low B.E. to high B.E., as observed. The negative signal in the difference spectrum therefore reveals the initial position of the pyridinium C⁴ signal, while the positive signal shows the resulting C⁴ signal of the bipyridinium unit.

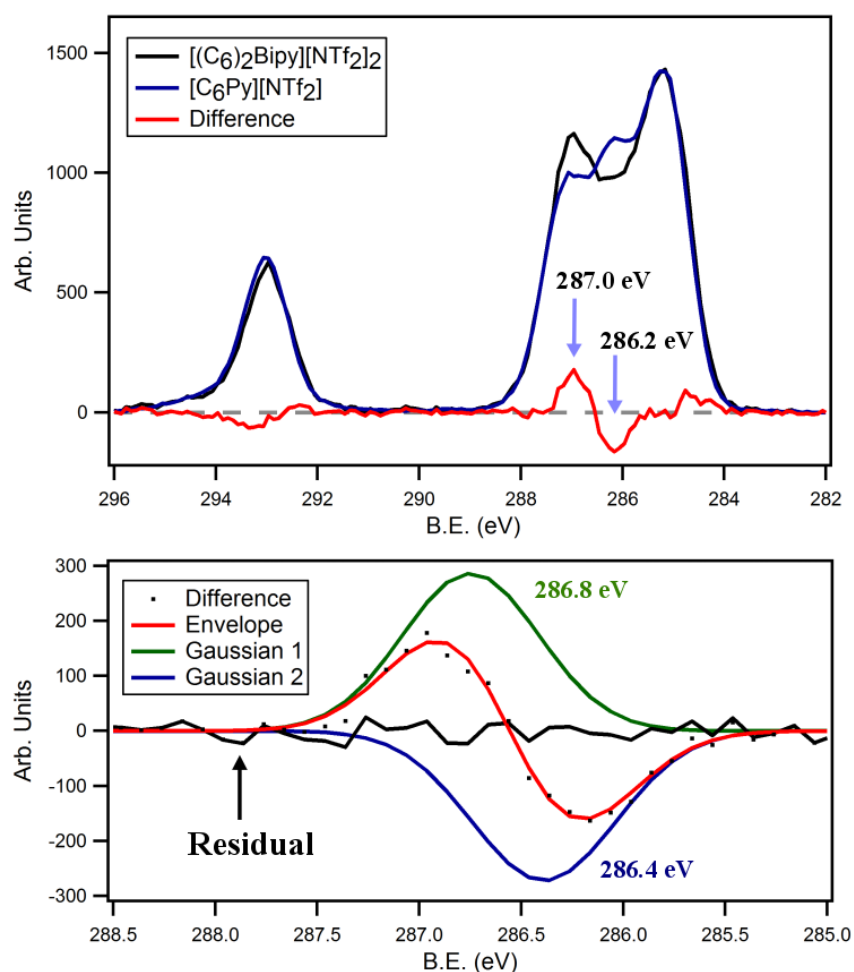


Figure 4.5 Plots for the C1s region of $[(C_6)_2Bipy][NTf_2]_2$ overlaid on the C 1s region of $[C_6Py][NTf_2]$. The spectra are normalised to the F 1s signal of the anion. The difference (top) between the two regions has been fitted with two oppositely phased Gaussian distributions (bottom), the envelope (red) is also displayed as a fit to the observed difference.

Integrating the positive signal of the difference spectrum gives an area that is equal to 0.46 carbon atoms, as calculated by the [(C₆)₂Bipy][NTf₂]₂ photoemission. A lower signal such as this may be the result of insufficient separation between the initial and final B.E.s of the shifting signal. Since subtraction of one spectrum from another involves positive and negative differences, overlapping signals may produce characteristic shapes with sharp drops between the two. The shift between the maxima and minima of the difference spectrum is only 0.8 eV. Individual carbon atoms usually produce FWHMs of around 0.8-1.2 eV. The structure of the derived difference spectrum is therefore most probably the result of slightly overlapping signals.

There may therefore be potential discrepancies in the true and observed peak positions. In order to address this issue, the calculated difference spectrum has been fitted with two oppositely phased Gaussian distributions. Each Gaussian curve has an area that is fixed to the calculated area for one sp² carbon atom. The FWHMs of the two curves have also been constrained between 0.8 and 1.2 eV and set to be equal. The Gaussian distributions and the resulting fit to the difference spectrum is also shown in **Figure 4.5**. The resulting fit appears to accurately reproduce the observed difference spectrum, with little residual signal.

Unfortunately, the maxima and minima of the difference do not coincide with the positions of the two Gaussian distributions. The new B.E. values are 286.8 eV for the positive signal and 286.4 eV for the negative signal. The positive signal being 0.2 eV lower than the observed peak and the negative signal being 0.2 eV higher than the observed peak. This discrepancy requires further investigations in order to obtain the true B.E. value for the C⁴ position. A larger B.E. shift between the positive and negative signals of the C⁴ carbon would provide distinct peaks that may lead to stronger evidence. This may be achieved by chlorination of the 4-position of the pyridinium ring,²³ as with the 2-chloropyridinium and 3-chloropyridinium salts analysed in the previous chapter. For the purpose of this work, the positive signal at 286.2 eV will be considered the more accurate B.E. for the C⁴ position, until future experiments provide further evidence to confirm or deny this observation.

4.2.1.3 Confirmation of the $[C_n\text{Py}][A]$ C 1s Peak Fitting Model

The current peak fitting model of the $[C_8\text{Py}][\text{NTf}_2]$ C 1s region is shown in **Figure 4.6**. Chlorination of the pyridine ring at the 2- and 3-positions has confirmed the location of the $C^{2,6}$ and $C^{3,4}$ components, see *Chapter 3*. Although the C^4 component is expected to have a similar B.E. to $C^{3,4}$, this assumption has not yet been confirmed through experimentation. However, the data provided from the comparison of the $[(C_n)_2\text{Bipy}][\text{NTf}_2]_2$ and $[C_n\text{Py}][\text{NTf}_2]$ C 1s regions has placed the C^4 component at a B.E. of exactly 286.2 eV. The C^4 peak position for $[C_n\text{Py}][\text{NTf}_2]$ C 1s XP spectra was previously placed at 286.1 eV, which is within the 286.2 eV signal by 0.1 eV. This finding confirms that the C^4 carbon emits photoelectron signals that are coincident with the $C^{3,5}$ carbons of the pyridinium ring.

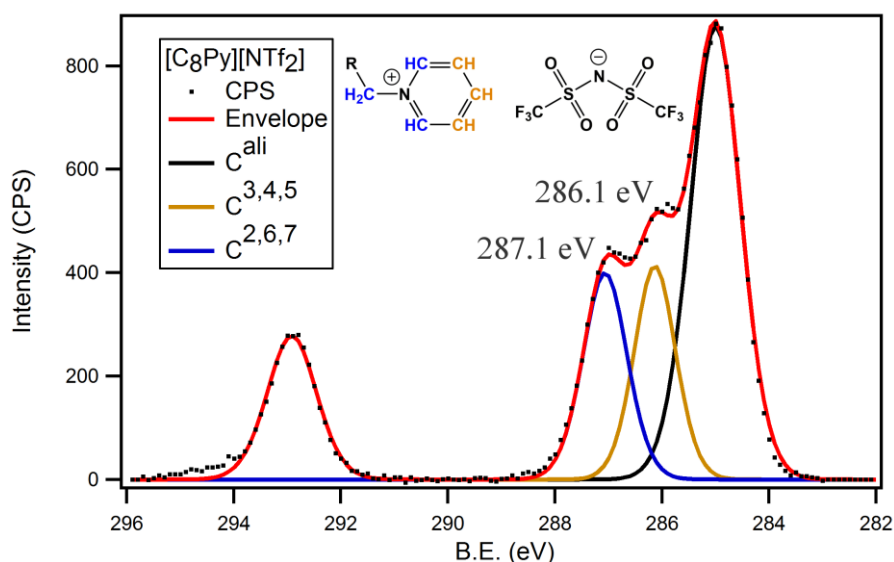


Figure 4.6 The peak fitted $[C_8\text{Py}][\text{NTf}_2]$ C 1s region with the component assignments shown on the appended structure.

Again, it is important to highlight that through the shifting of electron density, the exact location of the pyridinium C^4 component has been revealed. By comparing multiple C 1s regions, new data has been obtained that would otherwise be unavailable. The symmetrical dicationic $[(C_n)_2\text{Bipy}][\text{NTf}_2]_2$ salts have therefore been utilised in order to confirm the current pyridinium C 1s peak fitting procedures.

4.2.1.4 Peak Fitting the $[(C_n)_2Bipy][NTf_2]_2$ C 1s Region

A visual representation of the B.E. shifts observed in the difference spectra of the $[(C_n)_2Bipy][NTf_2]_2$ and $[C_nPy][NTf_2]$ salts is shown in **Figure 4.7**. The C^4 component increases in B.E. from 286.2 eV to 287.0 eV due to the neighbouring electron deficient pyridinium ring. The B.E. of the bipyridinium C^4 component is therefore coincident with the $C^{2,6,7}$ components of the pyridinium and bipyridinium rings. Since the exact location of the $C^{2,6}$ carbon components (287.0 eV) has been confirmed by chlorination of the pyridinium ring, these coincident peaks may be combined and fixed in B.E. for $[NTf_2]^-$ salts, e.g. the component becomes $C^{2,6,7} + C^4$. **Figure 4.7** shows the resulting carbon environment groups for the dialkyl-4,4'-bipyridinium C 1s region.

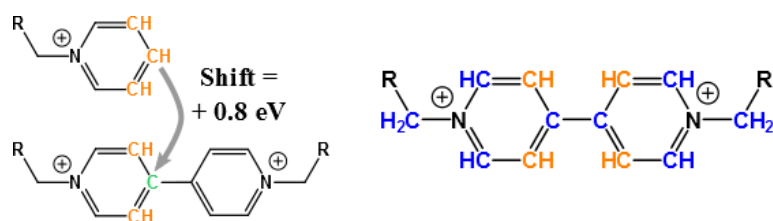


Figure 4.7 A visualised representation of the observed B.E. shift in the difference spectrum generated from $[(C_n)_2Bipy][NTf_2]_2$ and $[C_nPy][NTf_2]$ (left). The new fitting model for dialkyl-bipyridinium salts (right).

With the C^4 position of the bipyridinium salts being shifted by + 0.8 eV (relative to the C^4 component of the pyridinium ring), the $C^{3,5}$ component may also experience a positive B.E. shift due to the neighbouring charge withdrawal. For this reason the peak position of the $C^{3,5}$ photoemission were constrained to 285.8-286.5 eV. **Figure 4.8** shows the resulting peak fitted C 1s regions for the $[(C_n)_2Bipy][NTf_2]_2$ salts. The FWHMs for large C^{ali} components ($n = 6$ and 8) have been constrained to 0.8-1.5 eV, while all other components have been constrained to 0.8-1.2 eV.²⁰ The areas of the components have also been fixed according to the number of associated carbon environments. For example, the $[(C_8)_2Bipy][NTf_2]_2$ components $C^{3,5}$, $C^{2,6,7} + C^4$ and C^{ali} have areas set to the ratio 1.8:3.7:7, after accounting for shake up/off losses.

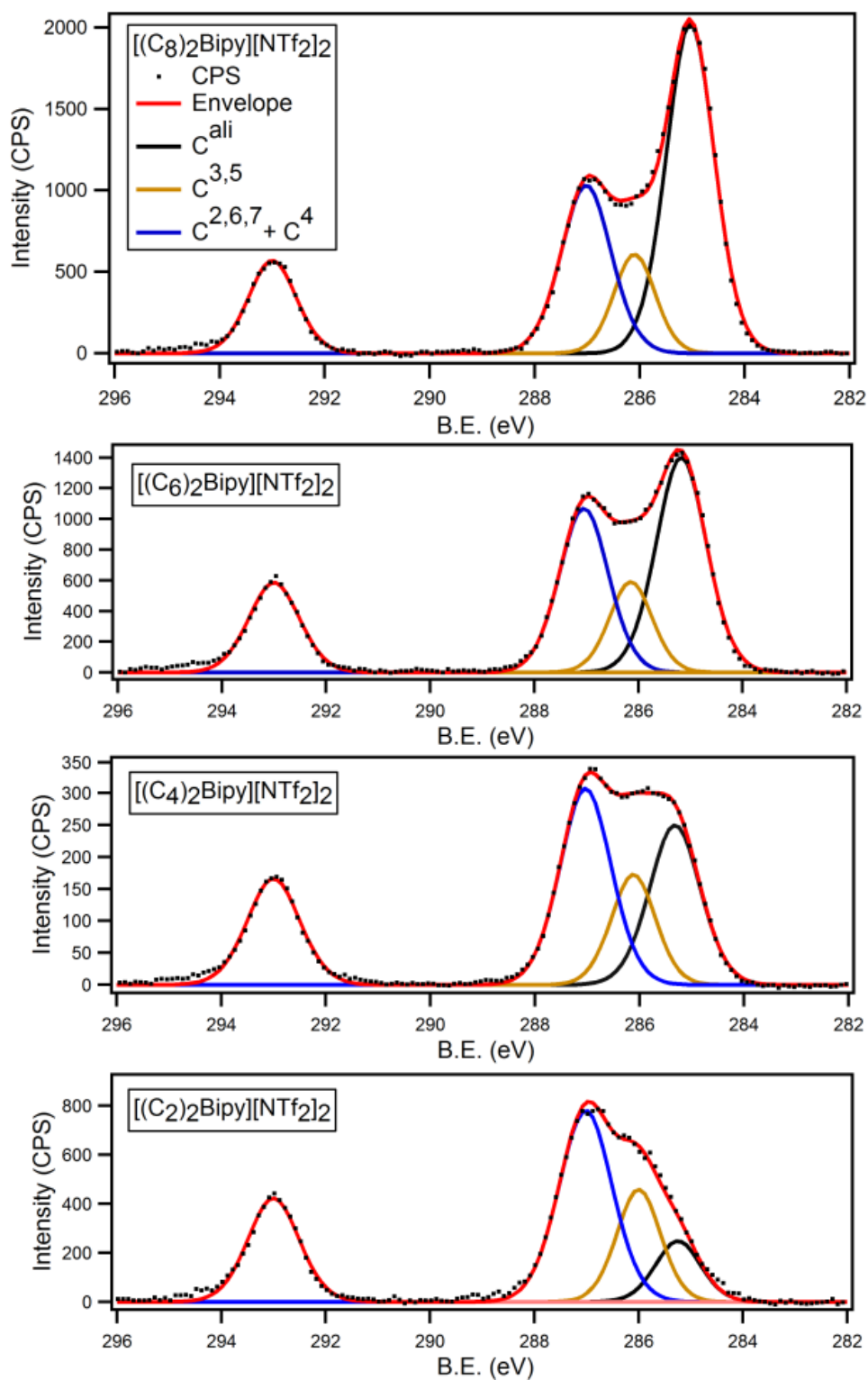


Figure 4.8 The peak fitted C 1s regions of the $[(C_n)_2Bipy][NTf_2]_2$ salts. The components are labelled on the $[(C_8)_2Bipy][NTf_2]_2$ graph (top).

Table 4.5 The binding energies for the C 1s components of the [(C_n)₂Bipy][NTf₂]₂ salts. The error for measurement is 0.1 eV.

Cation	Anion	Binding Energy (eV)			
		C ^{ali}	C ^{2,6,7} + C ⁴	C ^{3,5}	CF ₃
[(C ₂) ₂ Bipy] ²⁺	2[NTf ₂] ⁻	285.0	287.0	286.0	293.0
[(C ₄) ₂ Bipy] ²⁺	2[NTf ₂] ⁻	285.2	287.0	286.1	293.0
[(C ₆) ₂ Bipy] ²⁺	2[NTf ₂] ⁻	285.3	287.0	286.1	293.0
[(C ₈) ₂ Bipy] ²⁺	2[NTf ₂] ⁻	285.3	287.0	286.1	293.0

The B.E. values acquired from the peak fitting of the [(C_n)₂Bipy][NTf₂]₂ C 1s regions are shown in **Table 4.5**. The only significant changes in the B.E.s of the dicationic salts are associated with the aliphatic carbon chains. **Figure 4.8** shows this trend visually, as well as the corresponding change in the size of the C^{ali} component area. The shifting of the C^{ali} component with decreasing chain size was discussed in the previous chapter. The C^{3,5} components are consistent in their B.E.s and appear at the previously observed value of 286.1 eV,¹⁸ therefore the associated carbons do not experience XPS observable charge withdrawal.

By comparing the dicationic [(C_n)₂Bipy][NTf₂]₂ salts to the traditional mono-cationic [C_nPy][NTf₂] ILs, the peak fitting models of the C 1s spectra for each set of samples have been refined. In the same way, the di-alkylated bipyridinium salts may also provide further information when compared to the mono-alkylated bipyridinium products.

4.2.2 XPS of Alkyl-4,4'-bipyridinium Ionic Liquids

Unlike the di-cationic salts, the mono-cationic [C_nBipy][NTf₂] salts do not possess a centre of symmetry along the 4,4'-carbon to carbon bonds. One side of the bipyridinium unit is not alkylated and it contains a neutral free nitrogen atom. The C 1s signal for the mono-alkylated bipyridinium salt will therefore be considerably more complex than the dicationic C 1s photoemission.

4.2.2.1 Wide and High Resolution Scans

The wide and high resolution scans for the mono-cationic $[\text{C}_n\text{Bipy}][\text{NTf}_2]$ salts are shown in **Figure 4.9**. The wide scans show only the expected photoemissions, confirming a successful anion metathesis and a clean sample surface. The high resolution scans show good consistency between the various alkyl chain analogues of $[\text{C}_n\text{Bipy}][\text{NTf}_2]$. The spectra are charge corrected to the C 1s C^{ali} component for $n = 8$, set to 285.0 eV. The corresponding value for the N 1s signal (402.5 eV) was then used to reference $n = 2, 4$ and 6.

The calculated atomic percentages for the $[\text{C}_n\text{Bipy}][\text{NTf}_2]$ salts are displayed in **Table 4.6**. As with the dicationic salts, the measured values do not deviate from the calculated values by more than 10%; the error of measurement may be as high as 20%. The shake up/off losses from the $[\text{C}_n\text{Bipy}][\text{NTf}_2]$ salts have been calculated from the respective C 1s regions and the values are presented in **Table 4.7**. The average value is 9.79%, therefore the standard 10% signal deductions for sp^2 pyridinium carbons²² are also valid for the mono-cationic $[\text{C}_n\text{Bipy}][\text{NTf}_2]$ salts.

Table 4.6 The atomic percentages for the $[\text{C}_n\text{Bipy}][\text{NTf}_2]$ salts. The deviation (%) in the found and calculated values is also presented

Cation	Anion		Composition (%)				
			C	N	O	F	S
$[\text{C}_2\text{Bipy}]^+$	$[\text{NTf}_2]^-$	Found	50.48	9.36	13.60	20.28	6.28
		Calculated	48.28	10.34	13.79	20.69	6.90
		Deviation (%)	-4.36	10.47	1.40	2.02	9.87
$[\text{C}_4\text{Bipy}]^+$	$[\text{NTf}_2]^-$	Found	52.59	9.62	12.85	19.06	5.88
		Calculated	51.62	9.68	12.90	19.35	6.45
		Deviation (%)	-1.84	0.62	0.39	1.52	9.69
$[\text{C}_6\text{Bipy}]^+$	$[\text{NTf}_2]^-$	Found	55.55	8.55	12.16	18.13	5.61
		Calculated	54.55	9.09	12.12	18.18	6.06
		Deviation (%)	-1.80	6.32	-0.33	0.28	8.02
$[\text{C}_8\text{Bipy}]^+$	$[\text{NTf}_2]^-$	Found	58.90	7.96	11.35	16.36	5.43
		Calculated	57.15	8.57	11.43	17.14	5.71
		Deviation (%)	-2.97	7.66	0.70	4.77	5.16

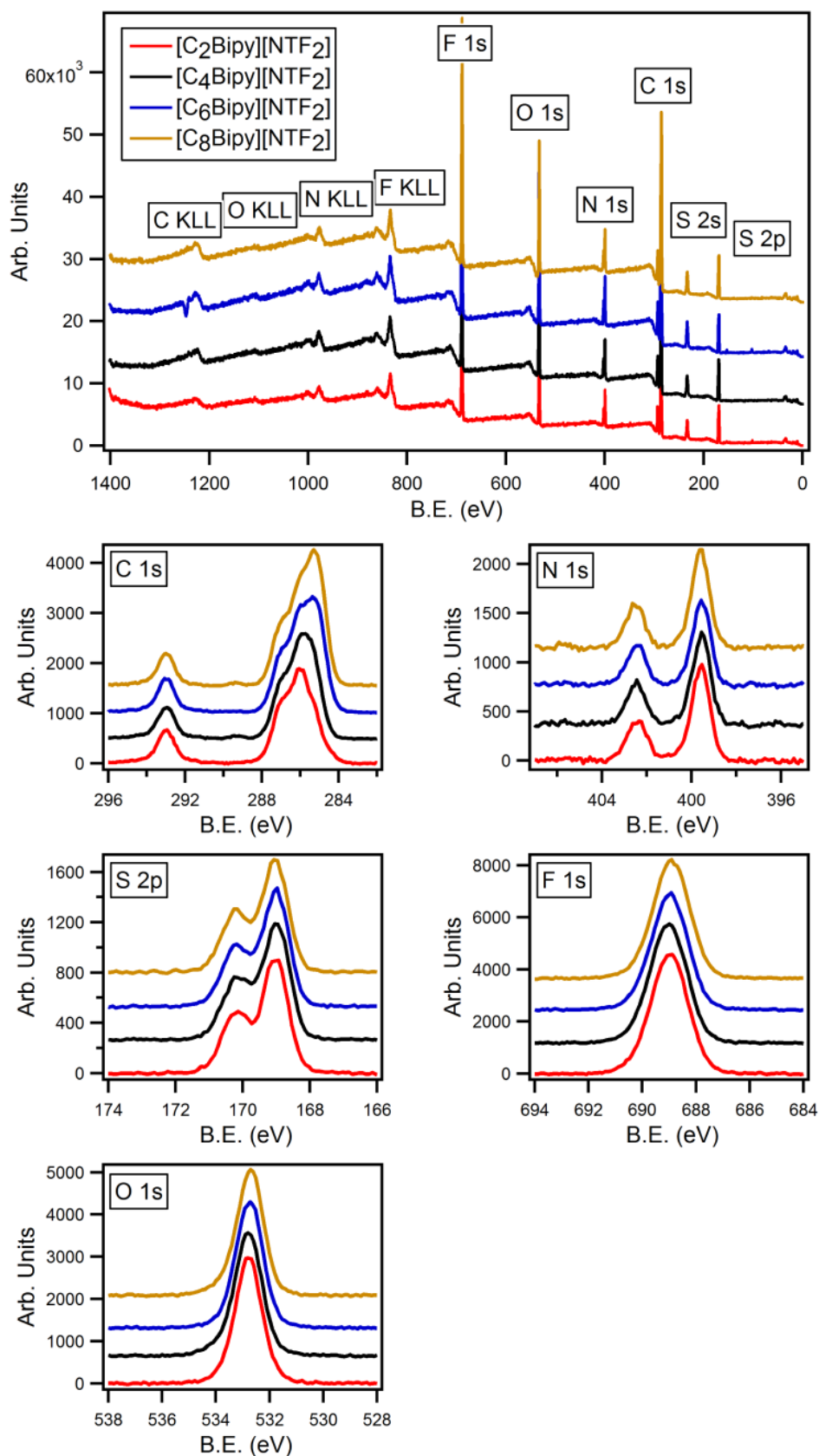


Figure 4.9 The wide and high resolution scans for the $[C_n\text{Bipy}][\text{NTf}_2]$ salts, where $n = 2$ (red), 4 (black), 6 (blue) and 8 (orange). The scans are colour coded to the legend shown on the top plot.

The C 1s region is the only photoemission that shows significant change between each alkyl chain analogue, as expected. The aliphatic chain is observed to grow and widen at the 285.0 eV position as previously observed and explained.²¹ The N 1s high resolution scans appear to show only two signals. Since three nitrogen environments are expected, these peaks require further analysis and investigation in order to present accurate B.E. for the dicationic salts.

Table 4.7 The percentage of shake up/off per aromatic carbon atom for the $[C_n\text{Bipy}][\text{NTf}_2]$ salts. Values are measured relative to the main C 1s photoemission.

Cation	Anion	Shake up/off per Sp ² carbon atom (%)
$[\text{C}_2\text{Bipy}]^+$	$[\text{NTf}_2]^-$	9.23
$[\text{C}_4\text{Bipy}]^+$	$[\text{NTf}_2]^-$	9.64
$[\text{C}_6\text{Bipy}]^+$	$[\text{NTf}_2]^-$	10.55
$[\text{C}_8\text{Bipy}]^+$	$[\text{NTf}_2]^-$	9.74
Average		9.79

4.2.2.2 N 1s Peak Fitting

The N 1s region for $[\text{C}_8\text{Bipy}][\text{NTf}_2]$ has been plotted against the N 1s region obtained from the $[(\text{C}_8)_2\text{Bipy}][\text{NTf}_2]_2$ sample, **Figure 4.10**. The spectra have been normalised to the F 1s signal areas of the anions. As with normalisation of the dicationic salts to the pyridinium spectra, this results in photoemissions from half of the $[(\text{C}_8)_2\text{Bipy}][\text{NTf}_2]_2$ salt. This time, one cationic nitrogen from the dication and one anionic nitrogen from the anion. When displayed relative to the $[\text{C}_8\text{Bipy}][\text{NTf}_2]$ signal, the peak at lower B.E. appears twice as intense in the mono-cationic spectrum compared to the dicationic spectrum. The additional electron density occurs from the neutral nitrogen from the non-alkylated side of the $[\text{C}_8\text{Bipy}][\text{NTf}_2]$ molecule.

By taking the difference between the $[\text{C}_8\text{Bipy}][\text{NTf}_2]$ and the $[(\text{C}_8)_2\text{Bipy}][\text{NTf}_2]_2$ N 1s regions, the exact peak position of the neutral nitrogen environment may be found, see **Figure 4.10**. Although this may be achieved by simple N 1s fitting models, uncertainty in peak areas and FWHMs may result in incorrect B.E. values for the constituent components. Both the anionic nitrogen and the neutral nitrogen appear exactly coincident at 399.5 eV. Simple data subtraction has therefore provided the exact B.E. for the neutral nitrogen species. The amount of electron density about the anionic and neutral nitrogen atoms is therefore the same. Although the $[\text{NTf}_2]^-$ species is negatively charged, electron density is delocalised across its structure reducing the amount of charge on the nitrogen atom.

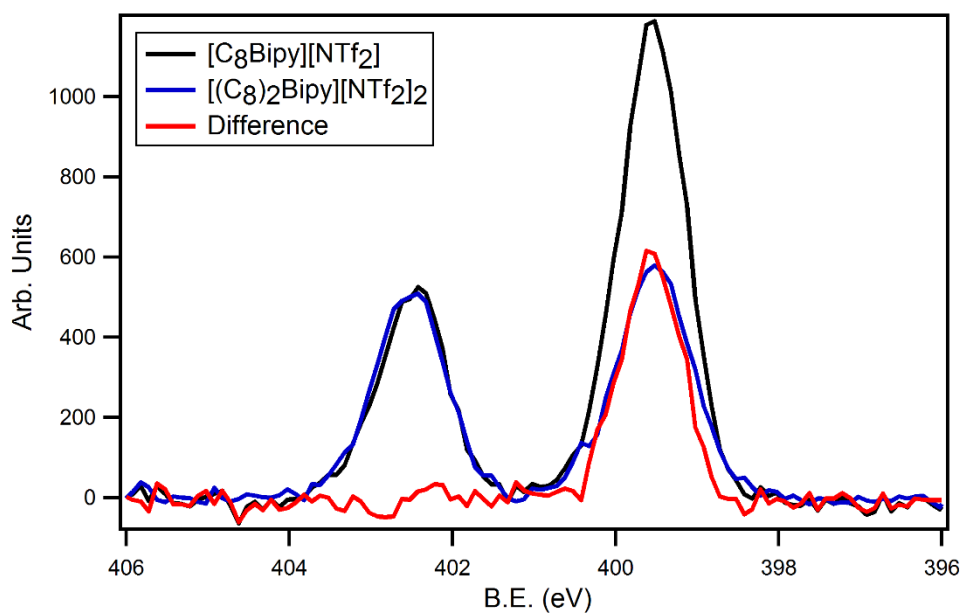


Figure 4.10 The plot of the N 1s region for $[\text{C}_8\text{Bipy}][\text{NTf}_2]$ (black) with the $[(\text{C}_8)_2\text{Bipy}][\text{NTf}_2]_2$ (blue) region overlaid. The difference (red) between the two spectra has been taken.

The B.E.s for all heteroatoms are presented in **Table 4.8**. The consistency in all of the obtained values supports the charge correction methods that have been applied to the spectra. All $[\text{C}_n\text{Bipy}][\text{NTf}_2]$ N 1s regions show peaks at 399.5 eV when producing difference spectra from the analogous $[(\text{C}_n)_2\text{Bipy}][\text{NTf}_2]_2$ salts. This supports the data subtraction process for the elucidation of the neutral nitrogen photoemission.

Table 4.8 The binding energies for the heteroatoms of the $[C_n\text{Bipy}][\text{NTf}_2]$ salts.

		Binding Energy (eV)					
		N 1s			F 1s	O 1s	S 2p _{3/2}
Cation	Anion	Cationic	Neutral	Anionic			
$[\text{C}_2\text{Bipy}]^+$	$[\text{NTf}_2]^-$	402.5	399.5	399.5	689.0	532.8	169.0
$[\text{C}_4\text{Bipy}]^+$	$[\text{NTf}_2]^-$	402.5	399.5	399.5	689.0	532.8	169.0
$[\text{C}_6\text{Bipy}]^+$	$[\text{NTf}_2]^-$	402.5	399.5	399.4	689.0	532.8	169.0
$[\text{C}_8\text{Bipy}]^+$	$[\text{NTf}_2]^-$	402.5	399.5	399.5	688.9	532.7	169.0

4.2.2.3 C 1s Peak Fitting

The $[C_n\text{Bipy}][\text{NTf}_2]$ structure contains a larger number of varied carbon environments than the dicationic salt, **Figure 4.11**. In addition to the $\text{C}^{2,6,7}$ (blue) and $\text{C}^{3,5}$ (orange) components, signals from the $\text{C}^{2',6'}$ (yellow) and $\text{C}^{3',5'}$ (dark red) carbons are expected. The 4- and 4'-carbon environments of the mono-cationic $[C_n\text{Bipy}][\text{NTf}_2]$ salts should also differ in B.E. due to the desymmetrisation of the bipyridinium ring. Most likely the $\text{C}^{4'}$ (yellow) will produce a B.E. similar to the $\text{C}^{2',6'}$ carbons as they are both bonded to electron withdrawing moieties. The C^4 carbon (dark green) of the $[C_n\text{Bipy}][\text{NTf}_2]$ salts should have a B.E. value in between the pyridinium C^4 component (286.2 eV) and the $[(C_n)_2\text{Bipy}][\text{NTf}_2]_2$ C^4 component (287.0 eV).

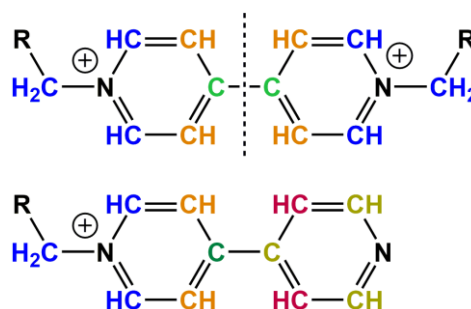


Figure 4.11 The structure of $[(C_n)_2\text{Bipy}][\text{NTf}_2]_2$ with the colour coded carbon environments (top) and the structure of $[C_n\text{Bipy}][\text{NTf}_2]$ with the corresponding and additional carbon environments (bottom).

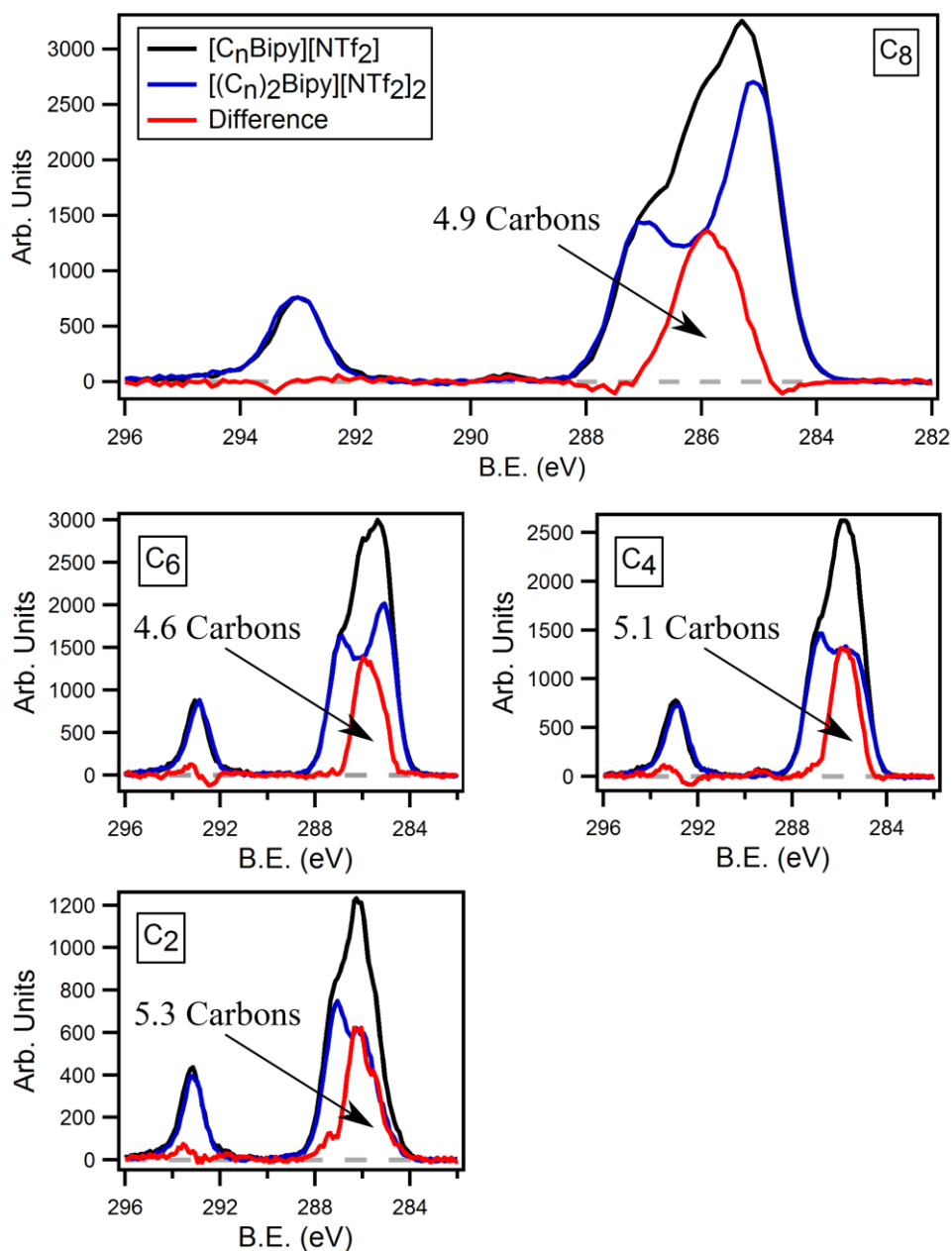


Figure 4.12 The C 1s regions for the mono-cationic $[C_n\text{Bipy}][\text{NTf}_2]$ salts (black), with the corresponding $[(C_2)_2\text{Bipy}][\text{NTf}_2]_2$ (blue) regions overlaid and the resulting difference spectra (red).

When the C 1s regions of the mono-cationic and di-cationic salts are overlaid and normalised to the F 1s signals of the anion, the difference between the spectra may be taken, **Figure 4.12**. Again, normalisation effectively halves the dicationic structure, in the same way as previously described. The resulting difference spectra show single wide peaks about the 286.0 eV position. The subtraction process may be represented schematically *via* the structures of the

bipyridinium units, **Figure 4.13**. The carbons involved in the generation of the difference spectra are colour coded to the C 1s photoemissions in **Figure 4.12**. By subtracting half of the $[(C_n)_2Bipy][NTf_2]_2$ spectra (blue carbons) from the $[C_nBipy][NTf_2]$ spectra (black carbons), the resulting signal should represent only the red carbons shown on the $[C_nBipy][NTf_2]$ structure.

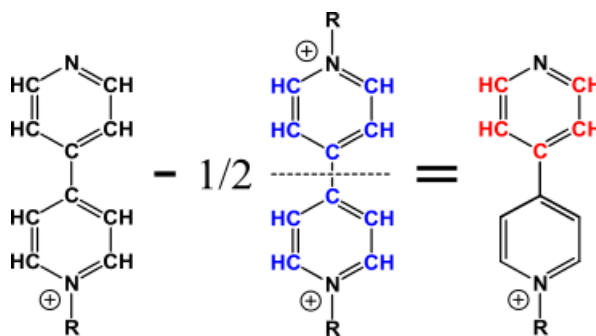


Figure 4.13 A schematic structural representation of the carbons involved in the difference spectrum generated by subtracting half of the $[(C_n)_2Bipy][NTf_2]_2$ C 1s photoemission (blue carbons) from the $[C_nBipy][NTf_2]$ photoemission (black carbons). The difference spectrum contains the photoelectron signals from the red carbons only.

If each generated difference spectrum is integrated and compared to the original $[C_nBipy][NTf_2]$ photoemission, the number of carbon atoms that the difference peak represents may be calculated (after accounting for shake up/off losses). The calculated values for the number of carbon atoms for each difference area are shown in **Figure 4.12**. The average calculated value is 5.0 carbon atoms which is exactly as expected. This means that the difference from the raw CPS data represents all 5 carbon atoms shown in red in **Figure 4.13**.

To check the validity of the generated difference spectra, this analytical procedure can be repeated with the $[C_nPy][NTf_2]$ photoemission in place of $[(C_n)_2Bipy][NTf_2]_2$. After normalising both mono-cationic salts, data subtraction should reveal the same difference spectra as obtained in **Figure 4.12**. For example, the $[C_4Py][NTf_2]$ C 1s photoemission may be subtracted from the $[C_4Bipy][NTf_2]$ C 1s region, see **Figure 4.14**. The signal shown in

green represents the difference between the $[\text{C}_4\text{Py}][\text{NTf}_2]$ and the $[\text{C}_4\text{Bipy}][\text{NTf}_2]$ C 1s photoemissions. The signal shown in red represents the original difference between the $[(\text{C}_4)_2\text{Bipy}][\text{NTf}_2]_2$ and the $[\text{C}_4\text{Bipy}][\text{NTf}_2]$ C 1s photoemissions. Both resulting signals are coincident, with little deviation in the structure of the peaks. This result significantly supports the assignment of the 5 red carbon environments to the $[\text{C}_n\text{Bipy}][\text{NTf}_2]$ C 1s difference spectra.

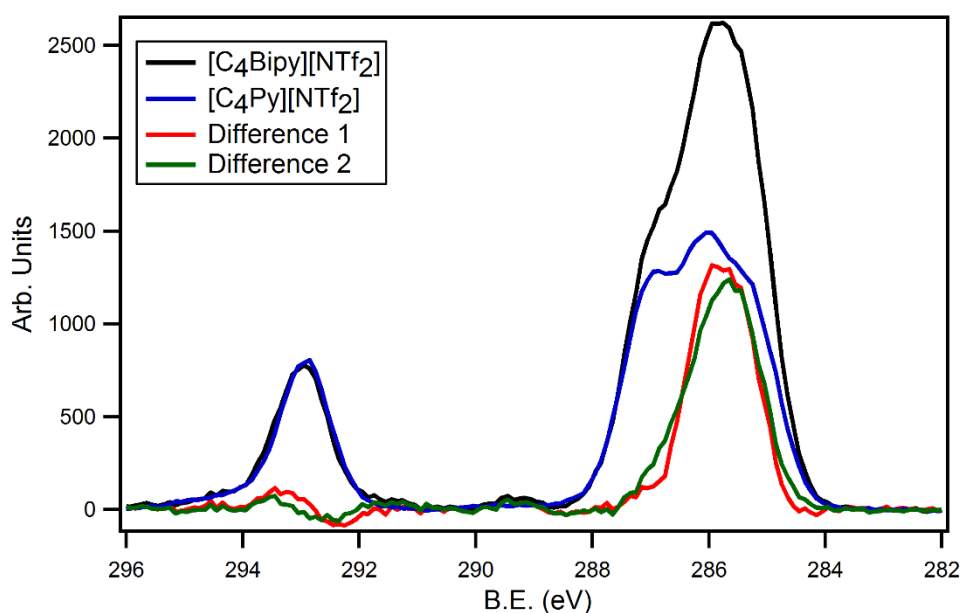


Figure 4.14 The plot of the difference (green) generated when the $[\text{C}_4\text{Py}][\text{NTf}_2]$ C 1s signal (blue) is subtracted from the $[\text{C}_4\text{Bipy}][\text{NTf}_2]$ C 1s photoemission (black). As a comparison, the difference (red) generated from the subtraction of the $[(\text{C}_4)_2\text{Bipy}][\text{NTf}_2]_2$ C 1s signal from the $[\text{C}_4\text{Bipy}][\text{NTf}_2]$ C 1s photoemission is shown.

Unfortunately, further peak identification is impossible without additional experimentation. However using parameter constrained GL (30) line shapes, peak fitting models may be used in order to examine the obtained difference spectra. **Figure 4.15** shows the resulting fits for a two component model based upon the $\text{C}^{2',4',6'}$ (yellow) and $\text{C}^{3',5'}$ (dark red) carbon environments. The FWHMs are constrained between 0.8 and 1.1 eV and the areas are constrained to be equal to the number of carbon environments, after accounting for shake up/off losses (2.7 : 1.8 for $\text{C}^{2',4',6'}$: $\text{C}^{3',5'}$). The measured B.E.s of the component peaks are also displayed in **Table 4.9**.

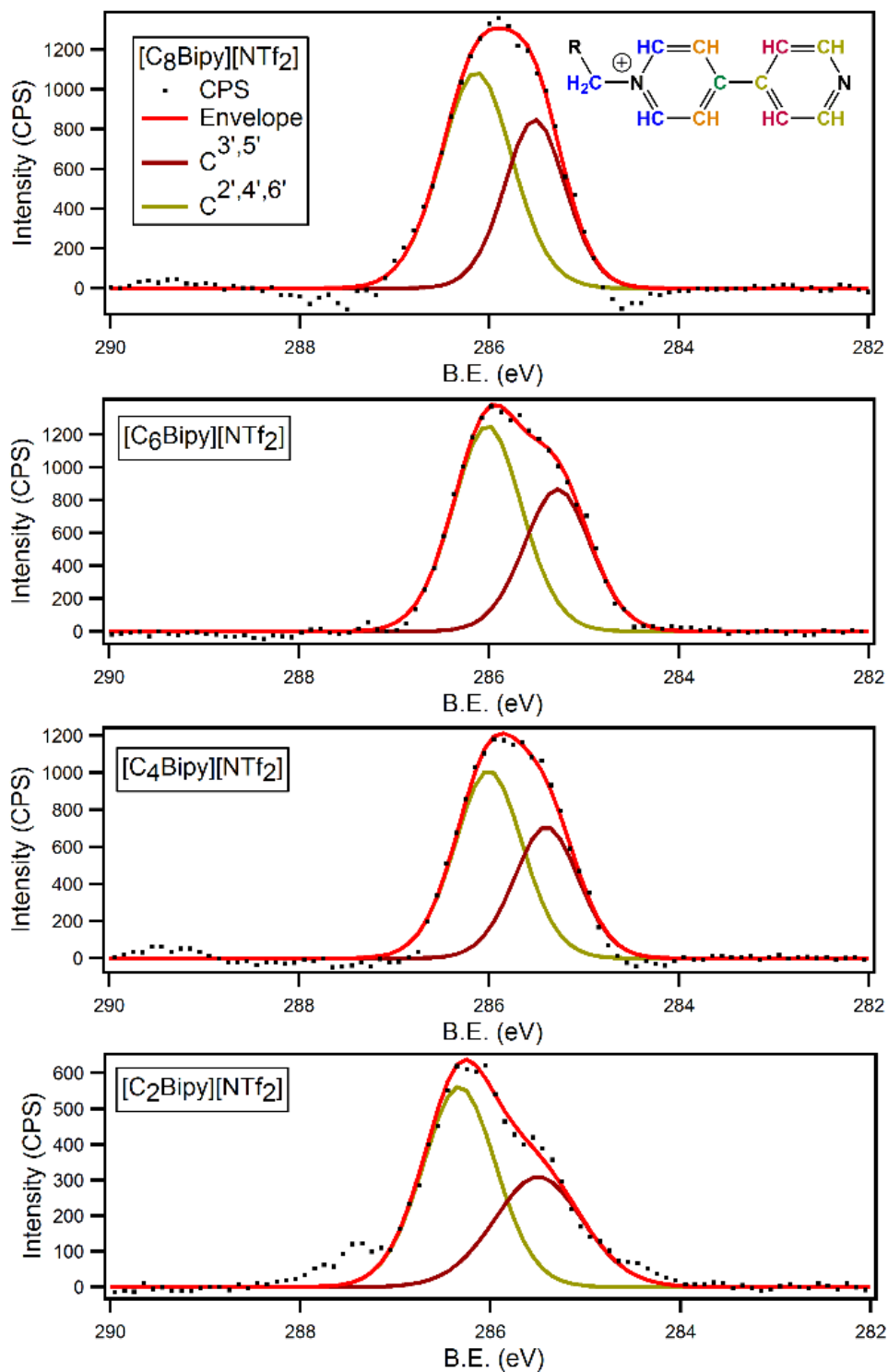


Figure 4.15 The individual difference spectra generated by the subtraction of the $[(C_n)_2\text{Bipy}][\text{NTf}_2]$ C 1s region from the $[\text{C}_n\text{Bipy}][\text{NTf}_2]$ C 1s region. The signal has been fitted with components that correspond to the $\text{C}^{2',4',6'}$ and $\text{C}^{3',5'}$ carbon environments.

Table 4.9 The B.E.s for the $C^{2,4,6'}$ and $C^{3,5'}$ components used to fit the difference spectra obtained from the subtraction of the $[(C_n)_2Bipy][NTf_2]$ C 1s region from the $[C_nBipy][NTf_2]$ C 1s region.

Cation	Anion	B.E. (eV)	
		$C^{2,4,6'}$	$C^{3,5'}$
$[C_2Bipy]^+$	$[NTf_2]^-$	286.2	285.5
$[C_4Bipy]^+$	$[NTf_2]^-$	286.0	285.4
$[C_6Bipy]^+$	$[NTf_2]^-$	286.0	285.3
$[C_8Bipy]^+$	$[NTf_2]^-$	286.1	285.5
		286.1±1	285.4±1

If the bipyridinium molecule was not bonded at the 4,4'-positions, the B.E. of the $C^{4'}$ carbon environment should be equal to the $C^{3,5'}$ carbon environments. This assumption is based upon the analysis of the dicationic $[(C_n)_2Bipy][NTf_2]_2$ salts at the beginning of this chapter, where the pyridinium C^4 B.E. was shown to be equal to the B.E. of the $C^{3,5}$ carbons. During this analysis, the observed B.E. shift (286.2 eV to 287.0 eV) in the C 1s difference of $[(C_n)_2Bipy][NTf_2]_2$ and $[C_nPy][NTf_2]$ revealed the impact of pyridinium functionalisation upon a carbon environment, **Figure 4.5**. This means that the $C^{3,5'}$ and the $C^{4'}$ carbon signals of the $[C_nBipy][NTf_2]$ C 1s molecule should be 0.8 eV apart. As **Table 4.9** shows, the B.E. for each component are separated by 0.7 eV, this is within the 0.1 eV measurement error and therefore the component assignments are supported in this simplified fitting model. **Figure 4.16** shows a schematic representation of the shifting B.E.s upon functionalisation.

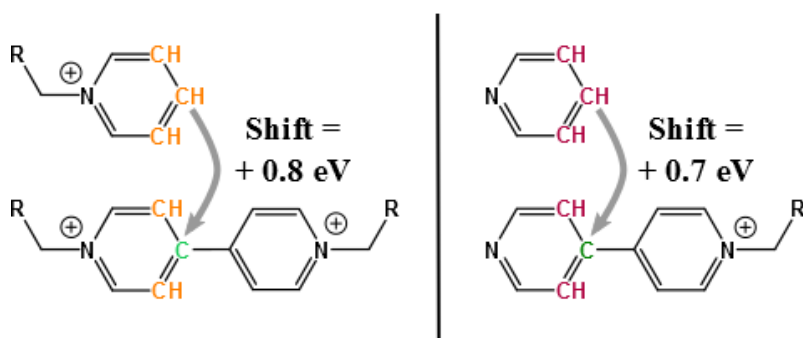


Figure 4.16 The B.E. impact in the C 1s region of functionalisation with a pyridinium ring bound via the 4-position of the aromatic ring.

In order to peak fit the entire C 1s regions of the mono-cationic $[\text{C}_n\text{Bipy}][\text{NTf}_2]$ salts, the intermediate values for the $\text{C}^{2',4',6'}$ (286.1 eV) and $\text{C}^{3',5'}$ (285.4 eV) components have been chosen. These values encompass all recorded B.E.s presented in **Table 4.9** by the error of 0.1 eV. The $\text{C}^{2',4',6'}$ component is coincident with the previously measured $\text{C}^{3,5}$ peak at 286.1 eV. For this reason both signals have been grouped into one component which is the sum of the two, e.g. $\text{C}^{3,5} + \text{C}^{2',4',6'}$. The B.E. of the $\text{C}^{2,6,7}$ component is known from the previous chlorination experiments and should appear around 287.1 eV. The C^4 carbon presents the only unknown B.E. for the $[\text{C}_n\text{Bipy}][\text{NTf}_2]$ salts. Although as previously stated, this value should be between the pyridinium C^4 component (286.2 eV) and the $[(\text{C}_n)_2\text{Bipy}][\text{NTf}_2]_2$ C^4 component (287.0 eV).

The full C 1s peak fittings for the $[\text{C}_n\text{Bipy}][\text{NTf}_2]$ salts are displayed in **Figure 4.17** and the corresponding component B.E.s are presented in **Table 4.10**. Each plot shows that the envelope closely resembles the experimental counts per second for each alkyl chain analogue. When a C 1s model contains multiple components, almost any photoemission shape may be represented by altering various peak parameters such as FWHM, area and position. However, in this case, the majority of the peak position have been deduced by the generation of difference spectra. For this reason, peaks are held in their known B.E.s (± 0.1 eV), with the exception of the C^4 and C^{ali} components of $n=2, 4$ and 6 ($n = 8$ is set to 285.0 eV).

Table 4.10 The B.E.s of the C 1s components used to peak fit the $[\text{C}_n\text{Bipy}][\text{NTf}_2]$ salts. The values in bold have been constrained to that particular B.E. position (± 0.1 eV) as they are known from previous difference spectra analyses. .

Cation	Anion	Binding Energy (eV)						CF_3
		C^{ali}	$\text{C}^{2,6,7}$	$\text{C}^{3,5}$	$\text{C}^{2',4',6'}$	$\text{C}^{3',5'}$	C^4	
$[\text{C}_2\text{Bipy}]^+$	$[\text{NTf}_2]^-$	285.3	287.1	286.1	286.1	285.4	286.6	293.0
$[\text{C}_4\text{Bipy}]^+$	$[\text{NTf}_2]^-$	285.3	287.1	286.1	286.1	285.4	286.6	293.0
$[\text{C}_6\text{Bipy}]^+$	$[\text{NTf}_2]^-$	285.1	287.1	286.0	286.1	285.4	286.6	293.0
$[\text{C}_8\text{Bipy}]^+$	$[\text{NTf}_2]^-$	285.0	287.1	286.1	286.1	285.4	286.6	293.0

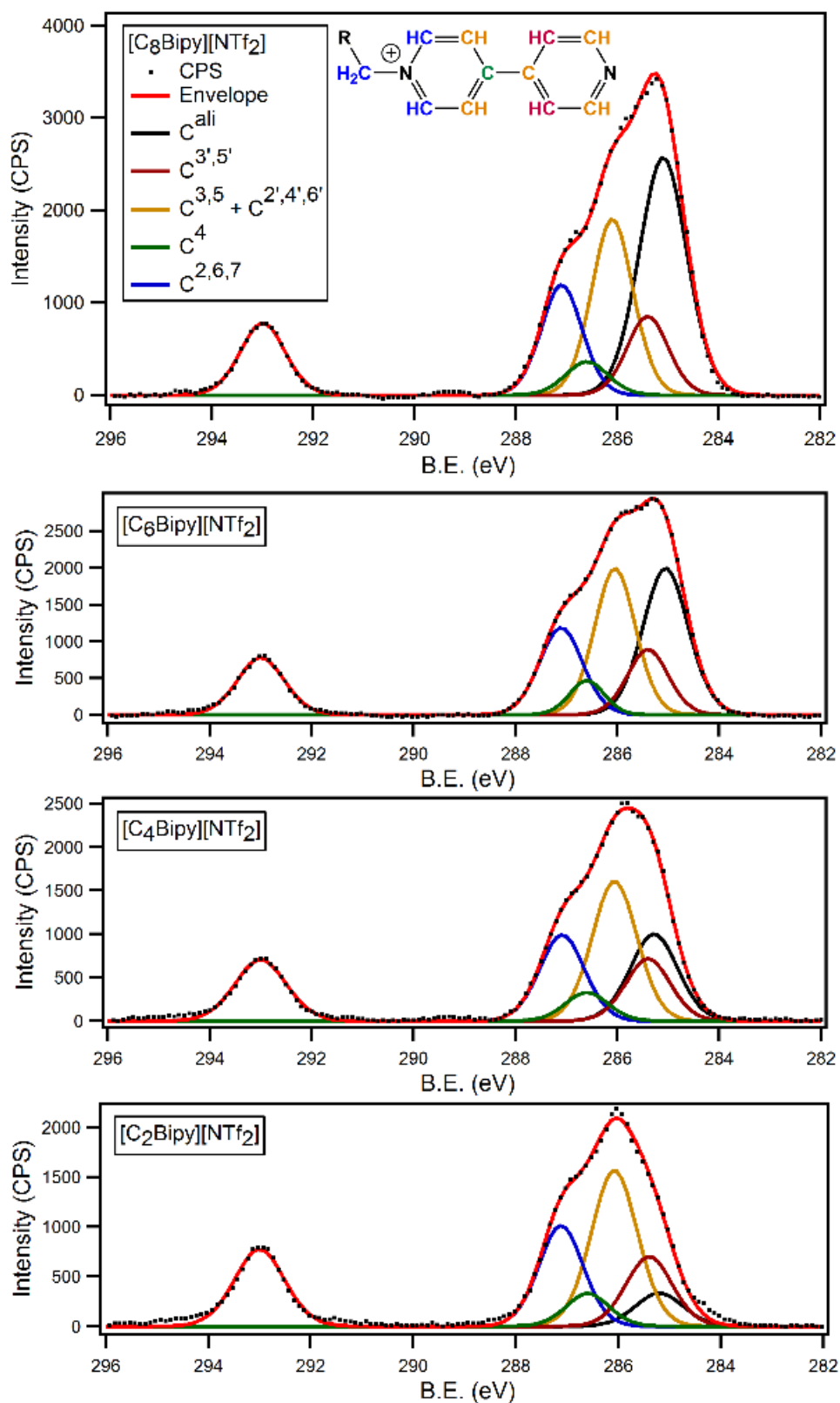


Figure 4.17 The peak fitted C 1s regions for the [C_nBipy][NTf₂] salts. The components are colour coded to the structure shown on the top plot.

The mono-cationic bipyridinium salts possess many different carbon environments. The carbon envelope is a sum of the individual carbon components which have each been fixed in B.E., area and FWHM. Most B.E.s have been derived from difference spectra generated from both this and alternative experiments. Therefore an envelope that accurately reproduces the observed C1s photoemissions significantly supports the data derived from each difference spectrum. As **Figure 4.17** shows, each obtained C 1s region is reproduced by the component envelope with very little deviation.

4.3 Conclusions

The XP spectra for mono- and di-alkylated 4,4-bipyridinium salts have been acquired. Analysis of the C 1s regions for both sets of salts has provided additional information on pyridinium C 1s peak fitting. The $[(C_n)_2Bipy][NTf_2]_2$ salts have been analysed relative to the traditional $[C_nPy][NTf_2]$ salts and difference spectra have been produced. The observed shift in electron density has revealed that the initial C⁴ carbon component is coincident with the C^{3,5} component of the pyridinium ring, as previously suspected.

The peak fitting of the mono-alkylated $[C_nBipy][NTf_2]$ C 1s region is more complicated than pyridinium and dicationic 4,4'-bipyridinium C 1s regions, due to the unsymmetrical nature of the monocation. Difference spectra generated between the $[C_nBipy][NTf_2]$ and $[(C_n)_2Bipy][NTf_2]_2$ salts has narrowed the location of the carbon environments from the non-alkylated portion of the $[C_nBipy]^+$ cation. GL (30) line shape components were used to fit the generated difference as exact identification of the individual components was not possible. A two component model with grouped C^{3',5'} and C^{2',4',6'} carbon environments was supported by the B.E. shift that was observed for the $[(C_n)_2Bipy][NTf_2]_2$ C 1s region, relative to the $[C_nPy][NTf_2]$ C 1s region. The C 1s region of the $[C_nBipy][NTf_2]$ salts were fitted with components of known B.E., which were generated through difference spectra presented in this and the previous chapter. The good agreement between the

predicted C 1s envelope and the acquired data shows that difference spectra present a powerful method for identifying individual carbon B.E.s.

When XP spectra of structurally related molecules are measured relative to each other, additional information is revealed that would otherwise be unknown. In this work the dicationic 4,4'-bipyridinium C1s XP spectra have been normalised to traditional pyridinium C 1s XP spectra. This process results in 4,4'-bipyridinium C 1s photoemissions that are equivalent to half of the 4,4'-bipyridinium salt (halved at the 4 and 4' C-C bond). The difference spectra that have been generated between the 'halved' 4,4'-bipyridinium and pyridinium C 1s regions are similar to those obtained in the previous chapter, where chlorination was used to shift specific carbon photoemissions to higher B.E.s. This type of analysis may provide useful information for future C 1s peak fitting models. For this work the 4,4'-bipyridinium salts were used due to the decomposition of 4-chloropyridinium salts on transfer to the XP spectrometer. Other symmetrical salts may be used for similar future experiments where chemical modifications are not easy to achieve.

4.4 References

- 1 J. Joseph, N. V. Eldho and D. Ramaiah, *Chem. Eur. J.*, 2003, **9**, 5926–5935.
- 2 R. P. Singh and J. M. Shreeve, *Chem. Commun.*, 2003, 1366–1367.
- 3 J. C. Xiao, C. Ye and J. M. Shreeve, *Org. Lett.*, 2005, **7**, 1963–1965.
- 4 A. Abebe, S. Admassie, I. J. Villar-Garcia and Y. Chebude, *Inorg. Chem. Commun.*, 2013, **29**, 210–212.
- 5 A. P. Abbott and K. J. McKenzie, *Phys. Chem. Chem. Phys.*, 2006, **8**, 4265–4279.
- 6 F. Endres, *ChemPhysChem*, 2002, **3**, 144–154.
- 7 H. Zhao, S. Xia and P. Ma, *J. Chem. Technol. Biotechnol.*, 2005, **80**, 1089–1096.
- 8 A. E. Visser, R. P. Swatloski, W. M. Reichert, J. H. Davis Jr., R. D. Rogers, R. Mayton, S. Sheff and A. Wierzbicki, *Chem. Commun.*, 2001, 135–136.
- 9 T. Welton, *Coord. Chem. Rev.*, 2004, **248**, 2459–2477.
- 10 P. Wasserscheid and W. Keim, *Angew. Chem. Int. Ed.*, 2000, **39**, 3772–3789.
- 11 J. P. Hallett and T. Welton, *Chem. Rev.*, 2011, **111**, 3508–3576.
- 12 M. Bonchio, M. Carraro, G. Casella, V. Causin, F. Rastrelli and G. Saielli, *Phys. Chem. Chem. Phys.*, 2012, **14**, 2710.
- 13 V. Causin and G. Saielli, *J. Mater. Chem.*, 2009, **19**, 9153.
- 14 V. Causin and G. Saielli, *J. Mol. Liq.*, 2009, **145**, 41–47.
- 15 G. Casella, V. Causin, F. Rastrelli and G. Saielli, *Phys. Chem. Chem. Phys.*, 2014, 5048–5051.
- 16 M. Currie, J. Estager, P. Licence, S. Men, P. Nockemann, K. R. Seddon, M. Swadźba-Kwaśny and C. Terrade, *Inorg. Chem.*, 2013, **52**, 1710–1721.
- 17 A. W. Taylor, S. Men, C. J. Clarke and P. Licence, *RSC Adv.*, 2013, **3**, 9436.

- 18 S. Men, D. S. Mitchell, K. R. J. Lovelock and P. Licence, *ChemPhysChem*, 2015, **16**, 2211-2218
- 19 E. F. Smith, I. J. V. Garcia, D. Briggs and P. Licence, *Chem. Commun. (Camb)*., 2005, 5633–5.
- 20 I. J. Villar-Garcia, E. F. Smith, A. W. Taylor, F. Qiu, K. R. J. Lovelock, R. G. Jones and P. Licence, *Phys. Chem. Chem. Phys.*, 2011, **13**, 2797.
- 21 I. J. Villar García, Thesis, The University of Nottingham, 2009.
- 22 S. Men, *Thesis*, The University of Nottingham, 2011.
- 23 S. K. Schneider, P. Roembke, G. R. Julius, H. G. Raubenheimer and W. A. Herrmann, *Adv. Synth. Catal.*, 2006, **348**, 1862–1873.

Chapter 5:
Nitrile Functionalised Ionic Liquids

5 Nitrile Functionalised Ionic Liquids

The mono-alkylated 4,4-bipyridinium ILs presented in the previous chapter provide a highly stable liquid medium that is capable of dissolving large quantities of inorganic salts.¹ Although their preparation is relatively straight forward, the majority of bipyridinium salts suffer from high melting points due to the increased order that arises from additional π - π stacking interactions.² As such, these salts lack the diversity that other task specific ILs may possess.

Functionalisation of traditional amine nucleophiles with an alkylnitrile species produces a range of thermally and chemically stable room temperature ILs.^{3,4} This functionalisation boosts the ability of the IL to dissolve inorganic salts and also acts to immobilise the dissolved species in the IL layer.⁵ The nitrile group is coordinating and therefore the liquid is able to act as both solvent and ligand.^{6,7} As a result, the physiochemical properties of nitrile ILs have recently become an important topic of study.⁸ Although many ILs have been shown to raise the activity of certain metal catalysts, the reuse and recycling of the active catalytic species is often problematic for IL solutions.^{6,9,10} The stabilising environment provided by nitrile functionalised ILs has been shown to significantly increase the recyclability of IL-metal solutions.^{11,12} This has important implications for the study of homogeneous catalysis in ILs, which is a rapidly expanding subset of IL research.¹³

As previously stated, XPS may be utilised as a unique tool for the investigation of IL solutions, particularly where multiple chemical species may arise due to complex interactions with the solvent itself. XPS is currently being used to obtain information regarding solvent-solute interactions,¹⁴ chemical speciation¹⁵ and surface concentrations of dissolved organic and inorganic species.¹⁶ The majority of this research is focused on the function of the anionic component, since different anions have different basicities and hence different coordinative abilities.^{17,18} As the XPS studies of ILs advance, investigations will undoubtedly turn towards more complicated solvent-solute systems, such as nitrile ILs with metal solutes.

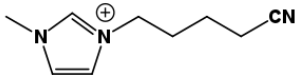
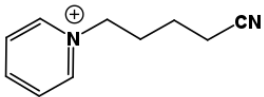
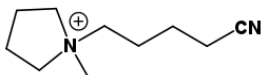
By applying current C 1s peak fitting procedures to IL-metal solutions, XP spectra may yield important information that other analytical techniques cannot provide. The small number of studies that present findings of this nature are built upon “best guess” peak fitting models, due to the complexities of the photoemissions in question.¹⁹ In order to extract the maximum amount of data available from XP spectra, complicated photoemissions must be deconvoluted. By utilising difference spectra of structurally related samples, photoemission peaks may be further resolved through the shifting of electron density.

This chapter will present the XP spectra for a range of nitrile functionalised salts. Various cation and anion combinations will be examined, however all salts have the valeronitrile, $-(\text{CH}_2)_4\text{-CN}$, functional group in common. Data analysis of the nitrile IL provides a logical progression in terms of XP difference spectra. *Chapter 3* showed how chlorine could be integrated into IL structures, providing an electron withdrawing moiety that shifted electron density in order to reveal the initial location of a photoemission, without adding any extra signals. *Chapter 4* showed how symmetrical molecules could be exploited for XP peak fitting. By normalising 4,4'-bipyridinium C 1s XP spectra to pyridinium C 1s XP spectra and subtracting one from another, the 4,4'-bipyridinium photoemission are equivalent to halved (at the 4 to 4' C-C bond) 4,4'-bipyridinium salts. This chapter will investigate more complicated XP difference spectra. If the C 1s region of nitrile functionalised ILs are compared to their traditional IL counterparts, simultaneous peak addition and shifting may be examined. Multiple C 1s difference spectra may need to be utilised in order to derive and validate the peak fitting models of the functionalised salts.

5.1 Structures and Synthesis

The structures of the nitrile functionalised ILs used in this work are shown in **Table 5.1**. The nucleophiles N-methylimidazole, N-methylpyrrolidine and pyridine were alkylated using 5-chlorovaleronitrile, see the example shown in **Figure 5.1**. Anion metatheses of the chloride salts were conducted in either water or acetone. The purity of the anions were measured by ion chromatography and XPS analysis. Salts are named according to the formula $[(C_4CN)Cat][A]$, where Cat = C₁Im (methylimidazolium), C₁Pyrr (methylpyrrolidinium) or Py (pyridinium) and A = anion. The conditions and yields for the alkylation and metathesis reactions are also shown in **Table 5.2**.

Table 5.1 The nitrile functionalised ionic liquids used in this work. The cationic structures are shown along with the corresponding anions.

Cations	Anions
	$[NTf_2]^- / [PF_6]^- / [BF_4]^- / Cl^-$
	$[NTf_2]^- / [PF_6]^- / Cl^-$
	$[NTf_2]^- / [PF_6]^- / Cl^-$

The yields shown in **Table 5.2** for the alkylation of the amine nucleophiles range from 63.6% to 91.1%. Metathesis reactions using either Li[NTf₂] or K[PF₆] were conducted in water at room temperature over 2 hours. [(C₄CN)C₁Im][BF₄] is a water miscible IL and so an anion metathesis with Na[BF₄] must be conducted in acetone at R.T. for 48 hr in order to eliminate the insoluble NaCl by product from the solvent.

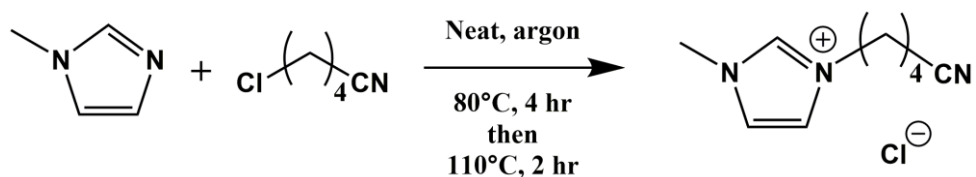


Figure 5.1 An example of the S_N2 alkylation reaction using the *N*-methylimidazole nucleophile and 5-chlorovaleronitrile as an electrophile. The imidazolium chloride salt is formed as the major product.

Although the pyrrolidinium and pyridinium chlorides were synthesised, their XPS wide scans showed iodine impurities and their high resolution scans showed unexpected photoemission peaks from unknown sources. For this reason the XP spectra for the [(C₄CN)C₁Pyrr]Cl and [(C₄CN)Py]Cl salts are not presented in the following sections of this thesis.

Table 5.2 The reaction conditions and yields for the synthesis of the nitrile functionalised ILs

Cation	Anion	Solvent	Temperature (Time)	Yield (%)
[(C ₄ CN)C ₁ Im] ⁺	Cl ⁻	Neat	80 °C (4 hr), 110 °C (2 hr)	91.1
[(C ₄ CN)C ₁ Pyrr] ⁺	Cl ⁻	Neat	70 °C (72 hr), 100 °C (2 hr)	69.4
[(C ₄ CN)Py] ⁺	Cl ⁻	Neat	70 °C (72 hr), 100 °C (2 hr)	85.2
[(C ₄ CN)C ₁ Im] ⁺	[NTF ₂] ⁻	H ₂ O	R.T. (2 hr)	84.3
[(C ₄ CN)C ₁ Pyrr] ⁺	[NTF ₂] ⁻	H ₂ O	R.T. (2 hr)	69.4
[(C ₄ CN)Py] ⁺	[NTF ₂] ⁻	H ₂ O	R.T. (2 hr)	85.4
[(C ₄ CN)C ₁ Im] ⁺	[PF ₆] ⁻	H ₂ O	R.T. (2 hr)	77.2
[(C ₄ CN)C ₁ Pyrr] ⁺	[PF ₆] ⁻	H ₂ O	R.T. (2 hr)	71.1
[(C ₄ CN)Py] ⁺	[PF ₆] ⁻	H ₂ O	R.T. (2 hr)	64.8
[(C ₄ CN)C ₁ Im] ⁺	[BF ₄] ⁻	Acetone	40 °C (48 hr)	63.6

5.2 XPS of Nitrile Functionalised ILs

The wide and high resolution scans for the nitrile functionalised ionic liquids will be presented as two groups for simplicity, the [NTf₂]⁻ salts followed by the [PF₆]⁻, [BF₄]⁻ and Cl⁻ salts. The scans are summed and offset for presentation purposes. Due to the complexity of the C 1s regions of nitrile functionalised ILs, the salts will be analysed *via* a series of difference spectra and so C 1s B.E.s will be presented later in the chapter.

5.2.1 Wide and High Resolution Scans for Nitrile Functionalised ILs

5.2.1.1 Nitrile Functionalised ILs with [NTf₂]⁻ anions

The acquired wide scans for the [NTf₂]⁻ salts are displayed in **Figure 5.2**. Only the expected elements are observed, confirming a successful anion metathesis and clean sample surface for each salt. Auger peaks are also labelled on the plots (> 800 eV). The atomic percentages measured for each sample are also displayed in **Table 5.3**. Most signals do not deviate by more than 10% of the expected values, the error is up to 20% when quantifying elemental regions.²⁰ Slightly larger deviations are noted for the O 1s regions for all samples. It is important to realise that a rise or fall in one region results in a corresponding change in the other atomic percentages.

The high resolution scans are also shown in **Figure 5.2** and the plots are colour coded to the signals displayed in the wide scans. Since the functionalised ILs have no rich aliphatic chains for charge correction,²¹ the XP spectra have been corrected to the F 1s signal for the [NTf₂]⁻ anion, which is set to 688.8 eV. The consistency in all other high resolution scans supports the charge referencing procedures for each salt.

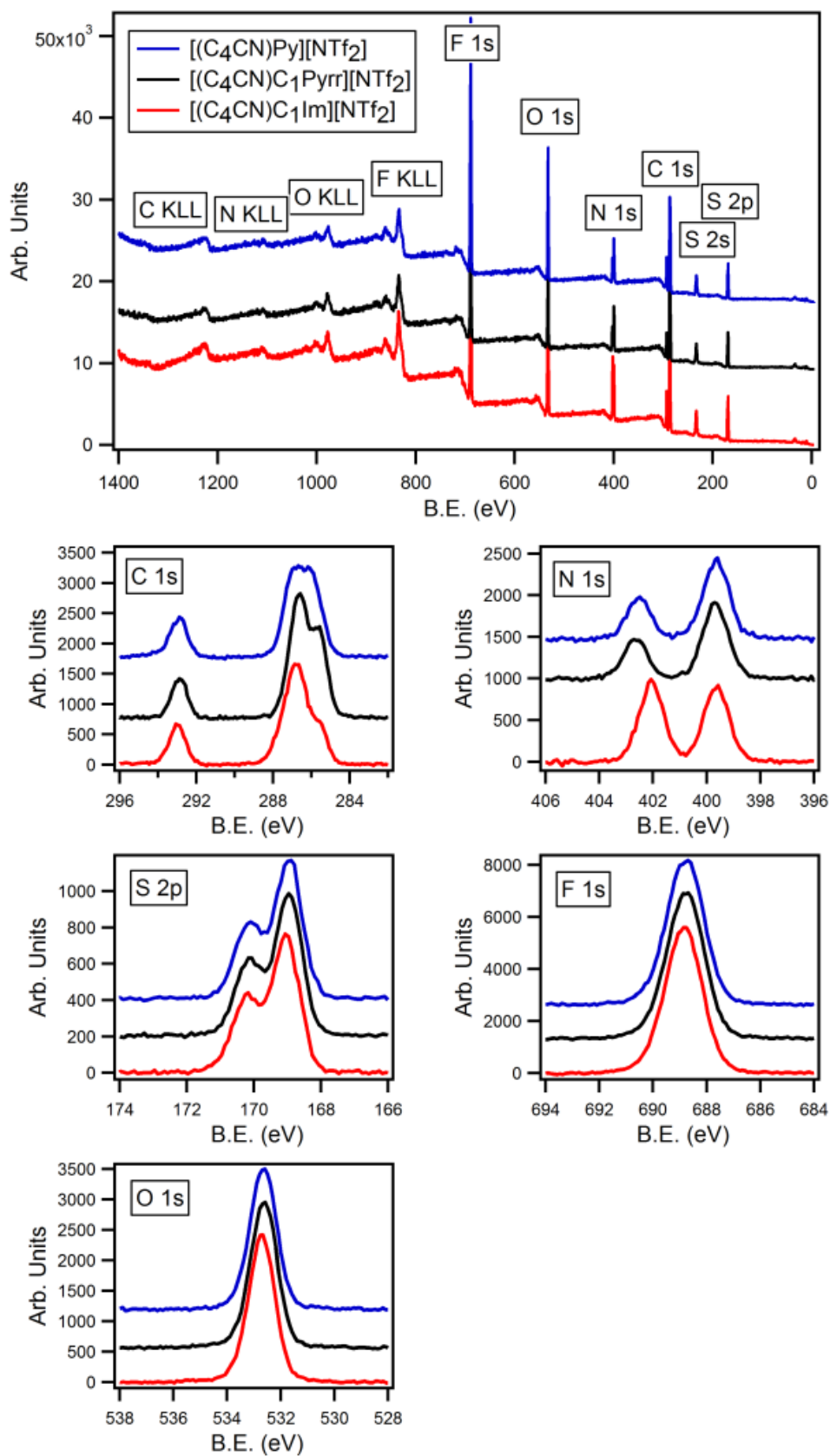


Figure 5.2 The wide scans (top) and high resolution scans for the $[NTf_2]^-$ salts of the nitrile functionalised ILs. The imidazolium (red), pyrrolidinium (black) and pyridinium (blue) scans are shown.

Table 5.3 The atomic percentages for the [NTf₂]⁻ nitrile functionalised salts. The deviation (%) and the found and calculated values are presented.

Cation	Anion		Composition (%)				
			C	N	O	F	S
[(C ₄ CN)C ₁ Im] ⁺	[NTf ₂] ⁻	Found	44.39	14.03	13.23	21.24	7.11
		Calculated	40.75	14.81	14.81	22.22	7.41
		Deviation (%)	-8.20	5.56	11.94	4.61	4.22
[(C ₄ CN)C ₁ Pyrr] ⁺	[NTf ₂] ⁻	Found	45.06	10.96	13.78	22.42	7.78
		Calculated	44.44	11.11	14.81	22.23	7.41
		Deviation (%)	-1.38	1.37	7.47	-0.85	-4.76
[(C ₄ CN)Py] ⁺	[NTf ₂] ⁻	Found	45.36	11.55	13.60	21.94	7.55
		Calculated	44.44	11.11	14.81	22.22	7.42
		Deviation (%)	-2.03	-3.81	8.90	1.28	-1.72

Figure 5.2 shows the distinct photoemission shapes for the C 1s regions of the pyridinium, imidazolium and pyrrolidinium salts. These will be discussed in greater detail later in this chapter. The N 1s region shows only two resolved peaks. Since three separate chemical states are expected for nitrogen, the nitrile and anionic nitrogen environments are most likely coincident, as with the bipyridinium salts from *Chapter 4*.

5.2.1.1.1 N 1s Difference and Peak Fitting

An N 1s difference spectrum generated from a traditional [NTf₂]⁻ containing IL and a corresponding nitrile functionalised [NTf₂]⁻ IL should provide additional information on the B.E.s of the individual nitrogen components. As an example, **Figure 5.3** shows the [(C₄CN)C₁Im][NTf₂]⁻ N 1s region with the [C₄C₁Im][NTf₂]⁻ N 1s signal overlaid. The generated difference clearly shows a higher B.E. for the neutral nitrile peak compared to the anionic [NTf₂]⁻ N 1s peak of the [C₄C₁Im][NTf₂]⁻ salt. This process has been repeated for all cation types and the resulting peak position have been included in **Table 5.4**, along with the other heteroatom B.E.s acquired from the high resolution scans.

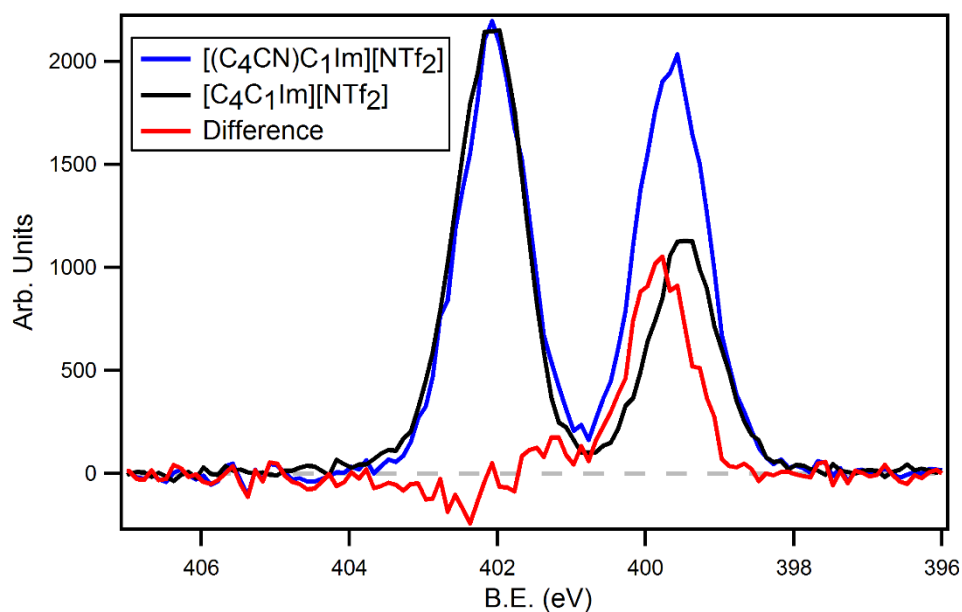


Figure 5.3 The N 1s region of $[(C_4CN)C_1Im][NTf_2]$ (blue) with the $[C_4C_1Im][NTf_2]$ N 1s region (black) overlaid. The spectra are normalised to the area of the F 1s signal of the anion. The generated difference spectrum (red) is also shown on the plot.

As expected, the anionic (399.5 eV) and nitrile (399.8 eV) N 1s signals are all at equal B.E.s for the analogous salts. As with the $[C_nBipy][NTf_2]$ salts, the neutral nitrogen atom appears to have a similar amount of electron density as the anionic $[NTf_2]^-$ nitrogen atom. The neutral nitrogen of the nitrile functionality is 0.2 eV higher than the neutral nitrogen from the mono-alkylated bipyridinium $[C_nBipy][NTf_2]$ sample. The nitrile group therefore has a slightly lower amount of electron density about the nitrogen atom.

Table 5.4 The B.E. for the heteroatoms of the $[NTf_2]^-$ nitrile functionalised salts. The nitrile N 1s signals were deduced by difference spectra.

		Binding Energy (eV)					
		N 1s			F 1s	O 1s	S 2p _{3/2}
Cation	Anion	Cation	Anion	Nitrile			
$[(C_4CN)C_1Im]^+$	$[NTf_2]^-$	402.1	399.5	399.8	688.8	532.7	169.1
$[(C_4CN)C_1Pyrr]^+$	$[NTf_2]^-$	402.6	399.5	399.8	688.8	532.6	169.0
$[(C_4CN)Py]^+$	$[NTf_2]^-$	402.5	399.5	399.8	688.8	532.7	169.0

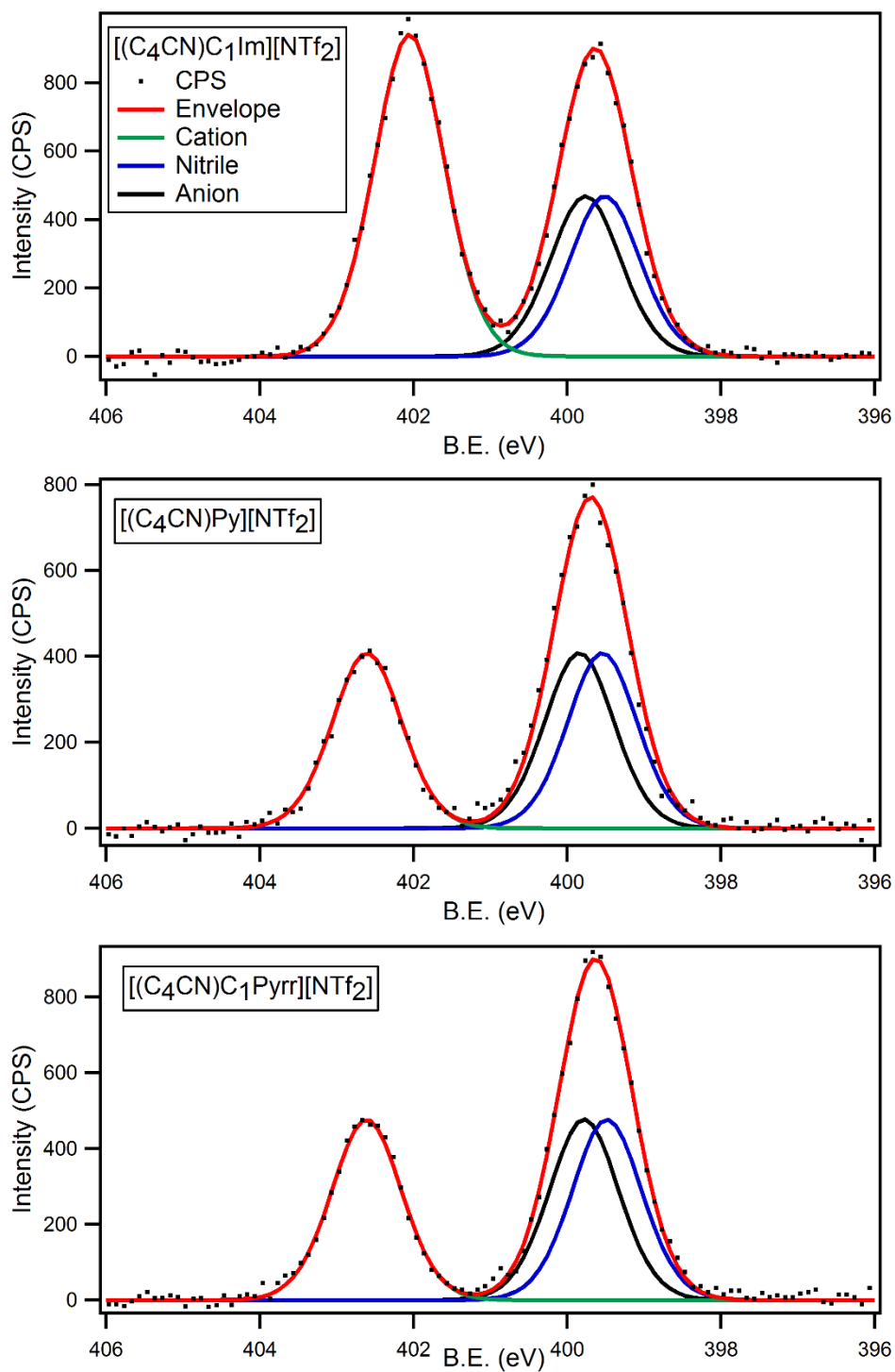


Figure 5.4 The peak fitted N 1s regions of the nitrile functionalised $[NTf_2]^-$ salts. The components are colour coded to the assignments shown for the imidazolium salt (top).

Figure 5.4 shows the peak fitted N 1s regions for the nitrile functionalised [NTf₂]⁻ salts. The imidazolium cation contains two nitrogen atoms, therefore the anionic [NTf₂]⁻ and neutral nitrile N 1s signals have been constrained to equal half the area of the imidazolium N 1s signal, e.g. cationic:anionic:nitrile = 2:1:1. The pyridinium and pyrrolidinium cations contain only one nitrogen atom and so all three components have areas that are set to be equal. The nitrile N 1s signals for all salts have been set to equal the B.E. obtained from the difference spectra, 399.8 eV. All N 1s regions present a good fit between the measured CPS and the theoretical envelope. The C 1s regions of the nitrile functionalised [NTf₂]⁻ salts will be further analysed later in this chapter. The [PF₆]⁻, [BF₄]⁻ and Cl⁻ nitrile functionalised IL XP spectra will be presented in the following section.

5.2.1.2 Nitrile Functionalised ILs with [PF₆]⁻, [BF₄]⁻ and Cl⁻ anions

The wide and high resolution scans for the [PF₆]⁻ and [BF₄]⁻ nitrile functionalised ILs are shown in **Figure 5.5**. The wide scans show the expected elements with no signal from bromine, confirming a successful anion metathesis for all salts. A small O 1s signal is visible on four of the wide scans. Oxygen impurities are common for IL salt and relatively easy to remove via sample etching. The O 1s signal is <1% of the observed C 1s signals for each of the three salts. The atomic percentages acquired from the wide scans are displayed in **Table 5.5**. The majority of values are far below the associated 20% error.

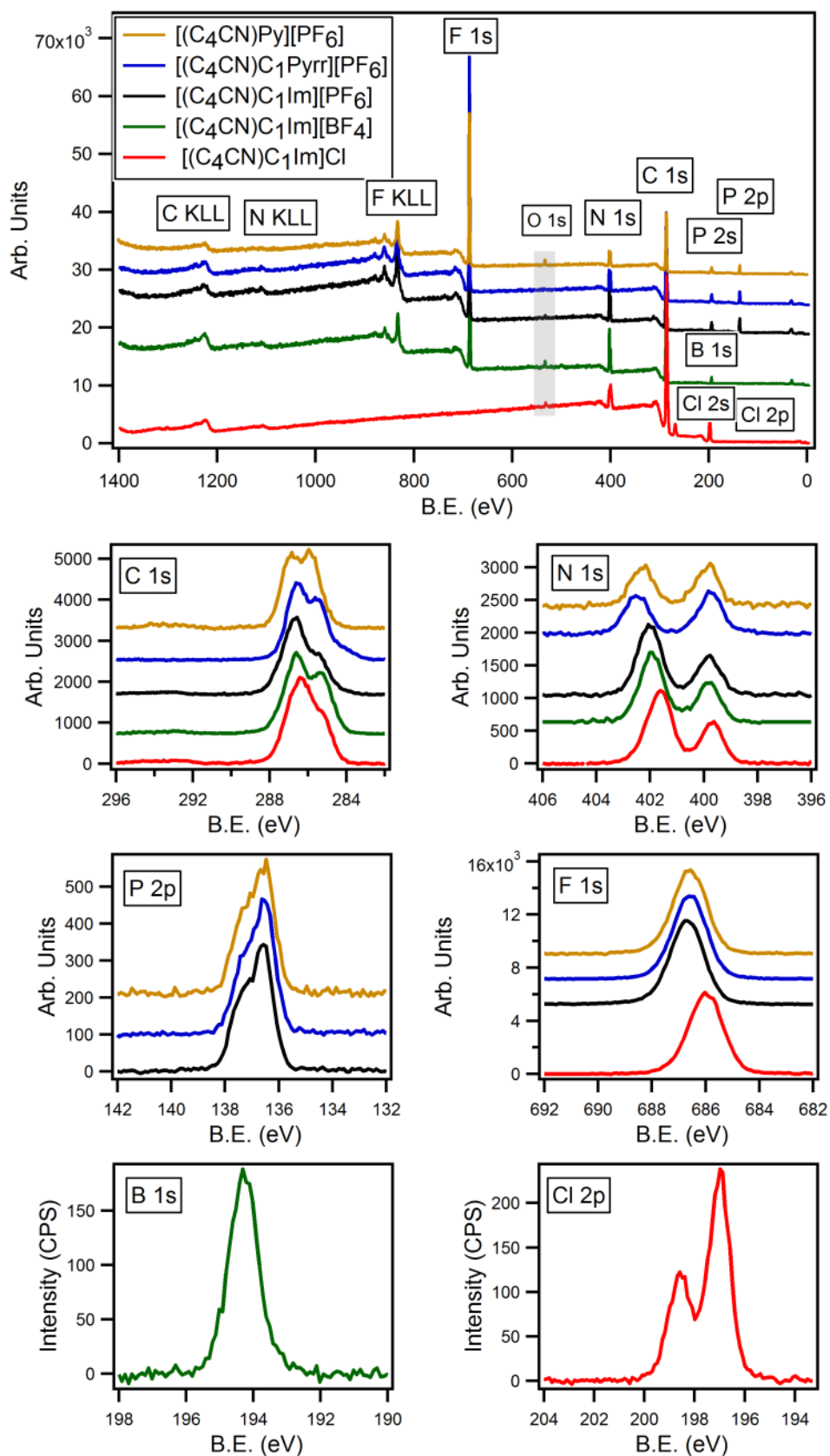


Figure 5.5 The wide scans (top) and high resolution scans for the $[PF_6]$, $[BF_4]$ and Cl salts of the nitrile functionalised ILs. The high resolution scans are colour coded to the wide scan signals. The $O 1s$ signal is highlighted on the wide scan.

Table 5.5 The atomic percentages for the $[PF_6]^-$ and $[BF_4]^-$ nitrile functionalised salts. The deviation (%) and the found and calculated values are presented.

Cation	Anion		Composition (%)					
			C	N	F	B	P	Cl
$[(C_4CN)C_1Im]^+$	$[PF_6]^-$	Found	51.68	14.52	28.8		5.00	
		Calculated	47.37	15.79	31.58		5.26	
		Deviation (%)	-8.34	8.75	9.65		5.20	
$[(C_4CN)C_1Pyrr]^+$	$[PF_6]^-$	Found	56.93	9.92	28.41		4.74	
		Calculated	52.63	10.53	31.58		5.26	
		Deviation (%)	-7.55	6.15	11.16		10.97	
$[(C_4CN)Py]^+$	$[PF_6]^-$	Found	55.89	9.48	29.95		4.68	
		Calculated	52.63	10.53	31.58		5.26	
		Deviation (%)	-5.83	11.08	5.44		12.39	
$[(C_4CN)C_1Im]^+$	$[BF_4]^-$	Found	57.35	15.83	20.89	5.93		
		Calculated	52.94	17.65	23.53	5.88		
		Deviation (%)	-7.69	11.5	12.64	-0.84		
$[(C_4CN)C_1Im]^+$	Cl^-	Found	72.37	21.36				6.27
		Calculated	69.23	23.08				7.69
		Deviation (%)	4.54	7.45				18.47

Again, these nitrile functionalised ILs lack a rich aliphatic chain for charge correction. Therefore the F 1s signals have been referenced to the F 1s photoemission obtained from the charge corrected $[C_8C_1Im][A]$ salts,^{14,20} where $[PF_6]^- = 686.7$ eV and $[BF_4]^- = 686.0$ eV. The $[(C_4CN)C_1Im]Cl$ spectra have been corrected in the same way using the Cl $2p_{3/2}$ peak at 197.0 eV. The C 1s regions show the unique photoemissions from each cationic structure. The N 1s regions show two peaks for each sample. However for the imidazolium salts, the peaks at higher B.E. has double the area of the peak at lower B.E. upon integration. The higher B.E. peak is attributed to the electron deficient cation, in the case of imidazolium there are two cationic nitrogens per nitrile nitrogen. The B.E.s for the $[PF_6]^-$, $[BF_4]^-$ and Cl^- nitrile functionalised salts are shown in **Table 5.6**

Table 5.6 The B.E. for the heteroatoms of the [PF₆]⁻, [BF₄]⁻ and Cl⁻ nitrile functionalised salts. The error of measurement is 0.1 eV.

		Binding Energy (eV)					
		N 1s		F 1s	P 2p _{3/2}	B 1s	Cl 2p _{3/2}
Cation	Anion	Cation	Nitrile				
[(C ₄ CN)C ₁ Im] ⁺	[PF ₆] ⁻	402	399.8	686.7	136.6		
[(C ₄ CN)C ₁ Pyrr] ⁺	[PF ₆] ⁻	402.5	399.8	686.7	136.5		
[(C ₄ CN)Py] ⁺	[PF ₆] ⁻	402.3	399.9	686.7	136.6		
[(C ₄ CN)C ₁ Im] ⁺	[BF ₄] ⁻	402.0	399.8	686.0		194.3	
[(C ₄ CN)C ₁ Im] ⁺	Cl ⁻	401.7	399.7				197.0

5.2.2 Shake up/off Quantification of Nitrile Functionalised ILs

The measured shake up/off signals for the nitrile functionalised imidazolium ILs are presented in **Table 5.7**. The values are calculated relative to the main photoemission of the C 1s region. The average value of 21.4% is close to the previously 20% signal loss as measured for imidazolium ILs.²⁰ Therefore aromatic carbons will be deducted 20% of their signal when imidazolium C 1s fitting models are developed.

Table 5.7 The measured shake up/off values from the nitrile functionalised imidazolium C 1s spectra. The values are measured relative to the main C 1s photoemission.

Cation	Anion	Shake up/off per Sp ² carbon atom (%)
[(C ₄ CN)C ₁ Im] ⁺	[NTf ₂] ⁻	23
[(C ₄ CN)C ₁ Im] ⁺	[PF ₆] ⁻	23.1
[(C ₄ CN)C ₁ Im] ⁺	[BF ₄] ⁻	19.9
[(C ₄ CN)C ₁ Im] ⁺	Cl ⁻	19.7
Average		21.4

The measured shake up/off values for the nitrile functionalised pyridinium ILs are presented in **Table 5.8**. The averaged value of 10.9% is also close to the previously measured 10% loss found for traditional pyridinium ILs.²² Therefore aromatic carbons will be deducted 10% of their signal when developing C 1s peak fitting models.

Table 5.8 The measured shake up/off values for the nitrile functionalised pyridinium C 1s spectra. The values are measured relative to the main C 1s photoemission.

Cation	Anion	Shake up/off per Sp ² carbon atom (%)
[(C ₄ CN)Py] ⁺	[NTf ₂] ⁻	10.4
[(C ₄ CN)Py] ⁺	[PF ₆] ⁻	11.4
Average		10.9

The calculated shake up/off values include the sp hybridised carbon atom from the nitrile functionality. Imidazolium and pyridinium ILs produce noticeable shake up/off signals which are relatively easy to identify. Theoretically the pyrrolidinium ILs should contain a signal in the C 1s region for the shake up/off emission from the nitrile carbon.²³ However, no distinct signals are observed, meaning that the shake up/off cannot be measured for these salts. For peak fitting C 1s models, the shake up/off losses of nitrile carbons will be assumed to be equal to those found for pyridinium carbons. Therefore the sp hybridised nitrile carbons will be deducted 10% of their signal when developing C 1s fitting models.

5.2.3 Nitrile Interactions with Anions and Cations

Theoretically, interactions between the dipole of the nitrile group and the anions and cations of the IL should be observed. The -CN functionality has a high polarity which appears to produce additional hydrogen bonding and nitrile-ion association.²⁴ These interactions cause significant changes in certain physiochemical properties, relative to traditional ILs.⁸ The N 1s signals of the nitrile IL can be examined in order to investigate and possibly quantify these interactions. **Table 5.9** shows summarised B.E.s for the N 1s photoemissions from a range of nitrile functionalised and traditional ILs.

Table 5.9 The N 1s B.E.s for selected nitrile functionalised and traditional ILs. The positions of the nitrile N 1s signals for the [NTf₂]⁻ salts were deduced via difference spectra.

		B.E. (eV)				
		N 1s				
Cation	Anion	Cation	Nitrile	Anion	reference	
[(C ₄ CN)C ₁ Im] ⁺	[NTf ₂] ⁻	402.1	399.8	399.5	this work	
[C ₄ C ₁ Im] ⁺	[NTf ₂] ⁻	402.1		399.5	20	
[(C ₄ CN)Py] ⁺	[NTf ₂] ⁻	402.5	399.8	399.5	this work	
[C ₄ Py] ⁺	[NTf ₂] ⁻	402.6		399.5	14	
[(C ₄ CN)C ₁ Pyrr] ⁺	[NTf ₂] ⁻	402.6	399.8	399.5	this work	
[C ₄ C ₁ Pyrr] ⁺	[NTf ₂] ⁻	402.7		399.5	14	
[(C ₄ CN)C ₁ Im] ⁺	[PF ₆] ⁻	402	399.8		this work	
[C ₄ C ₁ Im] ⁺	[PF ₆] ⁻	402.1			20	
[(C ₄ CN)C ₁ Im] ⁺	[BF ₄] ⁻	402	399.8		this work	
[C ₄ C ₁ Im] ⁺	[BF ₄] ⁻	402			20	
[(C ₄ CN)C ₁ Im] ⁺	Cl ⁻	401.7	399.7		this work	
[C ₄ C ₁ Im] ⁺	Cl ⁻	401.7			20	

If the N 1s signals of the cation are inspected for the imidazolium salts, there appears to be no change between the functionalised and non-functionalised ILs. The N 1s signals of the nitrile functionality are also consistent for the [(C₄CN)C₁Im][A] series. This implies that anionic variation has no effect upon the electron density of the nitrile group. The imidazolium cation shifts by + 0.4 eV when comparing the Cl⁻ salt to the [NTf₂]⁻ salt.

The functionalised and non-functionalised pyridinium and pyrrolidinium [NTf₂]⁻ salts also show similar B.E.s (within the 0.1 eV error) to their butyl chain counterparts. All nitrile N 1s signals are also the same (± 0.1 eV) for each cationic type, 399.8 eV. This is unexpected as the shift in the cationic N 1s B.E. from imidazolium (402.1 eV) to pyrrolidinium (402.6 eV) is 0.5 eV. The -CN functionality is therefore not affected by either cationic or anionic variation, according to XP spectroscopy.

5.2.4 C 1s Difference Spectra Examples: [(C₄CN)Py][NTf₂]

The [(C₄CN)Py][NTf₂] IL will be analysed first since a large portion of this investigation has involved the pyridinium C 1s region. Since all difference spectra in this chapter involve peaks originating from nitrile functionalised aliphatic chains, each carbon environment will be labelled according to the example shown in **Figure 5.6**. The nitrile carbon is labelled according to the functionality, e.g. the C^{CN} component. Imidazolium and pyrrolidinium ILs also follow the same labelling system.

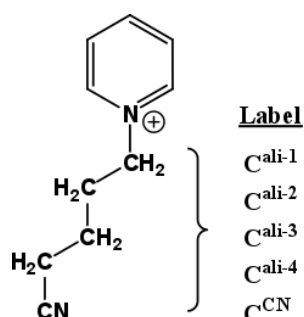


Figure 5.6 The general labelling scheme for nitrile functionalised ILs. The same scheme has been used for imidazolium and pyrrolidinium ILs. Note: C^{ali-1} is also included in the C^{2,6,7} component as C⁷, for the pyridinium C 1s model.

If the [(C₄CN)Py][NTf₂] C 1s region is displayed and the corresponding [C₄Py][NTf₂] C 1s region is overlaid, the difference between the two photoemissions may be taken, **Figure 5.7**. The difference between the two spectra is labelled as difference 1 and is shown in red. A sharp peak at low B.E. (285.1 eV) appears to be redistributed over a broad B.E. range that is approximately 1.8 eV wide. **Figure 5.8** shows a structural representation of the generated difference spectrum, pyridinium carbons have been omitted for clarity.

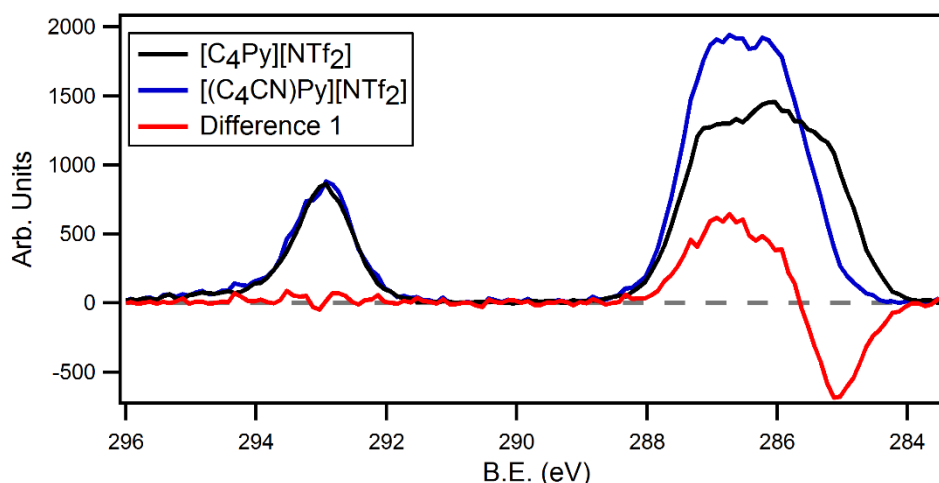


Figure 5.7 The $[(C_4CN)Py][NTf_2]$ C 1s region (blue) with the $[C_4Py][NTf_2]$ C 1s emission overlaid (black). The generated difference spectrum is shown in red and is labelled as difference 1.

The negative peak from difference 1 integrates to 1.4 carbon atoms and the positive peak integrates to 2.3 carbon atoms, relative to the $[(C_4CN)Py][NTf_2]$ photoemission. These values indicate the addition of one carbon atom from the nitrile functionality and the shifting of one carbon atom only. However, as previously shown, a difference spectrum may provide maxima and minima that are not fully resolved. The net result is a decrease in the areas of the positive and negative peaks of the difference, with loss of signal at the point where the two meet.

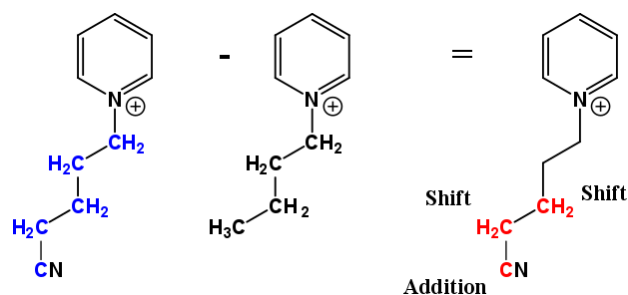


Figure 5.8 The structural representation of the difference generated between $[(C_4CN)Py][NTf_2]$ and $[C_4Py][NTf_2]$. The colours represent the scans shown in the difference spectrum. Pyridinium carbons have been omitted for simplicity.

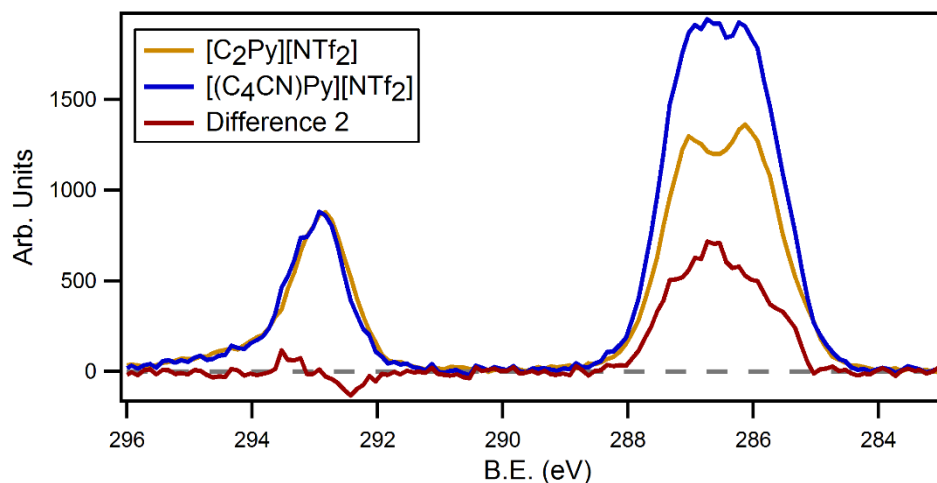


Figure 5.9 The [(C₄CN)Py][NTf₂] C 1s region (blue) with the [C₂Py][NTf₂] C 1s emission overlaid (yellow). The generated difference spectrum is shown in dark red and is labelled as difference 2.

Although the difference created between [(C₄CN)Py][NTf₂] and [C₄Py][NTf₂] does show a shift in B.E., the resulting difference spectrum is difficult to interpret alone. To further investigate the shifting B.E.s of the aliphatic chain, additional difference spectra may be considered. **Figure 5.9** shows the difference spectrum generated between the [(C₄CN)Py][NTf₂] (blue) and [C₂Py][NTf₂] (yellow) C 1s photoemissions. The resulting spectrum is shown in dark red and is labelled difference 2. A structural representation of the generated difference is also shown in **Figure 5.10**. Pyridinium carbons have again been omitted for simplicity.

The dark red carbons should only provide additional signals relative to [C₂Py][NTf₂]. Since difference 2 does not contain any negative signals, this carbon assignment is supported. Therefore the difference spectrum does not show relative shifts in electron density, instead signals are either added or subtracted to the respective photoemissions until one spectrum becomes the other. Although the C^{ali-2} carbon of the [C₂Py][NTf₂] may be slightly shifted relative to the C^{ali-2} signal of the [(C₄CN)Py][NTf₂] salt, the large difference spectrum probably masks this relatively small shift.

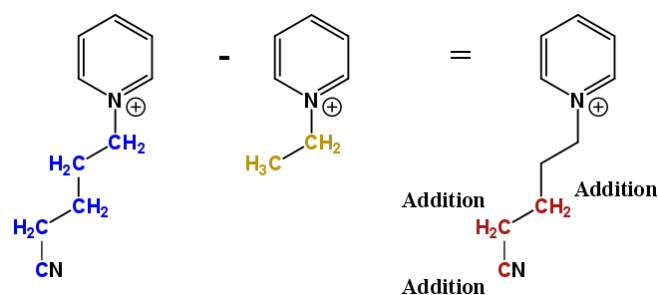


Figure 5.10 The structural representation of difference 2, as generated by the $[(C_4CN)Py][NTf_2]$ and $[C_2Py][NTf_2]$ C 1s photoemissions. The colours are coded to the difference spectrum. Pyridinium carbons have been omitted for simplicity

The difference shown in **Figure 5.9** is about 2.0 eV wide. This makes peak fitting the difference 2 region relatively simple, especially when considering the diversity of the individual carbon environments. The resulting peak fitting is shown in **Figure 5.11**. The C^{ali-3} , C^{ali-4} and C^{CN} components appear at 286.0, 286.6 and 287.1 eV, respectively. The electron deficient C^{CN} carbon has the highest B.E. due to the bound nitrogen atom. The neighbouring C^{ali-4} and C^{ali-3} carbon environments then decrease in B.E. due to the increasing distance from the nitrile group. The areas of the components are fixed to the ratio 0.9 : 1 : 1, 10% of the signal from the C^{CN} component has been deducted due to shake up/off processes.

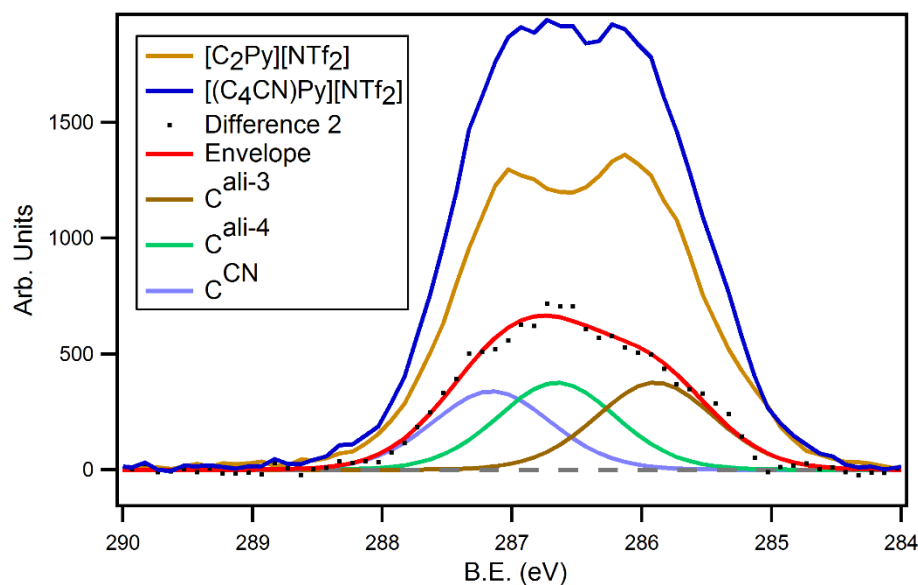


Figure 5.11 The peak fitted difference spectrum for difference 2 (black dots) with the resulting envelope (red) fitting. The individual components are labelled.

The peak fitted difference 2 spectrum may be used to further analyse the shifts observed in difference 1. The overlaid difference spectra are shown in **Figure 5.12**. Relative to difference 2, the loss in signal between the negative peak and positive peak is clearly visible. Using the peak fitting information from **Figure 5.11**, difference 1 may also be fitted by inverse Gaussian summation, as in *Chapter 4*.

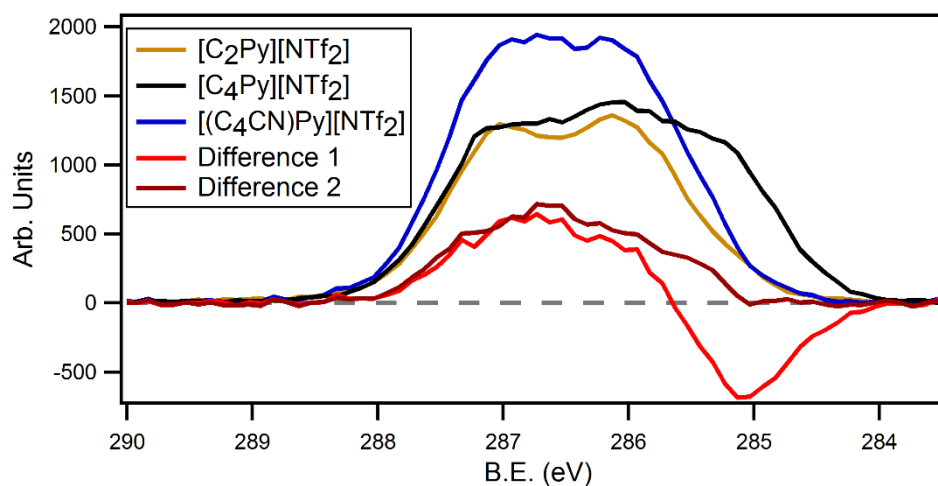


Figure 5.12 The overlaid difference 1 and difference 2 with the associated C 1s photoemissions.

Figure 5.13 shows the inverse Gaussian summation used to fit difference 1. The individual components and their resulting envelope (red) are shown, along with difference 1 (black dots) and the photoemissions from [C₄Py][NTf₂] (black) and [(C₄CN)Py][NTf₂] (blue). The C^{ali-3,4} component (grey) is equivalent to both the C^{ali-3} and C^{ali-4} carbons from the [C₄Py][NTf₂] salt. Since the C^{ali-3,4} component represents two similar carbon environments, the area of this component has been fixed to an area equal to two carbon atoms, as calculated from the [(C₄CN)Py][NTf₂] photoemission. All other components are fixed to an area equivalent to only one carbon atom, with a 10% signal deduction for the C^{CN} component to account for aromatic shake up/off losses.

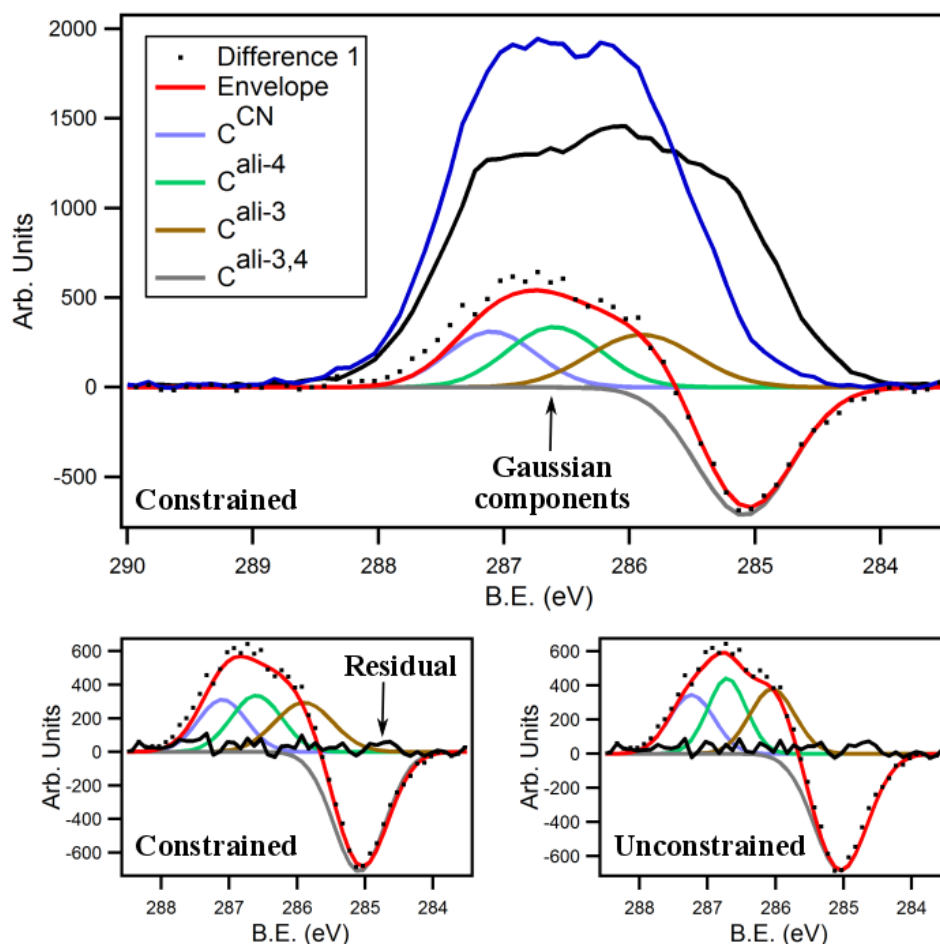


Figure 5.13 The Gaussian summation for difference 1 with the envelope fitting and individual components. The photoemissions from $[C_4Py][NTf_2]$ (black) and $[(C_4CN)Py][NTf_2]$ (blue) are also shown. The expanded fittings with the associated residuals for the position restrained and unrestrained components are also presented (bottom left and right).

Figure 5.13 also shows an expansion of the constrained component model fit, with a corresponding unrestrained models for comparison. The constrained model utilises the peak positions as obtained from the peak fitting of difference 2, **Figure 5.11**. The positions are constrained to the obtained B.E.s by ± 0.1 eV, the error of measurement. The B.E. values for the constrained and unconstrained fits for difference 1 are presented in **Table 5.10**, along with the B.E.s from the analogous difference 2 fitting. The unconstrained model has no B.E. restrictions for each individual peak, however the peaks are initially positioned at the same B.E. values before the fit is calculated. The residuals for the constrained and unconstrained fits are also plotted on the respective graphs.

Table 5.10 The B.E. values as obtained from the fitting of difference 1 and difference 2. The values obtained from the difference 2 fit have been used to constrain the peak positions for difference 1. The B.E.s for an unconstrained position model are also shown.

		B.E. (eV)			
		C ^{ali-3,4}	C ^{ali-3}	C ^{ali-4}	CCN
Difference 1	Constrained	285.1	286.1	286.7	287.2
	Unconstrained	285.1	285.9	286.6	287.1
Difference 2	Unconstrained		285.9	286.6	287.1

Both models provide a good agreement between the component envelope and the calculated CPS for difference 1. The component FWHMs have been limited to between 0.8 eV and 1.1 eV. Both difference 1 fitting models appear to provide similar results, with most B.E. values being within the 0.1 eV error of measurement. The C^{ali-3} components deviate slightly more, however both B.E.s are within the 0.1 eV error of a 286.0 eV value. By applying the peak fitting of difference 2 to the more complex signal of difference 1, the positions of the individual carbon components are independently confirmed. Importantly, the unconstrained model provides similar results to the constrained model of difference 1. Therefore prior knowledge of peak positions may not be a necessary requirement for future analysis of similar difference spectra.

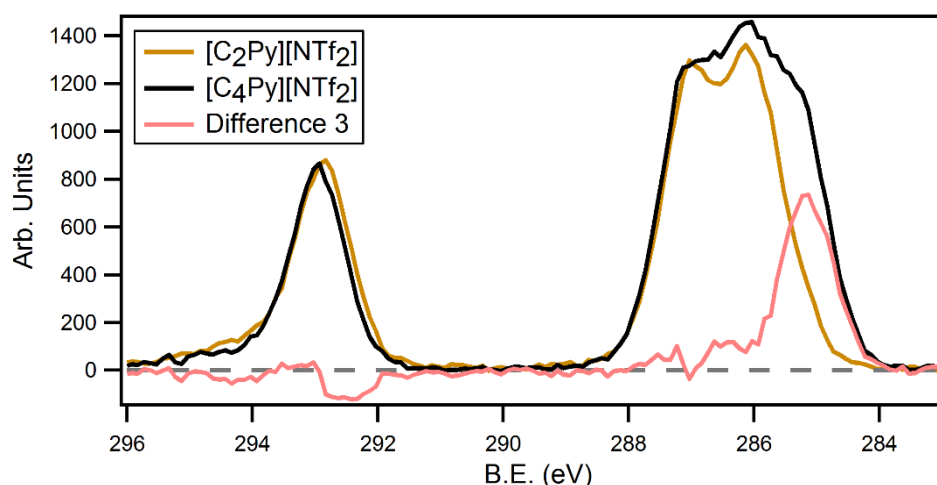


Figure 5.14 The $[C_4Py][NTf_2]$ C 1s region (black) with the $[C_2Py][NTf_2]$ C 1s emission overlaid (yellow). The generated difference spectrum is shown in pink and is labelled as difference 3.

As previously stated, the $C^{\text{ali-3,4}}$ component from **Figure 5.13** is equivalent to the $C^{\text{ali-3}}$ and $C^{\text{ali-4}}$ carbon atoms from the $[C_4\text{Py}][\text{NTf}_2]$ salt. To check this assumption, the difference between $[C_4\text{Py}][\text{NTf}_2]$ and $[C_2\text{Py}][\text{NTf}_2]$ may be taken and compared to the $C^{\text{ali-3,4}}$ component. **Figure 5.14** shows the resulting spectrum, which is labelled as difference 3 (pink). The structural representation of this generated spectrum is shown in **Figure 5.15**, where the pyridinium carbons have again been omitted for simplicity.

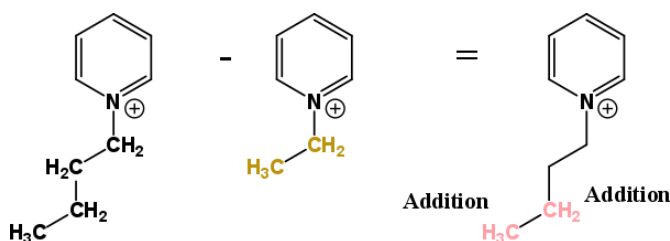


Figure 5.15 The structural representation of the difference generated between $[C_4\text{Py}][\text{NTf}_2]$ and $[C_2\text{Py}][\text{NTf}_2]$. The colours represent the scans shown in the difference 3 spectrum. Pyridinium carbons have been omitted for simplicity

The B.E. of difference 3 is 285.2 eV, while the B.E. of the $C^{\text{ali-3,4}}$ component is 285.1 eV. As expected, the area under difference 3 integrates to exactly 2.0 carbon atoms, relative to the $[C_4\text{Py}][\text{NTf}_2]$ photoemission. **Figure 5.16** shows all three difference spectra displayed together, along with their originating photoemissions. The combined spectra and area integrations highlight that the nitrile functionality of the alkyl chain cause a shifting of the $C^{\text{ali-3}}$ and $C^{\text{ali-4}}$ carbon environments, relative to the non-functionalised butyl chain. The C^{CN} carbon environment has also been located through the investigation of multiple C 1s regions. The difference spectra generated in this section only involve carbon environments from the alkyl chain of the nitrile functionalised IL. Therefore this data should be reproducible for alternative cationic heads.

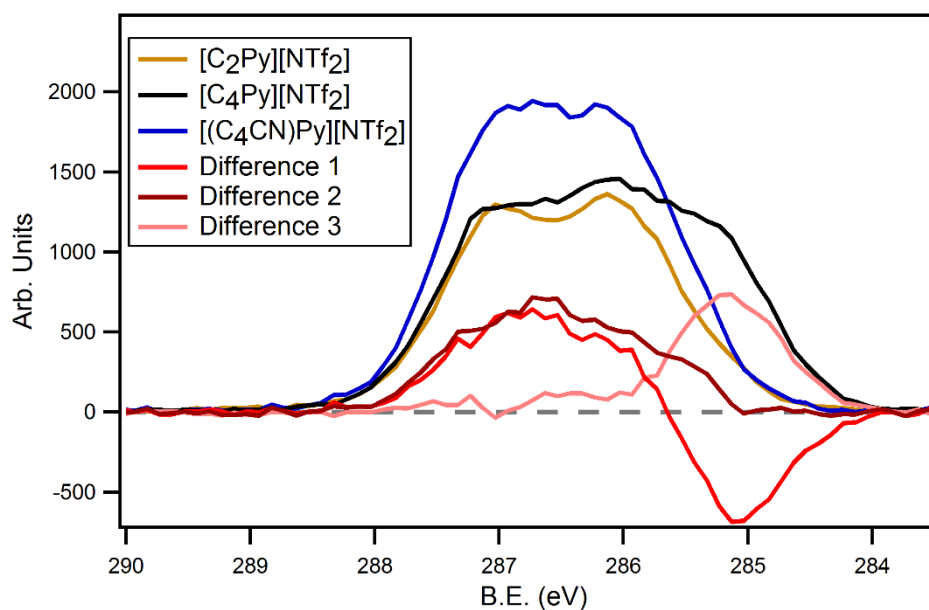


Figure 5.16 The plot showing difference 1 (red), 2 (dark red) and 3 (pink), along with the originating photoemissions from $[C_2Py][NTf_2]$ (yellow) $[C_4Py][NTf_2]$ (black) and $[(C_4CN)Py][NTf_2]$ (blue).

5.2.5 Cationic Variation: $[(C_4CN)C_1Im][NTf_2]$ and $[(C_4CN)C_1Pyrr][NTf_2]$ C 1s Difference Spectra

The differences observed so far for the $[(C_4CN)Py][NTf_2]$ C 1s photoemission should also be produced by both $[(C_4CN)C_1Im][NTf_2]$ and $[(C_4CN)C_1Pyrr][NTf_2]$ C 1s regions. The functionalised aliphatic tail of the cation is common to all ILs in this nitrile series and therefore a similar analysis should yield similar results. This type of independent confirmation, i.e. the generation of identical difference spectra from unique C 1s regions, should justify the data processing presented in this chapter.

5.2.5.1 $[(C_4CN)C_1Im][NTf_2]$ Difference Spectra

As with the $[(C_4CN)Py][NTf_2]$ XP spectra, the non-functionalised $[C_4C_1Im][NTf_2]$ C 1s photoemission may be subtracted from the C 1s region of the $[(C_4CN)C_1Im][NTf_2]$ nitrile functionalised salt. The structural representation of this process is shown in **Figure 5.17**, where the methyl- and

imidazolium carbons have been omitted for simplicity. The layout in **Figure 5.18** displays the generated difference spectrum and the resulting position constrained fitting model (according to the $[(C_4CN)Py][NTf_2]$ difference 2 fit). The locations of the C^{ali-3} , C^{ali-4} and C^{CN} components are therefore shown; the B.E.s for both constrained and unconstrained models are presented in **Table 5.11**.

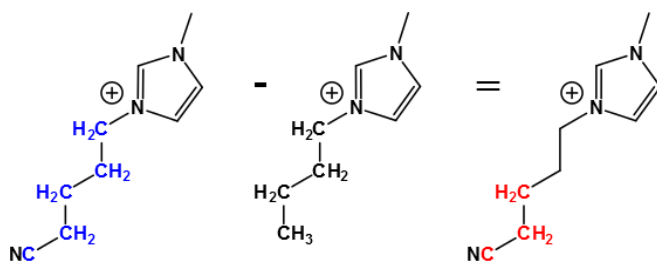


Figure 5.17 The structural representation of the difference generated (red carbons) when the $[C_4C_1Im][NTf_2]$ C 1s photoemission (black carbons) is subtracted from the $[(C_4CN)C_1Im][NTf_2]$ C 1s photoemission (blue carbons). The methyl- and imidazolium carbon atoms have been omitted for simplicity.

Both models appear to be within 0.1 eV of each other, with the exception of the C^{ali-3} component. The values for C^{ali-3} are however within the error of 286.0 eV, this was also observed for the fitting of difference 1 and difference 2 of the $[(C_4CN)Py][NTf_2]$ salt. The consistencies in the constrained and unconstrained component of the imidazolium fitting highlights the overall stability of the model. The observed residual for the constrained model does not deviate significantly from an ideal fit. Although the unconstrained envelope presents a slightly better agreement to the obtained difference spectrum, the B.E. values for both models are sufficiently close to consider the fits equivalent.

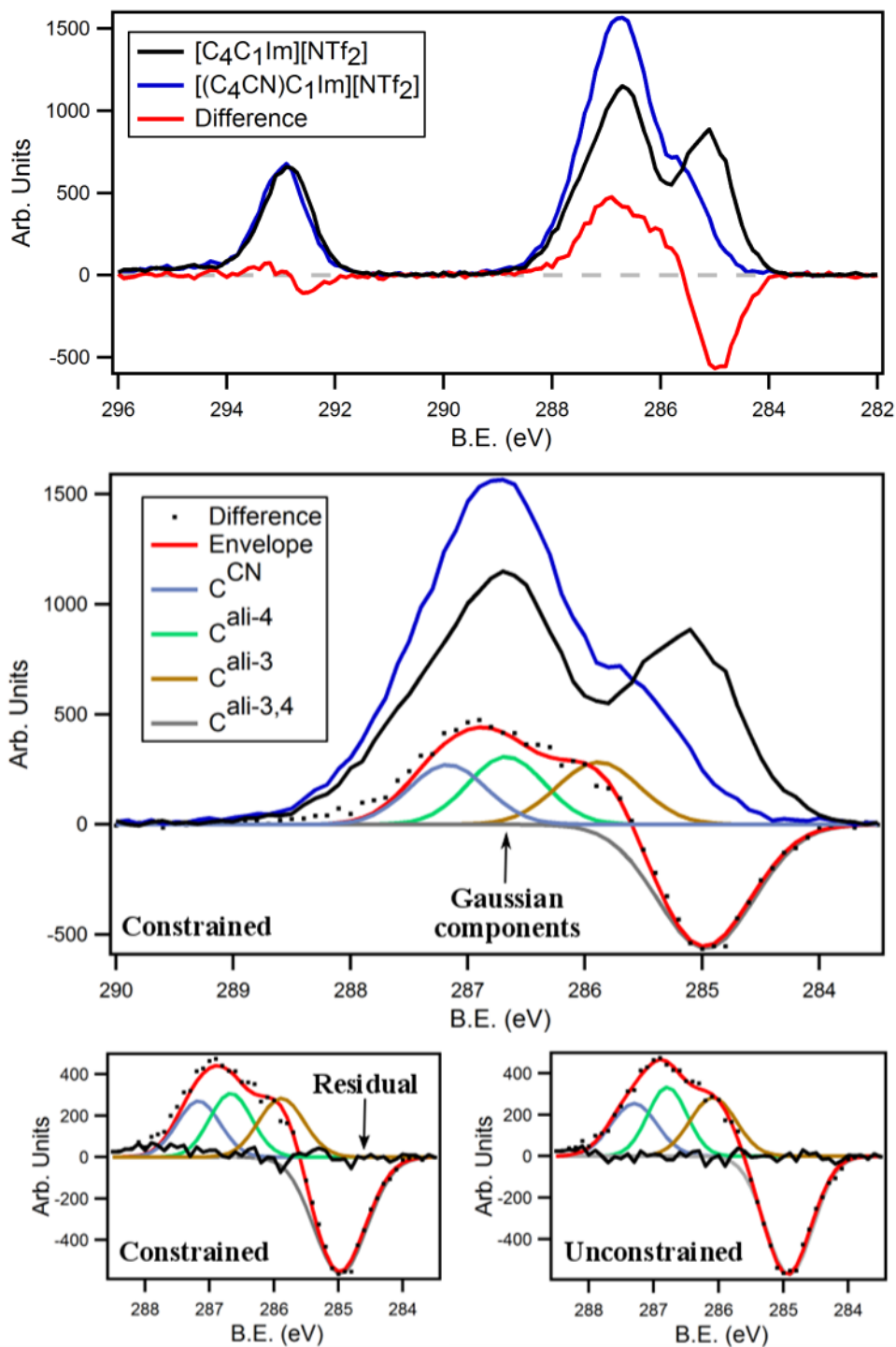


Figure 5.18 Top: The difference (red) generated from the subtraction of the $[C_4C_1Im][NTf_2]$ C 1s photoemission from the $[(C_4CN)C_1Im][NTf_2]$ photoemission. Middle: The peak fitted C 1s difference spectrum, peak positions are constrained to the B.E.s used for the $[(C_4CN)C_1Im][NTf_2]$ difference 2 fitting model. Bottom: An expansion of the constrained peak fitting model with the unconstrained model for comparison.

Table 5.11 The B.E.s for the position constrained and unconstrained fittings of the difference spectrum generated from the $[C_4C_1Im][NTf_2]$ and $[(C_4CN)C_1Im][NTf_2]$ C 1s photoemissions. The B.E.s for the C 1s components of the $[(C_4CN)Py][NTf_2]$ difference 2 fit are also shown.

		B.E. (eV)			
		Cali ^{-3,4}	Cali ⁻³	Cali ⁻⁴	C ^{CN}
$[(C_4CN)C_1Im][NTf_2]$	Constrained	285.0	285.9	286.7	287.2
	Unconstrained	284.9	286.1	286.8	287.3
$[(C_4CN)Py][NTf_2]$	Difference 2	285.1	286.0	286.7	287.2

5.2.5.2 $[(C_4CN)C_1Pyrr][NTf_2]$ Difference Spectra

Subtraction of the $[C_4C_1Pyrr][NTf_2]$ C 1s photoemission from the $[(C_4CN)C_1Pyrr][NTf_2]$ C 1s region should also produce a difference that may be peak fitted in the same way. The structural representation for this process is shown in **Figure 5.19**, where the methyl- and pyrrolidinium carbon atoms have been omitted for simplicity. The layout in **Figure 5.20** presents the difference spectrum for the pyrrolidinium nitrile IL, along with the associated peak fittings that were also used for the pyridinium and imidazolium nitrile difference spectra. Again, the peak positions have been constrained to the B.E. values obtained from the difference 2 peak fitting of the $[(C_4CN)Py][NTf_2]$ and $[C_2Py][NTf_2]$ C 1s difference.

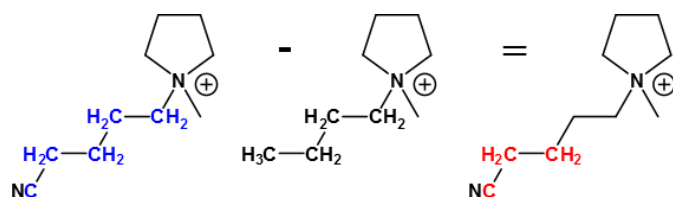


Figure 5.19 The structural representation of the difference generated (red carbons) when the $[C_4C_1Pyrr][NTf_2]$ C 1s photoemission (black carbons) is subtracted from the $[(C_4CN)C_1Pyrr][NTf_2]$ C 1s photoemission (blue carbons). The methyl- and imidazolium carbon atoms have been omitted for simplicity.

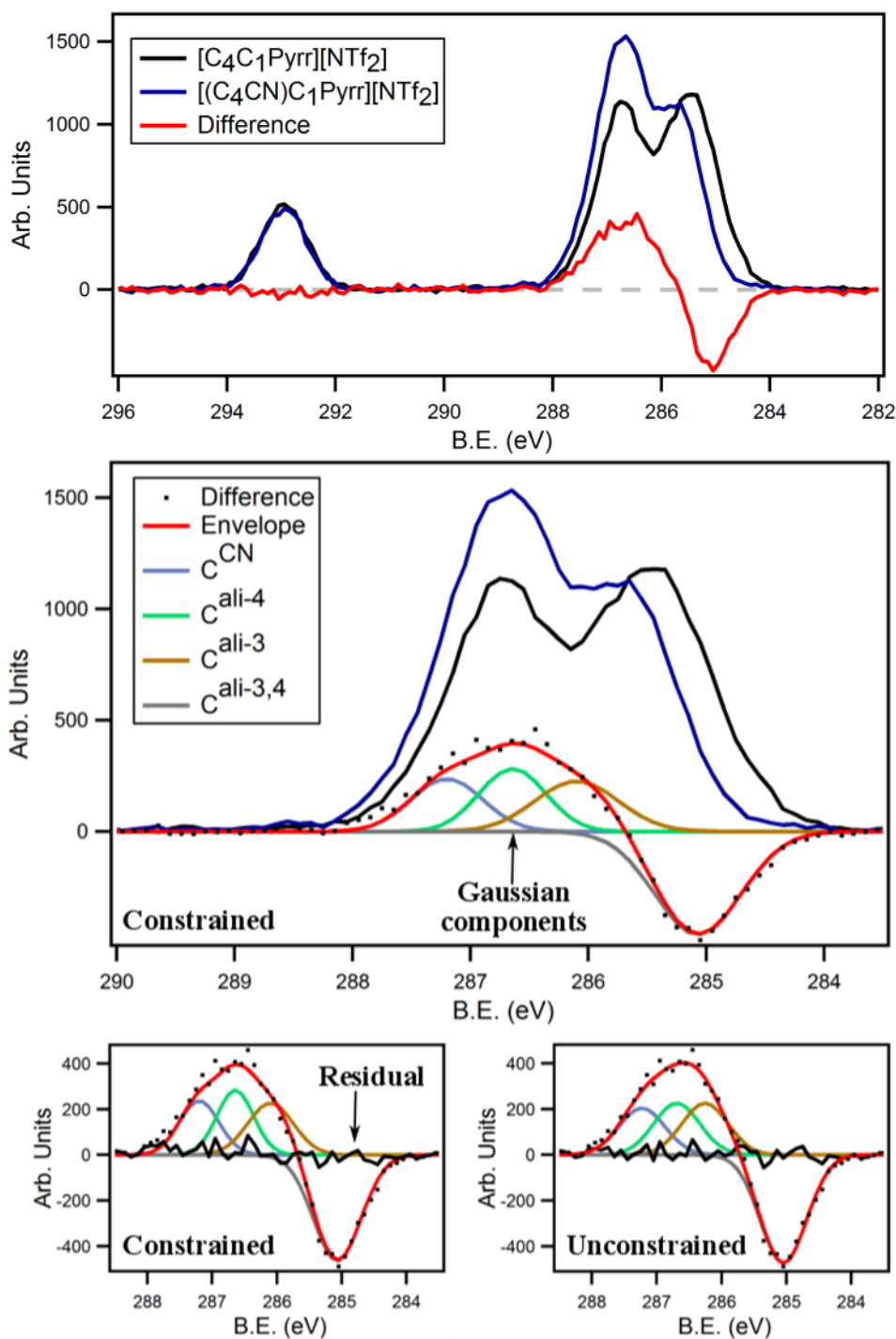


Figure 5.20 Top: The difference (red) generated from the subtraction of the $[C_4C_1Pyrr][NTf_2]$ C 1s photoemission from the $[(C_4CN)C_1Pyrr][NTf_2]$ photoemission. Middle: The peak fitted C 1s difference spectrum, peak positions are constrained to the B.E.s used for the $[(C_4CN)C_1Pyrr][NTf_2]$ difference 2 fitting model. Bottom: An expansion of the constrained peak fitting model with the unconstrained model for comparison.

The B.E.s for the position constrained and unconstrained difference models are summarised in **Table 5.12**. All values appear to be within 0.1 eV of the [(C₄CN)Py][NTf₂]⁻ difference 2 B.E.s, again with the exception of the C^{ali-3} component. Since this B.E. is situated at the point where the two inverse Gaussian peaks meet, there should be a greater deviation in the unconstrained C^{ali-3} peak position. Of course, the curve fitting function will attempt to replicate the CPS of the difference spectrum as best as possible. The degree of deviation from the best possible fit can be determined by inspecting the residual plots for each constrained and unconstrained fitting. As **Figure 5.20** shows, both residuals appear almost identical, with no significant differences between the two.

Table 5.12 The B.E.s for the position constrained and unconstrained fittings of the difference spectrum generated from the [C₄C₁Pyrr][NTf₂]⁻ and [(C₄CN)C₁Pyrr][NTf₂]⁻ C 1s photoemissions. The B.E.s for the C 1s components of the [(C₄CN)Py][NTf₂]⁻ difference 2 fit are also shown.

		B.E. (eV)			
		Cali ^{-3,4}	Cali ⁻³	Cali ⁻⁴	C ^{CN}
[(C ₄ CN)C ₁ Pyrr][NTf ₂] ⁻	Constrained	285.1	286.1	286.6	287.2
	Unconstrained	285.1	286.3	286.7	287.2
[(C ₄ CN)Py][NTf ₂] ⁻	Difference 2	285.1	286.0	286.7	287.2

All three differences generated from the [NTf₂]⁻ containing nitrile functionalised ILs have been overlaid and displayed together in **Figure 5.21**. The spectra are normalised to the area of the positive signals in the difference spectra. The same characteristic shapes are observed for each spectrum, with only a small deviation in the blue imidazolium difference at about 285.0 eV. This is most likely due to a small aliphatic surface contamination of either the nitrile functionalised or traditional imidazolium IL C 1s XP spectra. Despite this contamination, all difference spectra show a remarkable consistency. The data subtraction procedure has therefore eliminated all contribution from the cationic head groups, and the shifting signals of the aliphatic alkyl chains are revealed.

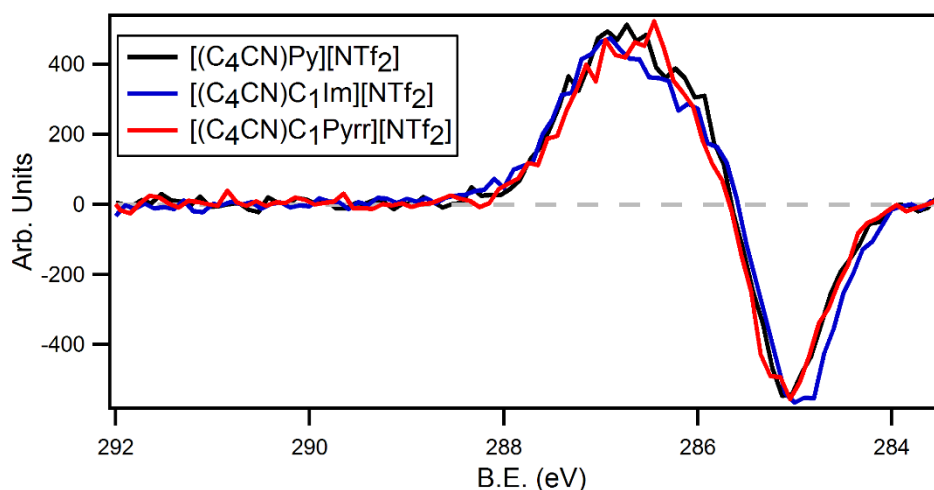


Figure 5.21 The differences generated from the pyridinium (black), imidazolium (blue) and pyrrolidinium (red) nitrile functionalised IL C 1s regions when the traditional butyl-chain analogues C 1s photoemissions are subtracted from the respective C 1s regions. The spectra are normalised to the area measured for the positive signals of each difference spectrum.

The same consistencies may not be observed for alternative counter ions as changing the anion produces an IL with different intermolecular interactions.²⁵ This process was discussed briefly in terms of XPS analysis in the introduction of this *thesis*. To examine any potential changes in the B.E.s of the -CN components as a function of the anion, the imidazolium nitrile functionalised ILs will be analysed in the following section.

5.2.6 Anionic Variation: [(C₄CN)C₁Im][A] C 1s Difference Spectra

The XP spectra for the [(C₄CN)C₁Im][A] (where A = [NTf₂]⁻, [PF₆]⁻, [BF₄]⁻ and Cl⁻) were shown in the beginning sections of this chapter. Since the [(C₄CN)C₁Im][NTf₂] salt has already been analysed, this section will present the C 1s region of the imidazolium [PF₆]⁻, [BF₄]⁻ and Cl⁻ salts. An identical method of analysis may be employed to again produce difference spectra relating to the shifts of the alkyl chain, relative to a non-functionalised butyl chain analogue.

Figure 5.22 shows the C1s regions and resulting difference spectra for the [(C₄CN)C₁Im][PF₆] and [C₄C₁Im][PF₆] salts. The spectra are charge corrected and normalised to the F 1s signal of the [PF₆]⁻ anion. The low quality of the [C₄C₁Im][PF₆] C 1s scan is unfortunately imparted onto the associated difference spectrum. The same fitting model utilising the C^{ali-3,4}, C^{ali-3}, C^{ali-4} and C^{CN} components has been applied to the difference spectrum. The areas are again fixed to 2 carbon atoms for the C^{ali-3,4} component, 1 carbon atom for the C^{ali-3} and C^{ali-4} components and 0.9 carbon atoms for the C^{CN} component (due to shake up/off losses). It should be noted that the functionalised and non-functionalised C 1s regions are both used when calculating the area per carbon atom. The values are usually identical as the spectra are normalised before the difference is taken. Although the peak positions are unconstrained, the signals are initially placed at the B.E. values found for the [(C₄CN)Py][NTf₂]⁻ difference 2 spectrum, before the curve fitting process is started.

The individual B.E.s for each component are presented later in **Table 5.12**, along with the results for the [BF₄]⁻ and Cl⁻ salts. Although the difference spectrum is of a lower quality than the analogous [NTf₂]⁻ spectrum, the same distinctive shape is present. The negative peak is again situated about the 285.0 eV position, while the positive peak spans a region that is approximately 1.8 eV wide, about the 286.5 eV position. The residual shows how the low quality C 1s spectrum has affected the degree of fit between the envelope and the observed difference. This fit may be improved with better quality XP spectra for the [C₄C₁Im][PF₆] C 1s region.

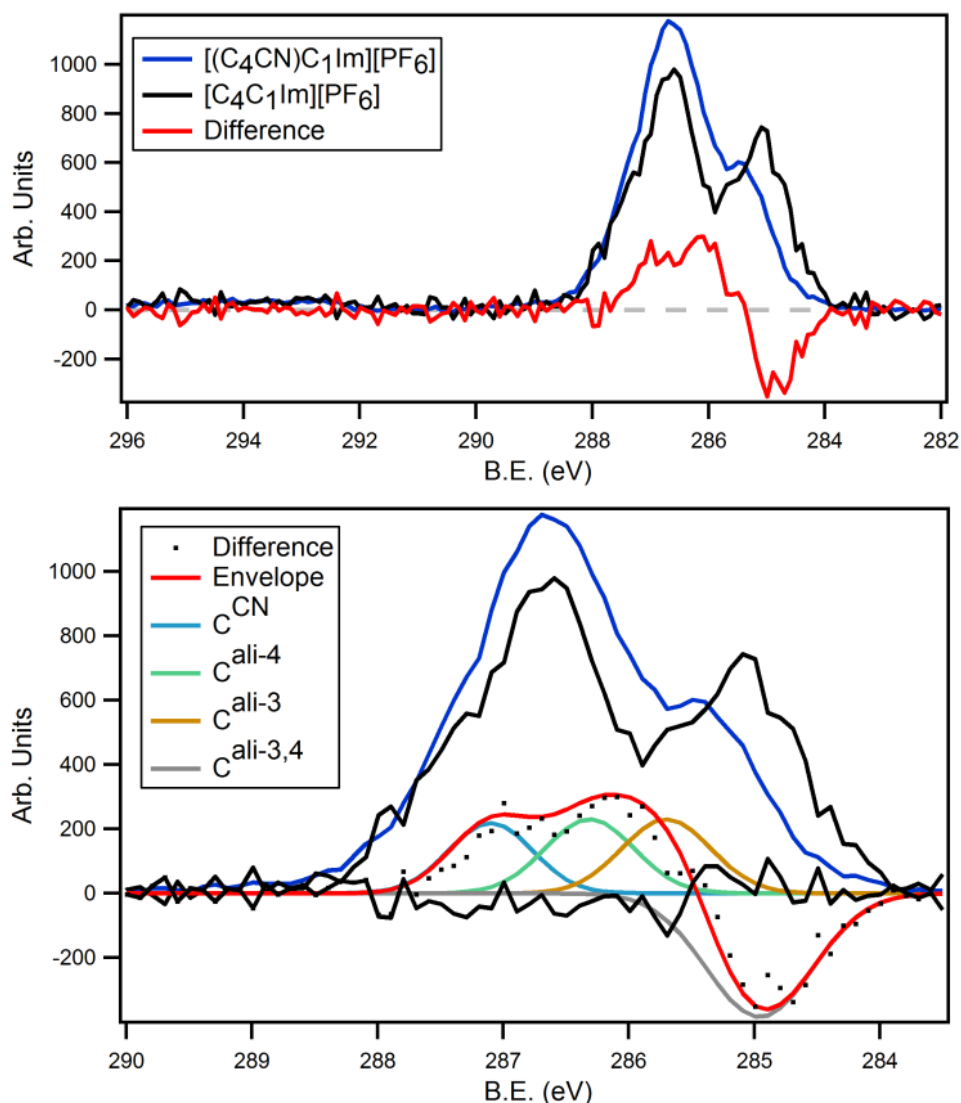


Figure 5.22 The $[(C_4CN)C_1Im][PF_6]$ C 1s region (blue) with the corresponding $[C_4C_1Im][PF_6]$ C 1s region (black) overlaid. The difference (red) between the two regions is also shown. The peak fitting of the difference spectrum is also shown, with the same unconstrained peaks used in the previous section.

The difference generated from the $[(C_4CN)C_1Im][BF_4]$ and $[C_4C_1Im][BF_4]$ C 1s photoemissions is displayed in **Figure 5.23**. The $[BF_4]^-$ nitrile IL XP spectra have been charge corrected to the F 1s signal of the anion, as obtained from the $[C_8C_1Im][BF_4]$ salt.²⁰ The spectra are also normalised to the F 1s signal area. The same unconstrained fitting model has also been applied to the obtained difference spectrum. The residual shows a good agreement between the difference and the envelope.

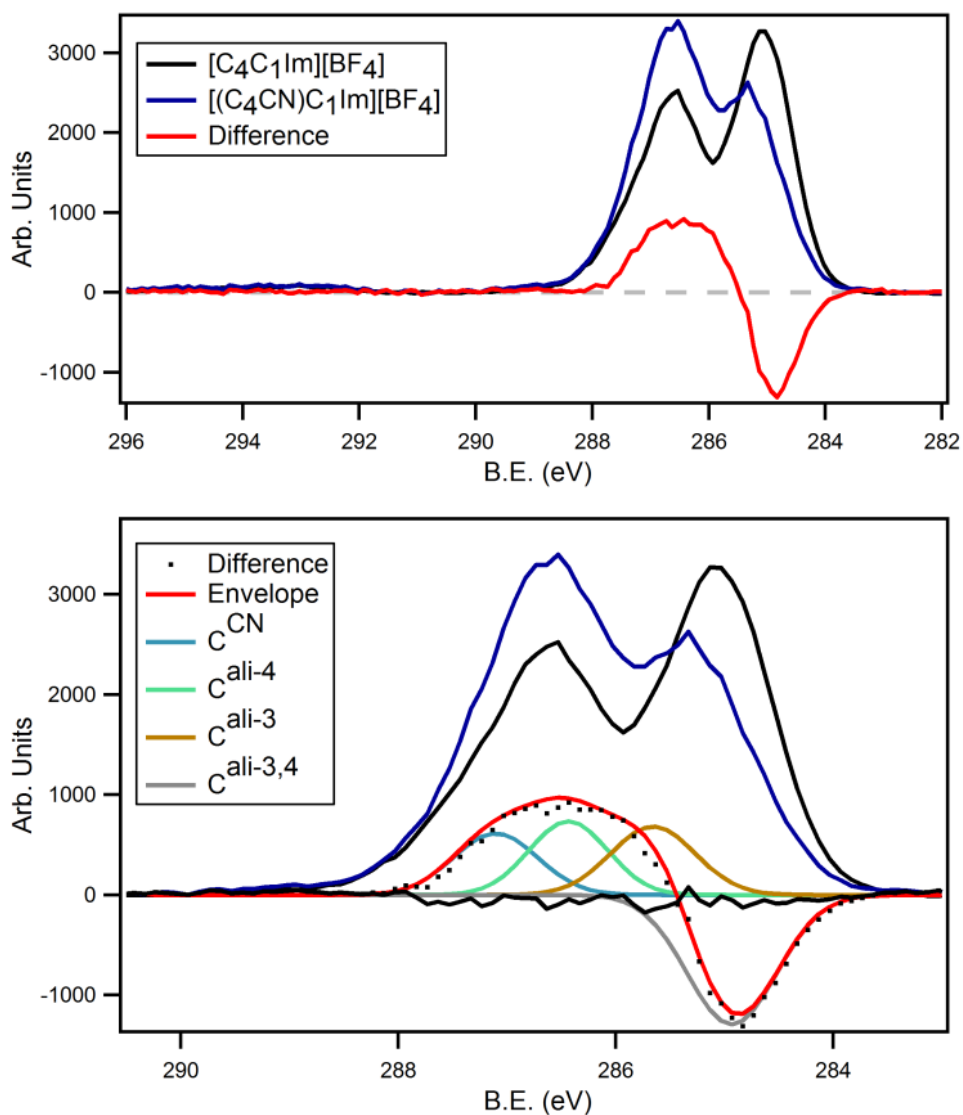


Figure 5.23 The $[(C_4CN)C_1Im][BF_4]$ C 1s region (blue) with the corresponding $[C_4C_1Im][BF_4]$ C 1s region (black) overlaid. The difference (red) between the two regions is also shown. The peak fitting of the difference spectrum is also shown, with the same unconstrained peaks used in the previous section.

The difference generated from the $[(C_4CN)C_1Im]Cl$ and $[C_4C_1Im]Cl$ C 1s photoemissions is also overlaid in **Figure 5.24**. The $[(C_4CN)C_1Im]Cl$ XP spectra have been corrected to the Cl $2p_{3/2}$ signal as obtained from the corrected $[C_8C_1Im]Cl$ salt. Since the samples do not contain fluorine, the spectra have been normalised to the area of the N 1s imidazolium signal. The good agreement between the envelope and the difference spectrum is reflected in the relatively small residual that is also plotted on the graph. As previously stated, the B.E.s for the unconstrained difference fittings of the imidazolium nitrile salts are summarised in **Table 5.13**.

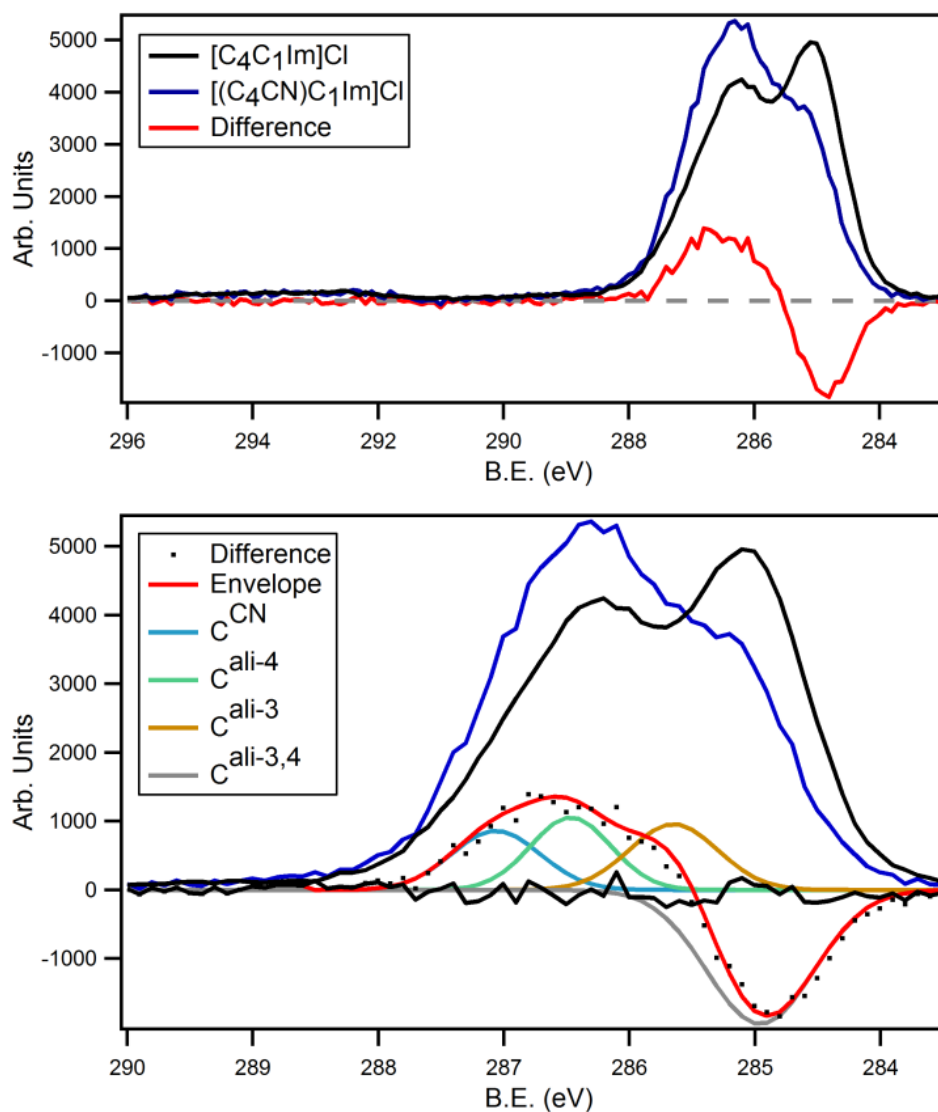


Figure 5.24 The $[(C_4CN)C_1Im]Cl$ C 1s region (blue) with the corresponding $[C_4C_1Im]Cl$ C 1s region (black) overlaid. The difference (red) between the two regions is also shown. The peak fitting of the difference spectrum is also shown, with the same unconstrained peaks used in the previous section.

Since the samples contain anions that may provide higher levels of charge transfer to the cationic species, peaks may shift to slightly lower B.E.s relative to the $[NTf_2]^-$ salts. Each unconstrained model appears to provide consistent results, with the peak positions being within 0.1 eV of each other.

Table 5.13 The B.E. values obtained when peak fitting the imidazolium nitrile difference spectra with the position unconstrained model that was previously used for the $[\text{NTf}_2]^-$ salts.

Cation	Anion	B.E. (eV)			
		$\text{C}^{\text{ali-3,4}}$	$\text{C}^{\text{ali-3}}$	$\text{C}^{\text{ali-4}}$	C^{CN}
$[(\text{C}_4\text{CN})\text{C}_1\text{Im}]^+$	$[\text{NTf}_2]^-$	285.0	286.0	285.9	287.2
$[(\text{C}_4\text{CN})\text{C}_1\text{Im}]^+$	$[\text{PF}_6]^-$	285.0	285.7	286.3	287.1
$[(\text{C}_4\text{CN})\text{C}_1\text{Im}]^+$	$[\text{BF}_4]^-$	284.9	285.7	286.4	287.1
$[(\text{C}_4\text{CN})\text{C}_1\text{Im}]^+$	Cl^-	285.0	285.7	286.5	287.1

When compared to the $[\text{NTf}_2]^-$ anions the other counter ions provide models with consistent $\text{C}^{\text{ali-3,4}}$ and C^{CN} components, however the $\text{C}^{\text{ali-3}}$ and $\text{C}^{\text{ali-4}}$ components deviate by as much as 0.6 eV. Due to their proximity to the edges of the difference spectrum, the $\text{C}^{\text{ali-3,4}}$ and C^{CN} signals are easily identified when peak fitting. The $\text{C}^{\text{ali-3}}$ and $\text{C}^{\text{ali-4}}$ peak positions are rather more difficult to distinguish due to the nature of the difference spectrum and their proximity to the boundary between the positive and negative signals.

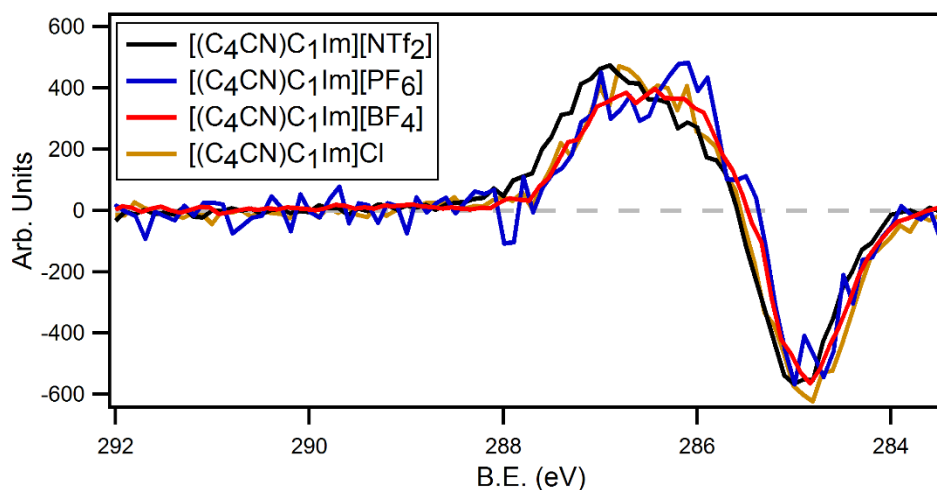


Figure 5.25 The overlaid difference spectra from the subtraction of the $[(\text{C}_4\text{CN})\text{C}_1\text{Im}][\text{A}]$ C 1s photoemission from the $[(\text{C}_4\text{CN})\text{C}_1\text{Im}][\text{A}]$ C 1s region ($\text{A} = [\text{NTf}_2]^-$, $[\text{PF}_6]^-$, $[\text{BF}_4]^-$ and Cl^-). The spectra are normalised to the area of the positive signals.

The overlaid difference spectra from the $[\text{C}_4\text{C}_1\text{Im}][\text{A}]$ and $[(\text{C}_4\text{CN})\text{C}_1\text{Im}][\text{A}]$ C 1s data subtractions are shown in **Figure 5.25**. Although the spectra have acquired some noise from the original photoemissions, the differences appear relatively consistent. The positive peak for the $[\text{NTf}_2]^-$ salt does appear to occupy a slightly higher B.E. region than the peaks from the other nitrile salts, however this is to be expected. Again, the characteristic difference spectra shapes have been reproduced by the data subtraction process, further supporting the results obtained for the $[\text{NTf}_2]^-$ salts.

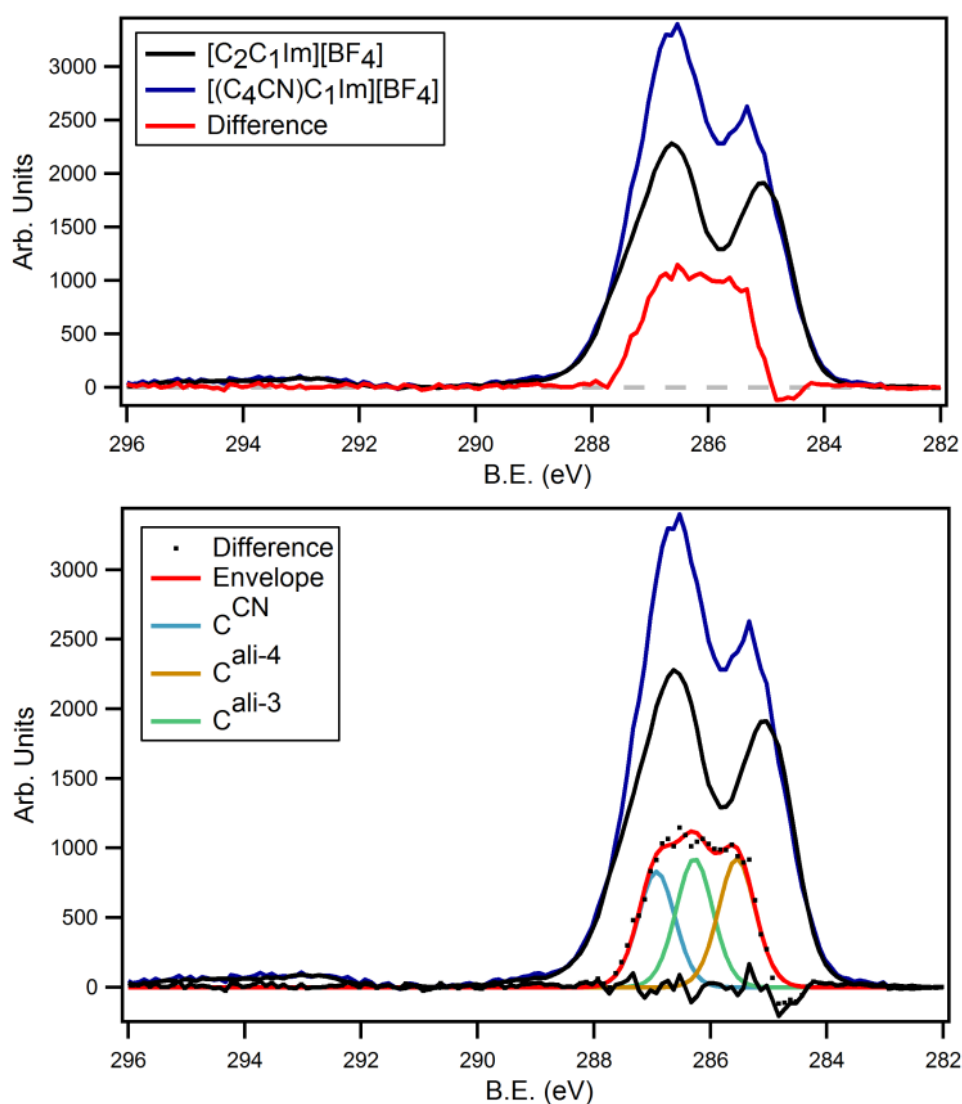


Figure 5.26 The $[(\text{C}_4\text{CN})\text{C}_1\text{Im}][\text{BF}_4]$ C 1s region (blue) with the corresponding $[\text{C}_2\text{C}_1\text{Im}][\text{BF}_4]$ C 1s region (black) overlaid. The difference (red) between the two regions is also shown. The peak fitting of the difference spectrum is also shown.

In order to support the observed shifting in the difference spectrum of the $[\text{BF}_4]^-$ salt, the difference between the $[\text{C}_2\text{C}_1\text{Im}][\text{BF}_4]$ and the $[(\text{C}_4\text{CN})\text{C}_1\text{Im}][\text{BF}_4]$ C 1s photoemissions may be examined. **Figure 5.26** shows both C 1s regions and the resulting difference spectrum, along with individual components and the residual fit. As with the fitting of difference 2 (from the $[\text{C}_2\text{Py}][\text{NTf}_2]$ and $[(\text{C}_4\text{CN})\text{Py}][\text{NTf}_2]$ C 1s photoemissions), this model utilises the standard GL(30) line shapes with unconstrained positions. Without the negative signal the three components are relatively easy to fit to the acquired difference spectrum. The B.E.s are shown in **Table 5.14**, along with the B.E.s for the unconstrained fitting of the difference generated from the $[\text{C}_4\text{C}_1\text{Im}][\text{BF}_4]$ C 1s photoemission.

Table 5.14 The B.E.s for the difference spectra generated from the $[(\text{C}_4\text{CN})\text{C}_1\text{Im}][\text{BF}_4]$ and the $[\text{C}_n\text{C}_1\text{Im}][\text{BF}_4]$ (where $n = 2$ or 4) C 1s photoemissions.

Initial Spectrum	Subtracted Spectrum	B.E. (eV)			
		Cali ^{-3,4}	Cali ⁻³	Cali ⁻⁴	C ^{CN}
$[(\text{C}_4\text{CN})\text{C}_1\text{Im}][\text{BF}_4]$	$[\text{C}_2\text{C}_1\text{Im}][\text{BF}_4]$		285.6	286.3	286.9
$[(\text{C}_4\text{CN})\text{C}_1\text{Im}][\text{BF}_4]$	$[\text{C}_4\text{C}_1\text{Im}][\text{BF}_4]$	284.9	285.7	286.4	287.1

The B.E.s are all within 0.1 eV of each other, with the exception of the C^{CN} component where both values are within 0.1 eV of a 287.0 eV value. Overall the peak fitting of the difference generated from the butyl imidazolium ionic liquid appears to provide reasonable B.E.s. The additional GL(30) fitting of the difference spectrum derived from the $[\text{C}_2\text{C}_1\text{Im}][\text{BF}_4]$ IL further supports the B.E.s that have been acquired through complicated inverse Gaussian summations. Due to the similarity of the $[\text{BF}_4]^-$ difference spectra from the $[\text{PF}_6]^-$ and Cl^- salts, no further analysis is required as each component is likely to occupy similar positions.

5.2.7 Accurate C 1s Peak Fitting for Nitrile ILs

If the individual components of the nitrile C 1s regions are constrained to ± 0.1 eV of the expected values, the resulting envelope should equal the observed CPS. The pyridinium and imidazolium C 1s regions have been analysed throughout this research and B.E.s have been produced for the majority of carbon environments. By utilising the known B.E. signals that have been derived through multiple difference spectra, the nitrile ILs may essentially be assembled from individual components. **Figure 5.27** presents the $[(C_4CN)Py][NTf_2]$ C 1s region with the associated peak fitting model. The residual shows a good agreement between the envelope and the measured photoemission.

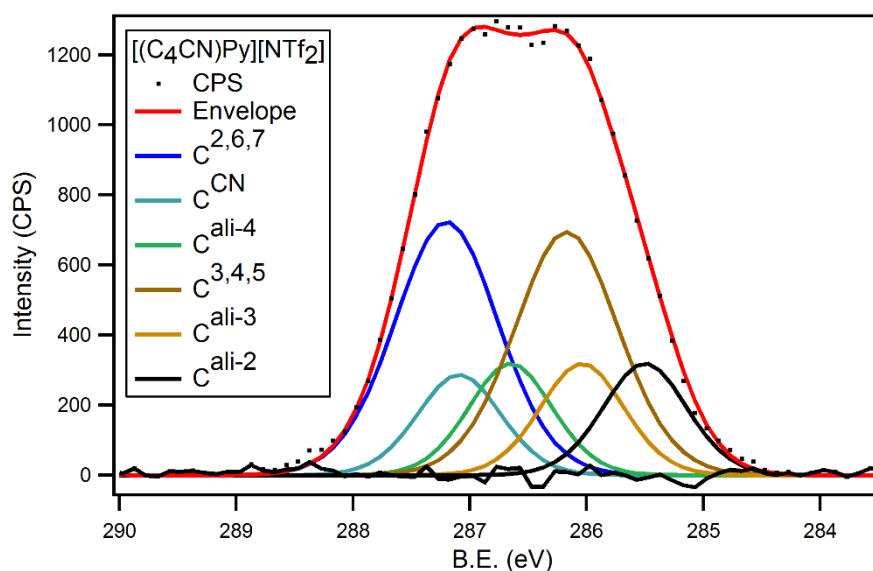


Figure 5.27 The $[(C_4CN)Py][NTf_2]$ C 1s spectrum with the peak fitting model that has been derived through numerous difference spectra found throughout this thesis. The component B.E.s are fixed to ± 0.1 eV of their expected values. Note: C^{ali-1} has been included in the pyridinium fitting as C^7 , from the $C^{2,6,7}$ component.

The analogous fitting for the $[(C_4CN)C_1Im][NTf_2]$ C 1s region is shown in **Figure 5.28**. Again, the individual components have been constrained to ± 0.1 eV of their expected values, as derived from various difference spectra throughout this thesis. A good agreement between the envelope and the recorded photoemission signals is also observed for the imidazolium salt, as reflected by the relatively small residual.

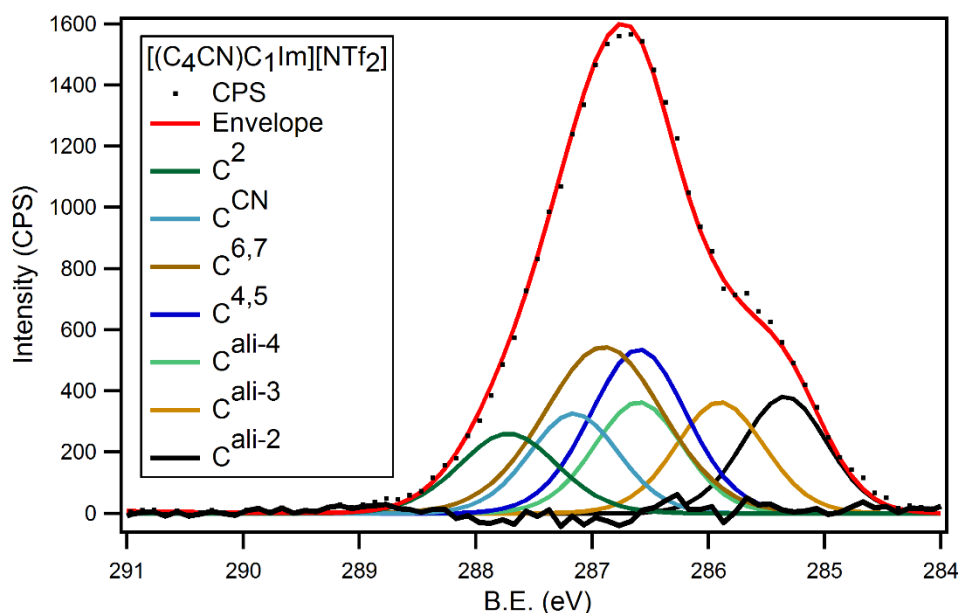


Figure 5.28 The $[(C_4CN)C_1Im][NTf_2]$ C 1s spectrum with the peak fitting model that has been derived through numerous difference spectra found throughout this thesis. The component B.E.s are fixed to ± 0.1 eV of their expected values.

The B.E.s used for the imidazolium and pyrrolidinium nitrile fitting models are summarised in **Table 5.14** and **Table 5.15**, respectively. The pyrrolidinium ILs have been fitted according to the previously published peak fitting model,^{14,23,26} combined with the position constrained carbons from the functionalised nitrile chain. In this model, the C^{ali-2} component is contained within the C^{inter} component, **Table 5.16**. The B.E. values have been constrained to ± 0.1 eV of the expected values, as taken from the appropriate source. The B.E.s may therefore deviate from the fixed value by the error of measurement. The B.E.s that provide the best fit to the recorded CPS have been selected and are presented.

		B.E. (eV)								
Cation	Anion	C ²	C ^{6,7}	C ^{4,5}	C ^{ali-2}	C ^{ali-3}	C ^{ali-4}	C ^{CN}	CF ₃	Residual STD
[(C ₄ CN)C ₁ Im] ⁺	[NTf ₂] ⁻	287.7 ^a	286.9 ^a	286.6 ^a	285.3	285.9	286.6	287.1	292.9	1.09
[(C ₄ CN)C ₁ Im] ⁺	[PF ₆] ⁻	287.7	286.9	286.4	285.2	285.5	286.4	286.9		1.11
[(C ₄ CN)C ₁ Im] ⁺	[BF ₄] ⁻	287.5	286.7	286.3	285.2	285.6	286.3	286.9		1.41
[(C ₄ CN)C ₁ Im] ⁺	Cl ⁻	287.5	286.6	285.8	285.0	285.5	286.2	286.9		1.29

^a Values taken from Chapter 3

		B.E. (eV)								
Cation	Anion	C ^{2,6,7}	C ^{3,4,5}	C ^{ali-2}	C ^{ali-3}	C ^{ali-4}	C ^{CN}	CF ₃	Residual STD	
[(C ₄ CN)Py] ⁺	[NTf ₂] ⁻	287.2 ^a	286.2 ^{a,b}	285.4	286.0	286.7	287.1	293.0	1.21	
[(C ₄ CN)Py] ⁺	[PF ₆] ⁻	286.9	285.9	285.3	285.5	286.4	286.9		1.08	

^a Values taken from Chapter 3, ^b C⁴ value confirmed in Chapter 4

		B.E. (eV)							
Cation	Anion	C ^{Hetero}	C ^{Inter}	C ^{ali-3}	C ^{ali-4}	C ^{CN}	CF ₃	Residual STD	
[(C ₄ CN)C ₁ Pyrr] ⁺	[NTf ₂] ⁻	286.7 ^c	285.6 ^c	285.9	286.7	287.2	292.9	1.18	
[(C ₄ CN)C ₁ Pyrr] ⁺	[PF ₆] ⁻	286.6	285.4	285.5	286.4	287.1		1.36	

^c Values taken from reference¹⁴

Table 5.14 The B.E.s for the [(C₄CN)C₁Im][A] C 1s peak fittings with the resulting residual STD. The component B.E.s were fixed to ± 0.1 eV of their expected values.

Table 5.15 The B.E.s for the [(C₄CN)Py][A] C 1s peak fittings with the resulting residual STD. The component B.E.s were fixed to ± 0.1 eV of their expected values.

Table 5.16 The B.E.s for the [(C₄CN)C₁Pyrr][A] C 1s peak fittings with the resulting residual STD. The component B.E.s were fixed to ± 0.1 eV of their expected values.

In order to gauge the degree of component fittings without presenting excessive numbers of spectra, residual STDs may be reported. The ideal residual STD for the C 1s region of the nitrile ILs has been measured at an average value of 0.88, see *Appendix* for more details. The residual STDs reduce the degree of fit between the envelope and CPS to a single value. A complex system such as this will certainly require further peak fitting error analysis in the future. However, for the purpose of this investigation the values may be used to examine the stability of a model with respect to certain variables, such as changing the counter ion of a salt. The majority of the peak fittings provide residuals that are close to unity, with no major deviations. The residual plots are therefore comparable to those shown in **Figure 5.27** and **Figure 5.28**.

5.3 Conclusions

A range of nitrile functionalised ILs have been synthesised with pyridinium, imidazolium and pyrrolidinium cations and various anions. The XP spectra of the nitrile salts have been acquired and analysed. The N 1s signal of the nitrile nitrogen from the -CN functionality appears to be independent of both anionic and cationic variations. This implies that the nitrile group does not experience significant changes in intermolecular interaction for different anion and cation sets. Elsewhere, the physiochemical properties of nitrile functionalised ILs have been found to differ significantly from traditional ILs. The changes have been attributed to the increased levels of hydrogen bonding and the additional interactions between the nitrile group and the anions and cations. Therefore, these interactions are most likely too weak to be XPS observable.

The C 1s regions of the nitrile functionalised ILs have also been thoroughly analysed *via* a series of difference spectra. By subtracting the C 1s photoemissions of the butyl chain analogues from the [(C₄CN)Cat][A] salts, complex difference spectra with positive and negative signals have been produced. **Figure 5.7** showed 'difference 1' as an example of the difference process. The spectral patterns display the shift in electron density relative to

the two samples. Hence, the initial and final location of the $C^{\text{ali-3}}$ and $C^{\text{ali-4}}$ peaks have been revealed, alongside the additional photoemission from the C^{CN} carbon environment.

Although all photoemissions are not fully resolved, the difference spectra have been modelled with Gaussian peaks that accurately reproduce the sinusoidal like shape of the calculated spectra. This model is based upon the GL(30) peak fitting of ‘difference 2’, a difference spectrum generated by the subtraction of the $[\text{C}_2\text{C}_1\text{Py}][\text{NTf}_2]$ C 1s photoemission from the $[(\text{C}_4\text{CN})\text{Py}][\text{NTf}_2]$ C 1s photoemission. This difference was later reproduced *via* the same process using the $[(\text{C}_4\text{CN})\text{C}_1\text{Im}][\text{BF}_4]$ C 1s region, albeit with slightly lower B.E.s due to the more basic $[\text{BF}_4]^-$ anion. ‘Difference 3’ was generated from the subtraction of the $[\text{C}_2\text{Py}][\text{NTf}_2]$ C 1s photoemission from the $[\text{C}_4\text{Py}][\text{NTf}_2]$ C 1s photoemission. This difference was used to confirm the initial location of the $C^{\text{ali-3}}$ and $C^{\text{ali-4}}$ components (grouped as $C^{\text{ali-3,4}}$).

The Gaussian model used to fit ‘difference 1’ was also applied to the imidazolium and pyrrolidinium $[\text{NTf}_2]^-$ nitrile difference spectra. The envelope of the constrained model showed a good agreement to each difference spectrum. A comparison of the spectra showed consistent peak shapes, highlighting the independence of the spectra with respect to the cationic head of the nitrile salts, **Figure 5.21**. Similar shapes were also observed for various anions of the imidazolium nitrile salt, although the spectra were shifted slightly to lower binding energies. Again, the consistent shapes have supported the difference process in terms of the associated photoemissions. By constraining the C 1s peak positions of the nitrile chain and combining these with the known B.E.s of the imidazolium and pyrrolidinium ILs, the entire C 1s regions have been modelled. The residual STDs reflect the ability of the predicted models to reproduce the photoemissions of the nitrile salts.

The B.E.s for the individual components of the C 1s regions for a range of nitrile functionalised ILs have been resolved. Further XPS studies utilising nitrile ILs as coordinating liquid media may benefit to a greater extent from this advanced knowledge of the B.E.s of the carbon framework. Other studies

that have utilised fitting models based upon chemical intuition may also find that the applications of these models yield supporting or alternative arguments. However, for this work, the greater impact is upon the C 1s peak fitting process and the application of difference spectroscopy.

Overall, analysis of the C 1s regions of nitrile IL salts has presented another technique that may be exploited with XP difference spectra. By utilising multiple differences from multiple IL that are structurally related, the impact of the additional nitrile group upon the alkyl chain has been deduced. The complexity of the difference spectra means that one difference alone is insufficient to examine the C 1s region. For example, the chlorinated ILs presented in *chapter 3* provided spectra that showed the shifting of one carbon atom in the related C 1s regions. This section has presented data analysis to clearly identify the shifting of two carbon atoms and the addition of one carbon atom.

So far, the level of peak fitting refinement provided by difference spectra surpasses any current peak fitting method for XP spectra. This technique is not necessarily limited to ILs, in fact any structurally related samples should provide reasonable difference spectra to deduce peak positions. However, the ability to modify the IL structure provides a great advantage for this method of XPS post data-acquisition analysis. By combining known B.E. peaks, molecules may essentially be assembled one piece at a time. This has important implications for future XP spectra and XP spectra calculations.

5.4 References

- 1 A. Abebe, S. Admassie, I. J. Villar-Garcia and Y. Chebude, *Inorg. Chem. Commun.*, 2013, **29**, 210–212.
- 2 N. Jordão, L. Cabrita, F. Pina and L. C. Branco, *Chem. Eur. J.*, 2014, **20**, 3982–3988.
- 3 K. C. Lethesh, K. Van Hecke, L. Van Meervelt, P. Nockemann, B. Kirchner, S. Zahn, T. N. Parac-Vogt, W. Dehaen and K. Binnemans, *J. Phys. Chem. B*, 2011, **115**, 8424–8438.
- 4 D. Zhao, Z. Fei, R. Scopelliti and P. J. Dyson, *Inorg. Chem.*, 2004, **43**, 2197–2205.
- 5 V. I. Pârvulescu and C. Hardacre, *Chem. Rev.*, 2007, **107**.
- 6 Z. Fei, D. Zhao, D. Pieraccini, W. H. Ang, T. J. Geldbach, R. Scopelliti, C. Chiappe and P. J. Dyson, *Organometallics*, 2007, **26**, 1588–1598.
- 7 P. Nockemann, M. Pellens, K. Van Hecke, L. Van Meervelt, J. Wouters, B. Thijs, E. Vanecht, T. N. Parac-Vogt, H. Mehdi, S. Schaltin, J. Fransaer, S. Zahn, B. Kirchner and K. Binnemans, *Chem. Eur. J.*, 2010, **16**, 1849–58.
- 8 Q. Zhang, Z. Li, J. Zhang, S. Zhang, L. Zhu, J. Yang, X. Zhang and Y. Deng, *J. Phys. Chem. B*, 2007, **111**, 2864–2872.
- 9 D. Zhao, Z. Fei, T. J. Geldbach, R. Scopelliti and P. J. Dyson, *J. Am. Chem. Soc.*, 2004, **126**, 15876–15882.
- 10 Y. Cui, I. Biondi, M. Chaubey, X. Yang, Z. Fei, R. Scopelliti, C. G. Hartinger, Y. Li, C. Chiappe and P. J. Dyson, *Phys. Chem. Chem. Phys.*, 2010, **12**, 1834–1841.
- 11 Z. Fei, D. Zhao, D. Pieraccini, W. H. Ang, T. J. Geldbach, R. Scopelliti, C. Chiappe and P. J. Dyson, *Organometallics*, 2007, **26**, 1588–1598.
- 12 C. Chiappe, D. Pieraccini, D. Zhao, Z. Fei and P. J. Dyson, *Adv. Synth. Catal.*, 2006, **348**, 68–74.

- 13 R. Sheldon, *Chem. Commun.*, 2001, 2399–2407.
- 14 S. Men, *Thesis*, The University of Nottingham, 2011.
- 15 A. W. Taylor, S. Men, C. J. Clarke and P. Licence, *RSC Adv.*, 2013, **3**, 9436.
- 16 S. Caporali, C. Chiappe, T. Ghilardi, C. S. Pomelli and C. Pinzino, *Chemphyschem*, 2012, **13**, 1885–92.
- 17 B. B. Hurisso, K. R. J. Lovelock and P. Licence, *Phys. Chem. Chem. Phys.*, 2011, **13**, 17737–48.
- 18 T. Cremer, C. Kolbeck, K. R. J. Lovelock, N. Paape, R. Wölfel, P. S. Schulz, P. Wasserscheid, H. Weber, J. Thar, B. Kirchner, F. Maier and H.-P. Steinrück, *Chem. Eur. J.*, 2010, **16**, 9018–33.
- 19 F. Bernardi, J. D. Scholten, G. H. Fecher, J. Dupont and J. Morais, *Chem. Phys. Lett.*, 2009, **479**, 113–116.
- 20 I. J. Villar García, *Thesis*, The University of Nottingham, 2009.
- 21 I. J. Villar-Garcia, E. F. Smith, A. W. Taylor, F. Qiu, K. R. J. Lovelock, R. G. Jones and P. Licence, *Phys. Chem. Chem. Phys.*, 2011, **13**, 2797.
- 22 S. Men, D. S. Mitchell, K. R. J. Lovelock and P. Licence, *ChemPhysChem*, 2015, **16**, 2211.
- 23 S. Men, K. R. J. Lovelock and P. Licence, *Phys. Chem. Chem. Phys.*, 2011, **13**, 15244–15255.
- 24 C. Hardacre, J. D. Holbrey, C. L. Mullan, M. Nieuwenhuyzen, W. M. Reichert, K. R. Seddon and S. J. Teat, *New J. Chem.*, 2008, **32**, 1953.
- 25 J. Dupont and P. a Z. Suarez, *Phys. Chem. Chem. Phys.*, 2006, **8**, 2441–2452.
- 26 D. S. Mitchell, *Thesis*, The University of Nottingham, 2014.

Conclusions and Future Work

6 Conclusions and Future Work

This *Thesis* has demonstrated a new method for the determination of exact B.E.s from complex XP spectra. By utilising the designer aspect of ILs and appending structural modifications to certain positions of the IL framework, the shifting of electron density between two structurally related samples has been examined *via* XPS. The subtraction of one photoemission from another has produced difference spectra that expose the initial and final positions of the shifting signals. Due to the large variety of chemical states and the ease of modification, this analysis is best suited for the identification of C 1s photoemissions that are otherwise unknown. Previous work has attempted to interpret the complex C 1s regions through peak fitting models based upon chemical knowledge and parameter constraints. Each results chapter has shown how XP difference spectra may be used in various ways in order to determine unknown information from complex photoemissions. To summarise:

Chapter 3:

Chlorine was used as an electron withdrawing group to remove electron density from certain carbon environments of imidazolium and pyridinium ILs. The observed C 1s differences relative to analogous non-chlorinated salts were easily interpreted due to the large B.E. shifts of the single carbon photoemission. The current peak fitting model of the imidazolium C 1s region was subsequently found to be incorrect. A new fitting model that accurately represented the imidazolium C 1s region was proposed based upon the exact B.E.s that were obtained. The current C 1s peak fitting model of pyridinium ILs was found to be correct with regards to the C², C³, C⁵ and C⁶ carbon environment photoemissions. Exact B.E.s were found to be within the error of the previous B.E. assignments.

Chapter 4:

The C 1s regions of di-alkylated 4,4'-bipyridinium salts were normalised to pyridinium and mono-alkylated 4,4'-bipyridinium C 1s regions to provide photoemissions equal to the 'halved' di-alkylated bipyridinium structures. The resulting difference spectra were more complex due to small B.E. shifts and the presence of multiple carbon environments. However, the acquired B.E. shifts were used to confirm that the B.E. of the pyridinium C⁴ carbon photoemission was correctly assigned by the previous peak fitting model. The photoemissions of the neutral portion of the mono-alkylated 4,4'-bipyridinium ring were also determined using difference spectra generated from the mono- and dicationic 4,4'-bipyridinium C 1s XP spectra. The model was found to accurately replicate the experimentally measured photoemissions when peaks were constrained to their known B.E. values.

Chapter 5:

A series of valeronitrile functionalised ILs were compared to their traditional butyl chain counterparts and the C 1s photoemissions were used to create difference spectra. The resulting differences were complex due to the presence of multiple unresolved carbon photoemissions. Other difference spectra derived from the nitrile ILs and various alkyl chain analogues were used to investigate and fit the complex nitrile-butyl chain difference spectra. The differences were found to be independent of cationic and anionic variation, due to the data subtraction process. The resulting C 1s peak fittings of the nitrile ILs were composed of known B.E.s derived from separate XPS experiments. When each photoemission was constrained in position, area and FWHM, the resulting sum of each signal was found to reproduce the observed photoemissions with little to no deviations.

With the growing number of IL applications, the ability to monitor IL solutions, mixtures and surfaces will become more important. The element specific nature and surface sensitivity of XPS has so far proven to yield valuable information on the IL surface-vacuum interface, solvent-solvent and solvent-solute interactions of ILs. Unfortunately, XPS investigations are often

limited by the resolution of the spectrometer, meaning that complicated photoemission spectra are difficult to interpret.

The work presented in this *Thesis* has demonstrated how, by exploiting the designer aspect of ILs, chemical modifications can be utilised in order to indirectly resolve coincident photoemission peaks. Therefore, by implementing the procedures outlined here, the information obtained from XP spectra may be significantly increased. For example, the interactions of solutes with IL cations or anions may be resolved, as well as the coordination modes of IL ligands and metal catalysts. The electronic distributions of IL structures may also be better understood, revealing additional information on the physicochemical properties of neat IL and IL mixtures.

Overall, this work has demonstrated the power of structural variation in the determination of exact B.E.s from XP spectra. Although this technique is not necessarily limited to ILs, there are many unique advantages that make them ideally suited for this particular purpose. Besides their extremely low vapour pressures, the ease of structural modification is perhaps the most significant. Elaborating upon this feature, the following future experiments are suggested:

1. To synthesise and XPS an imidazolium IL chlorinated at the C⁶ position, i.e. the methyl group. The resulting C 1s difference spectra will provide the reverse experiment to the C⁴ chlorinated imidazolium IL presented in this work.
2. To acquire the XP spectra of a 4-chloropyridinium IL in order to complete the known C 1s photoemission B.E.s for pyridinium ILs. This data will also provide information that may be used to scrutinise the difference spectra obtained from the di-alkylated 4,4'-bipyridinium ILs.
3. The preparation and XPS of a large complex salt that is composed of a carbon framework for which the B.E.s are known. This will enable the 'building' of C 1s photoemissions from smaller known pieces. If the acquired C 1s signals can be constructed and accurately replicated in this way, this technique may be used to predict XP spectra.

4. To extend difference spectra to other functionalised ILs. Non-shifting C 1s photoemissions may be cancelled out by subtracting the analogous traditional IL C 1s photoemissions. Therefore ILs may be used as ‘anchors’ to potentially XPS a range of chemical groups that may not be suited for UHV spectroscopy (i.e. volatile compounds)
5. To coordinate the functional nitrile and mono-alkylated bipyridinium ILs to metal centres and acquire the XPS analysis. Since the majority of C 1s and N 1s peaks are now known, the impact of coordination upon the electronic structures may be quantified for each particular environment.
6. To develop a library of exact B.E.s and photoemission shapes for future XPS analysis.

Appendix

7 Appendix

7.1 Generating Difference Spectra

Since the generation of difference spectra relies on analysing one spectrum relative to another, clear procedures must be outlined in order to understand the data that is produced upon photoemission subtraction. During analysis, non-uniform charging of the sample surface results in various degrees of B.E. shifts for all emitted photoelectrons during data acquisition. All XP spectra therefore require charge correction to provide accurate B.E. values for the reliable comparisons of different XP scans. The charge correction and referencing procedures of IL XP spectra are explained at the beginning of this *Thesis*. All of the difference spectra presented in this work were produced *via* the following procedures:

1. The two spectra of interest are charge corrected or charge referenced according to previously established procedures.
2. One spectrum is plotted against the B.E. of the reference spectrum (in this work all traditional ILs are used as the reference spectrum. The difference spectra generated from the mono- and dicationic 4,4'-bipyridinium C 1s and N 1s spectra were initially referenced to the charge corrected dicationic XP spectra).
3. Both spectra are overlaid and displayed on the common B.E. scale and then normalised to a common photoemission peak (For this work the majority of the spectra are normalised to the $-\text{CF}_3$ signal of the $[\text{NTf}_2]^-$ anion. In the absence of this peak the spectra are normalised to the area of the main photoemission peak).

Note: The signal area per atom may also be calculated and compared for each spectrum to ensure that the signals are accurately normalised.

4. Any resulting visual discrepancies are adjusted by aligning the spectra to a common peak. (Again, for this work the majority of the spectra are aligned by the $-\text{CF}_3$ signal of the $[\text{NTf}_2]^-$ anion. In the absence of this peak the spectra are aligned by the main photoemission signal).

5. The reference spectrum is then subtracted from the aligned spectrum to generate the difference.

7.2 Gaussian Peak Fittings:

Two types of peak fitting were used for the high resolution XP spectra reported in this work. GL(30) peak shapes were used to fit standard XP spectra using the CasaXPS program. Since CasaXPS is not designed to fit negative signals, all difference spectra were analysed using custom Gaussian peak fits in Igor Pro. Two custom fitting functions were used in this work, they are:

1. A two component Gaussian fitting used for the 4,4'-bipyridinium difference spectra, made using the equation:

$$f(B.E.) = a_1 \times e^{-\left(\frac{(B.E.-p_1)^2}{2w_1^2}\right)} - a_2 \times e^{-\left(\frac{(B.E.-p_2)^2}{2w_2^2}\right)}$$

where : $a_n = \left(\frac{A}{(w_n\sqrt{2\pi})}\right)$

and:

$A =$ the area of the peak (set to be equal for both peaks in this fitting)

$w =$ the Gaussian RMS width ($FWHM = 2.35 \times w$, $w = FWHM/2.35$)

$p =$ the position of the centre of the peak

2. A four component Gaussian fitting for the nitrile functionalised difference spectra, made using the equation:

$$f(B.E.) = a_1 \times e^{-\left(\frac{(B.E.-p_1)^2}{2w_1^2}\right)} + a_2 \times e^{-\left(\frac{(B.E.-p_2)^2}{2w_2^2}\right)} + a_3 \times e^{-\left(\frac{(B.E.-p_3)^2}{2w_3^2}\right)} - a_4 \times e^{-\left(\frac{(B.E.-p_4)^2}{2w_4^2}\right)}$$

where : $a_n = \left(\frac{A_n}{(w_n \sqrt{2\pi})} \right)$

and:

A = the area of the peak (A was set to the area for the appropriate number of carbons, as calculated from the nitrile C 1s photoemission area).

e.g. $C^{ali-3} = 1$ carbon, $C^{ali-4} = 1$ carbon, $C^{CN} = 0.9$ carbons and $C^{ali-3,4} = 2$ carbons.

w = the Gaussian RMS width ($FWHM = 2.35 \times w$, $w = FWHM/2.35$)

p = the position of the centre of the peak

Notes:

1. The pre-exponential is equal to the normalised area of the curve.
2. The Gaussian RMS width was limited to 0.34-0.51, as $w = FWHM/2.35$.

7.3 Gaussian Peak Fitting Results:

Fitting from **Figure 4.5**, Chapter 4: 4,4'-bipyridinium ILs:

Coefficient values \pm one standard deviation:

$$w_1 = 0.47331 \pm 0.0406 \text{ eV (FWHM} = 1.10 \text{ eV, positive peak)}$$

$$w_2 = 0.49831 \pm 0.0501 \text{ eV (FWHM} = 1.17 \text{ eV, negative peak)}$$

$$p_1 = 286.75 \pm 0.048 \text{ eV (taken as } 286.8 \text{ eV, positive peak)}$$

$$p_2 = 286.39 \pm 0.0475 \text{ eV (taken as } 286.4 \text{ eV, negative peak)}$$

$$A = 340 \pm 0$$

(Area constrained to equal 1.0 carbon atom, as found from the [(C₆)₂Bipy][NTf₂]₂ C 1s photoemission)

Fitting from **Figure 5.13**, Chapter 5: Nitrile Functionalised Ionic Liquids:

Constrained positions:

$$A_1 = 398 \pm 0 \text{ (constrained to 0.9 carbon atoms)}$$

$$A_2 = 443 \pm 0 \text{ (constrained to 1.0 carbon atoms)}$$

$$A_3 = 443 \pm 0 \text{ (constrained to 1.0 carbon atoms)}$$

$$A_4 = 886 \pm 0 \text{ (constrained to 2.0 carbon atoms)}$$

$$w_1 = 0.42433 \pm 0.18 \text{ eV (FWHM} = 0.99 \text{ eV, C}^{\text{CN}})$$

$$w_2 = 0.5 \pm 0.681 \text{ eV (FWHM} = 1.18 \text{ eV, C}^{\text{ali-4}})$$

$$w_3 = 0.48623 \pm 0.218 \text{ eV (FWHM} = 1.14 \text{ eV, C}^{\text{ali-3}})$$

$$w_4 = 0.44283 \pm 0.0254 \text{ eV (FWHM} = 1.04 \text{ eV, C}^{\text{ali-3,4}})$$

$$p_1 = 287.1 \pm 0.428 \text{ eV (C}^{\text{CN}} \text{ component, constrained to } 287.1 \pm 0.1 \text{ eV)}$$

$$p_2 = 286.7 \pm 0.236 \text{ eV (C}^{\text{ali-4}} \text{ component, constrained to } 286.6 \pm 0.1 \text{ eV)}$$

$$p_3 = 286.07 \pm 0.198 \text{ eV (C}^{\text{ali-3}} \text{ component, constrained to } 286.0 \pm 0.1 \text{ eV)}$$

$$p_4 = 285.06 \pm 0.0184 \text{ eV (C}^{\text{ali-3,4}} \text{ component, constrained to } 285.0 \pm 0.1 \text{ eV)}$$

Unconstrained positions:

$$A_1 = 398 \pm 0 \text{ (constrained to 0.9 carbon atoms)}$$

$$A_2 = 443 \pm 0 \text{ (constrained to 1.0 carbon atoms)}$$

$$A_3 = 443 \pm 0 \text{ (constrained to 1.0 carbon atoms)}$$

$$A_4 = 886 \pm 0 \text{ (constrained to 2.0 carbon atoms)}$$

$$w_1 = 0.4 \pm 0.0802 \text{ eV (FWHM} = 0.94 \text{ eV, C}^{\text{CN}})$$

$$w_2 = 0.424 \pm 0.129 \text{ eV (FWHM} = 0.99 \text{ eV, C}^{\text{ali-4}})$$

$$w_3 = 0.5 \pm 0.105 \text{ eV (FWHM} = 1.18 \text{ eV, C}^{\text{ali-3}})$$

$$w_4 = 0.43349 \pm 0.0214 \text{ eV (FWHM} = 0.97 \text{ eV, C}^{\text{ali-3,4}})$$

$$p_1 = 287.1 \pm 0.0681 \text{ eV (C}^{\text{CN}} \text{ component)}$$

$$p_2 = 286.6 \pm 0.0494 \text{ eV (C}^{\text{ali-4}} \text{ component)}$$

$$p_3 = 285.9 \pm 0.0535 \text{ eV (C}^{\text{ali-3}} \text{ component)}$$

$$p_4 = 285.09 \pm 0.0138 \text{ eV (C}^{\text{ali-3,4}} \text{ component)}$$

Fitting from **Figure 5.18**, Chapter 5: Nitrile Functionalised Ionic Liquids:

Constrained positions:

$$A_1 = 319 \pm 0 \text{ (constrained to 0.9 carbon atoms)}$$

$$A_2 = 355 \pm 0 \text{ (constrained to 1.0 carbon atoms)}$$

$$A_3 = 355 \pm 0 \text{ (constrained to 1.0 carbon atoms)}$$

$$A_4 = 710 \pm 0 \text{ (constrained to 2.0 carbon atoms)}$$

$$w_1 = 0.46936 \pm 0.0466 \text{ eV (FWHM} = 1.10 \text{ eV, C}^{\text{CN}})$$

$$w_2 = 0.46022 \pm 0.0469 \text{ eV (FWHM} = 1.08 \text{ eV, C}^{\text{ali-4}})$$

$$w_3 = 0.5 \pm 0.0302 \text{ eV (FWHM} = 1.18 \text{ eV, C}^{\text{ali-3}})$$

$$w_4 = 0.57717 \pm 0.0166 \text{ eV (FWHM} = 1.35 \text{ eV, C}^{\text{ali-4}})$$

$$p_1 = 287.2 \pm 0.0323 \text{ eV (C}^{\text{CN}} \text{ component, constrained to } 287.1 \pm 0.1 \text{ eV)}$$

$$p_2 = 286.7 \pm 0.0315 \text{ eV (C}^{\text{ali-4}} \text{ component, constrained to } 286.6 \pm 0.1 \text{ eV)}$$

$$p_3 = 285.92 \pm 0.0323 \text{ eV (C}^{\text{ali-3}} \text{ component, constrained to } 286.0 \pm 0.1 \text{ eV)}$$

$$p_4 = 285 \pm 0.0126 \text{ eV (C}^{\text{ali-3,4}} \text{ component, constrained to } 285.0 \pm 0.1 \text{ eV)}$$

Unconstrained positions:

$$A_1 = 319 \pm 0 \text{ (constrained to 0.9 carbon atoms)}$$

$$A_2 = 355 \pm 0 \text{ (constrained to 1.0 carbon atoms)}$$

$$A_3 = 355 \pm 0 \text{ (constrained to 1.0 carbon atoms)}$$

$$A_4 = 710 \pm 0 \text{ (constrained to 2.0 carbon atoms)}$$

$$w_1 = 0.5 \pm 0.0386 \text{ eV (FWHM} = 1.18 \text{ eV, C}^{\text{CN}})$$

$$w_2 = 0.42446 \pm 0.0302 \text{ eV (FWHM} = 1.00 \text{ eV, C}^{\text{ali-4}})$$

$$w_3 = 0.5 \pm 0.026 \text{ eV (FWHM} = 1.18 \text{ eV, C}^{\text{ali-3}})$$

$$w_4 = 0.50862 \pm 0.0123 \text{ eV (FWHM} = 1.19 \text{ eV, C}^{\text{ali-3,4}})$$

$$p_1 = 287.33 \pm 0.0243 \text{ eV (C}^{\text{CN}} \text{ component)}$$

$$p_2 = 286.82 \pm 0.0203 \text{ eV (C}^{\text{ali-4}} \text{ component)}$$

$$p_3 = 286.12 \pm 0.022 \text{ eV (C}^{\text{ali-3}} \text{ component)}$$

$$p_4 = 284.94 \pm 0.00859 \text{ eV (C}^{\text{ali-3,4}} \text{ component)}$$

Fitting from **Figure 5.20**, Chapter 5: Nitrile Functionalised Ionic Liquids:

Constrained positions:

$$A_1 = 256 \pm 0 \text{ (constrained to 0.9 carbon atoms)}$$

$$A_2 = 284 \pm 0 \text{ (constrained to 1.0 carbon atoms)}$$

$$A_3 = 284 \pm 0 \text{ (constrained to 1.0 carbon atoms)}$$

$$A_4 = 570 \pm 0 \text{ (constrained to 2.0 carbon atoms)}$$

$$w_1 = 0.43078 \pm 0.0378 \text{ eV (FWHM} = 1.01 \text{ eV, C}^{\text{CN}})$$

$$w_2 = 0.4 \pm 0.0439 \text{ eV (FWHM} = 0.94 \text{ eV, C}^{\text{ali-4}})$$

$$w_3 = 0.5 \pm 0.0547 \text{ eV (FWHM} = 1.18 \text{ eV, C}^{\text{ali-3}})$$

$$w_4 = 0.51694 \pm 0.0192 \text{ eV (FWHM} = 1.21 \text{ eV, C}^{\text{ali-3,4}})$$

$$p_1 = 287.2 \pm 0.0271 \text{ eV (C}^{\text{CN}} \text{ component, constrained to } 287.1 \pm 0.1 \text{ eV)}$$

$$p_2 = 286.64 \pm 0.0297 \text{ eV (C}^{\text{ali-4}} \text{ component, constrained to } 286.6 \pm 0.1 \text{ eV)}$$

$$p_3 = 286.1 \pm 0.0398 \text{ eV (C}^{\text{ali-3}} \text{ component, constrained to } 286.0 \pm 0.1 \text{ eV)}$$

$$p_4 = 285.07 \pm 0.0147 \text{ eV (C}^{\text{ali-3,4}} \text{ component, constrained to } 285.0 \pm 0.1 \text{ eV)}$$

Unconstrained positions:

$$A_1 = 256 \pm 0 \text{ (constrained to 0.9 carbon atoms)}$$

$$A_2 = 284 \pm 0 \text{ (constrained to 1.0 carbon atoms)}$$

$$A_3 = 284 \pm 0 \text{ (constrained to 1.0 carbon atoms)}$$

$$A_4 = 570 \pm 0 \text{ (constrained to 2.0 carbon atoms)}$$

$$w_1 = 0.5 \pm 0.0803 \text{ eV (FWHM} = 1.18 \text{ eV, C}^{\text{CN}})$$

$$w_2 = 0.5 \pm 0.188 \text{ eV (FWHM} = 1.18 \text{ eV, C}^{\text{ali-4}})$$

$$w_3 = 0.5 \pm 0.121 \text{ eV (FWHM} = 1.18 \text{ eV, C}^{\text{ali-3}})$$

$$w_4 = 0.49937 \pm 0.0159 \text{ eV (FWHM} = 1.17 \text{ eV, C}^{\text{ali-3,4}})$$

$$p_1 = 287.23 \pm 0.066 \text{ eV (C}^{\text{CN}} \text{ component)}$$

$$p_2 = 286.69 \pm 0.0855 \text{ eV (C}^{\text{ali-4}} \text{ component)}$$

$$p_3 = 286.26 \pm 0.106 \text{ eV (C}^{\text{ali-3}} \text{ component)}$$

$$p_4 = 285.05 \pm 0.0115 \text{ eV (C}^{\text{ali-3,4}} \text{ component)}$$

Fitting from **Figure 5.22**, Chapter 5: Nitrile Functionalised Ionic Liquids:

Unconstrained positions:

$$A_1 = 260 \pm 0 \text{ (constrained to 0.9 carbon atoms)}$$

$$A_2 = 289 \pm 0 \text{ (constrained to 1.0 carbon atoms)}$$

$$A_3 = 289 \pm 0 \text{ (constrained to 1.0 carbon atoms)}$$

$$A_4 = 570 \pm 0 \text{ (constrained to 2.0 carbon atoms)}$$

$$w_1 = 0.46931 \pm 0.0411 \text{ eV (FWHM} = 1.10 \text{ eV, C}^{\text{CN}})$$

$$w_2 = 0.49581 \pm 0.0732 \text{ eV (FWHM} = 1.17 \text{ eV, C}^{\text{ali-4}})$$

$$w_3 = 0.5 \pm 0.0855 \text{ eV (FWHM} = 1.18 \text{ eV, C}^{\text{ali-3}})$$

$$w_4 = 0.6 \pm 0.0346 \text{ eV (FWHM} = 1.41 \text{ eV, C}^{\text{ali-3,4}})$$

$$p_1 = 287.09 \pm 0.0323 \text{ eV (C}^{\text{CN}} \text{ component)}$$

$$p_2 = 286.3 \pm 0.0428 \text{ eV (C}^{\text{ali-4}} \text{ component)}$$

$$p_3 = 285.69 \pm 0.042 \text{ eV (C}^{\text{ali-3}} \text{ component)}$$

$$p_4 = 284.96 \pm 0.0219 \text{ eV (C}^{\text{ali-3,4}} \text{ component)}$$

Fitting from **Figure 5.23**, Chapter 5: Nitrile Functionalised Ionic Liquids:

Unconstrained positions:

$$A_1 = 847 \pm 0 \text{ (constrained to 0.9 carbon atoms)}$$

$$A_2 = 942 \pm 0 \text{ (constrained to 1.0 carbon atoms)}$$

$$A_3 = 942 \pm 0 \text{ (constrained to 1.0 carbon atoms)}$$

$$A_4 = 1884 \pm 0 \text{ (constrained to 2.0 carbon atoms)}$$

$$w_1 = 0.5 \pm 0.0817 \text{ eV (FWHM} = 1.18 \text{ eV, C}^{\text{CN}})$$

$$w_2 = 0.5 \pm 0.127 \text{ eV (FWHM} = 1.18 \text{ eV, C}^{\text{ali-4}})$$

$$w_3 = 0.5 \pm 0.102 \text{ eV (FWHM} = 1.18 \text{ eV, C}^{\text{ali-3}})$$

$$w_4 = 0.60003 \pm 0.0445 \text{ eV (FWHM} = 1.41 \text{ eV, C}^{\text{ali-3,4}})$$

$$p_1 = 287.17 \pm 0.0521 \text{ eV (C}^{\text{CN}} \text{ component)}$$

$$p_2 = 286.5 \pm 0.0568 \text{ eV (C}^{\text{ali-4}} \text{ component)}$$

$$p_3 = 285.9 \pm 0.0581 \text{ eV (C}^{\text{ali-3}} \text{ component)}$$

$$p_4 = 285 \pm 0.0343 \text{ eV (C}^{\text{ali-3,4}} \text{ component)}$$

Fitting from **Figure 5.24**, *Chapter 5: Nitrile Functionalised Ionic Liquids*:

Unconstrained positions:

$$= 1080 \pm 0 \text{ (constrained to 0.9 carbon atoms)}$$

$$= 1200 \pm 0 \text{ (constrained to 1.0 carbon atoms)}$$

$$= 1200 \pm 0 \text{ (constrained to 1.0 carbon atoms)}$$

$$= 2760 \pm 0 \text{ (constrained to 2.3 carbon atoms) Note: 2.3 C atoms required for fit.}$$

$$= 0.5 \pm 0.0555 \text{ eV (FWHM = 1.18 eV, C}^{\text{CN}})$$

$$= 0.45301 \pm 0.0478 \text{ eV (FWHM = 1.06 eV, C}^{\text{ali-4}})$$

$$= 0.5 \pm 0.0532 \text{ eV (FWHM = 1.18 eV, C}^{\text{ali-3}})$$

$$= 0.6 \pm 0.0261 \text{ eV (FWHM = 1.41 eV, C}^{\text{ali-3,4}})$$

$$= 287.06 \pm 0.0363 \text{ eV (C}^{\text{CN}} \text{ component)}$$

$$= 286.47 \pm 0.0331 \text{ eV (C}^{\text{ali-4}} \text{ component)}$$

$$= 285.65 \pm 0.0385 \text{ eV (C}^{\text{ali-3}} \text{ component)}$$

$$= 284.96 \pm 0.017 \text{ eV (C}^{\text{ali-3,4}} \text{ component)}$$

Notes:

1. All areas are calculated relative to the nitrile functionalised IL C 1s photoemissions and are checked to the traditional IL C 1s regions.
2. The FWHMs for the C^{CN}, C^{ali-4} and C^{ali-3} components are constrained to 0.8-1.2 eV, while the FWHM for the C^{ali-3,4} component has been constrained to 0.8-1.5 eV (since it contains multiple photoemission signals).

7.4 Residual STDs for nitrile ILs:

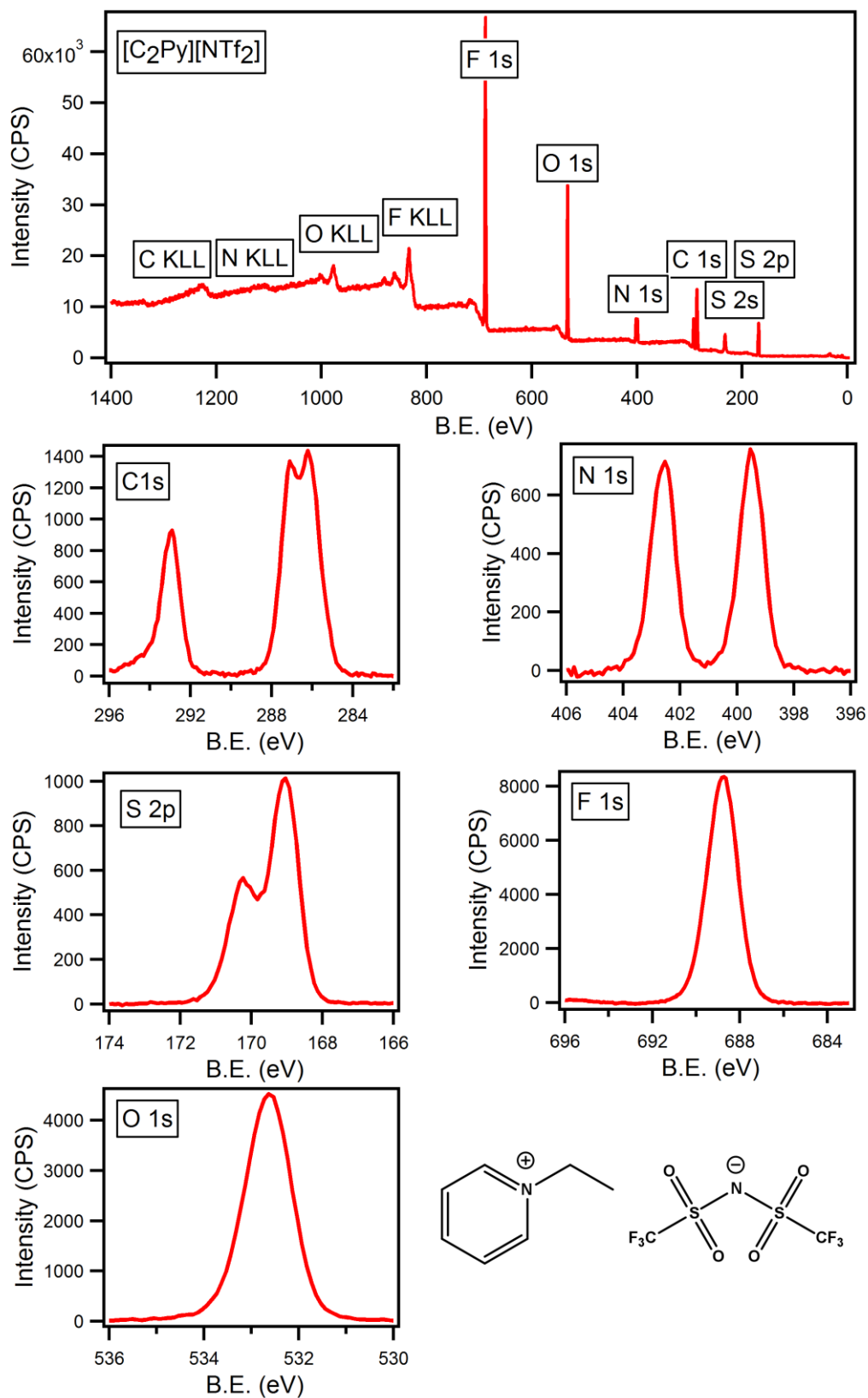
In an XP spectrum, Poisson statistics dictates that noise is proportional to the square root of the counts per data bin. Residual STDs are therefore automatically normalised by CasaXPS by dividing by the square root of the counts per bin of each bin. Modern XPS instruments have complex detectors that merge multiple data streams, e.g. multi-channel plates, and as such the pulse counting does not obey Poisson statistics. Since multi-channel detectors effectively smooth the data, the value for the residual STD may be less than one. The ideal residual STD can be calculated by applying a regression background to an area of a spectrum without any peaks, then the residual plot can be recorded. Residual STDs in the 0.87 range are common for modern instruments. The ideal residual STD from the nitrile IL C 1s regions. An area with no peaks was fitted with a regression background and the residual STD was taken.

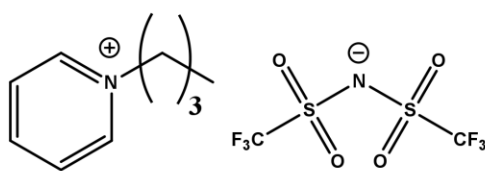
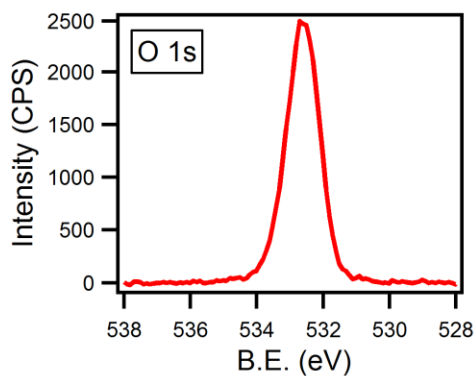
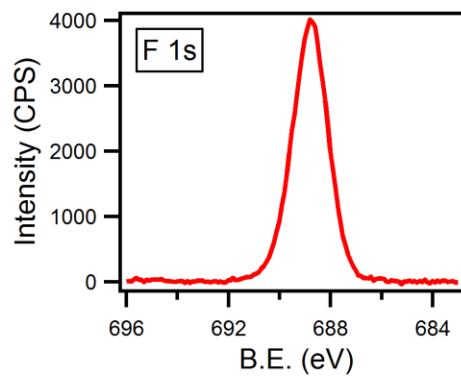
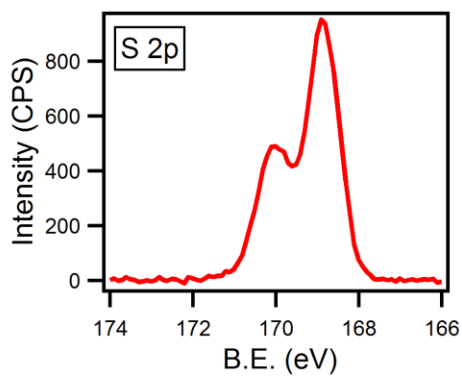
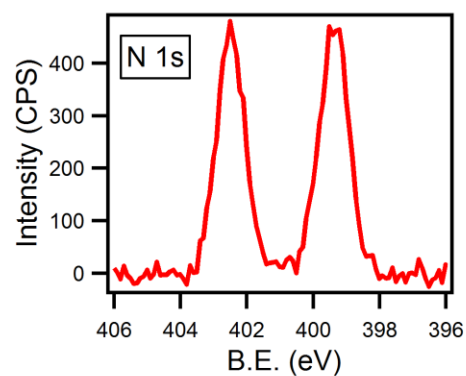
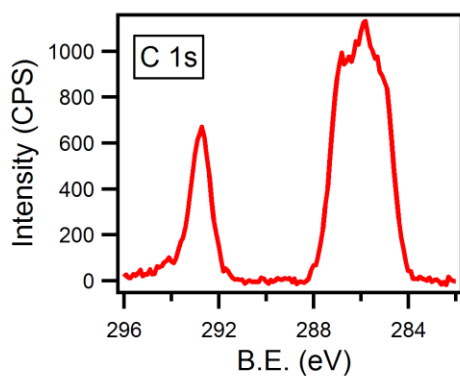
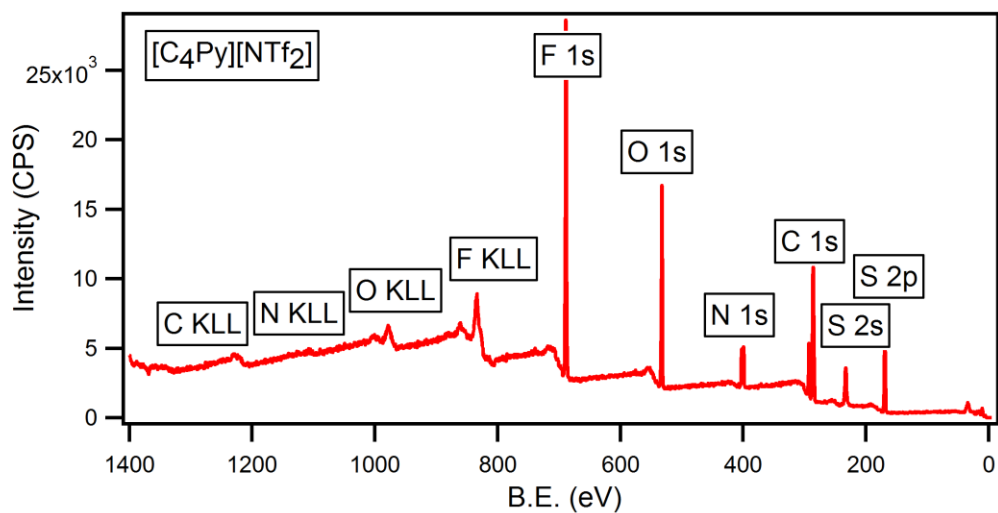
Appendix 1 The residual STDs as measured for the C 1s regions of the nitrile functionalised ILs. The individual cation and anion pairs are shown. The data was obtained by fitting a section of the C 1s region without any peaks with a regression background and then measuring the residual signal.

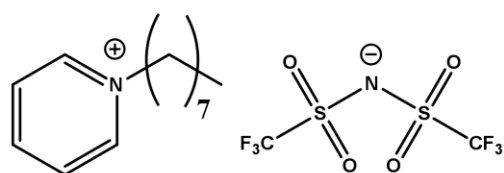
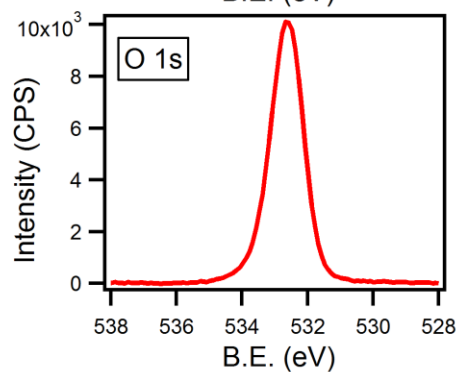
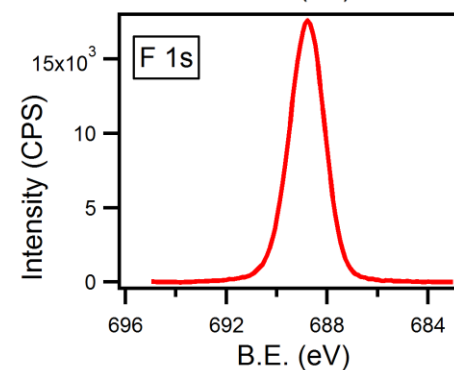
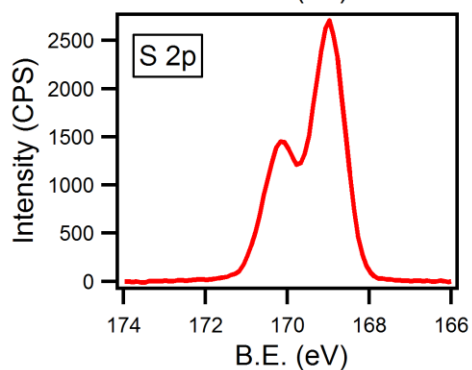
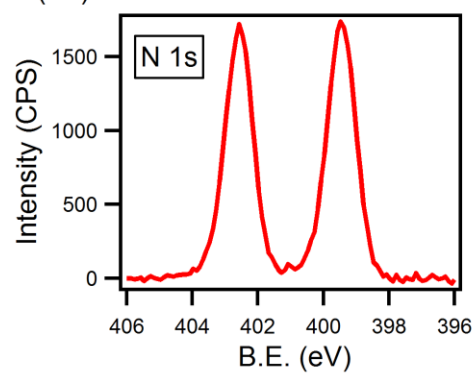
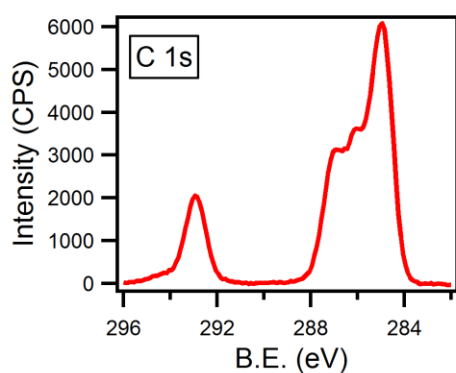
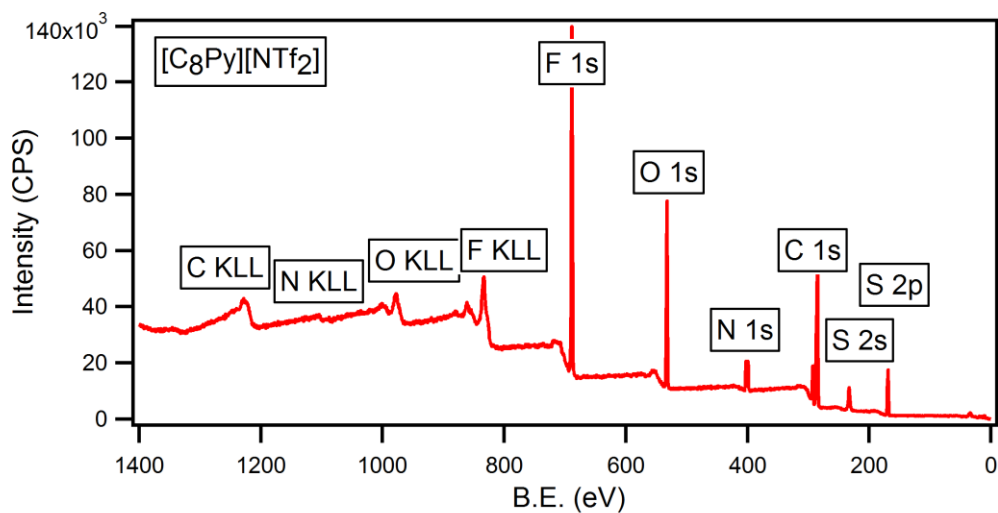
Cation	Anion	Residual STD
[(C ₄ CN)Py] ⁺	[NTf ₂] ⁻	0.82
[(C ₄ CN)C ₁ Im] ⁺	[NTf ₂] ⁻	0.75
[(C ₄ CN)C ₁ Pyrr] ⁺	[NTf ₂] ⁻	0.89
[(C ₄ CN)Py] ⁺	[PF ₆] ⁻	0.92
[(C ₄ CN)C ₁ Im] ⁺	[PF ₆] ⁻	0.83
[(C ₄ CN)C ₁ Pyrr] ⁺	[PF ₆] ⁻	0.93
[(C ₄ CN)C ₁ Im] ⁺	[BF ₄] ⁻	0.89
[(C ₄ CN)C ₁ Im] ⁺	Cl ⁻	0.99
Average		0.88

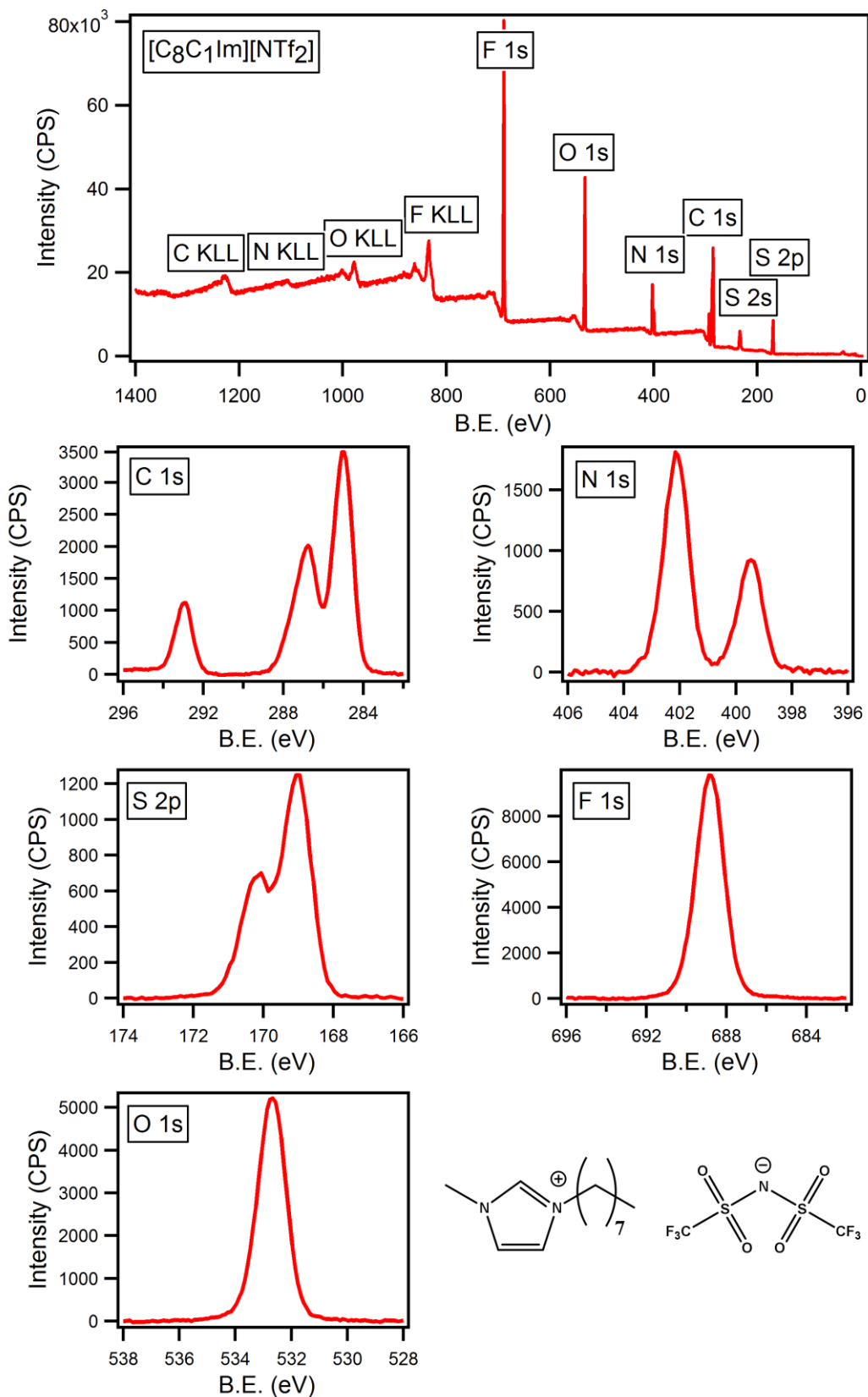
7.5 Reference Spectra:

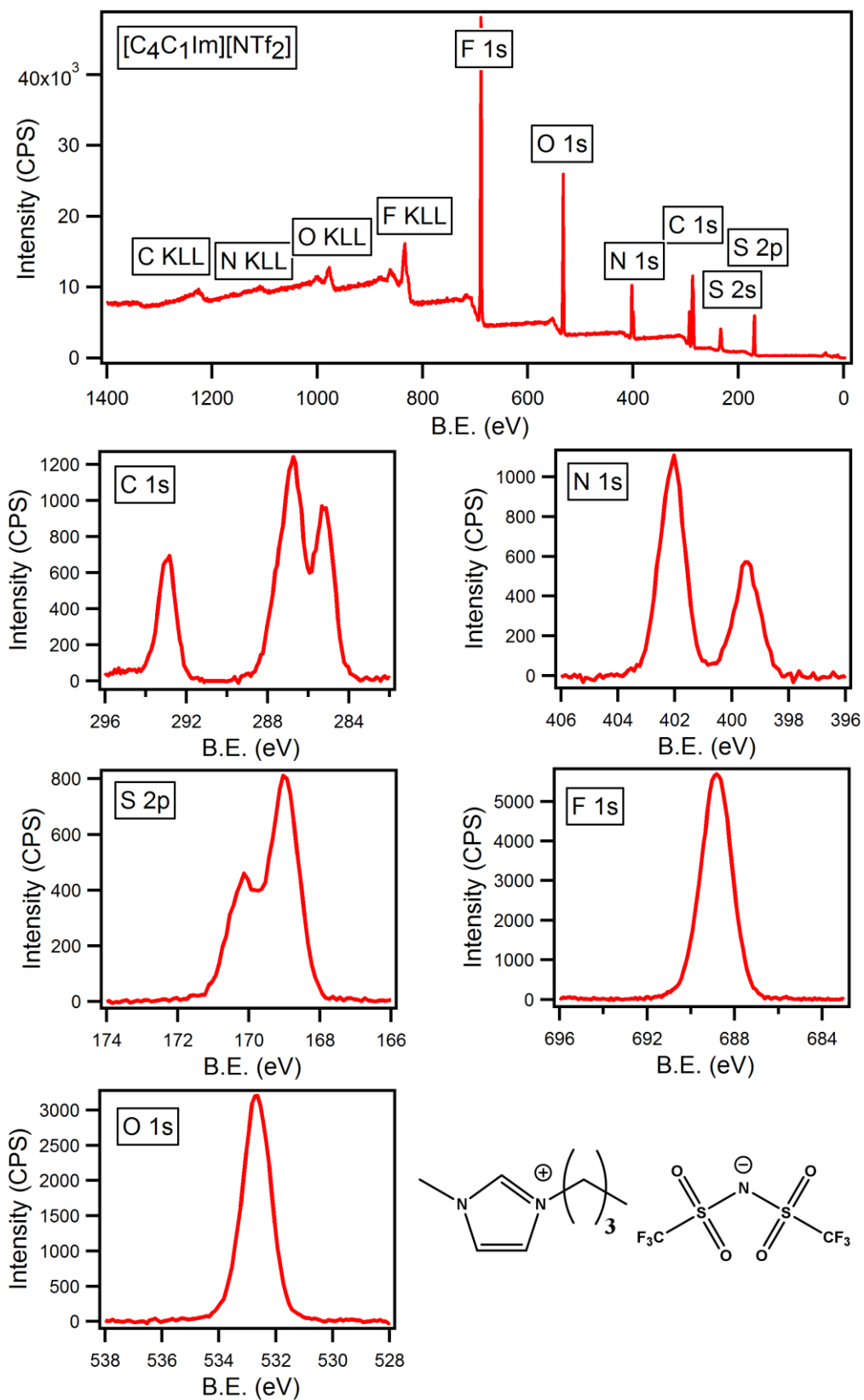
The imidazolium and pyridinium reference spectra used in this thesis were previously obtained by Dr. Shaung Men and Dr. Ignacio Villar-Garcia. The full XPS analysis of both pyridinium and imidazolium ILs have previously been thoroughly reported.^{1,2}

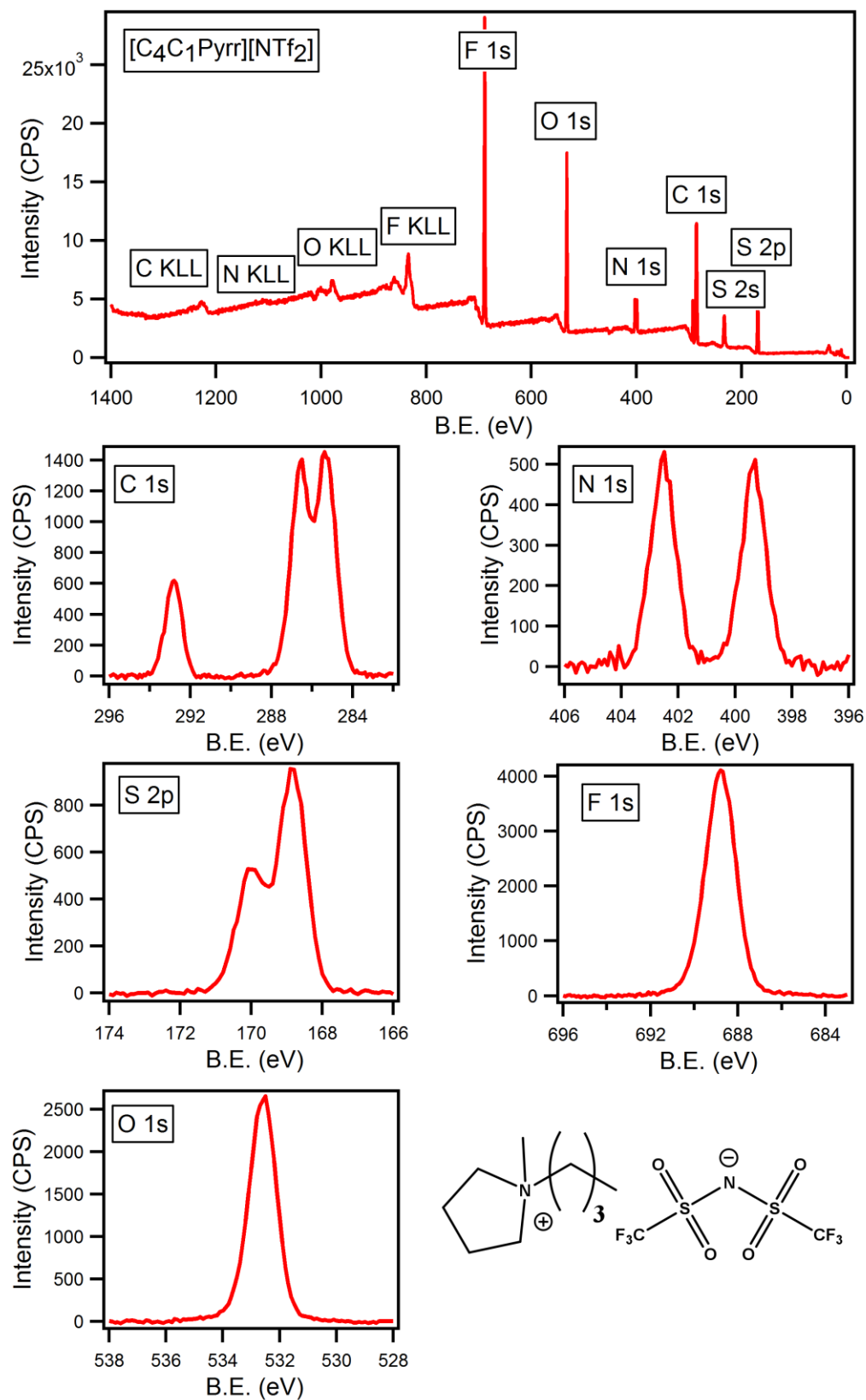


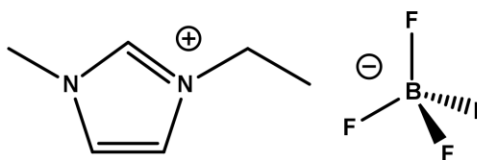
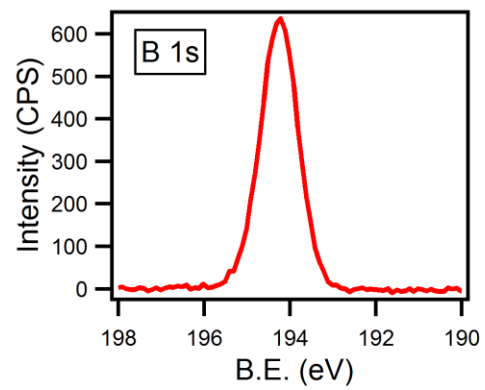
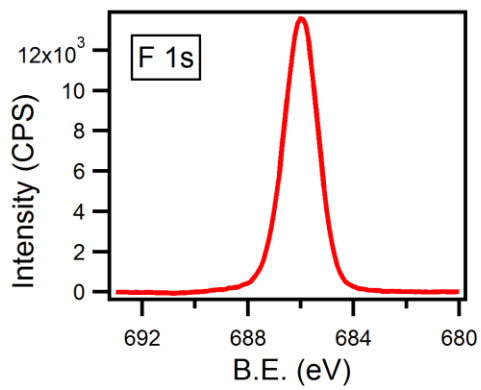
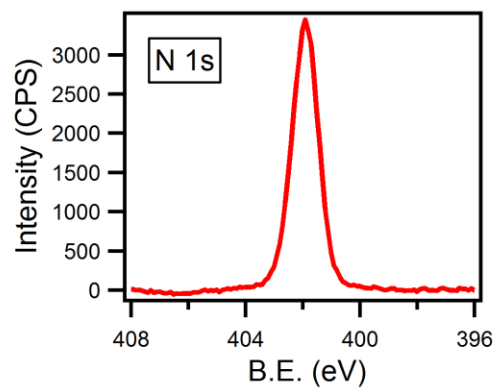
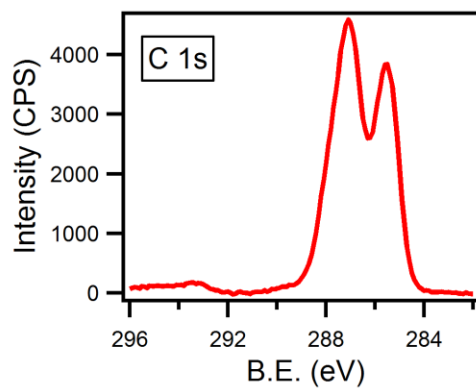
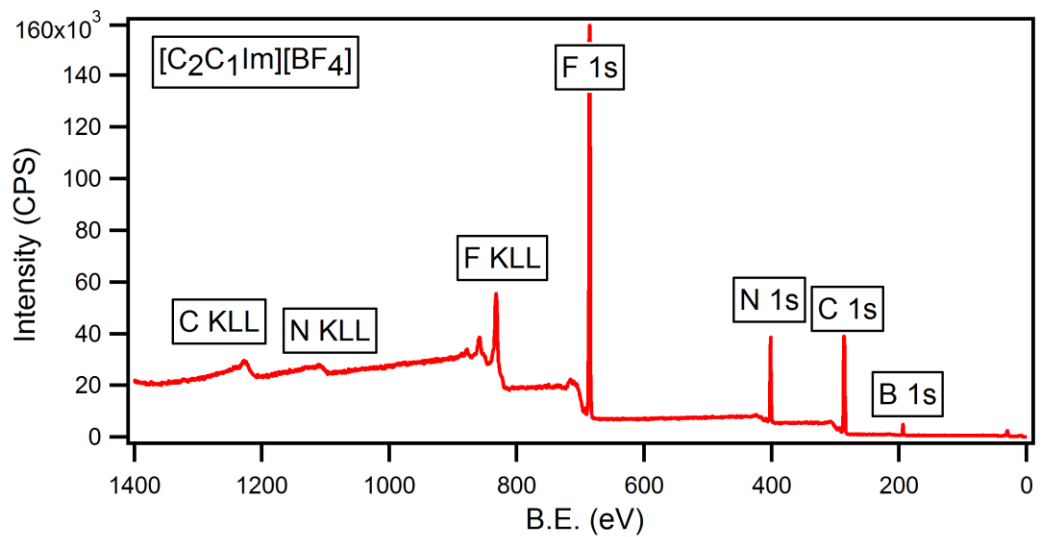


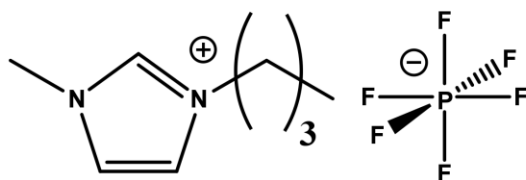
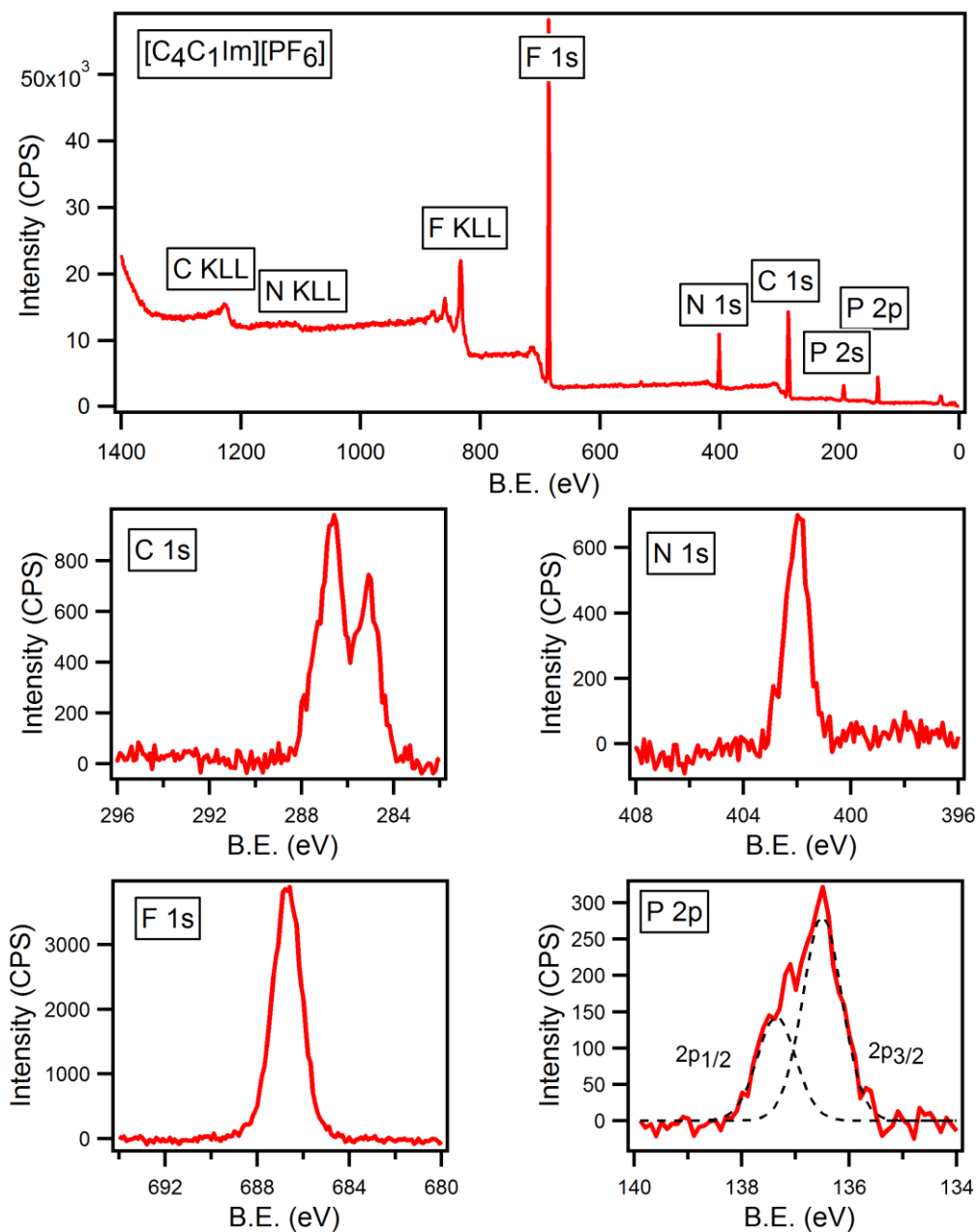


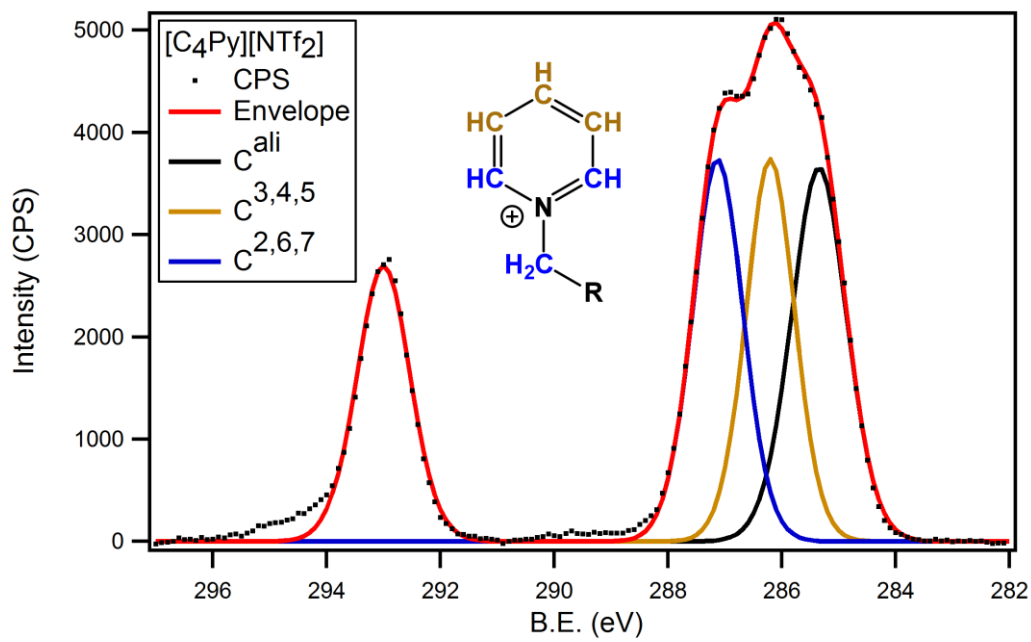
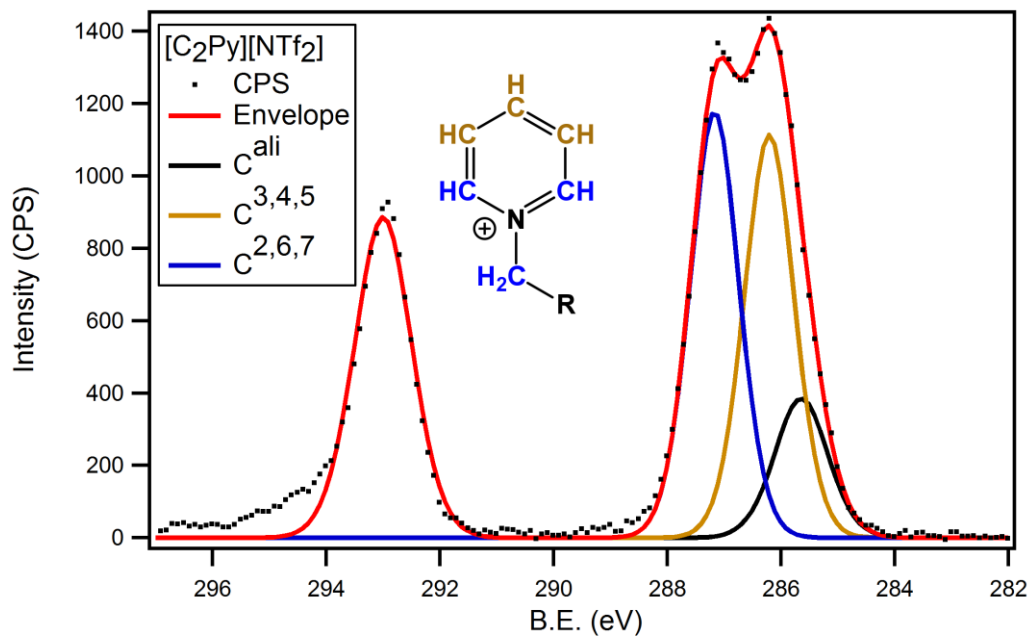


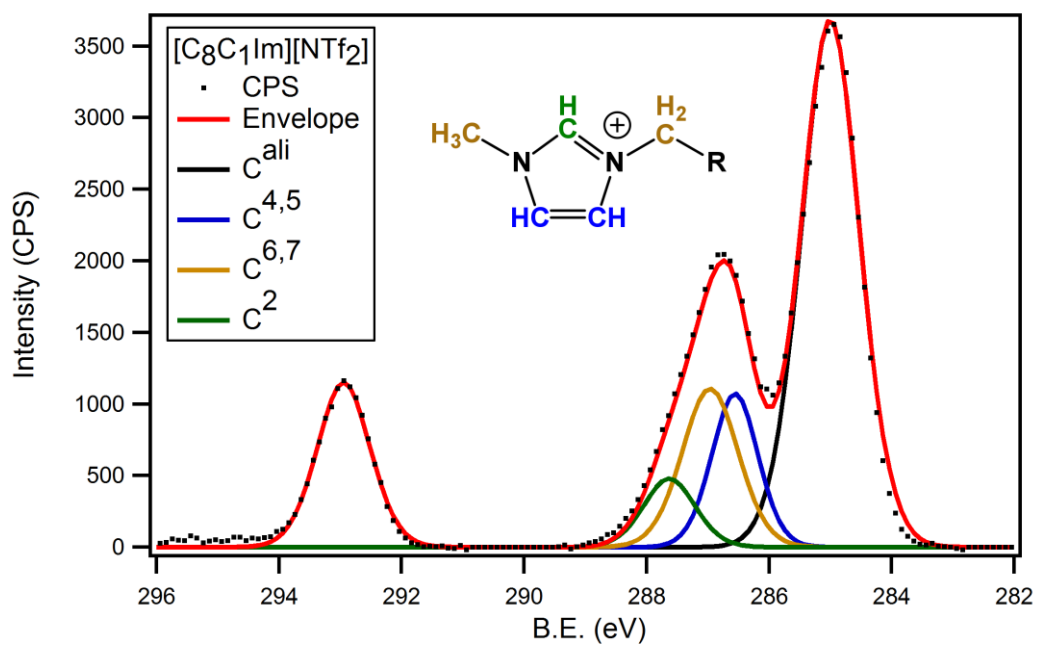
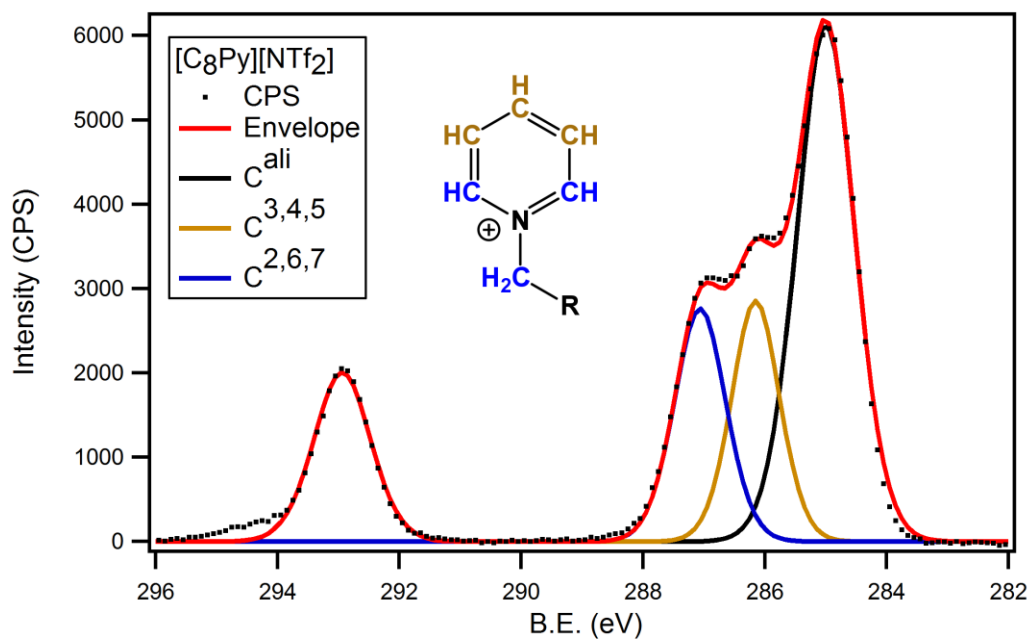


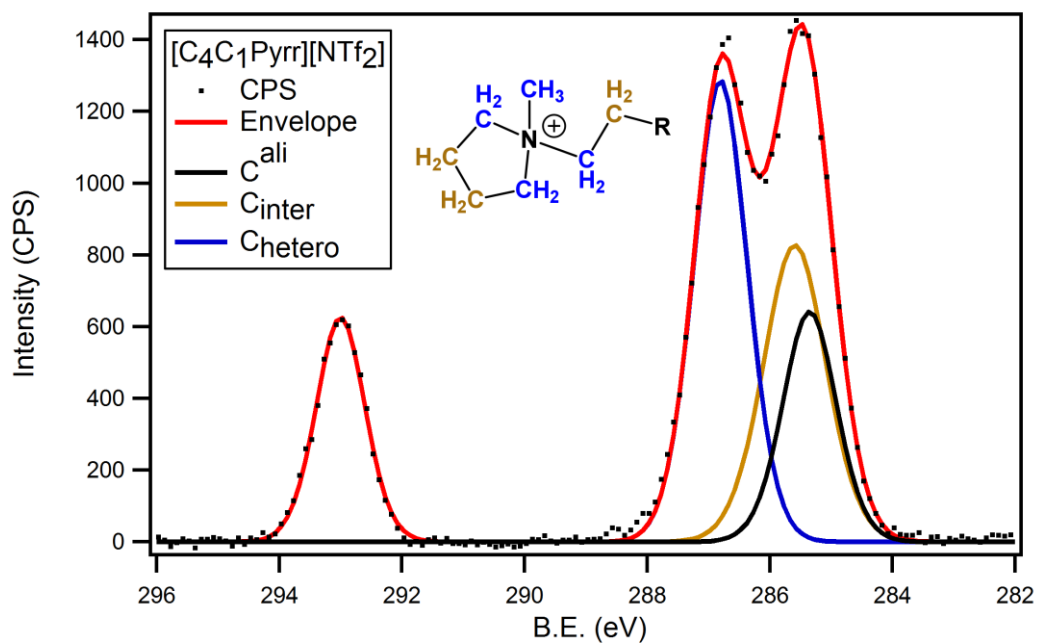
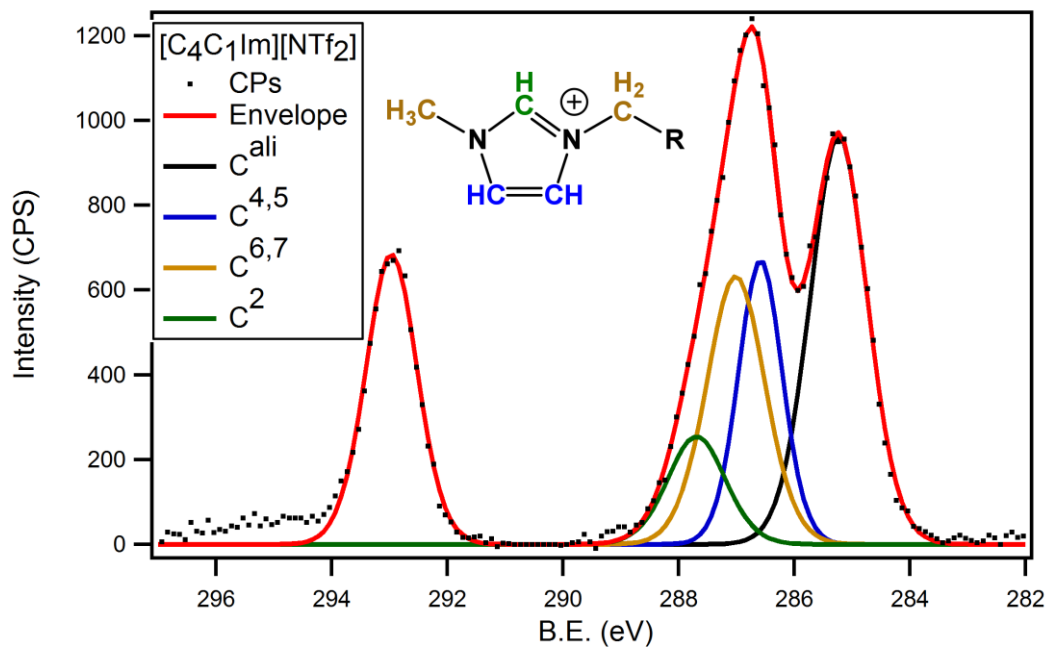












References:

- 1 S. Men, *Thesis*, The University of Nottingham, 2011.
- 2 I. J. Villar García, *Thesis*, The University of Nottingham, 2009.